ISSN 2500-316X (Online)

RUSSIAN TECHNOLOGICAL JOURNAL

РОССИЙСКИЙ ТЕХНОЛОГИЧЕСКИЙ ЖУРНАЛ

Information systems.
Computer sciences.
Issues of information security

Multiple robots (robotic centers) and systems.
Remote sensing and non-destructive testing

Modern radio engineering and telecommunication systems

Micro- and nanoelectronics.
Condensed matter physics

Analytical instrument engineering and technology

Mathematical modeling

Economics of knowledge-intensive and high-tech enterprises and industries.
Management in organizational systems

Product quality management. Standardization

Philosophical foundations of technology and society

12+
www.rtj-mirea.ru

МИРЭА
Российский технологический университет

10(5) 2022

ISSN 2500-316X (Online)

RUSSIAN TECHNOLOGICAL JOURNAL

РОССИЙСКИЙ ТЕХНОЛОГИЧЕСКИЙ ЖУРНАЛ

- Information systems. Computer sciences. Issues of information security
- Multiple robots (robotic centers) and systems. Remote sensing and non-destructive testing
- Modern radio engineering and telecommunication systems
- Micro- and nanoelectronics. Condensed matter physics
- Analytical instrument engineering and technology
- Mathematical modeling
- Economics of knowledge-intensive and high-tech enterprises and industries. Management in organizational systems
- Product quality management. Standardization
- Philosophical foundations of technology and society

- Информационные системы. Информатика. Проблемы информационной безопасности
- Роботизированные комплексы и системы. Технологии дистанционного зондирования и неразрушающего контроля
- Современные радиотехнические и телекоммуникационные системы
- Микро- и наноэлектроника. Физика конденсированного состояния
- Аналитическое приборостроение и технологии
- Математическое моделирование
- Экономика наукоемких и высокотехнологичных предприятий и производств. Управление в организационных системах
- Управление качеством продукции. Стандартизация
- Мировоззренческие основы технологии и общества

Russian Technological Journal
2022, Vol. 10, No. 5

Russian Technological Journal
2022, том 10, № 5

https://www.rtj-mirea.ru

https://doi.org/10.32362/2500-316X

ISSN 2500-316X (Online)

Russian Technological Journal
2022, Vol. 10, No. 5

Publication date September 30, 2022.

The peer-reviewed scientific and technical journal highlights the issues of complex development of radio engineering, telecommunication and information systems, electronics and informatics, as well as the results of fundamental and applied interdisciplinary researches, technological and economical developments aimed at the development and improvement of the modern technological base.

Periodicity: bimonthly.
The journal was founded in December 2013. The titles were «Herald of MSTU MIREA» until 2016 (ISSN 2313-5026) and «Rossiiskii tekhnologicheskii zhurnal» from January 2016 until July 2021 (ISSN 2500-316X).

Founder and Publisher:
Federal State Budget
Educational Institution
of Higher Education
«MIREA – Russian Technological University»
78, Vernadskogo pr., Moscow, 119454 Russia.

The Journal is included in RSL (Russian State Library), Russian citation index, elibrary, Socionet, Directory of Open Access Journals (DOAJ), Directory of Open Access Scholarly Resources (ROAD), Google Scholar, Open Archives Initiative, Ulrich's International Periodicals Directory.

The registration number ПИ № ФС 77 - 81733 was issued in August 19, 2021 by the Federal Service for Supervision of Communications, Information Technology, and Mass Media of Russia.

The subscription index of *Pressa Rossii*: **79641**.

Russian Technological Journal
2022, том 10, № 5

Дата опубликования 30 сентября 2022 г.

Научно-технический рецензируемый журнал освещает вопросы комплексного развития радиотехнических, телекоммуникационных и информационных систем, электроники и информатики, а также результаты фундаментальных и прикладных междисциплинарных исследований, технологических и организационно-экономических разработок, направленных на развитие и совершенствование современной технологической базы.

Периодичность: один раз в два месяца.
Журнал основан в декабре 2013 года. До 2016 г. издавался под названием «Вестник МГТУ МИРЭА» (ISSN 2313-5026), а с января 2016 г. по июль 2021 г. под названием «Российский технологический журнал» (ISSN 2500-316X).

Учредитель и издатель:
федеральное государственное бюджетное
образовательное учреждение
высшего образования
«МИРЭА – Российский технологический университет»
119454, РФ, г. Москва, пр-т Вернадского, д. 78.

Журнал индексируется в РГБ, РИНЦ, elibrary, Соционет, Directory of Open Access Journals (DOAJ), Directory of Open Access Scholarly Resources (ROAD), Google Scholar, Open Archives Initiative, Ulrich's International Periodicals Directory.

Регистрационный номер и дата принятия решения о регистрации СМИ ПИ № ФС 77 - 81733 от 19.08.2021 г. СМИ зарегистрировано Федеральной службой по надзору в сфере связи, информационных технологий и массовых коммуникаций (Роскомнадзор).

Индекс по объединенному каталогу «Пресса России» **79641**.

https://www.rtj-mirea.ru

Editorial Board

Редакционная коллегия

Contents

Содержание

Information systems. Computer sciences. Issues of information security
Информационные системы. Информатика. Проблемы информационной безопасности

UDC 004.825
https://doi.org/10.32362/2500-316X-2022-10-5-7-15

RESEARCH ARTICLE

Structure of associative heterarchical memory

Roman V. Dushkin [@], Vasilisa A. Lelekova [@], Vladimir Y. Stepankov, Sandra Fadeeva

Artificial Intelligence Agency, Moscow, 127591 Russia
[@] Corresponding authors, e-mail: drv@aiagency.ru, lv@aiagency.ru

Abstract

Objectives. Since the 20th century, artificial intelligence methods can be divided into two paradigms: top-down and bottom-up. While the methods of the ascending paradigm are difficult to interpret as natural language outputs, those applied according to the descending paradigm make it difficult to actualize information. Thus, natural language processing (NLP) by artificial intelligence remains a pressing problem of our time. The main task of NLP is to create applications that can process and understand natural languages. According to the presented approach to the construction of artificial intelligence agents (AI-agents), processing of natural language should be conducted at two levels: at the bottom, methods of the ascending paradigm are employed, while symbolic methods associated with the descending paradigm are used at the top. To solve these problems, the authors of the present paper propose a new mathematical formalism: associative heterarchical memory (AH-memory), whose structure and functionality are based both on bionic principles and on the achievements of top-down and bottom-up artificial intelligence paradigms.

Methods. Natural language recognition algorithms were used in conjunction with various artificial intelligence methods.

Results. The problem of character binding as applied to AH-memory was explored by the research group in earlier research. Here, abstract symbol binding was performed using multi-serial integration, eventually converting the primary symbols produced by the program into integrated abstract symbols. The present paper provides a comprehensive description of AH-memory in the form of formulas, along with their explanations and corresponding schemes.

Conclusions. The most universal structure of AH-memory is presented. When working with AH-memory, a developer should select from a variety of possible module sets those AH-memory components that support the most successful and efficient functioning of the AI-agent.

Keywords: artificial intelligence, natural language processing, associative heterarchical memory, AI-agent, abstract symbols, hypernet, predicate symbol control model, actant role classifier, hypergraph

• **Submitted:** 16.03.2022 • **Revised:** 13.07.2022 • **Accepted:** 12.09.2022

For citation: Dushkin R.V., Lelekova V.A., Stepankov V.Y., Fadeeva S. Structure of associative heterarchical memory. *Russ. Technol. J.* 2022;10(5):7–15. https://doi.org/10.32362/2500-316X-2022-10-5-7-15

Financial disclosure: The authors have no a financial or property interest in any material or method mentioned.

The authors declare no conflicts of interest.

НАУЧНАЯ СТАТЬЯ

Структура ассоциативно-гетерархической памяти

Р.В. Душкин [@], В.А. Лелекова [@], В.Ю. Степаньков, С. Фадеева

Агентство Искусственного Интеллекта, Москва, 127591 Россия
[@] Авторы для переписки, e-mail: drv@aiagency.ru, lv@aiagency.ru

Резюме

Цели. Начиная с XX века методы искусственного интеллекта разделяют на две парадигмы – нисходящую и восходящую. Методы восходящей парадигмы сложно интерпретировать в виде вывода естественного языка, а в методах нисходящей парадигмы затруднена актуализация информации. Обработка естественного языка (NLP, от англ. Natural Language Processing) искусственным интеллектом остается актуальной проблемой современности. Основная задача NLP – создание программ, способных обрабатывать и понимать естественные языки. С учетом авторского подхода к построению агентов искусственного интеллекта (ИИ-агентов) обработка естественного языка должна также вестись на двух уровнях: на нижнем – при помощи методов восходящей парадигмы и на верхнем – при помощи символьных методов нисходящей парадигмы. Для решения этих задач авторами предложен новый математический формализм – ассоциативно-гетерархическая память (АГ-память), структура и функционирование которой основаны как на бионических принципах, так и на достижениях обеих парадигм искусственного интеллекта.

Методы. Использованы методы искусственного интеллекта и алгоритмы распознавания естественного языка.

Результаты. Ранее авторским коллективом была исследована проблема привязки символов в приложении к АГ-памяти. В ней привязка абстрактных символов осуществлялась с помощью мультисенсорной интеграции. При этом первичные символы, получаемые программой, преобразовывались в интегрированные абстрактные символы. В данной статье приведено полное описание АГ-памяти в виде формул, пояснений к ним и соответствующим схемам.

Выводы. В статье представлена максимально универсальная структура АГ-памяти. При работе с АГ-памятью из множества возможных модулей следует выбирать те части АГ-памяти, которые обеспечивают успешное и эффективное функционирование ИИ-агента.

Ключевые слова: искусственный интеллект, обработка естественного языка, ассоциативно-гетерархическая память, ИИ-агент, абстрактные символы, гиперсеть, модель управления предикатного символа, классификатор ролей актантов, гиперграф

• **Поступила:** 16.03.2022 • **Доработана:** 13.07.2022 • **Принята к опубликованию:** 12.09.2022

Для цитирования: Душкин Р.В., Лелекова В.А., Степаньков В.Ю., Фадеева С. Структура ассоциативно-гетерархической памяти. *Russ. Technol. J.* 2022;10(5):7–15. https://doi.org/10.32362/2500-316X-2022-10-5-7-15

Прозрачность финансовой деятельности: Авторы не имеют финансовой заинтересованности в представленных материалах или методах.

Авторы заявляют об отсутствии конфликта интересов.

Glossarium

Artificial intelligence (AI) is a set of technological solutions for simulating human cognitive functions (including self-learning, finding solutions without a predetermined algorithm, and obtaining insights) and yielding specific, practically significant results that are at least comparable with those gained through human intellectual activity.

Natural language processing is a subfield of computer science and AI dedicated to the analysis of natural (human) languages using computers.

AI-agent is a fully-fledged cybernetic machine encompassing a control system that continuously receives information from its sensory systems and operates on its environment by means of actuators.

INTRODUCTION

Artificial intelligence methods [1] can be divided into two paradigms: top-down and bottom-up [2]. Methods associated with the bottom-up paradigm are used to build models of cognitive processes that rely on large amounts of data. Thus, while the accuracy of results from the thus constructed "black box" model can be brought to the required value, the relevant decision-making processes are difficult (or even almost impossible) to interpret from a human point of view [3]. Conversely, when using knowledge-based "white-box" models generated according to the top-down paradigm, difficulties arise in maintaining the relevance of the state when the structure of the problem area changes; moreover, the construction of such models is an inherently complex and time-consuming process [4].

Thus, natural language[1] processing (NLP) by artificial intelligence remains an urgent problem [5, 6]. The main challenge for NLP is to create applications for processing and understanding natural languages. Taking into account the presented approach to the construction of AI-agents [7], natural language processing should be carried out at two levels: (1) at the lower level using methods of the ascending paradigm (deep learning neural networks for solving linguistic problems); (2) at the upper level using symbolic methods of the descending paradigm (semantic networks and an associated ontology for knowledge representation and machine inference).

To solve these problems, the authors propose a novel mathematical formalism referred to as associative heterarchical memory (AH-memory), whose structure and functionality are based both on bionic principles and on the achievements of both paradigms of artificial intelligence. AH memory is based on this understanding of the structure of the *cognitome*. In terms of its structure, it comprises a hypergraph [8], in which nodes are comprised of symbols, while links and hyperlinks between symbols represent a mapping of relationships between concepts.

This article presents a complete description of the set-theoretic structure of AH-memory.

STRUCTURE OF ASSOCIATIVE HETERARCHICAL MEMORY

AH-memory comprises a tuple, i.e., an ordered set of elements of a fixed length, further presented in formula (1), between whose elements are five sets of links shown in Fig. 1 in the form of a graph [9].

[1] Natural language is a language that human beings speak or write.

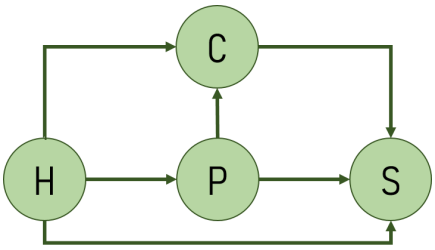

Fig. 1. Graph of links between AH-memory objects

A link between two sets on a graph denotes the entire set of associative links between their objects.

$$AG = <S, C, P, H, L>,$$

where S is the set of abstract symbols, whose formation scheme is shown in Fig. 2; C is the AG-hypernetwork of general knowledge; P is the AG-hypernetwork of particular knowledge; H is the AG-hypernetwork of personal history; L is the set of associative links between the objects of the sets S, C, P, and H.

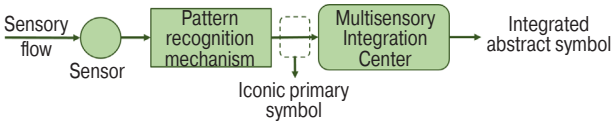

Fig. 2. Scheme for the formation of an abstract symbol

The formation of an abstract symbol takes place as follows:

1. The sensory channel input of the AI agent receives a discrete or continuous sensory data stream, which is filtered by the corresponding sensor and sent for processing to the image recognition mechanism.
2. After selecting and isolating the perceived images from the sensory stream, the image recognition mechanism of the corresponding sensory modality sends them to the multisensory integration center. Sensory modalities may consist of one or more sensory systems, each consisting of one or more sensory channels [10].
3. The multisensory integration center collects selected and recognized images from all sensory modalities of the AI agent and builds an integrated abstract symbol associated with all recognized sensory perception images. Thus, the AI agent solves the problem of symbol binding [11].

The S object represents the following structure:

$$S = \{s_i\}_{i=1}^{N},$$

where s_i is an abstract symbol with identifier i having N abstract symbols in the set S. Moreover, each abstract symbol s_i is the following object:

$$s_i = <UID, \mathrm{R}>,$$

where s_i is an arbitrary unique sequence of characters from the selected alphabet V; *UID* is a unique identifier [12] of an abstract symbol; R is a labeled set of primary sensory symbols to which the abstract symbol s_i is attached.

$$\mathrm{R} = \bigcup_{i=1}^{K} \mathrm{R}_i, \text{ wherein } \mathrm{R}_i \cap \mathrm{R}_j = \emptyset, \text{ if } i \neq j.$$

The AI-agent has K sensory modalities; the sets R_i (i = 1, ..., K) are the sets of primary sensory symbols for each sensory modality i. From a mathematical standpoint, the AH-hypernets C, P, and H comprise hypergraphs [13], i.e., generalized cases of a graph, in which any subset of vertices can be connected by an edge. AH memory elements C, P, and H comprise the following tuple:

$$e = <(s^*|m|m^*|g|\mathrm{k}|\mathrm{T}|N), x, f>, \quad (2)$$

where N is a hyperlink between AH-memory objects from sets C, P, or H; x is the current level of excitation of the AH-memory element; f is the activation function of the AH-memory element; m is a second-order abstract symbol m = <*UID*, Pr, Mt>, where *UID* is a unique symbol identifier; Pr and Mt are sets of properties and meta-properties of symbols, respectively; s^* and m^* are a link to an abstract symbol from the set S and a link to an abstract symbol of the second order from the sets C, P and H, respectively, which are symbol identifiers with additional information by which you can identify the link type and the link itself:

$$\mathrm{s}^* = <S', UID, UID^*>, m^* = <M', UID, UID^*>.$$

Here *S'* and *M'* are labels confirming the relevance of links; *UID* is the unique identifier of s and m, to which there is a corresponding link; UID^* is the unique identifier of the link itself.

Meta-properties from the set Mt comprise a semantic set of properties reflected in the patterns of the AI agent and directly embedded in the code. Properties from the Pr set are purely syntactic constructions, whose semantics are unknown to the AI agent at the program level and which are revealed only during the functioning of the AH memory, taking into account the binding of all symbols to sensory information. Both sets comprise a set of elements of the following form:

$$p = <name, value, type, unit>,$$

where all the objects that make up the p property are strings: *name*—name of the property; *value*—the value of the property must be non-empty; *type*—the type of the property; *unit*—the unit of measurement of the property (value can be empty).

A property of a particular AH-memory element can be identified by a unique identifier such as UID.name, i.e., there cannot be two properties having the same name in a single element of AH-memory.

In (2) g is a functional symbol designated for those elements of knowledge of the AI-agent that have special behavioral responses or special processing procedures, such as quantifiers or logical propositional connectives (conjunctions "and," "or," etc.). Function symbols used to describe arbitrary relationships between some elements of the AH-memory represent the following tuple:

$$g = \left\langle UID, ID, \{e_i^*\}_{i=1}^{Z} \right\rangle,$$

where *UID* is the unique identifier of the functional symbol; *ID* is the identifier of the type of functionality, necessary to indicate which behavioural pattern of the AI agent corresponds to the selected functional symbol; e_i^* is the ith reference to the AH-memory element from the set of operands (value, variable or expression located to the left or right of the operator) of the function symbol; Z is the number of operands of the function symbol.

The symbol k in (2) denotes a list of AH-memory elements for grouping AH-memory elements into a single object: this is necessary for the formation of hierarchies and heterarchies. In actuality, k is an identified and ordered set of references to arbitrary AH-memory objects, expressed in the following tuple:

$$\mathrm{k} = <UID, \{e_i^*\}_{i=1}^{Y}, \mathrm{Pr}, \mathrm{Mt}>,$$

where *UID* is a unique identifier of the list of AH-memory elements; e_i^* is the ith link to the AH-memory element; Y is the number of elements in the list; Pr and Mt are sets of properties and meta-properties of the list of AH-memory elements, respectively, defined similarly to symbol *m*.

In (2), the control model template of the predicate symbol T [14] is the following tuple:

$$\mathrm{T} = <UID, s^*, \mathrm{A}>,$$

where *UID* is the unique ID of the predicate symbol control model template; s^* is a reference to an abstract symbol from the set S, which corresponds to the predicate of the described control model template; $\mathrm{A} = \{a_i\}_{i=1}^{Q}$ is the set of actants in the control model of the predicate symbol, consisting of the ith number of actants of valence Q (the total number of actants) of the predicate symbol. The actant in the control model of the predicate symbol a represents the role of the element that occupies

a vacant place in the case of the implementation of the control model template [15].

For a specific AI-agent, a classifier of the roles of elements in control models of predicate symbols should be compiled. The proposed classifier of the roles of actants (language expressions that fill the valence of a predicate symbol), which solves the problems of natural language processing, is given as follows:

1. SUBJECT is the actant role that performs the action of a predicate symbol, whose control model is described by a template. In natural language, this can be expressed as a subject in the syntactic construction of a predicate.
2. OBJECT is the actant role on which the action of the predicate symbol is performed, whose control model is described by the template. In natural language, this can be expressed as a direct object in the syntactic construction of the predicate.
3. LOCATION is the actant role indicating the place of the action execution of the predicate symbol, whose control model is described by the template. In natural language, this can be expressed as an adverbial place in the syntactic construction of the predicate, or as an object in some grammatical locative. This role can also be divided into several sub-roles, among which there can be such frequently used ones as LOCATION-FROM (LOC-FROM) and LOCATION-TO (LOC-TO), denoting places—source and destination—of the motion realized by the action of the predicate symbol.
4. TIME is the actant role indicating the execution time of the action of the predicate symbol, the control model of which is described by the template. In natural language, this can be expressed as a time circumstance in the syntactic construction of the predicate.
5. CAUSE is the actant role indicating the reason for the execution of the action of the predicate symbol, whose control model is described by the template. This is usually expressed in natural language as a subordinate syntactic construction that introduces causal relations into the statement.
6. PURPOSE is the actant role indicating the purpose of performing the action of the predicate symbol, the control model of which is described by the template. In natural language, this can be expressed as a subordinate syntactic construction that introduces causal relations into the statement. In this case, the predicate itself, describing the action, acts as a reason for the actant-goal.
7. TOOL is the actant role indicating the method (tool) for performing the action of the predicate symbol, whose control model is described by the template. In natural language, this can be expressed as an indirect object in the syntactic construction of the predicate in the instrumental grammatical case.
8. MATERIAL is the actant role indicating the material from which the object is produced during the execution of the action of the predicate symbol, whose control model is described by the template. In natural language, this role can be expressed by means of an indirect object in the prepositional case using prepositions such as “of” (or similar grammatical constructions in other languages).
9. IMAGE OF ACTION (HOW-TO) is the actant role, which indicates the method (attribute) of performing the action of the predicate symbol, the control model of which is described by the template. Usually, in natural language it is expressed using an adverb referring to the predicate in the sentence describing the fact.

Here, the action also means the state of the subject or the change of such a state; this can also be expressed by predicate symbols in natural language.

Since the predicate with its control model is a description of the fact about the existence of an AI being, the presented classifier of the roles of actants in the control model holistically and fully describes the possible situations in which an AI-agent finds itself within the framework of various facts of its personal history.

For a particular predicate, the control model template may contain a subset of distinguished actants. At the same time, almost any predicate must comprise in its control model actants with the roles of SUBJECT and OBJECT.

As an example, consider the CREATE predicate. Its template will have 7 actants listed in the presented actant role classifier. Figure 3 shows the scheme of the CREATE predicate template.

Here, it should be noted that not all vacant roles of actants can be filled when implementing the predicate symbol template.

The hyperlink N between AH-memory objects from the sets C, P, or H is a specific implementation of the predicate symbol control model. Each hyperlink in AH-memory is a predicate symbol describing some fact from the personal history of the AI-agent. Thus, the hyperlink N comprises the following object:

$$N = <UID, w, t^*, \{s_i^* \mid e_i^*\}_{i=1}^{Q}>,$$

where UID is a unique hyperlink identifier; w are all hyperlink activations ($w \in [0,1]$); t^* is the reference to the control template of the predicate symbol; s_i^* is a reference to the abstract symbol of the set S, replacing the vacant role i in the control model of the predicate symbol; e_i^* is a reference to an element of the sets C, P, or H, replacing the vacant role i in the control model of the predicate symbol.

The most interesting option from the presented possibilities for replacing the vacant actant of the control model of the predicate symbol is the element of e_i^* type, since this actually allows any other element of the sets C, P or H to act as an actant of the predicate, including hyperlinks *N*. Since any actant can be another fact from personal history, this makes the AG-hypernetwork very flexible for describing facts from the personal history of an AI-agent; thus, the AH-hypernet becomes a hypergraph from a mathematical standpoint. This structure allows a very flexible processing of facts as revealed in natural language texts describing the personal history of an AI-agent.

Finally, the set of associative links L consists of objects of the following form:

$$l = <UID, ID, w(e_1^*, e_2^*)>,$$

where *UID* is a unique identifier for a specific connection; *ID* is a non-unique identifier (type) of the connection; *w* is the connection activation weight ($w \in [0,1]$); e_1^* and e_2^* are the references to elements of sets C, P, or H. (In this case, the link *l* is directed and goes from element e_1^* to element e_2^*.)

For a specific manifestation of an AI-agent, it is necessary to create an exhaustive set of possible link identifiers, the semantics of which can be written at the level of the program code of a specific AI-agent.

It remains to note that the activation weight $w[0,1]$ used in AH-memory links and hyperlinks, the level of excitation of the element *x* and the activation function of the AH-memory element *f* are used in the procedures of knowledge processing and inference on the facts recorded in the AH-memory, which will be described in detail in subsequent articles.

A summary diagram of the structure of the AH-memory is shown in Fig. 4.

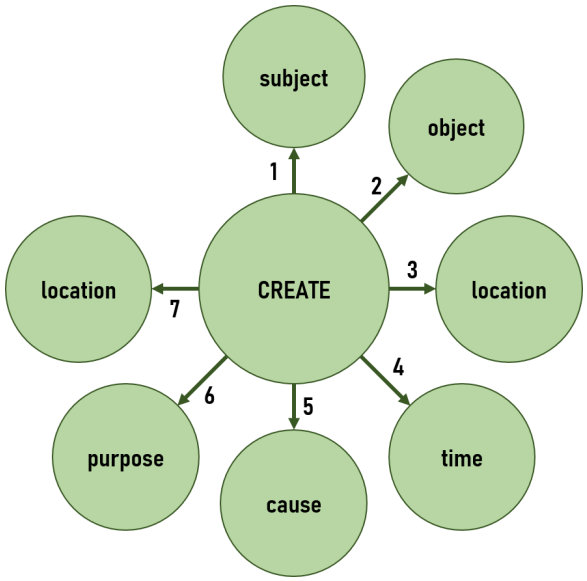

Fig. 3. Template of the control model of the CREATE predicate symbol

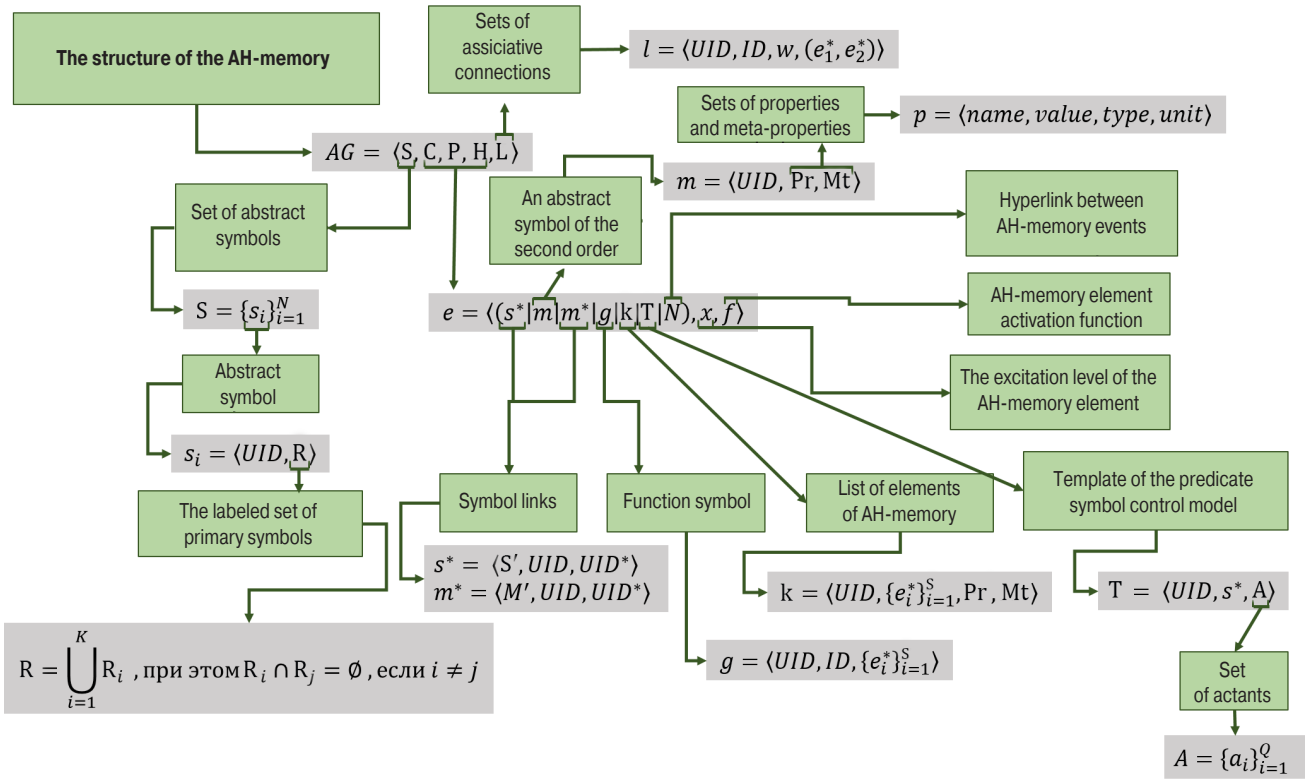

Fig. 4. Structure of AH-memory

CONCLUSIONS

When implementing a specific AI-agent, the designer and developer must select those elements of the AH-memory from those required for the successful and efficient functioning of this particular AI-agent. Although the most universal structure of the AH-memory has been presented in this article, it is necessary to decide which specific components are to be used in each specific case.

Authors' contributions

R.V. Dushkin—development of AG-memory, presentation of theoretical basis for implementation in the form of an article.

V.A. Lelekova—analysis of theoretical scientific materials, writing the text of the article.

V.Y. Stepankov—development of AG-memory, consultations on technical details of AG-memory.

S. Fadeeva—analysis of theoretical scientific materials, editing the text of the article.

REFERENCES

1. Dushkin R.V. *Iskusstvennyi intellekt* (*Artificial intelligence*). Moscow: DMK-Press; 2019. 280 p. (in Russ.). ISBN 978-5-97060-787-9
2. Dushkin R.V. Review of artificial intelligence approaches and methods. *Radioelektronnye tekhnologii*. 2018;3: 85–89 (in Russ.).
3. Nikolenko S., Arkhangel'skaya E., Kadurin A. *Glubokoe obuchenie. Pogruzhenie v mir neironnykh setei* (*Deep learning. Immersion in the world of neural networks*). St. Petersburg: Piter; 2018. 480 p. (in Russ.). ISBN 978-5-496-02536-2
4. Sarker M.K., Zhou L., Eberhart A., Hitzler P. Neuro-symbolic artificial intelligence: Current trends. *AI Communications*. 2021. 13 p. https://doi.org/10.48550/arXiv.2105.05330
5. Raina V., Krishnamurthy S. Natural language processing. In: *Building an Effective Data Science Practice*. Apress, Berkeley, CA; 2022. https://doi.org/10.1007/978-1-4842-7419-4_6
6. Zadeh L.A. From computing with numbers to computing with words – From manipulation of measurements to manipulation of perceptions. *Int. J. Appl. Math. Comput. Sci*. 2002;12(3):307–324. Available from URL: https://www.zbc.uz.zgora.pl/Content/2928/1zade.pdf
7. Dushkin R.V. Development of adaptive learning methods using intelligent agents. *Iskusstvennyi intellekt i prinyatie reshenii*. 2019;1:87–96 (in Russ.). https://doi.org/10.14357/20718594190108
8. Zhu L., Gao W. Hypergraph ontology sparse vector representation and its application to ontology learning. In: Tan Y., Shi Y., Zomaya A., Yan H., Cai J. (Eds.). *Data Mining and Big Data*. International Conference on Data Mining and Big Data (DMBD 2021). Part of the *Communications in Computer and Information Science*. Book series. Singapore: Springer; 2021. V. 1454. P. 16–27. https://doi.org/10.1007/978-981-16-7502-7_2
9. Kormen T., Leizerson Ch., Rivest R., Shtain K. *Algoritmy. Postroenie i analiz*. Moscow: Vil'yams; 2011. 1296 p. (in Russ.). ISBN 0-07-013151-1
[Cormen T.H., Leiserson C.E., Rivest R.L., Stein C. *Introduction to Algorithms*. London: The MIT Press; 2009. 1312 p.]
10. Horiguchi H., Winawer J., Dougherty R.F., Wandell B.A. Human trichromacy revisited. *Proceedings of the National Academy of Sciences* (*PNAS*). 2012;110(3):E260–E269. https://doi.org/10.1073/pnas.1214240110

СПИСОК ЛИТЕРАТУРЫ

1. Душкин Р.В. *Искусственный интеллект*. М.: ДМК-Пресс; 2019. 280 с. ISBN 978-5-97060-787-9.
2. Душкин Р.В. Обзор подходов и методов искусственного интеллекта. *Радиоэлектронные технологии*. 2018;3:85–89.
3. Николенко С., Архангельская Е., Кадурин А. *Глубокое обучение. Погружение в мир нейронных сетей*. СПб: Питер; 2018. 480 с. ISBN 978-5-496-02536-2.
4. Sarker M.K., Zhou L., Eberhart A., Hitzler P. Neuro-symbolic artificial intelligence: Current trends. *AI Communications*. 2021. 13 p. https://doi.org/10.48550/arXiv.2105.05330
5. Raina V., Krishnamurthy S. Natural language processing. In: *Building an Effective Data Science Practice*. Apress, Berkeley, CA; 2022. https://doi.org/10.1007/978-1-4842-7419-4_6
6. Zadeh L.A. From computing with numbers to computing with words – From manipulation of measurements to manipulation of perceptions. *Int. J. Appl. Math. Comput. Sci*. 2002;12(3):307–324. URL: https://www.zbc.uz.zgora.pl/Content/2928/1zade.pdf
7. Душкин Р.В. Развитие методов адаптивного обучения при помощи использования интеллектуальных агентов. *Искусственный интеллект и принятие решений*. 2019;1:87–96. https://doi.org/10.14357/20718594190108
8. Zhu L., Gao W. Hypergraph ontology sparse vector representation and its application to ontology learning. In: Tan Y., Shi Y., Zomaya A., Yan H., Cai J. (Eds.). *Data Mining and Big Data*. International Conference on Data Mining and Big Data (DMBD 2021). Part of the *Communications in Computer and Information Science*. Book series. Singapore: Springer; 2021. V. 1454. P. 16–27. https://doi.org/10.1007/978-981-16-7502-7_2
9. Кормен Т., Лейзерсон Ч., Ривест Р., Штайн К. *Алгоритмы. Построение и анализ*. М.: Вильямс; 2011. 1296 с. ISBN 0-07-013151-1
10. Horiguchi H., Winawer J., Dougherty R.F., Wandell B.A. Human trichromacy revisited. *Proceedings of the National Academy of Sciences* (*PNAS*). 2012;110(3):E260–E269. https://doi.org/10.1073/pnas.1214240110
11. Harnad S. The symbol grounding problem. *Physica D: Nonlinear Phenomena*. 1990;42(1–3):335–346. https://doi.org/10.1016/0167-2789(90)90087-6
12. Jentzsch R., Feustel D., Topf B. *Unique identifier, method for providing the unique identifier and use of the unique identifier*: US Pat. US8578162B2. Publ. 05.11.2013.

11. Harnad S. The symbol grounding problem. *Physica D: Nonlinear Phenomena*. 1990;42(1–3):335–346. https://doi.org/10.1016/0167-2789(90)90087-6
12. Jentzsch R., Feustel D., Topf B. *Unique identifier, method for providing the unique identifier and use of the unique identifier*: US Pat. US8578162B2. Publ. 05.11.2013.
13. Kaminski B., Pralat P., Theberge F. Hypergraphs. In: *Mining Complex Networks*. NY: Chapman and Hall/CRC; 2021. https://doi.org/10.1201/9781003218869-7
14. Popov E.V. *Obshchenie s EVM na estestvennom yazyke* (*Communication with a computer in natural language*). Moscow: Nauka; 1982. 360 p. (in Russ.).
15. Malchukov A., De Swart P. Differential case marking and actancy variation. In: *The Oxford Handbook of Case*. Oxford: Oxford University Press; 2012.

13. Kaminski B., Pralat P., Theberge F. Hypergraphs. In: *Mining Complex Networks*. NY: Chapman and Hall/CRC; 2021. https://doi.org/10.1201/9781003218869-7
14. Попов Э.В. *Общение с ЭВМ на естественном языке*. М.: Наука; 1982. 360 с.
15. Malchukov A., De Swart P. Differential case marking and actancy variation. In: *The Oxford Handbook of Case*. Oxford: Oxford University Press; 2012.

About the authors

Roman V. Dushkin, Expert in the Field of Artificial Intelligence, Science and Technology Director, Artificial Intelligence Agency (75B, build. 2, off. 10, Dubninskaya ul., Moscow, 127591 Russia). E-mail: drv@aiagency.ru. Scopus Author ID 14070035900, RSCI SPIN-code 1371-0337, https://orcid.org/0000-0003-4789-0736

Vasilisa A. Lelekova, Analyst, Artificial Intelligence Agency (75B, build. 2, off. 10, Dubninskaya ul., Moscow, 127591 Russia). E-mail: lv@aiagency.ru. https://orcid.org/0000-0002-6150-980X

Vladimir Y. Stepankov, Technical Director, Artificial Intelligence Agency (75B, build. 2, off. 10, Dubninskaya ul., Moscow, 127591 Russia). E-mail: svu@aiagency.ru. Scopus Author ID 57226776426, https://orcid.org/0000-0003-0783-000X

Sandra Fadeeva, Chief Analyst, Artificial Intelligence Agency (75B, build. 2, off. 10, Dubninskaya ul., Moscow, 127591 Russia). E-mail: sf@aiagency.ru. https://orcid.org/0000-0001-9064-0017

Об авторах

Душкин Роман Викторович, эксперт в области искусственного интеллекта, директор по науке и технологиям, Агентство искусственного интеллекта (127591, Россия, Москва, ул. Дубнинская, д. 75Б, стр. 2, офис 10). E-mail: drv@aiagency.ru. Scopus Author ID 14070035900, SPIN-код РИНЦ 1371-0337, https://orcid.org/0000-0003-4789-0736

Лелекова Василиса Алексеевна, аналитик, Агентство искусственного интеллекта (127591, Россия, Москва, ул. Дубнинская, д. 75Б, стр. 2, офис 10). E-mail: lv@aiagency.ru. https://orcid.org/0000-0002-6150-980X

Степаньков Владимир Юрьевич, технический директор, Агентство искусственного интеллекта (127591, Россия, Москва, ул. Дубнинская, д. 75Б, стр. 2, офис 10). E-mail: svu@aiagency.ru. Scopus Author ID 57226776426, https://orcid.org/0000-0003-0783-000X

Фадеева Сандра, главный аналитик, Агентство искусственного интеллекта (127591, Россия, Москва, ул. Дубнинская, д. 75Б, стр. 2, офис 10). E-mail: sf@aiagency.ru. https://orcid.org/0000-0001-9064-0017

Translated from Russian into English by Evgenii I. Shklovskii
Edited for English language and spelling by Thomas A. Beavitt

Information systems. Computer sciences. Issues of information security
Информационные системы. Информатика. Проблемы информационной безопасности

UDC 004.41
https://doi.org/10.32362/2500-316X-2022-10-5-16-27

RESEARCH ARTICLE

Framework for experimental evaluation of software solutions in a virtual environment

Dmitry Ilin @

MIREA – Russian Technological University, Moscow, 119454 Russia
@ *Corresponding author, e-mail: i@dmitryilin.com*

Abstract

Objectives. Ready-made information technology solutions used when developing software have various characteristics depending on the objectives to be experimentally obtained. While the selection of appropriate technologies and software tools used in experimental software engineering can be time-consuming, experimental complexity can be reduced by providing the researcher with domain-specific tools. The aim of the study is to design and develop a domain-specific software framework for experimental evaluation of the characteristics of information technology solutions in a virtual environment.

Methods. To determine the required characteristics of the software framework, an analysis of software tools for conducting experimental studies to evaluate the characteristics of information technology solutions in a virtual environment was conducted. Methods of decomposition, structural design, and software development were applied to design and develop the framework.

Results. A software framework for conducting experimental research has been developed. The design results, key features of the framework and a description of the functionality are presented. The implementation of the framework comprises commands for managing virtual machines and commands for scaffolding. A technique for conducting experimental studies using the framework is proposed.

Conclusions. The developed domain-specific software framework addresses shortcomings of existing tools to reduce labor costs when conducting experiments to evaluate information technology solutions. The developed framework and proposed methodology allows the number of programming and markup languages required for setting up a software experiment to be reduced from 3 to 1.

Keywords: software framework, virtual machines, experimental evaluation of software solutions, resource utilization monitoring, scaffolding

• **Submitted:** 04.03.2022 • **Revised:** 13.07.2022 • **Accepted:** 05.09.2022

For citation: Ilin D. Framework for experimental evaluation of software solutions in a virtual environment. *Russ. Technol. J.* 2022;10(5):16–27. https://doi.org/10.32362/2500-316X-2022-10-5-16-27

Financial disclosure: The author has no a financial or property interest in any material or method mentioned.

The author declares no conflicts of interest.

НАУЧНАЯ СТАТЬЯ

Программный фреймворк для экспериментальной оценки характеристик информационно-технологических решений в виртуальной среде

Д.Ю. Ильин [@]

МИРЭА – Российский технологический университет, Москва, 119454 Россия
[@] *Автор для переписки, e-mail: i@dmitryilin.com*

Резюме

Цель. При разработке программного обеспечения, как правило, применяются готовые информационно-технологические решения. Они обладают различными характеристиками, объективные данные о которых можно получить экспериментально. Постановка корректного и воспроизводимого эксперимента требует от исследователя применения целого ряда разрозненных технологий и программных инструментов, что делает задачу трудоемкой. Снизить трудоемкость постановки эксперимента возможно, предоставив исследователю предметно-ориентированный инструментарий. Цель работы – проектирование и разработка предметно-ориентированного программного фреймворка для экспериментальной оценки характеристик информационно-технологических решений в виртуальной среде.

Методы. Для определения требуемых характеристик программного фреймворка проведен анализ программных инструментов проведения экспериментальных исследований по оценке характеристик информационно-технологических решений в виртуальной среде. При проектировании и разработке фреймворка применены методы декомпозиции, структурного проектирования, разработки программного обеспечения.

Результаты. Спроектирован и разработан программный фреймворк для экспериментальной оценки характеристик информационно-технологических решений в виртуальной среде. Представлены результаты проектирования, ключевые особенности фреймворка и программные технологии, примененные для разработки. Приведено описание функциональных возможностей фреймворка. Реализация фреймворка содержит 12 команд для управления виртуальными машинами и 4 команды для скаффолдинга. Предложена методика проведения экспериментальных исследований с применением фреймворка.

Выводы. Проведенное исследование позволило идентифицировать недостатки применения существующего инструментария, разработать предметно-ориентированный программный фреймворк и предложить методику его использования, что может сократить трудозатраты при проведении экспериментов по оценке информационно-технологических решений в виртуальной среде. Фреймворк позволяет сократить количество языков программирования и разметки, необходимых исследователю для постановки эксперимента, с 3 до 1.

Ключевые слова: программный фреймворк, виртуальные машины, экспериментальная оценка характеристик программного обеспечения, мониторинг вычислительных ресурсов, скаффолдинг

• **Поступила:** 04.03.2022 • **Доработана:** 13.07.2022 • **Принята к опубликованию:** 05.09.2022

Для цитирования: Ильин Д.Ю. Программный фреймворк для экспериментальной оценки характеристик информационно-технологических решений в виртуальной среде. *Russ. Technol. J.* 2022;10(5):16–27. https://doi.org/10.32362/2500-316X-2022-10-5-16-27

Прозрачность финансовой деятельности: Автор не имеет финансовой заинтересованности в представленных материалах или методах.

Автор заявляет об отсутствии конфликта интересов.

INTRODUCTION

Software development is largely based on the integration of ready-made information technology solutions including software libraries, frameworks, database management systems or entire software products.

Integrated solutions may have different quality characteristics, including those evaluated under different operating conditions [1–3]. The assessment of quality characteristics such as performance [2–4] is especially important when designing systems that serve a large number of users. To do this, the considered information technology solutions or the result of their integration are tested experimentally [3–5]. As a rule, such experiments are carried out on a cloud infrastructure, although this is not always advisable. In some cases, the necessary infrastructure can be organized at the workstations [6, 7] of researchers. In both cases, the organization of the infrastructure requires the preparation of virtual machines or containers [8, 9], which allow information technology solutions to be evaluated in an isolated environment.

Researchers generally agree that the results of experimental assessments should be reproducible [7, 10–13]. However, there are different approaches for ensuring reproducibility. In some works, the importance of detailed infrastructure documentation and experimental protocols [12] is noted; in others, tools are proposed for recording software actions at the level of system calls [10, 11]. In some cases, infrastructure is not manually prepared but with organized using widely used DevOps[1] technologies [14–17]. These technologies have proven themselves, including for research purposes [5, 18], as a means of ensuring the reproducibility of experiments. In addition, they can be used as part of pedagogical activities [19–21] to provide participants in the educational process with an identical working environment.

However, according to some studies, the implementation of a reproducible experiment requires the use of many software tools [10, 11], which requires additional knowledge and skills from the researcher. It is also noted that the use of such tools can increase labor costs when setting up experiments.

The present work is devoted to the analysis of tools used to implement infrastructure on researchers' workstations and the development of a framework for conducting experimental studies to evaluate the characteristics of information technology solutions in a virtual environment.

To achieve this goal, it is necessary to:

- analyze the tasks for the researcher when setting up the experiment, as well as to determine the tools used to solve them;
- based on the analysis, prepare architectural solutions that define the key characteristics of the software framework;
- develop a framework corresponding to the subject area and architecture solutions, as well as present a methodology for its application.

TOOLS FOR CARRYING OUT EXPERIMENTS FOR ASSESSING INFORMATION TECHNOLOGY SOLUTIONS

Before proceeding to the development of a software framework, it is necessary to analyze the tasks for the researcher when setting up a reproducible experiment, as well as the tools used to solve them.

Although experimental studies for assessing the characteristics of information technology solutions can be conducted without using the software tools listed below, the feasibility of their use is justified.

The use of virtual machines (for example, using *VirtualBox*[2] [9, 22]) makes it possible to conduct experiments using a smaller number of devices including conducting an experiment on a single physical device.

However, the virtual environment itself can take up a significant amount of disk space, making it difficult to transfer virtual machines between researchers. Moreover, the virtual environment does not provide tools for formally describing its own configuration or that of any virtual machines used. Thus, in post-factum descriptions of the experimental bench, there is a possibility that documenting errors will arise.

This can be compensated by using special tools for creating and configuring a virtual environment (for example, *Vagrant*[3] [9, 22]). If the virtual machines are defined using the configuration tool, a formal description of the characteristics of the virtual bench can be determined even prior to its operation. Cloud configuration tools (for example, *Ansible*[4] [22, 23]) can be used to manage the configuration of virtual machine software in a similar way. This "infrastructure as code" approach [14, 23] solves two identified problems: reducing the volume of the experimental bench when transferring between researchers and ensuring the reliability of experimental documentation.

[1] DevOps is an acronym for development & operations—a set of practices for automating the technological processes of building, configuring, and deploying software.

[2] https://www.virtualbox.org/. Accessed February 18, 2022.

[3] https://www.vagrantup.com/. Accessed February 18, 2022.

[4] https://www.ansible.com/. Accessed February 18, 2022.

However, such existing solutions to the described problems are not always sufficient for conducting experiments since the configuration of the virtual experimental bench does not always remain unchanged throughout the experiment. For example, restrictions on the utilization of computing resources may be required only at certain stages of the experiment. Since the above-described tools describe a static configuration, they cannot be used to change the characteristics of the bench.

A program-controlled experiment also requires a task manager (for example, *Gulp*[5]) that executes commands in a given order. Data collection tools are also important for monitoring the utilization of computing resources (for example, *Atop*[6]) and tools for preparing reports.

Summarizing the above, we can conclude that in order to conduct a well-documented program-controlled experiment in a virtual environment, it is necessary to prepare a virtual bench to solve the following tasks:

1) design of the experimental study;
2) preparation of a formal description of virtual machines;
3) preparation of a formal description of virtual machine software configuration;
4) installation of monitoring tools for resource utilization on each virtual machine (in addition to 3);
5) preparation of research materials (IT solution, experimental data, etc.);
6) development and debugging of the program code for managing the experiment;
7) ensuring correct restrictions on resource utilization at various stages of the experiment;
8) export of monitoring data and generation of a resource utilization report.

Fulfilling the above-mentioned conditions requires a researcher to know a large number of technologies and means of integrating them. The situation is also complicated by the fact that different technologies require knowledge of different programming languages and data markup. Table 1 shows a list of the technologies, as an example. It is important to note that knowledge of the listed technologies becomes mandatory.

Due to the significant list of tasks facing before the researcher, some of which are not solved by existing tools, it is necessary to design and develop a tool for:

- describing the experiment in the form of software configurations;
- using specific software configurations at specific stages of the experiment;
- reducing the number of programming languages, data markup and information technologies required for the experiment.

[5] https://gulpjs.com/. Accessed February 18, 2022.
[6] https://www.atoptool.nl/. Accessed February 18, 2022.

Table 1. Example of a list of technologies required for conducting experiments in a virtual environment

Category	Tool	Language (programming, markup)
Configuring virtual machines	*Vagrant*	Ruby[7]
Configuring Virtual Machine Software	*Ansible*	YAML[8]
Experiment management	*Gulp*, Shell script[9]	JavaScript[10], Bash[11]
Report generation	*Gulp* + *EJS*[12]+ *Plotly.js*[13]	JavaScript, HTML[14], JSON[15]
Export monitoring data	*Atop*, Shell script	Bash

FRAMEWORK DESIGN

In the process of designing the framework, an analysis of software requirements was carried out and a software architecture that meets the specified requirements was formed.

Since the configuration of a virtual machine and its software parameters are described statically, they can be specified using semi-structured formats. Such a format should be easy to read and edit, so it is suggested to use the YAML markup language. This language is used in the *Ansible* system for configuring virtual machine software and is familiar to researchers. Instead of using a general-purpose programming language, the algorithm for executing automated tasks can also be specified declaratively in YAML.

It is understood that the experimental framework will compile YAML source files into target configurations (for example, the configuration for the *Vagrant* tool in Ruby), and will contain a built-in task automation tool. Thus, the researcher, instead of using three different languages to configure virtual machines, their software and perform automated tasks, only needs the YAML markup language, as shown in Fig. 1.

In order to ensure that the experiment is carried out taking into account the configurations specific for each stage, the following is proposed. The experiment

[7] https://www.ruby-lang.org/. Accessed February 18, 2022 (in Russ.).
[8] https://yaml.org/. Accessed February 18, 2022.
[9] Shell script is a script written in Bash or a similar language.
[10] https://262.ecma-international.org/6.0/. Accessed February 18, 2022.
[11] http://www.gnu.org/software/bash/. Accessed February 18, 2022.
[12] https://ejs.co/. Accessed February 18, 2022.
[13] https://plotly.com/javascript/. Accessed February 18, 2022.
[14] https://html.spec.whatwg.org/multipage/. Accessed February 18, 2022.
[15] https://www.json.org/. Accessed February 18, 2022.

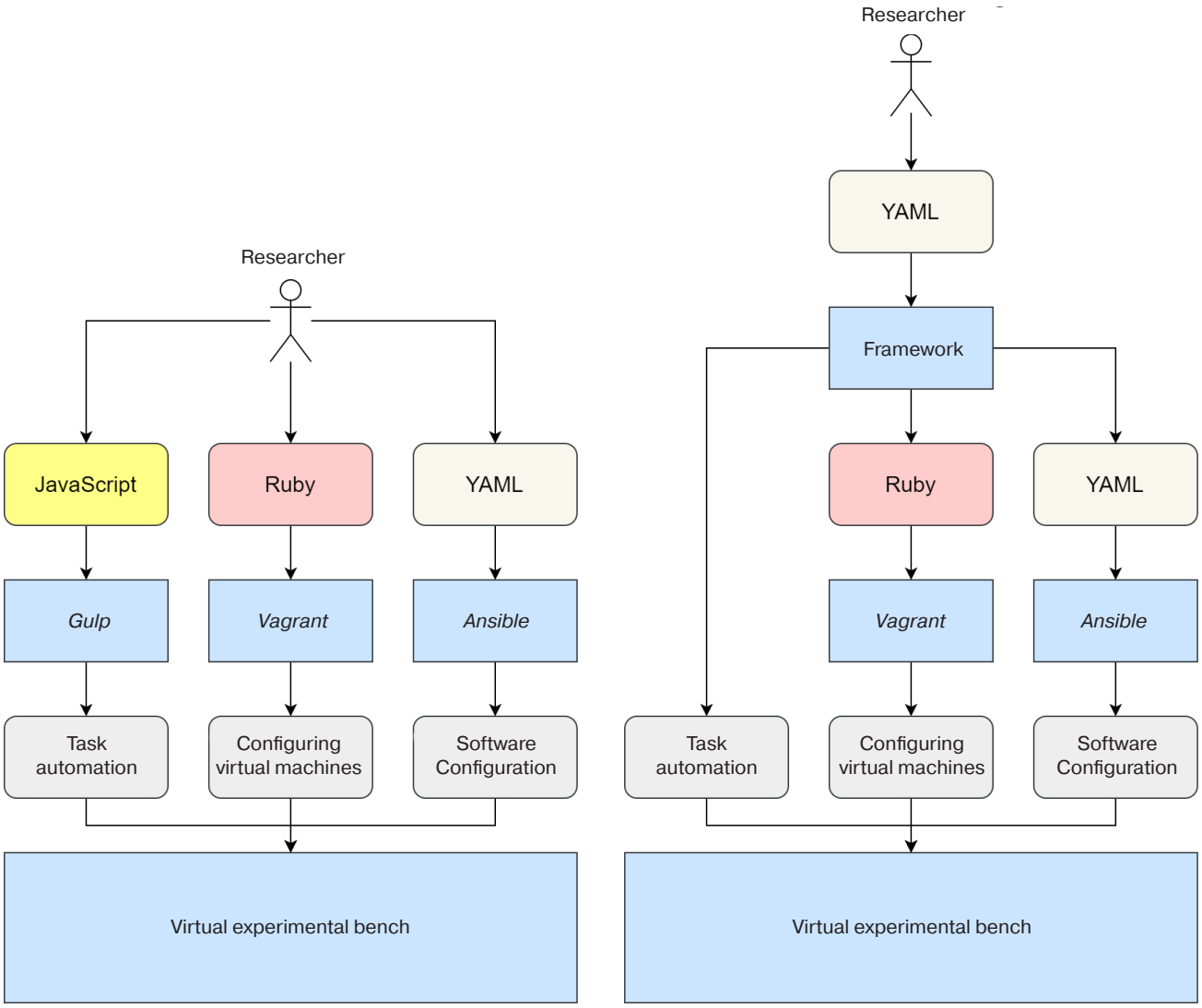

Fig. 1. Reducing the number of programming and data markup languages used by the researcher

is divided into stages, at each of which the compiled configurations are applied to each virtual machine. These consist of three components:

(1) a general configuration for the entire project;
(2) a configuration for a specific virtual machine;
(3) a configuration that addresses a specific stage of the experiment.

After compiling the selected configurations, a number of actions are performed to define the algorithm of the experiment at a particular stage. These actions can include any commands for virtual machines. The diagram illustrating the process of the experiment is shown in Fig. 2.

The file structure of the project for conducting an experimental study is shown in Fig. 3. A typical project consists of:

- configuration file;
- one or more virtual machines, for each of which there is also a separate configuration file and a set of provisioning files specific to the virtual machine;
- common provisioning files for all virtual machines;
- files with initial data (including the researched information technology solution);
- directories with reports on the utilization of virtual machine resources in the course of the experiments.

The experiment configuration file and virtual machine configuration files are implemented in a semi-structured YAML format. The structure of these files is schematically shown in Fig. 4, where at the top (file repex.yml) the configuration of the experiment is shown, and at the bottom (file vm.yml) the configuration of one of the virtual machines.

The content of the files is interconnected. The “path” property in the experimental configuration specifies the path to the vm.yml file. The experiment stage name (stage) used in the experiment configuration file can be used in the virtual machine configuration in order to apply its settings other than the default settings. These settings will be applied only at the specified stage of the experiment; however, the features of the hypervisor

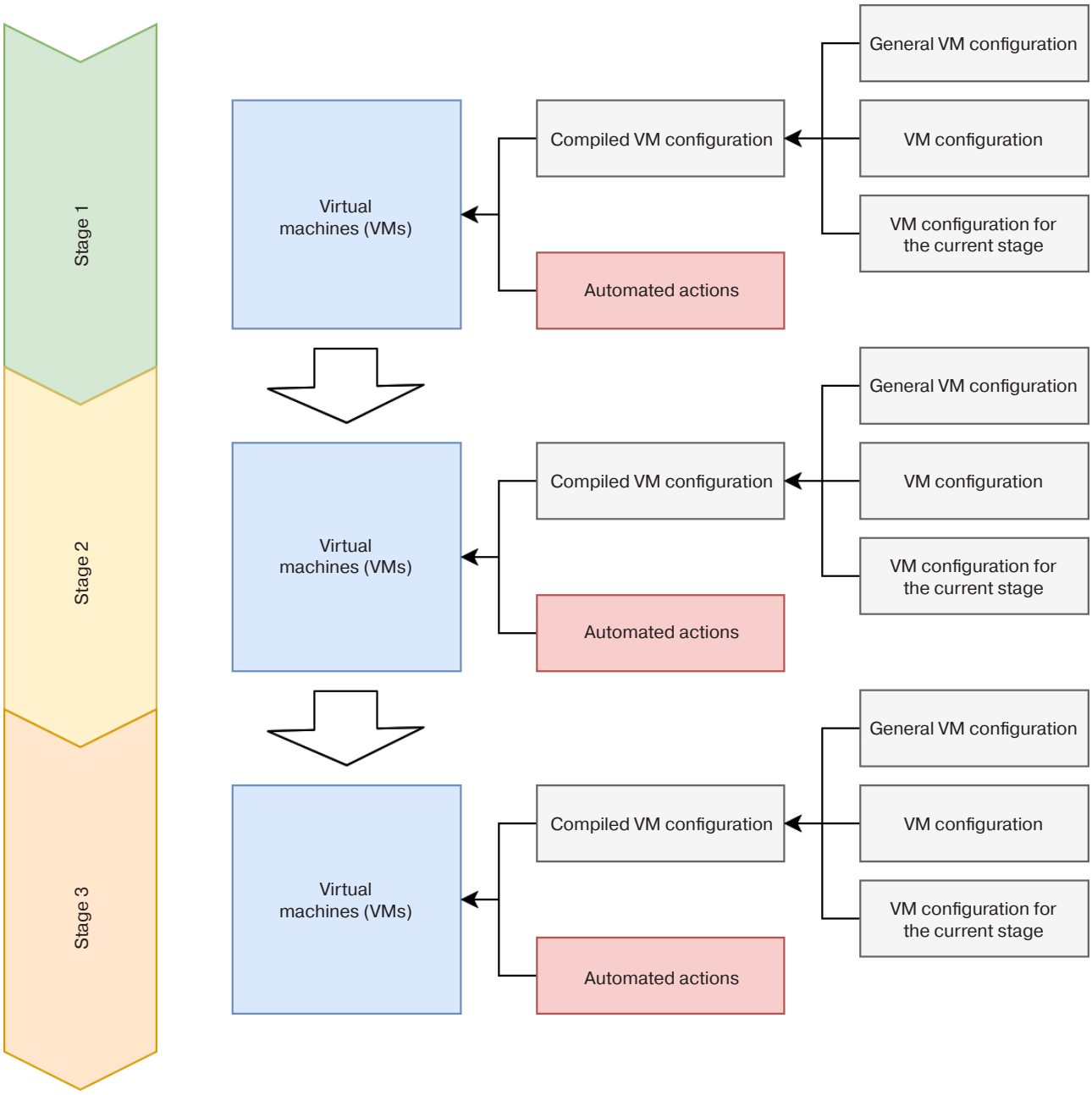

Fig. 2. Block-diagram of the experiment

should be taken into account. So, most of the settings will be applied only after rebooting the virtual machine. Some settings, such as disk subsystem or network bandwidth limits, are applied permanently, and you will need to create another stage of the experiment to remove the applied restrictions.

SOFTWARE IMPLEMENTATION OF THE FRAMEWORK

Based on the obtained design results, the *Repexlab* (reproducible experiment laboratory) software framework[16] was developed and published as an open source software. It is a tool with a command line interface (command line interface, hereinafter referred to as CLI), the main task of which is to support experimental studies in order to evaluate the characteristics of IT solutions. The framework sets the basic configuration of the project, ensures that the settings of the virtual environment are applied at various stages of the experiment.

The software framework is based on a number of existing tools:

VirtualBox is a virtualization system that allows you to organize the work of one or more virtual machines, including on a PC;

- *Vagrant* is a virtual environment creation and configuration tool. As a rule, it is used to prepare

[16] https://github.com/rnd-student-lab/repexlab. Accessed February 18, 2022.

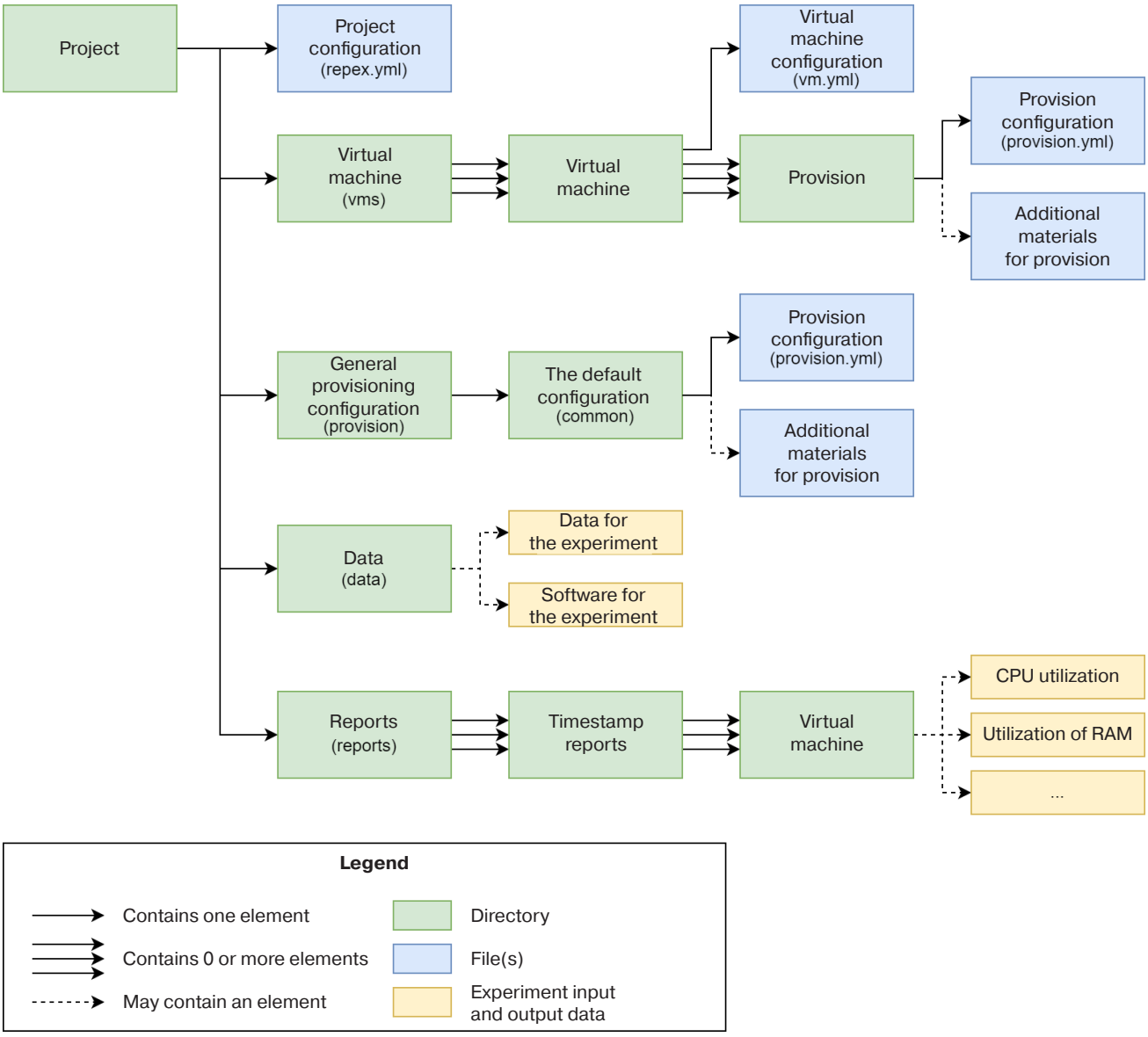

Fig. 3. File structure of the project for the experimental study

a virtual working environment for developers. The base version uses *VirtualBox* as a hypervisor;

- *Ansible* is a cloud configuration management tool. Used by the framework as the main means of provisioning virtual machines;
- *Atop* is a tool for monitoring processes in the operating system. Used by the framework to collect data on the utilization of the computing resources of virtual machines;
- *Node.js*[17] and *NPM*[18] is a JavaScript code execution platform and an accompanying package manager. Since *Repexlab* is developed in JavaScript, they are required to install and execute the framework code.

The main functions that distinguish the framework from the totality of technologies used in it include:

- creation of a basic project for conducting an experimental study;
- scaffolding[19] for managing virtual machines within the experimental bench;
- control of the virtual bench from the command line;
- built-in tools for automating the tasks of interaction with a virtual bench.

The developed tool has commands that can be used both from the command line and with the help of built-in tools for automating tasks. They are divided into two categories: commands for interacting with virtual machines within an experiment (Table 2) and commands for changing the configuration of a virtual experimental bench (Table 3).

[17] https://nodejs.org/. Accessed February 18, 2022.
[18] https://www.npmjs.com/. Accessed February 18, 2022.

[19] Scaffolding is a programming method that involves generating program code for solving typical tasks, such as, for example, building a project file structure or creating classes for accessing database tables.

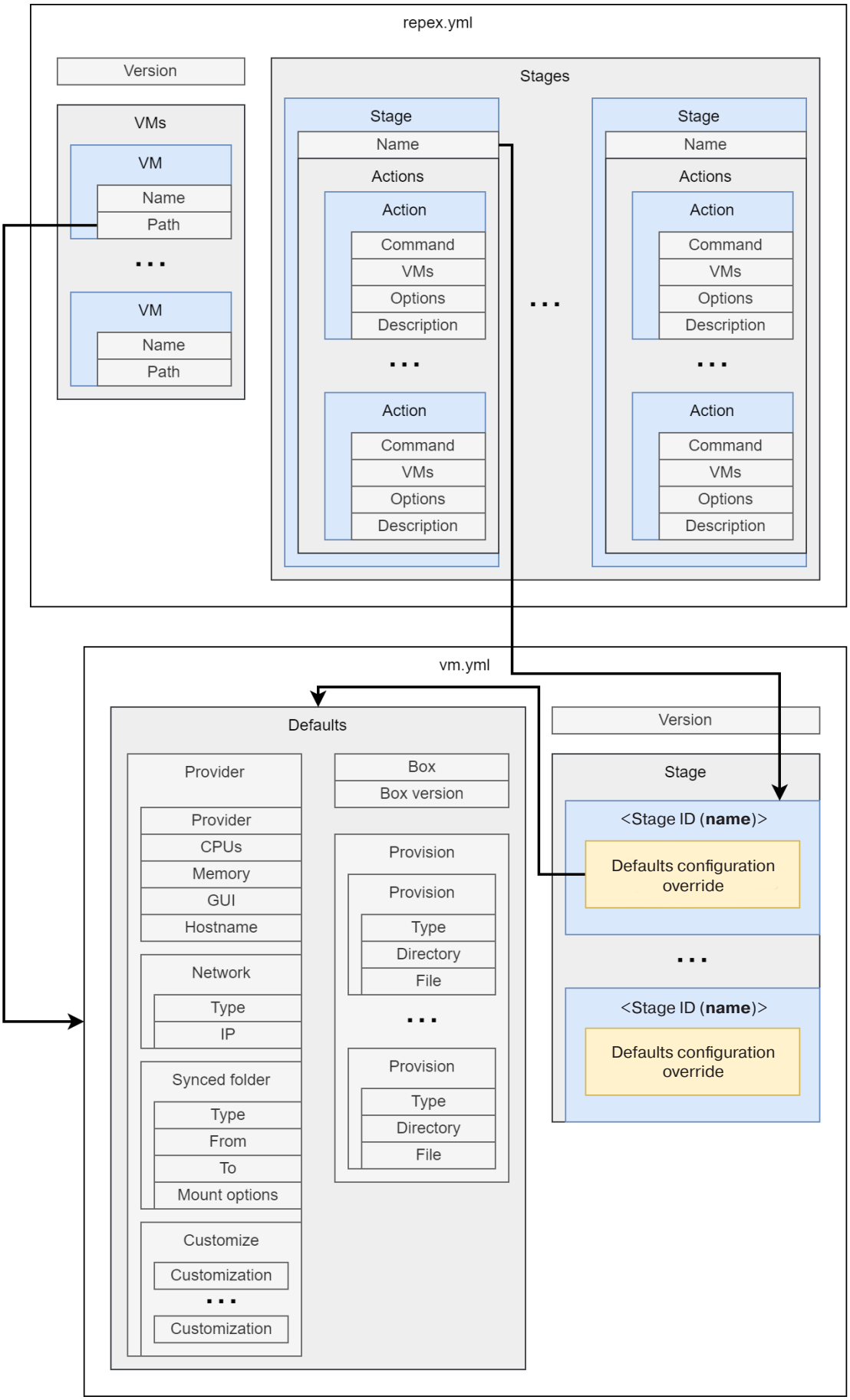

Fig. 4. Links to the configuration files of the project for conducting an experimental study

Table 2. List of commands for interacting with virtual machines

Command	Option		Command description
	Name	Description	
vm compile	-n, --name	Name of the virtual machine	Compiles virtual machine settings from a semi-structured data format to the configuration formats used by the tools
	-s, --stage	Experiment stage name	
vm copy	-n, --name	Name of the virtual machine	Copies a file or directory between the host system and the specified virtual machine
	-s, --stage	Experiment stage name	
	-d, --direction	Copy direction	
	-f, --from	Copy from	
	-t, --to	Copy to	
vm destroy	-n, --name	Name of the virtual machine	Deletes all data associated with the virtual machine (not configuration)
	-s, --stage	Experiment stage name	
vm exec	-n, --name	Name of the virtual machine	Execute a command on the specified virtual machine
	-s, --stage	Experiment stage name	
	-c, --command	Command to execute on a virtual machine	
vm provision	-n, --name	Name of the virtual machine	Performs installation and configuration of virtual machine software in accordance with the provisioning configurations
	-s, --stage	Experiment stage name	
vm report	-n, --name	Name of the virtual machine	Generates a report on the use of computing resources by virtual machines. In parentheses is the option in case of using automation
	-s, --stage	Experiment stage name	
	--start	The start time of the period for the report (or the name of the stage of the experiment)	
	--end	Report period end time (or experiment stage name)	
	-l, --labels	List of Atop labels to generate a report on them	
vm restart	-n, --name	Name of the virtual machine	Restarts the virtual machine
	-s, --stage	Experiment stage name	
vm setupHosts	-n, --name	Name of the virtual machine	Adds the IP-Hostname bindings of each virtual machine in the experiment to the /etc/hosts file of the virtual machines to simplify addressing
	-s, --stage	Experiment stage name	
vm ssh	-n, --name	Name of the virtual machine	Connecting to a virtual machine via SSH
vm start	-n, --name	Name of the virtual machine	Starts the virtual machine
	-s, --stage	Experiment stage name	
vm status	-n, --name	Name of the virtual machine	Displays the status of the virtual machine
	-s, --stage	Experiment stage name	
vm stop	-n, --name	Name of the virtual machine	Stops the virtual machine
	-s, --stage	Experiment stage name	

Table 3. List of commands for interacting with the project

Command	Option		Command description
	Name	Description	
project init	None, interactive parameter entry mode is used		Initializes the experiment project in the current directory and creates a base file structure
project run	-s, --stage	Experiment stage name	Starts the run of a configured experiment sequence or a specified experiment stage
project vm add	None, interactive parameter entry mode is used		Adds a new virtual machine configuration
project vm remove	-n, --name	Name of the virtual machine	Removes an existing virtual machine configuration

Since the commands from the Table 3 change the structure of the experiment, their use is possible only through the CLI. Most commands from the Table 2 are applicable both using the CLI for testing and debugging individual actions, as well as means of the built-in task automation tool. The exceptions are the "vm status" and "vm ssh" commands, which are only applicable via the CLI.

The application of the developed tool in practice is expected according to the following methodology:

1) planning and design of the experimental study;
2) initialization of the experimental study project with a given number of virtual machines;
3) preparation of a formal description of virtual machines and their configurations in YAML format;
4) development and debugging of the sequence of actions in the experiment using CLI tools;
5) automation of the sequence of actions in the experiment using tools for automating the execution of tasks;
6) conducting the experiment in a program-controlled mode;
7) analysis of exported data on the utilization of computing resources and other data obtained during the experiment.

CONCLUSIONS

In this work, tasks facing researchers when setting up experiments to assess the characteristics of information technology solutions have been analyzed along with the various tools used. It is shown that experimental studies require researchers who are knowledgeable and skillful at working with a large number of separate tools. Three key characteristics with which the framework must comply are formulated.

A domain-specific framework comprising some of the technologies used and providing the necessary functionality for conducting experimental research is presented. A scheme of interaction between the framework and the corresponding software for the experiment has been prepared. The general scheme of experiments based on virtual machines is determined. The formulated file structure of the experiment project includes the structure of the main project files and internal links between the project files.

A framework developed according to the results of the study contains 12 commands for working with virtual machines. Most commands can be executed both in CLI mode and in task automation mode. To simplify the process of preparing an experiment project, 4 scaffolding commands were implemented. The proposed methodology for using the framework in practice is described along with software technologies with which the framework is to be implemented.

Further research can be aimed at solving specific problems of evaluating information technology solutions using the framework, as well as identifying and eliminating the limitations of the framework, in order to develop the methodological basis for conducting experimental research using the proposed tools.

ACKNOWLEDGMENTS

The work was supported by the RTU MIREA grant "Innovations in the implementation of priority areas for the development of science and technology," Research Part project No. 28/22.

REFERENCES

1. Barrett E., Bolz-Tereick C.F., Killick R., Mount S., Tratt L. Virtual machine warmup blows hot and cold. In: *Proc. ACM Program. Lang.* 2017;1:52:1–52:27. https://doi.org/10.1145/3133876
2. Eismann S., Bezemer C.-P., Shang W., Okanović D., van Hoorn A. Microservices: A performance tester's dream or nightmare? In: *Proceedings of the ACM/SPEC International Conference on Performance Engineering*, Edmonton AB Canada: ACM; 2020. P. 138–149. https://doi.org/10.1145/3358960.3379124
3. Curino C., Godwal N., Kroth B., Kuryata S., Lapinski G., Liu S., et al. MLOS: An infrastructure for automated software performance engineering. In: *Proceedings of the Fourth International Workshop on Data Management for End-to-End Machine Learning.* 2020:1–5. https://doi.org/10.1145/3399579.3399927
4. Jiang Z.M., Hassan A.E. A survey on load testing of large-scale software systems. *IEEE Transactions on Software Engineering.* 2015;41(11):1091–1118. https://doi.org/10.1109/TSE.2015.2445340
5. Alankar B., Sharma G., Kaur H., Valverde R., Chang V. Experimental setup for investigating the efficient load balancing algorithms on virtual cloud. *Sensors.* 2020;20(24):7342. https://doi.org/10.3390/s20247342
6. Spanaki P., Sklavos N. Cloud Computing: security issues and establishing virtual cloud environment via Vagrant to secure cloud hosts. In: Daimi K. (Ed.). *Computer and Network Security Essentials*. Springer, Cham; 2018. P. 539–553. https://doi.org/10.1007/978-3-319-58424-9_31
7. Saingre D., Ledoux T., Menaud J.-M. BCTMark: a framework for benchmarking blockchain technologies. In: *2020 IEEE/ACS 17th International Conference on Computer Systems and Applications* (*AICCSA*). Antalya, Turkey: IEEE; 2020. P. 1–8. https://doi.org/10.1109/AICCSA50499.2020.9316536
8. Potdar A.M., Narayan D.G., Kengond S., Mulla M.M. Performance evaluation of Docker container and virtual machine. *Procedia Computer Science.* 2020;171:1419–1428. https://doi.org/10.1016/j.procs.2020.04.152

9. Kucek S., Leitner M. An empirical survey of functions and configurations of open-source Capture the Flag (CTF) environments. *J. Network Comput. Appl.* 2020;151:102470. https://doi.org/10.1016/j.jnca.2019.102470
10. Chirigati F., Rampin R., Shasha D., Freire J. ReproZip: Computational reproducibility with ease. In: *Proceedings of the 2016 International Conference on Management of Data*. New York, USA: Association for Computing Machinery; 2016. P. 2085–2088. https://doi.org/10.1145/2882903.2899401
11. Steeves V., Rampin R., Chirigati F. Using ReproZip for reproducibility and library services. *IASSIST Quarterly.* 2018;42(1):14–14. https://doi.org/10.29173/iq18
12. Jimenez I., Sevilla M., Watkins N., Maltzahn C., Lofstead J., Mohror K., et al. The Popper convention: making reproducible systems evaluation practical. In: *2017 IEEE International Parallel and Distributed Processing Symposium Workshops* (*IPDPSW*). 2017. P. 1561–1570. https://doi.org/10.1109/IPDPSW.2017.157
13. Papadopoulos A.V., Versluis L., Bauer A., Herbst N., von Kistowski J., Ali-Eldin A., et al. Methodological principles for reproducible performance evaluation in cloud computing. *IEEE Trans. Software Eng.* 2021;47(8): 1528–1543. https://doi.org/10.1109/TSE.2019.2927908
14. Artač M., Borovssak T., Di Nitto E., Guerriero M., Tamburri D.A. DevOps: introducing infrastructure-as-code. In: *2017 IEEE/ACM 39th International Conference on Software Engineering Companion* (*ICSE-C*). 2017. P. 497–498. https://doi.org/10.1109/ICSE-C.2017.162
15. Marquardson J. Infrastructure tools for efficient cybersecurity exercises. *Inform. Systems Education. J.* 2018;16(6):23–30.
16. Šimec A., Držanić B., Lozić D. Isolated environment tools for software development. In: *2018 International Conference on Applied Mathematics Computer Science* (*ICAMCS*). 2018. P. 48–484. https://doi.org/10.1109/ICAMCS46079.2018.00016
17. Stillwell M., Coutinho J.G.F. A DevOps approach to integration of software components in an EU research project. In: *Proceedings of the 1st International Workshop on Quality-Aware DevOps*. New York, USA: Association for Computing Machinery; 2015. P. 1–6. https://doi.org/10.1145/2804371.2804372
18. Magomedov S., Ilin D., Nikulchev E. Resource analysis of the log files storage based on simulation models in a virtual environment. *Appl. Sci.* 2021;11(11):4718. https://doi.org/10.3390/app11114718
19. Staubitz T., Brehm M., Jasper J., Werkmeister T., Teusner R., Willems C., et al. Vagrant virtual machines for hands-on exercises in massive open online courses. In: Uskov V.L., Howlett R.J., Jain L.C. (Eds.). *Smart Education and e-Learning 2016*. Springer, Cham; 2016. P. 363–373. https://doi.org/10.1007/978-3-319-39690-3_32
20. Berger O., Gibson J.P., Lecocq C., Bac C. Designing a virtual laboratory for a relational database MOOC. In: *Proceedings of the 7th International Conference on Computer Supported Education*. Lisbon, Portugal: SCITEPRESS – Science and and Technology Publications; 2015. P. 260–268. https://doi.org/10.5220/0005439702600268
21. Hobeck R., Weber I., Bass L., Yasar H. Teaching DevOps: a tale of two universities. In: *Proceedings of the 2021 ACM SIGPLAN International Symposium on SPLASH-E*, New York, USA: Association for Computing Machinery; 2021. P. 26–31. https://doi.org/10.1145/3484272.3484962
22. Shah J., Dubaria D., Widhalm J. A survey of DevOps tools for networking. In: *2018 9th IEEE Annual Ubiquitous Computing, Electronics Mobile Communication Conference* (*UEMCON*). 2018. P. 185–188. https://doi.org/10.1109/UEMCON.2018.8796814
23. Sandobalín J., Insfran E., Abrahão S. On the effectiveness of tools to support infrastructure as code: Model-driven versus code-centric. *IEEE Access.* 2020;8:17734–17761. https://doi.org/10.1109/ACCESS.2020.2966597

About the author

Dmitry Ilin, Cand. Sci. (Eng.), Associate Professor, Department of Data Processing Digital Technologies, Institute of Cybersecurity and Digital Technologies, MIREA – Russian Technological University (78, Vernadskogo pr., Moscow, 119454 Russia). E-mail: i@dmitryilin.com. ResearcherID J-7668-2017, Scopus Author ID 57203848706, https://orcid.org/0000-0002-0241-2733, https://www.researchgate.net/profile/Dmitry-Ilin-2

Об авторе

Ильин Дмитрий Юрьевич, к.т.н., доцент, кафедра «Цифровые технологии обработки данных» Института кибербезопасности и цифровых технологий ФГБОУ ВО «МИРЭА – Российский технологический университет» (119454, Россия, Москва, пр-т Вернадского, д. 78). E-mail: i@dmitryilin.com. ResearcherID J-7668-2017, Scopus Author ID 57203848706, https://orcid.org/0000-0002-0241-2733, https://www.researchgate.net/profile/Dmitry-Ilin-2

Translated from Russian into English by Evgenii I. Shklovskii
Edited for English language and spelling by Thomas A. Beavitt

Information systems. Computer sciences. Issues of information security
Информационные системы. Информатика. Проблемы информационной безопасности

UDC 004.93
https://doi.org/10.32362/2500-316X-2022-10-5-28-37

RESEARCH ARTICLE

Development of a neural network model for spatial data analysis

Ekaterina O. Yamashkina [1],
Stanislav A. Yamashkin [2],
Olga V. Platonova [1, @],
Sergey M. Kovalenko [1]

[1] *MIREA – Russian Technological University, Moscow, 119454 Russia*
[2] *National Research Mordovia State University, Saransk, 430005 Russia*
[@] *Corresponding author, e-mail: oplatonova@gmail.com*

Abstract

Objectives. The paper aimed to develop and validate a neural network model for spatial data analysis. The advantage of the proposed model is the presence of a large number of degrees of freedom allowing its flexible configuration depending on the specific problem. This development is part of the knowledge base of a deep machine learning model repository including a dynamic visualization subsystem based on adaptive web interfaces allowing interactive direct editing of the architecture and topology of neural network models.

Methods. The presented solution to the problem of improving the accuracy of spatial data analysis and classification is based on a geosystem approach for analyzing the genetic homogeneity of territorial-adjacent entities of different scales and hierarchies. The publicly available EuroSAT dataset used for initial validation of the proposed methodology is based on Sentinel-2 satellite imagery for training and testing machine learning models aimed at classifying land use/land cover systems. The ontological model of the repository including the developed model is decomposed into domains of deep machine learning models, project tasks and data, thus providing a comprehensive definition of the formalizing area of knowledge. Each stored neural network model is mapped to a set of specific tasks and datasets.

Results. Model validation for the EuroSAT dataset algorithmically extended in terms of the geosystem approach allows classification accuracy to be improved under training data shortage within 9% while maintaining the accuracy of ResNet50 and GoogleNet deep learning models.

Conclusions. The implemention of the developed model into the repository enhances the knowledge base of models for spatial data analysis as well as allowing the selection of efficient models for solving problems in the digital economy.

Keywords: neural network, deep learning, remote sensing data, geosystem, classification, machine learning

• **Submitted:** 20.12.2021 • **Revised:** 11.07.2022 • **Accepted:** 24.08.2022

For citation: Yamashkina E.O., Yamashkin S.A., Platonova O.V., Kovalenko S.M. Development of a neural network model for spatial data analysis. *Russ. Technol. J.* 2022;10(5):28–37. https://doi.org/10.32362/2500-316X-2022-10-5-28-37

Financial disclosure: The authors have no a financial or property interest in any material or method mentioned.

The authors declare no conflicts of interest.

НАУЧНАЯ СТАТЬЯ

Разработка нейросетевой модели для анализа пространственных данных

Е.О. Ямашкина [1], С.А. Ямашкин [2], О.В. Платонова [1, @], С.М. Коваленко [1]

[1] *МИРЭА – Российский технологический университет, Москва, 119454 Россия*
[2] *Национальный исследовательский Мордовский государственный университет им. Н.П. Огарёва, Саранск, 430005 Россия*
[@] *Автор для переписки, e-mail: oplatonova@gmail.com*

Резюме

Цели. Цели настоящего исследования – разработка и апробация нейросетевой модели для анализа пространственных данных. Преимуществом предложенной модели является наличие большого количества степеней свободы, что позволяет гибко конфигурировать модель, исходя из решаемой проблемы. Данная разработка входит в состав базы знаний репозитория моделей глубокого машинного обучения, включающего подсистему динамической визуализации на основе адаптивных веб-интерфейсов с интерактивной возможностью прямого редактирования архитектуры и топологии нейросетевых моделей.

Методы. Решение проблемы повышения точности анализа и классификации пространственных данных основано на привлечении геосистемного подхода, предполагающего анализ генетической однородности территориально-смежных образований различного масштаба и иерархического уровня. Для апробации предложенной методики применен открытый набор данных EuroSAT, сформированный для обучения и тестирования моделей машинного обучения с целью эффективного решения проблемы классификации систем землепользования и растительного покрова с использованием спутниковых снимков Sentinel-2. Онтологическая модель репозитория, в который входит модель, декомпозируется на домены моделей глубокого машинного обучения, решаемых задач и данных. Это позволяет дать комплексное определение формализуемой области знаний: каждая хранимая нейросетевая модель сопоставлена с набором конкретных задач и наборами данных.

Результаты. Апробация модели для набора EuroSAT, алгоритмически расширенного с позиции геосистемного подхода, дает возможность повысить точность классификации в условиях дефицита обучающих данных в пределах 9%, а также приблизиться к точности глубоких моделей ResNet50 и GoogleNet.

Выводы. Внедрение созданной модели в репозиторий позволит не только сформировать базу знаний моделей для анализа пространственных данных, но и решить проблему подбора эффективных моделей для решения задач в области цифровой экономики.

Ключевые слова: нейронная сеть, глубокое обучение, данные дистанционного зондирования, геосистема, классификация, машинное обучение

• **Поступила:** 20.12.2021 • **Доработана:** 11.07.2022 • **Принята к опубликованию:** 24.08.2022

Для цитирования: Ямашкина Е.О., Ямашкин С.А., Платонова О.В., Коваленко С.М. Разработка нейросетевой модели для анализа пространственных данных. *Russ. Technol. J.* 2022;10(5):28–37. https://doi.org/10.32362/2500-316X-2022-10-5-28-37

Прозрачность финансовой деятельности: Авторы не имеют финансовой заинтересованности в представленных материалах или методах.

Авторы заявляют об отсутствии конфликта интересов.

INTRODUCTION

Machine learning technologies including those based on deep neural network (DNN) models can be used to conduct high-precision automated monitoring of natural resource management (NRM) systems and analyze regularities of natural processes and phenomena. Here, a relevant scientific problem involves classification of land use (LU) and land cover (LC) system types on the basis of high-resolution remote sensing data. For this, deep machine learning (DML) methods and algorithms are applied under conditions of small quantities of labeled data obtained using the geosystem approach involving the genetic uniformity analysis of territorially adjacent entities of various scales and hierarchies.

The described geosystem territorial analysis model is characterized by a large number of degrees of freedom, allowing flexible tool configuration based on the current task and analyzed data. The proposed development is a part of the repository knowledge base of DML models including a dynamic visualization subsystem based on adaptive web interfaces offering interactive capability for directly editing the architecture and topology of neural network models (NNMs).

The NNM repository can be used not only to create a knowledge base for spatial data analysis but also to select efficient algorithms for solving problems arising in the digital economy. By decomposing the ontological model into domains of DML models, current tasks, and data, a comprehensive definition of the formalizing knowledge domain can be provided with each stored NNM being mapped to the set of specific tasks and datasets.

METHODOLOGY AND RESEARCH METHODS

DML can be used to reduce research costs when conducting spatial data analysis due to the possibility of accurate interpolation and extrapolation of measurements. The key to solving these problems is sought not only through improvements to the architecture of DML models, but also in developing methods and algorithms for the optimal enrichment of training datasets [1–3]. The present authors propose the use of a geosystem approach in which the state and properties of each territorial unit are determined by the features of its interaction with neighboring units. It is shown in [4] that a landscape has horizontal, vertical, and temporal structures; the vertical structure implies dividing the landscape into geohorizons, while the horizontal structure divides the landscape into facies and the temporal structure is related to the dynamics of landscape states.

This approach involves the assumption that land classification accuracy based on remote sensing could be increased by using a neural network to analyze not only the particular features of a system but also the features of the areas with which it interacts. In order to test this hypothesis, several datasets for model training should be prepared [5], including a basic (consisting of labeled areas fixed using satellite imagery) and extended (supplemented with data on neighboring and adjacent geosystems) dataset.

The methodology of spatial data analysis using DML and the formation of a DNN model comprising part of the repository and capable of efficiently analyzing the data can be described as follows. The graphical web interfaces of the DNN model repository justified in terms of UX system analysis allow a relevant machine learning model to be selected for solving specific tasks of spatial data analysis as well as obtaining systematized information on the required DNN model.

Figure 1 depicts the ontology model of the repository decomposed into DML model, project task, and spatial data domains. This allows the formalizing knowledge domain to be comprehensively defined as follows: each stored NNM is mapped to the set of specific tasks and

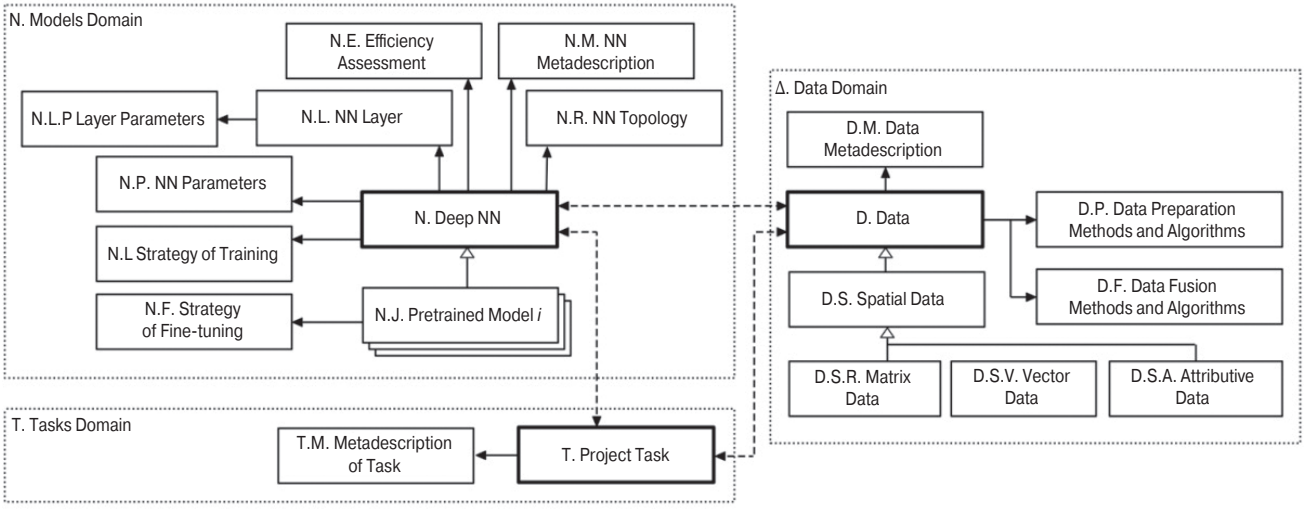

Fig. 1. Repository data model

datasets. This kind of system structure allows relevant searches for the most efficient architectural solution and fine tuning for solving project tasks to be carried out through the graphical web interface of the neural network repository.

The model storage scheme allows models to be converted into representations used by machine learning frameworks in order to integrate and use neural networks. In terms of the set-theoretic approach, the set of models of the *MODELS* repository comprises the universal set whose cardinality is determined by the number of repository models as follows:

$$MODELS = \{MODEL_i | 1 \le i \le N \wedge i \in \mathbb{Z}\}.$$

The topology of NNM $MODEL_i$ may be presented in the form of graph-scheme $GRAPH_i$ and structured meta-description $META_i$ (including the tuple of model parameters $COMPILATION_i$ describing methods and algorithms for NNM optimization as well as operating parameters). The $GRAPH_i$ element is an oriented graph where the vertex set $LAYERS_i$ defines the set of model layers while the arc set $LINKS_i$ defines the network topology for establishing connections between the layers, as follows:

$$MODEL_i = <META_i, GRAPH_i> = \\ = <META_i, <LAYERS_i, LINKS_i>>.$$

The key component of the graph model i is the layer $LAYER_{ij}$, which can be represented as a set of objects defining the architecture of the layer set $TYPE_{\text{layer}_{ij}}$, the interface set $INTERFACES_{ij}$, and arguments $PROPERTIES_{ij}$, as follows:

$$LAYER_{ij} = <TYPE_{\text{layer}_{ij}}, INTERFACES_{ij}, PROPERTIES_{ij}>.$$

During model training, the $TYPE_{\text{layer}}$ object specifies data processing features and hyperparameter settings, as well as defining the layer architecture. The interface $INTERFACES_{ij}$ parameters of layer $LAYER_{ij}$ (of inputs $INPUTS_{ij}$ and outputs $OUTPUTS_{ij}$) are defined by tuple <*name*, *type*>, where *name* specifies the interface name while *type* specifies the dimension and data type.

$$INTERFACES_{ij} = <INPUTS_{ij}, OUTPUTS_{ij}> = \\ = <\{INPUTS_{ij\lambda} | 1 \le \lambda \le \Lambda \wedge \lambda \in \mathbb{Z}\}, \\ \{OUTPUTS_{ij\mu} | 1 \le \mu \le M \wedge \mu \in \mathbb{Z}\}>.$$

The set $PROPERTIES_{ij}$ defines hyperparameters describing the layer $LAYER_{ij}$ features. This set of named arguments may include the definition of algorithms for weight initialization, regularization, and activation.

Taking tensors of data of different hierarchies on the classified territory and its host geosystems as inputs, DNN *MODEL* is designed for classifying spatial data. In terms of the black box, the deep classification model based on the geosystem approach comprises the functional element, whose input comprises images of the territory and its host geosystems obtained from satellite imagery, as well as synthetic maps [6, 7]. The number of inputs *INPUTS* may vary depending on the number of levels of the territory geosystem model. However, the temptation to increase them should be avoided since this would inevitably entail the need to increase the model capacity. The model has one output in the shape of vector with each i-th element determining the predicted probability of the territory belonging to the i-th category. The final hypothesis that the territory belongs to a certain category is made according to "the winner takes all" principle implying the object belongs to the class for which the model predicts the maximum probability. We now turn to the decomposition of the model.

The structure of each block is represented by the layer chain *LAYERS*. The first layer, which carries out depthwise separable convolution, allows features to be extracted from the original image, as well as making the model more compact and consequently resistant to retraining. This contrasts with using a conventional convolutional layer. The depthwise separable convolution having a kernel $\mathbf{W}$ of size K, which underlies the layer's functionality, comprises the linear transformation. Each value $y_{i,j}$ of the output matrix $\mathbf{Y}$ is calculated based on values x of the original matrix $\mathbf{X}$, according to the following formula:

$$y_{i,j} = \mathbf{W} \bullet \mathbf{X} = \sum_{a=0}^{K-1} \sum_{b=0}^{K-1} W_{a,b} x_{i+a,j+b}.$$

The convolution operation has important properties: as well as preserving the structure and geometry of the input, it is characterized by sparsity and multiple use of the same weights. The depthwise separable convolution deals not only with spatial dimensions, but also with depth measurements, such as image channels. Unlike conventional convolution, this involves using separate convolution kernels, on the basis of which two convolutions—depthwise and pointwise—are sequentially applied to the original tensor.

When solving the classification test problems described below, split testing of models with classical convolutional layers and depthwise separable convolution was performed to confirm the efficiency of the second approach. The batch normalization layer [8] providing regularization and stability of the model was the next layer of the feature extraction block to be efficiency-tested experimentally [9, 10]. The function ReLU[1] [11] performing the transformation of the form $x = \max(0, x)$

[1] https://pytorch.org/docs/stable/generated/torch.nn.ReLU.html. Accessed July 27, 2022.

was selected for activation. The feature extraction block is completed by the subsampling layer having external outputs and applying the maximum operation for reducing the size of the resulting representations. The experiments have shown the best result shown by applying the maximum operation. It is proposed that the number of output filters in convolution and the size of the convolution kernel be selected according to the principle of minimization of these values while maintaining acceptable classification accuracy. With every additional step comprising extraction of next-level features, the number of output filters for depthwise separable convolution should be increased.

The next model component block is the feature fusion module. This takes as input the features of level N extracted from the image of the classified territory along with geosystem images associated with it. The fusion modules of the second and subsequent levels also take as input the output data of the previous fusion module. All input data is concatenated into the single tensor and processed using the feature extraction pipeline, which consists of the layers of depthwise separable convolution, batch normalization, and activation and subsampling.

The output of the last feature fusion module is transformed into the vector and fed to the multilayer perceptron (MLP) input. The number of MLP dense layers and their capacity is selected according to the principle of minimization of these parameters while maintaining sufficient classification accuracy. In addition, applying batch normalization and thinning to the dense layer outputs is recommended for solving the overtraining problem. The function ReLU is selected for activating the output of the input and hidden layers with Sigmoid [12] for binary classification and Softmax [12] for multiclass classification selected for the output layer.

When training the classifier, the RMSProp algorithm[2] based on the stochastic gradient descent (SGD) method is used as the optimizer, while cross-entropy is used as the loss function. Fine-tuning of the model is influenced by the features of the particular classification problem being solved [13]. We now proceed to the model validation.

MODEL VALIDATION

The publicly available EuroSAT [14] dataset intended for training and testing machine learning models for effectively solving the problem of LU/LC system classification using Sentinel-2 satellite images[3] was used for initial validation of the proposed methodology [15]. The dataset, which is evenly divided into 10 classes (annual crops; forest; herbaceous vegetation; highway; industrial; pasture; permanent crop; residential; river; water), consists of 27 000 images containing information on areas distributed across the European Union in 13 spectral bands. Each element of the dataset, which has a size of 64 × 64 pixels and a spatial resolution of 10 m per pixel, is also characterized by georeferencing.

The characteristics of comparing the classification accuracy of different models for the EuroSAT dataset [16] based on different ratios of training and test samples are as follows. The ResNet-50 neural network model [17] shows the accuracy of 96.43% (for separating training and test data at the ratio of 80 to 20) and 75.06% (at the ratio of 10 to 90). The small convolutional network having two layers achieves an accuracy of 87.96% (80 to 20 splitting) and 75.88% (10 to 90 splitting). DML models based on convolutional layers show predominantly higher accuracy than support vector machines (SVM).

While modern deep convolutional networks offer excellent classification accuracy of satellite images with a relatively large size of the EuroSAT dataset training sample, these approaches entail significant accuracy losses under conditions of training data shortage. Thus, the problem of increasing the accuracy of methods and algorithms for spatial data analysis under their shortage remains a relevant research topic.

The data augmentation process is potentially subject to full automation. In the presence of information on geographic coordinates (latitude and longitude) of the classified area, the spatial data provider API can be requested for the fragment of satellite image including these coordinates and characterized by the required scale and resolution. In this way, it becomes possible to expand the training dataset algorithmically by importing the fragments of spatial imagery characterizing geosystems of a higher hierarchical level and containing the classified area.

Today, spatial data is publicly available via many Internet providers, some of which offer convenient application program interfaces (APIs) for fast retrieval [18, 19]. However, the low cost of this data is due to its poor temporal resolution (often, there is no possibility of selecting the specific date of spatial imagery). At the same time, this does not cease to be an informative source of information on host geosystems of different hierarchies. In the paper, the Mapbox API[4] is used by the authors for automated augmentation of the original dataset by satellite images of different scales.

The comparative accuracy values of the proposed model and CNN (2 layers) [12], ResNet-50, and GoogleNet [20] are presented in the Table. When

[2] Hinton G., Srivastava N., Swersky K. *Neural networks for machine learning. Lecture 6a. Overview of mini-batch gradient descent*. URL: http://www.cs.toronto.edu/~hinton/coursera/lecture6/lec6.pdf. Accessed July 27, 2022.

[3] https://sentinel.esa.int/web/sentinel/missions/sentinel-2. Accessed July 27, 2022.

[4] https://docs.mapbox.com/api/overview/. Accessed July 27, 2022.

Table. Classification accuracy of different models for the EuroSAT dataset

Method	Number of modules	Dataset	Testing range								
			10/90	20/80	30/70	40/60	50/50	60/40	70/30	80/20	90/10
CNN (2layers)	422 378	EuroSAT	75.88	79.84	81.29	83.04	84.48	85.77	87.24	87.96	88.66
ResNet-50	25 636 712	EuroSAT	75.06	88.53	93.75	94.01	94.45	95.26	95.32	**96.43**	**96.37**
GoogleNet	6 797 700	EuroSAT	77.37	90.97	90.57	91.62	**94.96**	**95.54**	**95.70**	96.02	96.17
Developed model	1 324 526	Extended EuroSAT	**86.23**	**91.52**	**93.98**	**94.11**	94.29	94.35	94.41	94.65	95.30

extracting test data from the EuroSAT dataset at a ratio of 40% and below, the proposed model shows the best result; the relative efficiency increases with the training sample decreasing as low as 10% (86.23% vs. 77.37% for the second result (GoogleNet)). With increased training data size, the model starts falling behind ResNet-50 and GoogleNet with the gap within the 2% range.

The developed model allows such results to be obtained due to the analysis of the EuroSAT dataset extended in terms of geosystem approach (while ResNet-50 and GoogleNet models been training and analyzing the original EuroSAT dataset). The difference in experimental conditions is negated by the low cost and rapidity of the fully automated training set expansion process, as well as by the lower model capacity: 1.3 mln units vs. 6.8 mln for GoogleNet and 25.6 mln for ResNet-50. Thus, the gained advantage in model training under data shortage is due to the low-cost automated geosystem-based expansion of the dataset and creation of an efficient model for its analysis.

Since training of neural networks is a probabilistic process, a series of 10 experiments was conducted to analyze the model training process, plotting the dependence of mathematical expectation and standard deviation of the classification accuracy on validation data on the training epoch. At early stages of the training process, the model demonstrates low classification accuracy of the extended set, which starts increasing from almost zero. The two-layer convolutional neural network and the ResNet-50 model may achieve above 40% accuracy from the first epoch. However, the developed model outperforms other models following the tenth training epoch to achieve the expected accuracy of 86%. A small standard deviation from the dependence mathematical expectation typical for training on small dataset should additionally be noted. This indicates greater stability of the model training process and high capability of generalizing information on the analyzed features correctly.

We now consider the cases of the developed model showing lower accuracy. The confusion matrix is shown in Fig. 2. Low matching values for such classes as “highway,” “industrial,” and “water” are due to the consideration of surrounding geosystem images during classification inevitably resulting in the increasing volume of data under analysis that may require a larger model capacity. Moreover, additional images may mislead the classification model in a number of cases; in terms of algorithm, it is definitely much easier to classify a single homogeneous image of water surface than an image supplemented by several fragments of smaller scale including coastal territories.

Thus, extending the EuroSAT dataset in terms of the geosystem approach and developing the model allows improving the classification accuracy under training data shortage (dividing the training set into the training and testing datasets at a ratio ranging from 10/90 to 40/60) as well as showing results exceeding the accuracy values of DML models while classifying the EuroSAT dataset.

CONCLUSIONS

Comprising part of the knowledge base of the repository of DML models, the developed neural network model allows the accuracy of analysis and classification of spatial data to be improved using a geosystem approach involving the genetic uniformity analysis of territorially adjacent entities of different scales and hierarchies. The repository may be deployed not only to create a model knowledge base for spatial data analysis but also to select efficient models for solving problems arising in various areas of the digital economy. The main advantage of the proposed model the high number of degrees of freedom it supports, which allows greater flexibility when configuring the model according to the particular problem to be solved.

The validation of the model according to the EuroSAT dataset algorithmically extended in terms of the geosystem approach shows the possibility of improving the classification accuracy under training

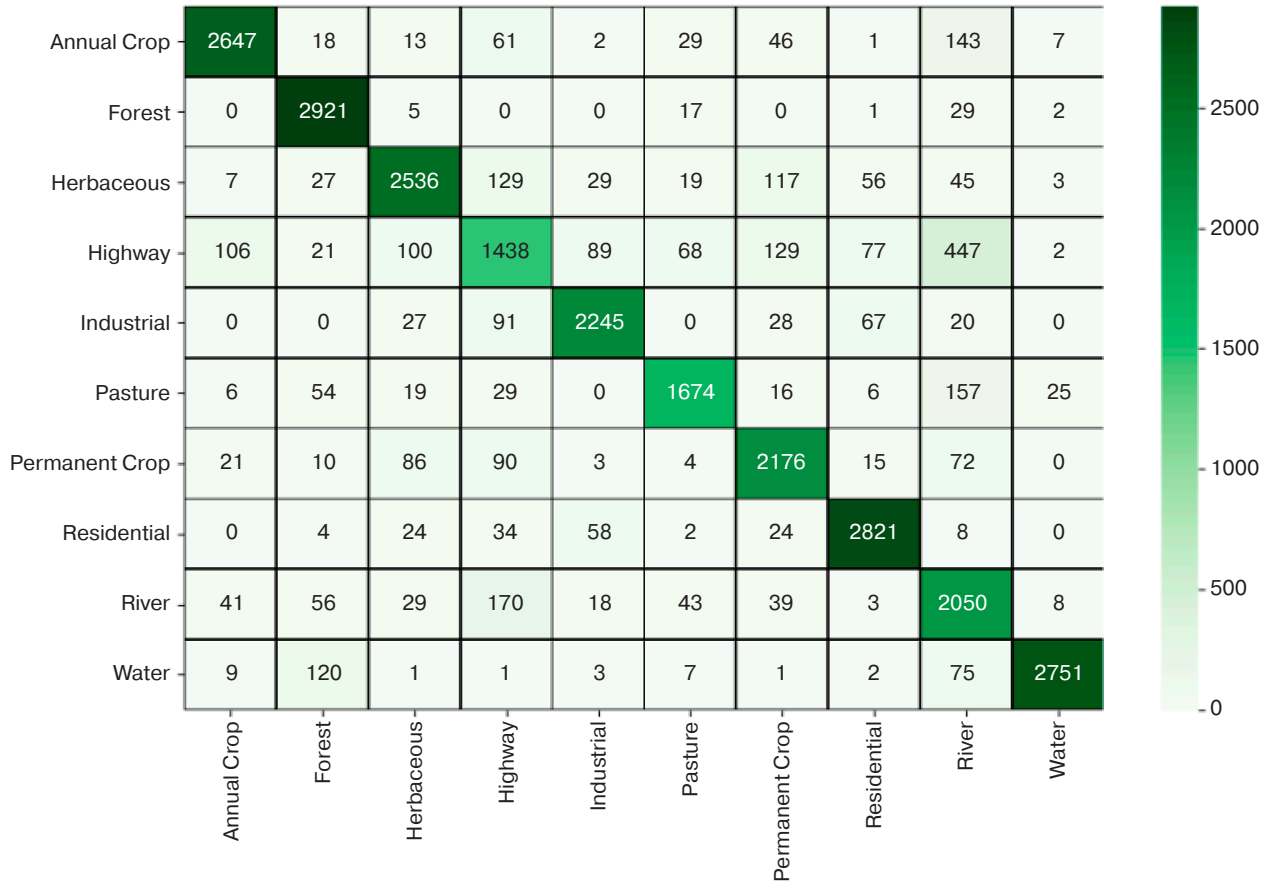

Fig. 2. Confusion matrix

data shortage within 9% while maintaining accuracy comparable with the ResNet50 and GoogleNet deep models. Following the tenth epoch of training, the developed model outperforms other models to achieve an expected accuracy of 86%.

ACKNOWLEDGMENTS

The study was supported by the grant from the President of the Russian Federation, project No. MK-199.2021.1.6).

Authors' contributions

E.O. Yamashkina—development and description of the research methodology, conducting experiments, and model optimization.

S.A. Yamashkin—statement of the problem and justification of the research concept, design and development of a neural network model.

O.V. Platonova—analysis of domestic and foreign experience in the field of interpretation of spatial data, work with the material, editing and preparation of the manuscript.

S.M. Kovalenko—planning of the experiment, interpretation and generalization of the results of the study.

REFERENCES

1. Saleh H., Alexandrov D., Dzhonov A. Uberisation business model based on blockchain for implementation decentralized application for lease/rent lodging. In: Rocha Á., Serrhini M., (Eds.). *Information Systems and Technologies to Support Learning* (*EMENA-ISTL 2018*). Smart Innovation, Systems and Technologies. *International Conference Europe Middle East & North Africa.* Springer, Cham. 2018;111:225–232. https://doi.org/10.1007/978-3-030-03577-8_26

СПИСОК ЛИТЕРАТУРЫ

1. Saleh H., Alexandrov D., Dzhonov A. Uberisation business model based on blockchain for implementation decentralized application for lease/rent lodging. In: Rocha Á., Serrhini M. (Eds.). *Information Systems and Technologies to Support Learning* (*EMENA-ISTL 2018*). Smart Innovation, Systems and Technologies. *International Conference Europe Middle East & North Africa.* Springer, Cham. 2018;111:225–232. https://doi.org/10.1007/978-3-030-03577-8_26

2. Sigov A.S., Tsvetkov V.Ya., Rogov I.E. Methods for assessing testing difficulty in education sphere. *Russ. Technol. J.* 2021;9(6):64–72 (in Russ.). https://doi.org/10.32362/2500-316X-2021-9-6-64-72
3. Liu Y., Sangineto E., Bi W., Sebe N., Lepri B., Nadai M. Efficient training of visual transformers with small datasets. *Advances in Neural Information Processing Systems.* 2021;34:23818–23830. Available from URL: https://arxiv.org/pdf/2106.03746.pdf
4. Zanozin V.V., Karabaeva A.Z., Koneeva A.V., Makeeva E.V., Molokova V.G. Features of the horizontal structure of the central part of the Volga delta landscape. In: *Geographic Sciences and Education: Proceedings of the XI All-Russian Conf.* 2018. P. 161–163 (in Russ.).
5. Yamashkina E.O., Kovalenko S.M., Platonova O.V. Development of repository of deep neural networks for the analysis of geospatial data. *IOP Conf. Ser.: Mater. Sci. Eng.* 2021;1047(1):012124. https://doi.org/10.1088/1757-899X/1047/1/012124
6. Weiss M., Jacob F., Duveiller G. Remote sensing for agricultural applications: A meta-review. *Remote Sens. Environ.* 2020;236(5):111402. https://doi.org/10.1016/j.rse.2019.111402
7. Yamashkin S.A., Yamashkin A.A. Improving the efficiency of remote sensing data interpretation by analyzing neighborhood Descriptors. *Inzhenernye tekhnologii i sistemy = Engineering Technologies and Systems* (*Vestnik Mordovskogo universiteta = Mordovia University Bulletin*). 2018; 28(3):352–365 (in Russ.). https:///doi.org/10.15507/0236-2910.028.201803.352-365
8. Ioffe S., Szegedy Ch. *Batch Normalization: accelerating deep network training by reducing internal covariate shift*. Preprint. March 2, 2015. Available from URL: https://arxiv.org/abs/1502.03167
9. Yao Z., Cao Y., Zheng S., Huang G., Lin S. Cross-iteration Batch Normalization. In: *Proceedings of the IEEE/CVF Conference on Computer Vision and Pattern Recognition* (*CVPR*). 2021:12331–12340. https://doi.org/10.1109/CVPR46437.2021.01215
10. Jung W., Jung D., Kim B., Lee S., Rhee W., Ahn J.H. Restructuring Batch Normalization to accelerate CNN training. In: *Proceedings of Machine Learning and Systems.* 2019;1:14–26. Available from URL: https://mlsys.org/Conferences/2019/doc/2019/18.pdf
11. Chen Y., Dai X., Liu M., Chen D., Yuan L., Liu Z. Dynamic ReLU. In: Vedaldi A., Bischof H., Brox T., Frahm J.M. (Eds.). *Computer Vision – ECCV 2020. ECCV 2020. Lecture Notes in Computer Science*. Cham: Springer; 2020. V. 12364. P. 351–367. https://doi.org/10.1007/978-3-030-58529-7_21
12. Gu J., et al. Recent advances in convolutional neural networks. *Pattern Recognition*. 2018;77:354–377. https://doi.org/10.1016/j.patcog.2017.10.013
13. Kozaev A., Saleh H., Alexandrov D. Simulation of emergency situations on main gas pipeline with MATLAB Simulink. In: *2019 Actual Problems of Systems and Software Engineering* (*APSSE*). IEEE. 2019:63–68. https://doi.org/10.1109/APSSE47353.2019.00015
14. Helber P., Bischke B., Dengel A., Borth D. Introducing Eurosat: A novel dataset and deep learning benchmark for land use and land cover classification. In: *IEEE International Symposium on Geoscience and Remote Sensing* (*IGARSS*). 2018:204–207. https://doi.org/10.1109/IGARSS.2018.8519248

2. Сигов А.С., Цветков В.Я., Рогов И.Е. Методы оценки сложности тестирования в сфере образования. *Russ. Technol. J.* 2021;9(6):64–72. https://doi.org/10.32362/2500-316X-2021-9-6-64-72
3. Liu Y., Sangineto E., Bi W., Sebe N., Lepri B., Nadai M. Efficient training of visual transformers with small datasets. *Advances in Neural Information Processing Systems.* 2021;34:23818–23830. URL: https://arxiv.org/pdf/2106.03746.pdf
4. Занозин В.В., Карабаева А.З., Конеева А.В., Макеева Е.В., Молокова В.Г. Особенности горизонтальной структуры центральной части ландшафта дельты Волги. *Географические науки и образование: сб. трудов XI Всероссийской научно-практической конференции.* 2018. С. 161–163.
5. Yamashkina E.O., Kovalenko S.M., Platonova O.V. Development of repository of deep neural networks for the analysis of geospatial data. *IOP Conf. Ser.: Mater. Sci. Eng.* 2021;1047(1):012124. https://doi.org/10.1088/1757-899X/1047/1/012124
6. Weiss M., Jacob F., Duveiller G. Remote sensing for agricultural applications: A meta-review. *Remote Sens. Environ.* 2020;236(5):111402. https://doi.org/10.1016/j.rse.2019.111402
7. Ямашкин С.А., Ямашкин А.А. Повышение эффективности процесса интерпретации данных дистанционного зондирования Земли за счет анализа дескрипторов окрестности. *Инженерные технологии и системы.* 2018;28(3):352–365. https://doi.org/10.15507/0236-2910.028.201803.352-365
8. Ioffe S., Szegedy Ch. *Batch Normalization: accelerating deep network training by reducing internal covariate shift*. Preprint. March 2, 2015. URL: https://arxiv.org/pdf/1502.03167.pdf
9. Yao Z., Cao Y., Zheng S., Huang G., Lin S. Cross-iteration Batch Normalization. In: *Proceedings of the IEEE/CVF Conference on Computer Vision and Pattern Recognition* (*CVPR*). 2021:12331–12340. https://doi.org/10.1109/CVPR46437.2021.01215
10. Jung W., Jung D., Kim B., Lee S., Rhee W., Ahn J.H. Restructuring Batch Normalization to accelerate CNN training. In: *Proceedings of Machine Learning and Systems*.2019;1:14–26. URL: https://mlsys.org/Conferences/2019/doc/2019/18.pdf
11. Chen Y., Dai X., Liu M., Chen D., Yuan L., Liu Z. Dynamic ReLU. In: Vedaldi A., Bischof H., Brox T., Frahm J.M. (Eds.). *Computer Vision – ECCV 2020. ECCV 2020. Lecture Notes in Computer Science*. Cham: Springer; 2020. V. 12364. P. 351–367. https://doi.org/10.1007/978-3-030-58529-7_21
12. Gu J., et al. Recent advances in convolutional neural networks. *Pattern Recognition*. 2018;77:354–377. https://doi.org/10.1016/j.patcog.2017.10.013
13. Kozaev A., Saleh H., Alexandrov D. Simulation of emergency situations on main gas pipeline with MATLAB Simulink. In: *2019 Actual Problems of Systems and Software Engineering* (*APSSE*). IEEE. 2019:63–68. https://doi.org/10.1109/APSSE47353.2019.00015
14. Helber P., Bischke B., Dengel A., Borth D. Introducing Eurosat: A novel dataset and deep learning benchmark for land use and land cover classification. In: *IEEE International Symposium on Geoscience and Remote Sensing* (*IGARSS*). 2018:204–207. https://doi.org/10.1109/IGARSS.2018.8519248

15. Phiri D., Simwanda M., Salekin S., Nyirenda V.R., Murayama Y., Ranagalage M. Sentinel-2 data for land cover/use mapping: a review. *Remote Sens*. 2020;12(14):2291. https://doi.org/10.3390/rs12142291
16. Helber P., Bischke B., Dengel A., Borth D. EuroSAT: A novel dataset and deep learning benchmark for land use and land cover classification. *IEEE Journal of Selected Topics in Applied Earth Observations and Remote Sensing.* 2019;12(7): 2217–2226. https://doi.org/10.1109/JSTARS.2019.2918242
17. Szegedy Ch., Ioffe S., Vanhoucke V., Alemi A. Inception-v4, Inception-ResNet and the impact of residual connections on learning. In: *Thirty-First AAAI Conference on Artificial Intelligence*. 2017;31(1). https://doi.org/10.1609/aaai.v31i1.11231
18. Yamashkin S.A., Radovanovic M.M., Yamashkin A.A., Barmin A.N., Zanozin V.V., Petrovic M.D. Problems of designing geoportal interfaces. *GeoJournal of Tourism and Geosites*. 2019;24(1):88–101. https://doi.org/10.30892/gtg.24108-345
19. Soni A., Ranga V. API features individualizing of web services: REST and SOAP. *Int. J. Innovative Technol. Exploring Eng.* 2019;8(9S):664–671. https://doi.org/10.35940/ijitee.I1107.0789S19
20. Szegedy Ch., et al. Going deeper with convolutions. In: *2015 IEEE Conference on Computer Vision and Pattern Recognition* (*CVPR*). 2015;1–9. https://doi.org/10.1109/CVPR.2015.7298594

15. Phiri D., Simwanda M., Salekin S., Nyirenda V.R., Murayama Y., Ranagalage M. Sentinel-2 data for land cover/use mapping: a review. *Remote Sens*. 2020;12(14):2291. https://doi.org/10.3390/rs12142291
16. Helber P., Bischke B., Dengel A., Borth D. EuroSAT: A novel dataset and deep learning benchmark for land use and land cover classification. *IEEE Journal of Selected Topics in Applied Earth Observations and Remote Sensing.* 2019;12(7): 2217–2226. https://doi.org/10.1109/JSTARS.2019.2918242
17. Szegedy Ch., Ioffe S., Vanhoucke V., Alemi A. Inception-v4, Inception-ResNet and the impact of residual connections on learning. In: *Thirty-First AAAI Conference on Artificial Intelligence*. 2017;31(1). https://doi.org/10.1609/aaai.v31i1.11231
18. Yamashkin S.A., Radovanovic M.M., Yamashkin A.A., Barmin A.N., Zanozin V.V., Petrovic M.D. Problems of designing geoportal interfaces. *GeoJournal of Tourism and Geosites*. 2019;24(1):88–101. https://doi.org/10.30892/gtg.24108-345
19. Soni A., Ranga V. API features individualizing of web services: REST and SOAP. *Int. J. Innovative Technol. Exploring Eng.* 2019;8(9S):664–671. https://doi.org/10.35940/ijitee.I1107.0789S19
20. Szegedy Ch., et al. Going deeper with convolutions. In: *2015 IEEE Conference on Computer Vision and Pattern Recognition* (*CVPR*). 2015;1–9. https://doi.org/10.1109/CVPR.2015.7298594

About the authors

Ekaterina O. Yamashkina, Postgraduate Student, Computer Technology Department, Institute of Information Technologies, MIREA – Russian Technological University (78, Vernadskogo pr., Moscow, 119454 Russia). E-mail: eoladanova@yandex.ru. Scopus Author ID 57222118879, RSCI SPIN-code 9940-1751

Stanislav A. Yamashkin, Cand. Sci. (Eng.), Associate Professor, Department of Automated Information Processing and Management Systems, Institute of Electronics and Lighting Engineering, Ogarev Mordovia State University (68, Bolshevistskaya ul., Saransk, 430005 Russia). E-mail: yamashkinsa@mail.ru. ResearcherID N-2939-2018, Scopus Author ID 9133286400, RSCI SPIN-code 5569-7314, https://orcid.org/0000-0002-7574-0981

Olga V. Platonova, Cand. Sci. (Eng.), Associated Professor, Head of the Computer Technology Department, Institute of Information Technologies, MIREA – Russian Technological University (78, Vernadskogo pr., Moscow, 119454 Russia). E-mail: oplatonova@gmail.com. Scopus Author ID 57222119478, RSCI SPIN-code 4680-5904

Sergey M. Kovalenko, Cand. Sci. (Eng.), Professor, Computer Technology Department, Institute of Information Technologies, MIREA – Russian Technological University (78, Vernadskogo pr., Moscow, 119454 Russia). E-mail: kovalenko@mirea.ru. Scopus Author ID 57222117274, RSCI SPIN-code 7308-8250

Об авторах

Ямашкина Екатерина Олеговна, аспирант, кафедра вычислительной техники Института информационных технологий ФГБОУ ВО «МИРЭА – Российский технологический университет» (119454, Россия, Москва, пр-т Вернадского, д. 78). E-mail: eoladanova@yandex.ru. Scopus Author ID 57222118879, SPIN-код РИНЦ 9940-1751, https://orcid.org/0000-0002-8086-7717

Ямашкин Станислав Анатольевич, к.т.н., доцент, кафедра автоматизированных систем обработки информации и управления Института электроники и светотехники Национального исследовательского Мордовского государственного университета им. Н.П. Огарёва (430005, Россия, Саранск, ул. Большевистская, д. 68). E-mail: yamashkinsa@mail.ru. ResearcherID N-2939-2018, Scopus Author ID 9133286400, SPIN-код РИНЦ 5569-7314, https://orcid.org/0000-0002-7574-0981

Платонова Ольга Владимировна, к.т.н., доцент, заведующий кафедрой вычислительной техники Института информационных технологий ФГБОУ ВО «МИРЭА – Российский технологический университет» (119454, Россия, Москва, пр-т Вернадского, д. 78). E-mail: oplatonova@gmail.com. Scopus Author ID 57222119478, SPIN-код РИНЦ 4680-5904

Коваленко Сергей Михайлович, к.т.н., профессор, кафедра вычислительной техники Института информационных технологий ФГБОУ ВО «МИРЭА – Российский технологический университет» (119454, Россия, Москва, пр-т Вернадского, д. 78). E-mail: kovalenko@mirea.ru. Scopus Author ID 57222117274, SPIN-код РИНЦ 7308-8250

Translated from Russian into English by Kirill V. Nazarov
Edited for English language and spelling by Thomas A. Beavitt

Multiple robots (robotic centers) and systems. Remote sensing and non-destructive testing

Роботизированные комплексы и системы. Технологии дистанционного зондирования и неразрушающего контроля

UDC 004.93'11
https://doi.org/10.32362/2500-316X-2022-10-5-38-48

RESEARCH ARTICLE

3D object tracker for sports events

Maria A. Volkova @,
Mikhail P. Romanov,
Alexander M. Bychkov

MIREA – Russian Technological University, Moscow, 119454 Russia
@ Corresponding author, e-mail: volkova_m@mirea.ru

Abstract

Objectives. Sports events are currently among the most promising areas for the application of tracking systems. In most cases, such systems are designed to track moving objects in a two-dimensional plane, e.g., players on the field, as well as to identify them by various features. However, as new sports such as drone racing are developed, the problem of determining the position of an object in a three-dimensional coordinate system becomes relevant. The aim of the present work was to develop algorithms and software for a method to perform 3D tracking of moving objects, regardless of the data segmentation technique, and to test this method to estimate the tracking quality.

Methods. A method for matching information on the speed and position of objects was selected based on a review and analysis of contemporary tracking methods.

Results. The structure of a set of algorithms comprising software for a moving-object tracker for sports events is proposed. Experimental studies were performed on the publicly available *APIDIS* dataset, where a MOTA metric of 0.858 was obtained. The flight of an FPV quadcopter along a track was also tracked according to the proposed dataset; the 3D path of the drone flight was reconstructed using the tracker data.

Conclusions. The results of the experimental studies, which demonstrated the feasibility of using the proposed method to track a quadcopter flight trajectory in a three-dimensional world coordinate system, is also showed that the method is suitable for tracking objects at sports events.

Keywords: tracker, moving object tracking, FPV quadcopter, localization, tracking system

• **Submitted:** 02.06.2022 • **Revised:** 19.07.2022 • **Accepted:** 26.08.2022

For citation: Volkova M.A., Romanov M.P., Bychkov A.M. 3D object tracker for sports events. *Russ. Technol. J.* 2022;10(5):38–48. https://doi.org/10.32362/2500-316X-2022-10-5-38-48

Financial disclosure: The authors have no a financial or property interest in any material or method mentioned.

The authors declare no conflicts of interest.

НАУЧНАЯ СТАТЬЯ

Трекер объектов на спортивных мероприятиях

М.А. Волкова [@], М.П. Романов, А.М. Бычков

МИРЭА – Российский технологический университет, Москва, 119454 Россия
[@] Автор для переписки, e-mail: volkova_m@mirea.ru

Резюме

Цели. На сегодняшний день спорт является одной из наиболее перспективных областей для применения систем слежения за объектами. Большинство методов, на базе которых реализованы эти системы, ориентированы на отслеживание движущихся объектов в двумерной плоскости, например, для локализации игроков на поле, а также на их идентификацию по различным признакам. С развитием дрон-рейсинга актуальной стала задача определения положения в трехмерной системе координат. Целями работы являются разработка программно-алгоритмического обеспечения метода, позволяющего отслеживать траекторию движущихся объектов в трехмерном пространстве, абстрагированного от способа сегментации данных, и тестирование предложенного решения для оценки качества работы трекера.

Методы. На основе проведенного обзора и анализа современных методов отслеживания траекторий движения был выбран метод сопоставления информации о скорости и положении объектов.

Результаты. Предложена структура программно-алгоритмического обеспечения трекера движущихся объектов на спортивных мероприятиях и представлены результаты экспериментальных исследований на общедоступном датасете *APIDIS*, который включает в себя фрагменты видеозаписи баскетбольной игры, где по критерию качества отслеживания MOTA был получен показатель 0.858. Также были проведены эксперименты с использованием предложенного авторами датасета с пролетом FPV квадрокоптера по трассе. В результате по полученным с трекера данным была восстановлена траектория полета дрона в трехмерном пространстве.

Выводы. Результаты проведенных экспериментальных исследований показали, что предложенное решение позволяет отслеживать траекторию полета квадрокоптера в трехмерной (мировой) системе координат, а также подходит для слежения за объектами на спортивных мероприятиях.

Ключевые слова: трекер, слежение за движущимися объектами, FPV квадрокоптер, определение положения, система слежения

• **Поступила:** 02.06.2022 • **Доработана:** 19.07.2022 • **Принята к опубликованию:** 26.08.2022

Для цитирования: Волкова М.А., Романов М.П., Бычков А.М. Трекер объектов на спортивных мероприятиях. *Russ. Technol. J.* 2022;10(5):38–48. https://doi.org/10.32362/2500-316X-2022-10-5-38-48

Прозрачность финансовой деятельности: Авторы не имеют финансовой заинтересованности в представленных материалах или методах.

Авторы заявляют об отсутствии конфликта интересов.

INTRODUCTION

Contemporary tracking systems for moving objects are widely used in various social and industrial areas of human activity, e.g., the creation of autonomous vehicles [1], detection of motoring offences [2], provision of safety and security at mass gatherings [3], and personnel tracking [4]. One of the most promising areas of application of such systems is sports, especially team sports: football, basketball, etc. By tracking participants in sports events, it becomes possible to evaluate group tactical actions, predict the results of matches, etc. During the broadcast of football games, for example, movement monitoring is used to view personal replays or obtain extended player statistics [5].

To track the movements of athletes during the competition, it is necessary to solve two main tasks:

1) detection and identification of moving objects using sensors;
2) determination of the parameters (e.g., position and speed) of objects, according to which the path of the movement is reconstructed.

Player identification is complicated by the difficulty that athletes in team sports are often similar in appearance (e.g., due to wearing the same sports uniform). In addition, the movement paths of the players can change dramatically, resulting in occlusion and the need for re-identification. Thus, the main problem affecting the tracking accuracy indicators is the frequent switching of object identifiers [6].

Among the various methods and algorithms for tracking moving objects, multi-athlete tracking (MAT) technology can be distinguished. This video tracking system comprises several cameras acting as sensors to provide video data for subsequent processing. The literature covering MAT systems can be divided into two groups. Works in the first group [6, 7] are more focused on identifying characteristic features in order to solve the object identification problem, which often results in long delays in information output, while works of the second group [8, 9] are aimed at determining other parameters. However, the correct functioning of the MAT algorithms requires the determination of a spatial plane against which objects move, making it less appropriate for tracking objects in the air or moving across complex terrain.

A relatively young and actively developing sport is first-person view (FPV) quadcopter (drone) racing. This competitive sport is based on the speed and quality of passing a predetermined track with real-time video broadcast from the camera of the drone to the monitor, goggles, or pilot helmet of its operator. Due to the need to evaluate the flight trajectory for fair refereeing, tracking the movement path of objects in 3D space becomes an important consideration. For example, because of the high speeds involved, it is often impossible to visually determine which of the quadcopters passed the finish gate first. Most of the works on this subject are aimed at increasing the autonomy of quadcopters and developing algorithms for finding the optimal route, as well as testing them [10–12].

The purpose of the present work was to develop algorithms and software for a method for 3D tracking of moving objects that do not require identification at the detection stage and to test this method to provide an estimate of its tracking quality.

Our contribution is as follows:

- a moving-object tracker for sports events is proposed based on a described method for matching information on the speed and position of objects [13];
- experimental studies were carried out both on the publicly available *APIDIS* dataset, where a multiple object tracking accuracy (MOTA) metric of 0.858 was obtained, and on the presented dataset for quadcopter flight along a track;
- the 3D path of the drone flight was reconstructed.

1. REVIEW OF WORKS ON THE SUBJECT OF INVESTIGATION

Most of the works studying the problem of tracking moving objects are applicable to the development of athlete tracking systems. These mainly comprise methods that include a preliminary stage of detection, i.e., segmentation of data obtained from sensors in various ways. Since object identification is typically carried out at this stage, many studies are aimed at improving its accuracy by modernizing existing methods for searching for singular points and descriptors [14]. As well as describing the most frequently used descriptors and methods for detecting objects, Chigrinskii and Matveev [15] also studied approaches for improving certain aspects of the algorithms. Experimental results demonstrated higher tracking accuracy as compared with using basic methods. Approaching the problem of object localization using RGB color models, Lan et al. [16] significantly improved the performance of the system by training the descriptor at two levels: directly on the obtained image, as well as on its infrared representation. Such methods are not suitable for real-time implementation because of the need to train descriptors, which leads to a delay in the output of information.

Detection-based tracking methods can be divided into three groups according to the way they represent the shape of an object: points, geometric shapes, and contours (silhouettes). While the latter group of methods is more often used to track people (pedestrians,

athletes, etc.) [17], the former, less resource-intensive, implementations are more suitable for other objects (cars, mobile robots, etc.). Volkova et al. [13] proposed a method for comparing information about the speed and position of objects, which allows them to be tracked in three-dimensional space. Identification is based on the obtained data on the speed and position of objects that can be represented as points, which is suitable for tracking small FPV quadcopters.

Wang et al. [18] proposed an online pedestrian tracking system. Segmented data are optimized by specifying the occlusion status. The position of the objects detected at the first stage is predicted using the Kalman filter, which, it should be noted, is often used in tracking algorithms. A comparison was made with the five most common trackers today (WVMF, SMOT-admm, SFCT, TLD, and DP + NMS). Experiments showed that the proposed system gives the best results. Linke et al. [19] compared two tracking systems in football: Gen4 and Gen5. The main difference between these systems is that Gen4 consists of two multi-camera systems, whereas Gen5 combines two stereo pairs on each side of the field and two monocular systems behind the goal areas. It was concluded that. the larger the number of cameras, the higher the accuracy of object tracking. On the basis of a comparative analysis of team sports tracking systems based on GPS data and multi-camera systems, Pons, et al. [20] concluded that higher tracking accuracy can be achieved with algorithms that use data from cameras.

Since many algorithms designed to solve the MAT problem require high-performance computers for their implementation, i.e., are costly [19], research is underway to create cheaper systems. Nishikawa et al. [21] proposed a tracking system based on the *k*-shortest path search algorithm. The results of the study proved the efficiency of the proposed solution when using relatively inexpensive cameras. Hui [22] investigated tracking the trajectory of sports objects using the mean shift algorithm. From the experimental results obtained, this approach demonstrated the possibility of reducing the required computing power.

Along with methods based on detection and identification, the MAT problem is often solved using algorithms based on the construction of occupancy maps. Taj and Cavallaro [23, 24] presented a tracking method based on a particle filter, where a priori information on the number of objects is not required. Liang et al. [25] and Yang et al. [26] used a hybrid method combining the construction of an occupancy map and the identification of the main features of the players. Although this approach provides a high MOTA, such methods are unsuitable for tracking quadcopters due to the need to implement a spatially deterministic plane.

Most studies of quadcopter flights along a track are aimed at increasing the autonomy of the flight to determine the optimal route [10–12], i.e., achieving superior technical vision and navigation. Moreover, there is an active development of datasets with complex trajectories containing a large number of sharp turns at high speeds [27], which significantly complicates tracking sports drones.

Thus, the results of the analysis performed suggest that to achieve the goal, the most appropriate approach for tracking the path of a sports object is based on comparing information about the speed and position of objects [13].

2. STRUCTURE OF ALGORITHMS AND SOFTWARE OF THE TRACKER

Figure 1 presents the structure of the algorithms and software of the tracker. In this work, it was decided to use only the main parameters, such as speed and spatial position (without using additional features) to reduce the delay in the output of information on objects.

A prerequisite for the tracker's operation is a preliminary calibration of all sensors, which determines the relative linear and angular displacements of the sensors' coordinate systems and chooses the origin of the world coordinate system. It is assumed that the position of the sensors relative to each other does not change throughout the tracker's work time.

The data obtained at the stage of object detection is fed to the tracker input. The result of the tracker is the state vector $\mathbf{x}_i$ of the object at time t. The vector consists of the basic geometric parameters (position L, speed V, and acceleration a; T is the transposition symbol) in the world (three-dimensional) coordinate system, as well as, if necessary, an identification number:

$$\mathbf{x}_i = (L, V, a)^{\mathrm{T}}.$$

Let us consider the blocks in the tracker structure. Table 1 compares the operations of the selected method and the blocks of algorithms and software.

The tracker algorithm consists of six blocks.

1. The input of the block "Creating a dataset on the position of objects" receives all segmented data on the position of objects O and O', comprising a set of projected vectors of coordinates of objects predicted using the Kalman filter in the coordinate system selected for localization. Thus, the output of the block is a set of vectors $O_t = \{O\ O'\}$.
2. The input of the block "Calculating the overall likelihood function" receives the data set O_t. Clustering in this case is performed by the mean shift method [24] and gives a set of clusters, the

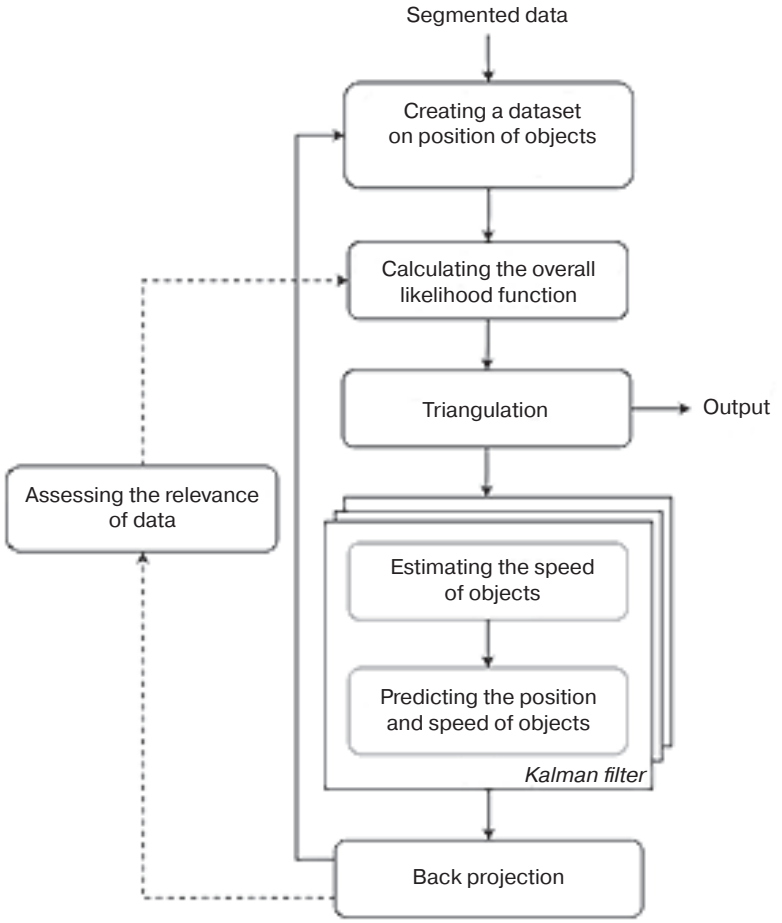

Fig. 1. Structure of algorithms and software of the tracker

Table 1. Comparison of the operations of the selected method and the blocks of algorithms and software of the tracker

Block	Operation
Creating a dataset on the position of objects	Creating a sample of observations O_t
Calculating the overall likelihood function	Calculating the overall likelihood function $p(O_t \mid \mathbf{x}_i)$
Triangulation	Obtaining vectors $\mathbf{x}_i(L)$
Estimating the speed of objects	Obtaining vectors $\mathbf{x}_i(V)$
Predicting the position and speed of objects	Calculating vectors $\hat{\mathbf{x}}_i$
Back projection	Creating a sample of observations O'
Assessing the relevance of data	Calculating the parameter characterizing the reliability of obtained information A_{M}

number of which corresponds to the number of objects. The segmented data from the sensors are assigned identification numbers of objects that are in the same cluster.

3. In the "Triangulation" block, data with equal identification numbers from all the sensors are triangulated [28]. The output of the block gives the position of objects in the three-dimensional (world) coordinate system $\mathbf{x}_i(L)$.
4. The data obtained at the previous stage enter the third order Kalman filter block, which, in turn, consists of two blocks, the calculations for which are performed sequentially: "Estimating the speed of objects" and "Predicting the speed and position of objects" [29]. To estimate the parameters in a three-dimensional coordinate system, three Kalman filters are needed. When calculating the predicted parameters for the X coordinate, the following

expressions are used (for Y and Z, the expressions are similar):

$$\mathbf{A} = \begin{bmatrix} 1 & T & 0 \\ 0 & 1 & T \\ 0 & 0 & 1 \end{bmatrix},$$

$$\mathbf{H} = [1\ 0\ 0],$$

$$\mathbf{x}_t = (L_X, V_X, a_X)^{\mathrm{T}},$$

$$\mathbf{Q} = \begin{bmatrix} \frac{T^4}{4\sigma^2} & \frac{T^3}{2\sigma^2} & 0 \\ \frac{T^3}{2\sigma^2} & \frac{T^2}{\sigma^2} & T\sigma^2 \\ 0 & T\sigma^2 & \sigma^2 \end{bmatrix},$$

$$\hat{\mathbf{x}} = \mathbf{A}\mathbf{x}_t,$$

$$\hat{\mathbf{P}}_{t+1} = \mathbf{A}\mathbf{P}\mathbf{A}^{\mathrm{T}} + \mathbf{Q},$$

$$K_{t+1} = \hat{\mathbf{P}}_{t+1|1\ldots3,1}(\hat{\mathbf{P}}_{t+1|1,1} + \mathbf{R})^{-1},$$

$$\mathbf{x}_{t+1} = \hat{\mathbf{x}} + K_{n+1}(\mathbf{x} - \hat{\mathbf{x}}_{1,1}),$$

where $\mathbf{Q}$ is the process noise covariance matrix; $\mathbf{R}$ is the sensor noise matrix; $\mathbf{P}$ is the noise covariance matrix; K is the matrix correction factor; $\mathbf{H}$ is a matrix that defines the output data; $\mathbf{A}$ is the state matrix; T is the measurement period, σ is a filter parameter, which depends on the dynamic characteristics of the observed object.

At the output of the block, data are generated on the predicted position and speed of objects in the three-dimensional coordinate system.

5. The block "Back projection" reprojects the data obtained in step 4 from the world coordinate system into the coordinate system of each sensor O'.
6. The block "Assessing the relevance of data" calculates the parameter A_{M} characterizing the reliability of the received information. It is calculated as follows:

$$A_{\mathrm{M}} = \exp\left(-\frac{t_{\mathrm{m}}}{d\Delta Ts}\right),$$

where t_{m} is the time elapsed since the last determination of feature, ΔTs is the sensor measurement period, and d is the coefficient of decrease in the relevance of data.

If, at the moment of time t, the data of none of the measurements of the object or the data of only one measurement has been received (the latter is unacceptable for triangulation), then the predicted reprojected position and speed are indicated as the data received from the sensors in the block "Creating a dataset on the position of objects." The A_{M} parameter in this case is necessary to correct the tracking duration according to the predicted data, i.e., to timely stop tracking the object.

3. EXPERIMENTAL INVESTIGATIONS

In the first experiment, the *APIDIS*[1] dataset was used to verify the proposed algorithms and software. This comprised seven video segments of a basketball game, which were taken from different cameras located around the court. Two cameras (first and seventh) were chosen, having different focal lengths but both aimed at the same corner of the court. Segmented data on objects were obtained by a previously proposed method [30]. During the experiment, for one minute (a sequence of 1500 frames), the parameters of the position and speed were estimated for four preselected objects, which most often intersected with each other and with other objects.

In Fig. 2, the black lines represent the reference trajectories for all objects in space on the XY plane (in this experiment, the displacement along the Z axis is 0), while the colored lines represent the selected targets. The reference trajectories were obtained by interpolating the coordinates of the objects presented on the dataset website at an interval of 1 s.

Figure 3 presents the reference trajectories of the selected targets and the trajectories reconstructed on the basis of the segmented data received from the cameras. Table 2 presents the results of calculating the MOTA tracking accuracy index in comparison with other modern methods.

Table 2. MOTA indicators of various trackers

Tracker	MOTA
[6]	0.752
[31]	0.796
[32]	0.811
Tracker proposed in this work	0.858

Based on the analysis of Table 2, it can be concluded that the proposed algorithms and software of the tracker provide a high tracking accuracy and is superior to known analogues.

For the second experiment, a stand was constructed in our laboratory (Fig. 4).

[1] https://sites.uclouvain.be/ispgroup/index.php/Softwares/APIDIS. Accessed January 1, 2022.

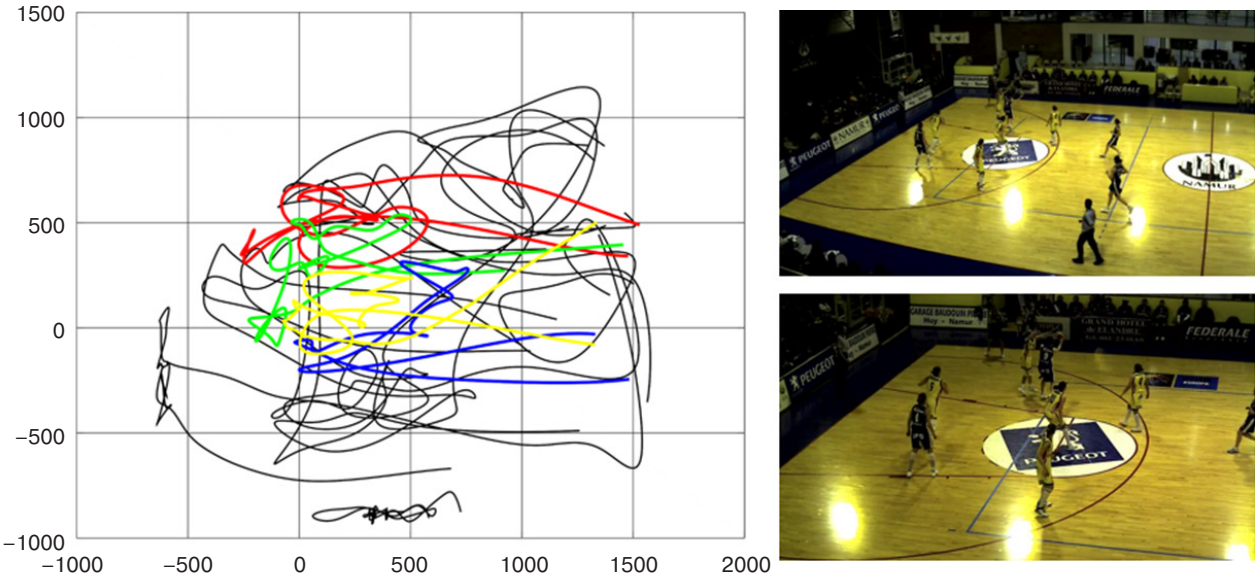

Fig. 2. Reference trajectories of players (left) and frames from the first and seventh cameras (right)

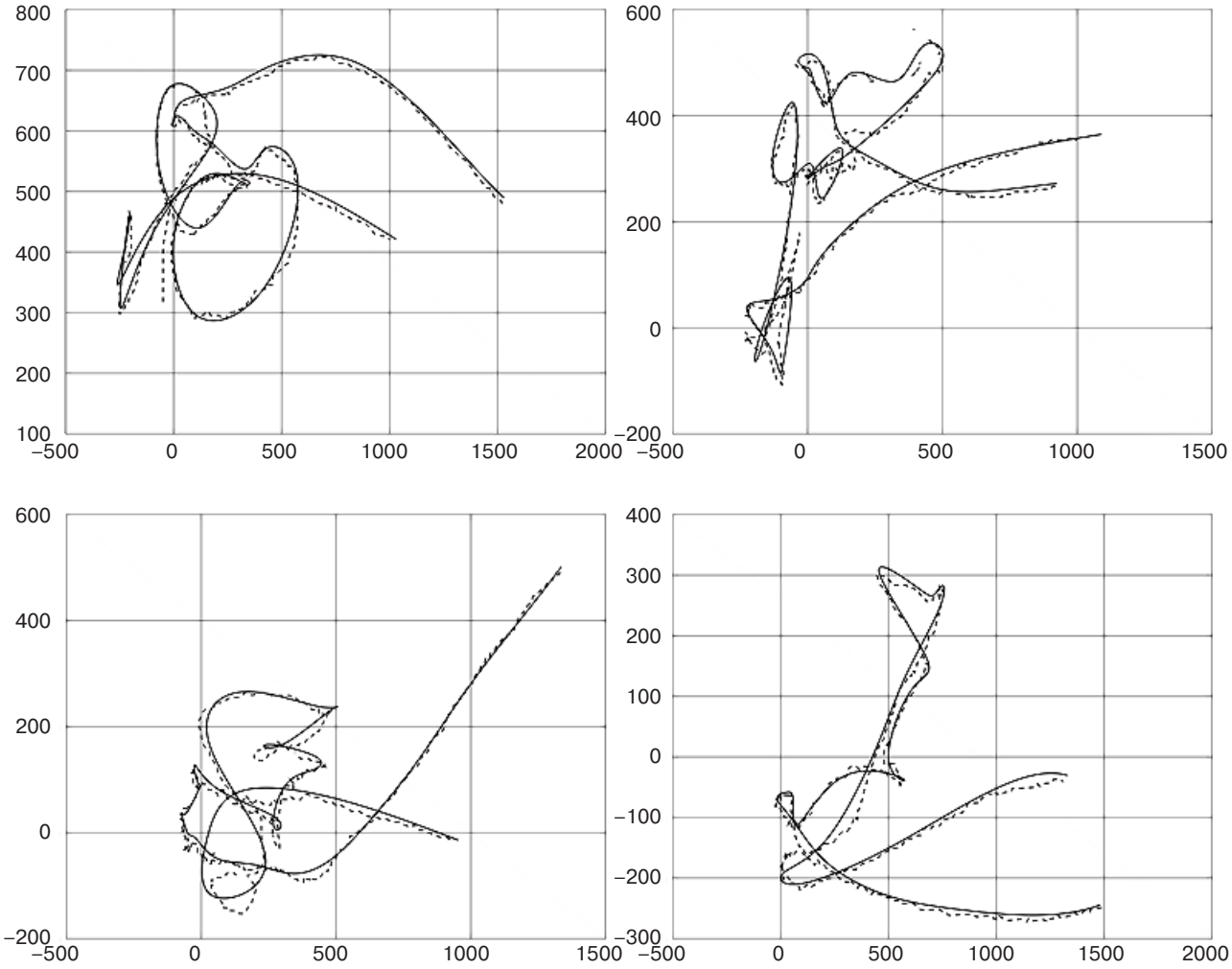

Fig. 3. Reference trajectories of objects (solid lines) and the trajectories reconstructed from segmented data (dashed lines)

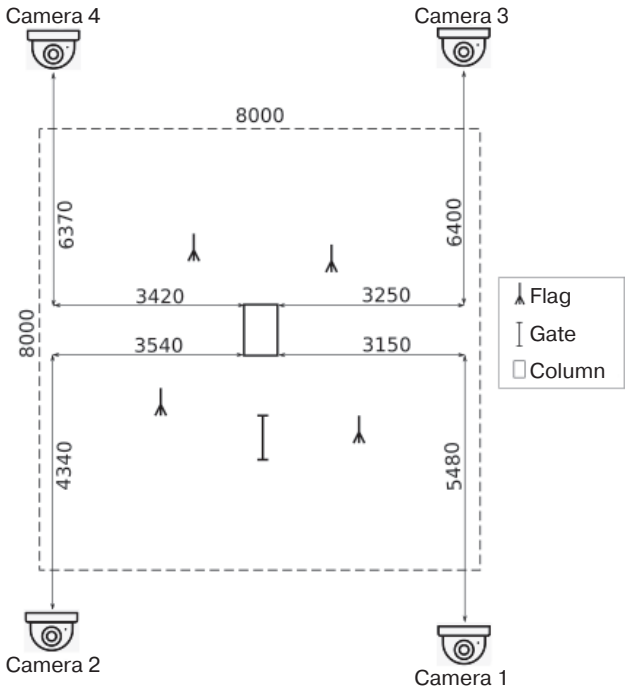

Fig. 4. Schematic of a test stand

The stand consisted of a video tracking system with four BD133 dome cameras (manufactured by Beward, Russia) and a quadcopter track. The track comprised five elements: four flags (range poles) and a gate. The dimensions of the working area were 8 × 8 × 3 m. Calibration of the cameras determined that the frame rate for the first camera should be 13 fps (frames per second), while for the other cameras, it should be 25 fps. During the experiment, a dataset was taken simultaneously from four cameras of the quadcopter Photon (manufactured by MIREA – Russian Technological University, Russia) flying along the track for 30 s. Segmentation of a moving object (quadcopter) was performed by the frame binarization method with a predetermined threshold. The quadcopter flight trajectory was reconstructed in the world coordinate system (Fig. 5). Then, for verification, this trajectory was projected back onto the images received from the cameras. The result is shown in Fig. 6.

The quadcopter flight trajectory was successfully restored. During the course of the experiment, it was also determined that the delay (latency) in the output of information for one object after the segmented data was sent to the tracker is 32 ms.

CONCLUSIONS

In this work, contemporary methods for tracking moving objects were reviewed and analyzed with special attention paid to MAT methods. The structure of a set of algorithms comprising software for the tracking of moving objects is proposed based on the

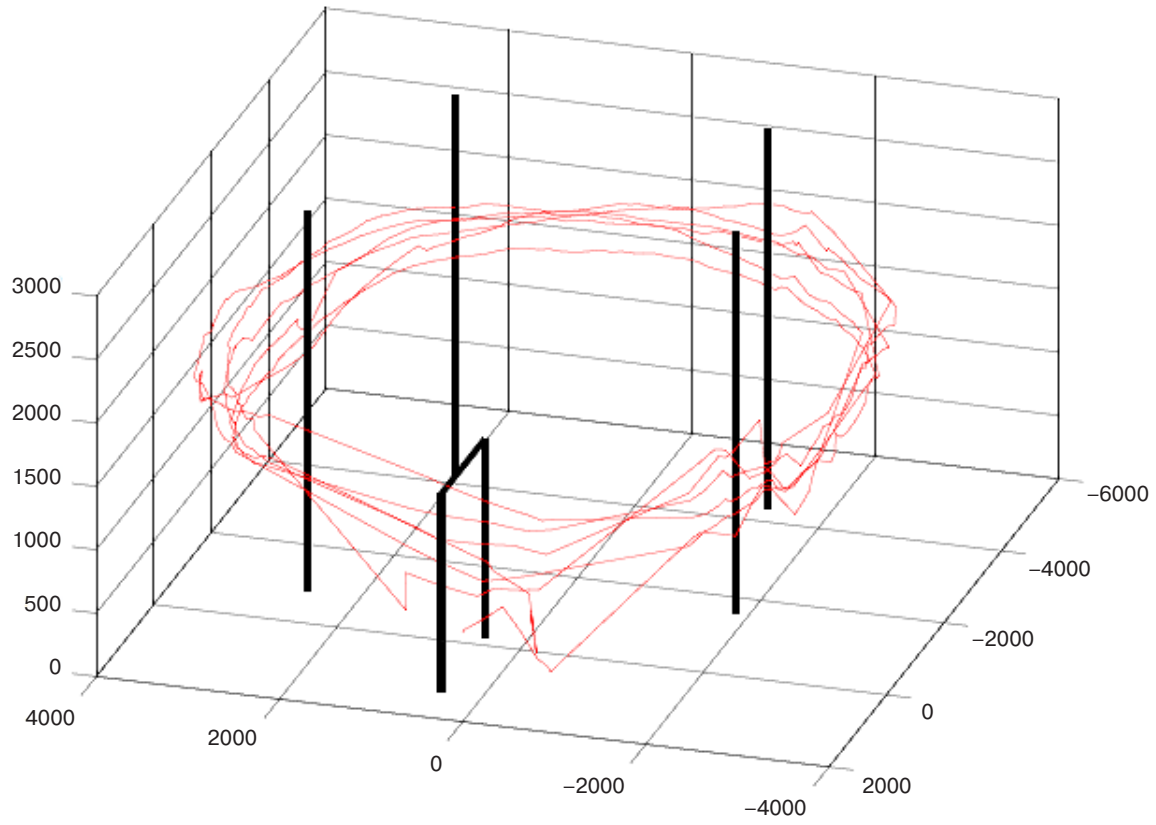

Fig. 5. 3D reconstructed quadcopter flight trajectory

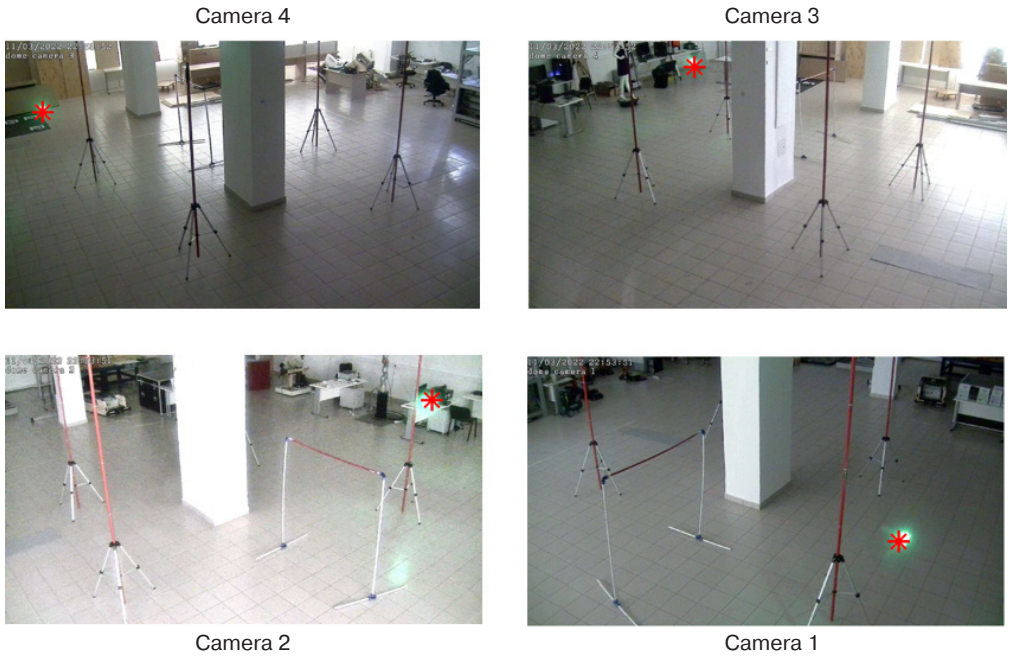

Fig. 6. Frames received from cameras and the tracked quadcopter (marked with a red marker)

method of comparing information on the position and speed of objects. The experimental studies demonstrated the possibility of using the proposed solution to track a quadcopter flight trajectory in a three-dimensional (world) coordinate system, as well as being suitable for tracking objects at sports events.

ACKNOWLEDGMENTS

This research is supported by the RTU MIREA grant "Innovations in the implementation of priority areas for the science and technology development," project No. 28/24.

Authors' contributions

M.A. Volkova has proposed the solution for implementing the object tracker for sports events, presented the results of experimental studies on the APIDIS dataset and a test stand, conducted an experiment with a quadcopter flying along the track, and written the text of the article.

M.P. Romanov has proposed the solution for implementing the object tracker for sports events.

A.M. Bychkov has presented a test stand and conducted an experiment with a quadcopter flying along the track.

REFERENCES

1. Zein Y., Darwiche M., Mokhiamar O. GPS tracking system for autonomous vehicles. *Alexandria Eng. J.* 2018;57(4): 3127–3137. https://doi.org/10.1016/j.aej.2017.12.002
2. Yu K., et al. Deep learning-based traffic safety solution for a mixture of autonomous and manual vehicles in a 5G-enabled intelligent transportation system. *IEEE Transactions on Intelligent Transportation Systems*. 2020;22(7): 4337–4347. https://doi.org/10.1109/TITS.2020.3042504
3. Ryan B.J., et al. COVID-19 contact tracing solutions for mass gatherings. *Disaster Medicine and Public Health Preparedness*. 2021;15(3):e1–e7. https://doi.org/10.1017/dmp.2020.241
4. Khan S., et al. Implementing traceability systems in specific supply chain management (SCM) through critical success factors (CSFs). *Sustainability*. 2018;10(1):204. https://doi.org/10.3390/su10010204
5. Cioppa A., Deliege A., Magera F., Giancola S., Barnich O., Ghanem B., Van Droogenbroeck M. Camera calibration and player localization in soccerNet-v2 and investigation of their representations for action spotting. In: *Proceedings of the IEEE/CVF Conference on Computer Vision and Pattern Recognition Workshops* (*CVPRW*). 2021. P. 4537–4546. https://doi.org/10.1109/CVPRW53098.2021.00511
6. Kong L., Zhu M., Ran N., Liu Q., He R. Online multiple athlete tracking with pose-based long-term temporal dependencies. *Sensors*. 2020;21(1):197. https://doi.org/10.3390/s21010197
7. Liu J., Tong X., Li W., Wang T., Zhang Y., Wang H. Automatic player detection, labeling and tracking in broadcast soccer video. *Pattern Recognition Lett*. 2009;30(2):103–113. https://doi.org/10.1016/j.patrec.2008.02.011
8. Possegger H., Sternig S., Mauthner T., Roth P.M., Bischof H. Robust real-time tracking of multiple objects by volumetric mass densities. In: *Proceedings of the IEEE Conference on Computer Vision and Pattern Recognition*. 2013. P. 2395–2402. https://doi.org/10.1109/CVPR.2013.310
9. Bialkowski A., Lucey P., Carr P., Denman S., Matthews I., Sridharan S. Recognising team activities from noisy data. In: *Proceedings of the IEEE Conference on Computer Vision and Pattern Recognition Workshops*. 2013. P. 984–990. https://doi.org/10.1109/CVPRW.2013.143

10. Foehn P., Brescianini D., Kaufmann E., et al. AlphaPilot: Autonomous drone racing. *Auton. Robot*. 2022;46(1): 307–320. https://doi.org/10.1007/s10514-021-10011-y
11. Spica R., Cristofalo E., Wang Z., Montijano E., Schwager M. A real-time game theoretic planner for autonomous two-player drone racing. *IEEE Transactions on Robotics*. 2020;36(5): 1389–1403. https://doi.org/10.1109/TRO.2020.2994881
12. Kaufmann E., et al. Beauty and the beast: Optimal methods meet learning for drone racing. In: *2019 International Conference on Robotics and Automation* (*ICRA*). IEEE. 2019. P. 690–696. https://doi.org/10.1109/ICRA.2019.8793631
13. Volkova M.A., Romanov A.M., Romanov M.P. Distributed system for objects localization in the working area of a modular reconfigurable mobile robot. *Mekhatronika, Avtomatizatsiya, Upravlenie*. 2021;22(12):634–643 (in Russ.). https://doi.org/10.17587/mau.22.634-643
14. Dai-Hong J., Lei D., Dan L., San-You Z. Moving-object tracking algorithm based on PCA-SIFT and optimization for underground coal mines. *IEEE Access*. 2019;7: 35556–35563. https://doi.org/10.1109/ACCESS.2019.2899362
15. Chigrinskii V.V., Matveev I.A. Optimization of a tracking system based on a network of cameras. *J. Comput. Syst. Sci. Int.* 2020;59(4):583–597. https://doi.org/10.1134/S1064230720040127
[Original Russian Text: Matveev I.A., Chigrinskii V.V. Optimization of a tracking system based on a network of cameras. *Izvestiya Rossiiskoi akademii nauk. Teoriya i sistemy upravleniya*. 2020;4:110–124 (in Russ.). https://doi.org/10.31857/S0002338820040125]
16. Lan X., Ye M., Shao R., Zhong B., Yuen P.C., Zhou H. Learning modality-consistency feature templates: A robust RGB-infrared tracking system. *IEEE Transactions on Industrial Electronics*.2019;66(12):9887–9897. https://doi.org/10.1109/TIE.2019.2898618
17. Bao Q., Liu W., Cheng Y., Zhou B., Mei T. Pose-guided tracking-by-detection: Robust multi-person pose tracking. *IEEE Transactions on Multimedia*. 2020;23:161–175. https://doi.org/10.1109/TMM.2020.2980194
18. Wang Z., Li M., Lu Y., Bao Y., Li Z., Zhao J. Effective multiple pedestrian tracking system in video surveillance with monocular stationary camera. *Expert Systems with Applications*. 2021;178:114992. https://doi.org/10.1016/j.eswa.2021.114992
19. Linke D., Link D., Lames M. Football-specific validity of TRACAB's optical video tracking systems. *PLoSONE*. 2020;15(3):e0230179. https://doi.org/10.1371/journal.pone.0230179
20. Pons E., García-Calvo T., Resta R., Blanco H., López del Campo R., Díaz García J., Pulido J.J. A comparison of a GPS device and a multi-camera video technology during official soccer matches: Agreement between systems. *PLoSONE*. 2019;14(8):e0220729. https://doi.org/10.1371/journal.pone.0220729
21. Nishikawa Y., Sato H., Ozawa J. Multiple sports player tracking system based on graph optimization using low-cost cameras. In: *2018 IEEE International Conference on Consumer Electronics* (*ICCE*). IEEE; 2018. P. 1–4. https://doi.org/10.1109/ICCE.2018.8326126
22. Hui Q. Motion video tracking technology in sports training based on Mean-Shift algorithm. *J. Supercomput*. 2019;75(9):6021–6037. https://doi.org/10.1007/s11227-019-02898-3
23. Taj M., Cavallaro A. Distributed and decentralized multicamera tracking. *IEEE Signal Processing Magazine.* 2011;28(3):46–58. https://doi.org/10.1109/MSP.2011.940281
24. Taj M., Cavallaro A. Simultaneous detection and tracking with multiple cameras. In: Cipolla R., Battiato S., Farinella G. (Eds.). *Machine Learning for Computer Vision. Studies in Computational Intelligence*. Berlin, Heidelberg: Springer; 2013. V. 411. P. 197–214. https://doi.org/10.1007/978-3-642-28661-2_8
25. Liang Q., Wu W., Yang Y., Zhang R., Peng Y., Xu M. Multi-player tracking for multi-view sports videos with improved k-shortest path algorithm. *Appl. Sci*. 2020;10(3):864. https://doi.org/10.3390/app10030864
26. Yang Y., Xu M., Wu W., Zhang R., Peng Y. 3D multiview basketball players detection and localization based on probabilistic occupancy. In: *2018 Digital Image Computing: Techniques and Applications* (*DICTA*). IEEE; 2018. P. 1–8. https://doi.org/10.1109/DICTA.2018.8615798
27. Delmerico J., Cieslewski T., Rebecq H., Faessler M., Scaramuzza D. Are we ready for autonomous drone racing? The UZH-FPV drone racing dataset. In: *2019 International Conference on Robotics and Automation* (*ICRA*). IEEE; 2019. P. 6713–6719. https://doi.org/10.1109/ICRA.2019.8793887
28. Chen J., Wu D., Song P., Deng F., He Y., Pang S. Multi-view triangulation: Systematic comparison and an improved method. *IEEE Access*. 2020;8:21017–21027. https://doi.org/10.1109/ACCESS.2020.2969082
29. Romanov A.M., et al. Modular reconfigurable robot distributed computing system for tracking multiple objects. *IEEE Systems J*. 2021;15(1):802–813. https://doi.org/10.1109/JSYST.2020.2990921
30. Delannay D., Danhier N., De Vleeschouwer C. Detection and recognition of sports(wo)men from multiple views. In: *2009 Third ACM/IEEE International Conference on Distributed Smart Cameras* (*ICDSC*). IEEE; 2009. P. 1–7. https://doi.org/10.1109/ICDSC.2009.5289407
31. Byeon M., et al. Variational inference for 3-D localization and tracking of multiple targets using multiple cameras. *IEEE Transactions on Neural Networks and Learning Systems*. 2019;30(11):3260–3274. https://doi.org/10.1109/TNNLS.2018.2890526
32. Zhang R., et al. Multi-camera multi-player tracking with deep player identification in sports video. *Pattern Recognition*. 2020;102:107260. https://doi.org/10.1016/j.patcog.2020.107260

About the authors

Maria A. Volkova, Senior Lecturer, Control Problems Department, Institute of Artificial Intelligence, MIREA – Russian Technological University (78, Vernadskogo pr., Moscow, 119454 Russia). E-mail: volkova_m@mirea.ru. Scopus Author ID 57194215422, RSCI SPIN-code 5939-6811, https://orcid.org/0000-0002-1219-5090

Mikhail P. Romanov, Dr. Sci. (Eng.), Professor, Director of the Institute of Artificial Intelligence, MIREA – Russian Technological University (78, Vernadskogo pr., Moscow, 119454 Russia). E-mail: m_romanov@mirea.ru. Scopus Author ID 14046079000, RSCI SPIN-code 5823-8795, https://orcid.org/0000-0003-3353-9945

Alexander M. Bychkov, Assistant, Control Problems Department, Institute of Artificial Intelligence, MIREA – Russian Technological University (78, Vernadskogo pr., Moscow, 119454 Russia). E-mail: bychkov@mirea.ru. https://orcid.org/0000-0003-0701-7529

Об авторах

Волкова Мария Александровна, старший преподаватель, кафедра проблем управления Института искусственного интеллекта ФГБОУ ВО «МИРЭА – Российский технологический университет» (119454, Россия, Москва, пр-т Вернадского, д. 78). E-mail: volkova_m@mirea.ru. Scopus Author ID 57194215422, SPIN-код РИНЦ 5939-6811, https://orcid.org/0000-0002-1219-5090

Романов Михаил Петрович, д.т.н., профессор, директор Института искусственного интеллекта ФГБОУ ВО «МИРЭА – Российский технологический университет» (119454, Россия, Москва, пр-т Вернадского, д. 78). E-mail: m_romanov@mirea.ru. Scopus Author ID 14046079000, SPIN-код РИНЦ 5823-8795, https://orcid.org/0000-0003-3353-9945

Бычков Александр Михайлович, ассистент, кафедра проблем управления Института искусственного интеллекта ФГБОУ ВО «МИРЭА – Российский технологический университет» (119454, Россия, Москва, пр-т Вернадского, д. 78). E-mail: bychkov@mirea.ru. https://orcid.org/0000-0003-0701-7529

Translated from Russian into English by Vladislav V. Glyanchenko
Edited for English language and spelling by Thomas A. Beavitt

Modern radio engineering and telecommunication systems

Современные радиотехнические и телекоммуникационные системы

UDC 004.94
https://doi.org/10.32362/2500-316X-2022-10-5-49-59

RESEARCH ARTICLE

Implementation of stochastic signal processing algorithms in radar CAD

Maxim Yu. Konopel'kin [@], Sergey V. Petrov, Daria A. Smirnyagina

"Almaz-Antey" Air and Space Defence Corporation, Moscow, 121471 Russia
[@] Corresponding author, e-mail: m.konopelkin@almaz-antey.ru

Abstract

Objectives. In 2020, development work on the creation of a Russian computer-assisted design system for radars (radar CAD) was completed. Radar CAD provides extensive opportunities for creating simulation models for developing the hardware-software complex of radar algorithms, which take into account the specific conditions of aerospace environment observation. The purpose of the present work is to review and demonstrate the capabilities of radar CAD in terms of implementing and testing algorithms for processing stochastic signals.

Methods. The work is based on the mathematical apparatus of linear algebra. Analysis of algorithms characteristics was carried out using the simulation method.

Results. A simulation model of a sector surveillance radar with a digital antenna array was created in the radar CAD visual functional editor. The passive channel included the following algorithms: algorithm for detecting stochastic signals; algorithm for estimating the number of stochastic signals; direction finding algorithm for stochastic signal sources; adaptive spatial filtering algorithm. In the process of simulation, the algorithms for detecting and estimating the number of stochastic signals produced a correct detection sign and an estimate of the number of signals. The direction-finding algorithm estimated the angular position of the sources with an accuracy of fractions of degrees. The adaptive spatial filtering algorithm suppressed interfering signals to a level below the antenna's intrinsic noise power.

Conclusions. The processing of various types of signals can be simulated in detail on the basis of the Russian radar CAD system for the development of functional radar models. According to the results of the simulation, coordinates of observing objects were obtained and an assessment of the effectiveness of the algorithms was given. The obtained results are fully consistent with the theoretical prediction. The capabilities of radar CAD systems demonstrated in this work can be used by specialists in the field of radar and signal processing.

Keywords: simulation modeling, radar information processing algorithm, computer-aided design system, radar station, adaptive spatial filtering

• **Submitted:** 05.05.2022 • **Revised:** 15.07.2022 • **Accepted:** 02.09.2022

For citation: Konopel'kin M.Yu., Petrov S.V., Smirnyagina D.A. Implementation of stochastic signal processing algorithms in radar CAD. *Russ. Technol. J.* 2022;10(5):49–59. https://doi.org/10.32362/2500-316X-2022-10-5-49-59

Financial disclosure: The authors have no a financial or property interest in any material or method mentioned.

The authors declare no conflicts of interest.

НАУЧНАЯ СТАТЬЯ

Реализация алгоритмов обработки стохастических сигналов в САПР РЛС

М.Ю. Конопелькин [@], **С.В. Петров**, **Д.А. Смирнягина**

Концерн воздушно-космической обороны «Алмаз-Антей», Москва, 121471 Россия
[@] *Автор для переписки, e-mail: m.konopelkin@almaz-antey.ru*

Резюме

Цели. В 2020 г. завершилась опытно-конструкторская работа по созданию российской системы автоматизированного проектирования (САПР) радиолокационных станций (РЛС). Отличительной особенностью САПР РЛС являются богатые возможности для создания имитационных моделей и имитационного моделирования, что позволяет отрабатывать аппаратную часть и комплекс боевых алгоритмов РЛС с учетом конкретных условий боевого применения, средств воздушно-космического нападения и фоно-целевой обстановки. Цель настоящей статьи – обзор и демонстрация возможностей САПР РЛС в части реализации и отработки алгоритмов обработки стохастических сигналов.

Методы. В работе использовался математический аппарат линейной алгебры. Анализ характеристик алгоритмов проведен методом имитационного моделирования.

Результаты. В визуальном функциональном редакторе САПР РЛС создана имитационная модель РЛС секторного обзора с цифровой антенной решеткой. В состав пассивного канала входили следующие алгоритмы: алгоритм обнаружения стохастических сигналов; алгоритм оценивания числа стохастических сигналов; алгоритм пеленгации источников стохастических сигналов; алгоритм адаптивной пространственной фильтрации. В процессе имитационного моделирования алгоритмы обнаружения и оценивания числа выдавали корректный признак обнаружения и оценку числа сигналов. Алгоритм пеленгации оценивал угловое положение источников с точностью до долей градусов. Алгоритм адаптивной пространственной фильтрации подавлял сигналы мешающих сигналов до уровня ниже мощности собственных шумов антенны.

Выводы. Обширные возможности по разработке моделей функционирования РЛС, имеющиеся в российской САПР РЛС, позволяют детально моделировать процессы обработки различных видов сигналов. По результатам моделирования получены координаты целей и приведена оценка эффективности работы алгоритмов. Полученные результаты полностью соответствуют теоретическому прогнозу. Продемонстрированные в настоящей работе возможности САПР РЛС могут быть использованы специалистами в области радиолокации и обработки сигналов.

Ключевые слова: имитационное моделирование, алгоритм обработки радиолокационной информации, система автоматизированного проектирования, радиолокационная станция, адаптивная пространственная фильтрация

• **Поступила:** 05.05.2022 • **Доработана:** 15.07.2022 • **Принята к опубликованию:** 02.09.2022

Для цитирования: Конопелькин М.Ю., Петров С.В., Смирнягина Д.А. Реализация алгоритмов обработки стохастических сигналов в САПР РЛС. *Russ. Technol. J.* 2022;10(5):49–59. https://doi.org/10.32362/2500-316X-2022-10-5-49-59

Прозрачность финансовой деятельности: Авторы не имеют финансовой заинтересованности в представленных материалах или методах.

Авторы заявляют об отсутствии конфликта интересов.

INTRODUCTION

In 2020, development work was completed on the creation of a computer-assisted design (CAD) system for radar stations, radar complexes and radar systems, as well as their various components [1–10]. Due to the outstanding capabilities of radar CAD in creating simulation models and simulation modeling, it is now possible to work out a hardware and algorithm set for the radar that takes specific conditions of aerospace environment observation. One of the most important applications of the developed CAD is the development of algorithms for processing radar information based on the results of end-to-end integrated simulation based on the requirements and operating conditions.

The study aimes to review and demonstrate the capabilities of radar CAD in terms of implementing and developing algorithms for processing stochastic signals.

1. RADAR CAD TOOLKIT

1.1. Visual functional editor

Radar CAD uses an approach known as dataflow programming to create simulation models. Employing the visual constructor, a user creates a calculation graph from blocks, configures the parameters of each block and the connections between them. By pressing the start calculation button, the graph is passed through; the output data of each block are calculated based on the input data and block parameters.

The advantages of this approach are the natural visual representation (in the form of a calculation graph) and support for parallelism. The visual functional editor developed as part of the radar CAD system provides the ability to create and calculate a data-flow graph. The graphical user interface resembles the classic *Simulink* interface for visual design of streaming data processing, consisting of interconnected parameterizable blocks (Fig. 1).

1.2. Module of engineering calculation and simulation

As well as the possibility of automating the radar development process, another of the key features of the developed CAD is its comprehensive modeling of radar behavior under operating conditions. In particular, an engineer has the possibility to set a scenario as part of the design process. When sending the scenario for calculation, a complete (close to reality) simulation of the behavior of the radar under operating conditions is carried out. A simulated raid on the radar includes the simulation of the movement of various air objects. At the same time, the operation of the radar antenna is modeled on the basis of the constructed radar model to scan the space. The reflection of an electromagnetic wave from an air object is simulated during the interaction of electromagnetic waves coming from the locator antenna and the air object to form the basis of calculated parameters of the signal received by the appropriate channel of the locator, where its processing can be further simulated. Various types of noise are superimposed on the incoming signal, due, for example, to reflection from the Earth's surface. When modeling the propagation of a beam through the atmosphere, various kinds of precipitation are also taken into account.

The modeling process is organized by the simulation modeling manager (SMM). The creation and editing of simulation scenarios is implemented in the module of engineering calculation and simulation (Fig. 2), which is part of the radar CAD system.

2. DESCRIPTION OF THE RADAR SIMULATION MODEL

2.1. Parameters of the radar simulation model

To demonstrate the capabilities of radar CAD in terms of implementing and testing algorithms for processing stochastic signals, a radar simulation model of an airspace surveillance was created. Figure 3 shows its block diagram, which includes the transmitting and receiving parts: the radio transmitter generates pulses with specified modulation parameters, while the radio receivers, together with the primary information processing system and the passive channel, provide amplification, conversion and optimal processing of the signals received by the antenna against a background of internal noise and external interference.

The radar type is active, single position, sector surveillance with electronic beam scanning. The selected signal parameters are typical for air traffic control radar [11]:

- signal type: chirp;
- carrier frequency: 3 GHz;
- signal bandwidth: 1 MHz;
- pulse duration: 67 μs;
- pulse repetition period: 0.67 ms;
- pulse power: 2.3 kW.

Antenna parameters are as follows:

- type of antenna: digital antenna array (DAA);
- size, in elements: 12 × 12;
- step of elements: 0.5 wavelength;
- gain factor: 32 dB;
- scanning sector in azimuth: (−45°)–(+45°);
- scanning sector in elevation: 0°–30°;
- antenna tilt to the horizon: 15°.

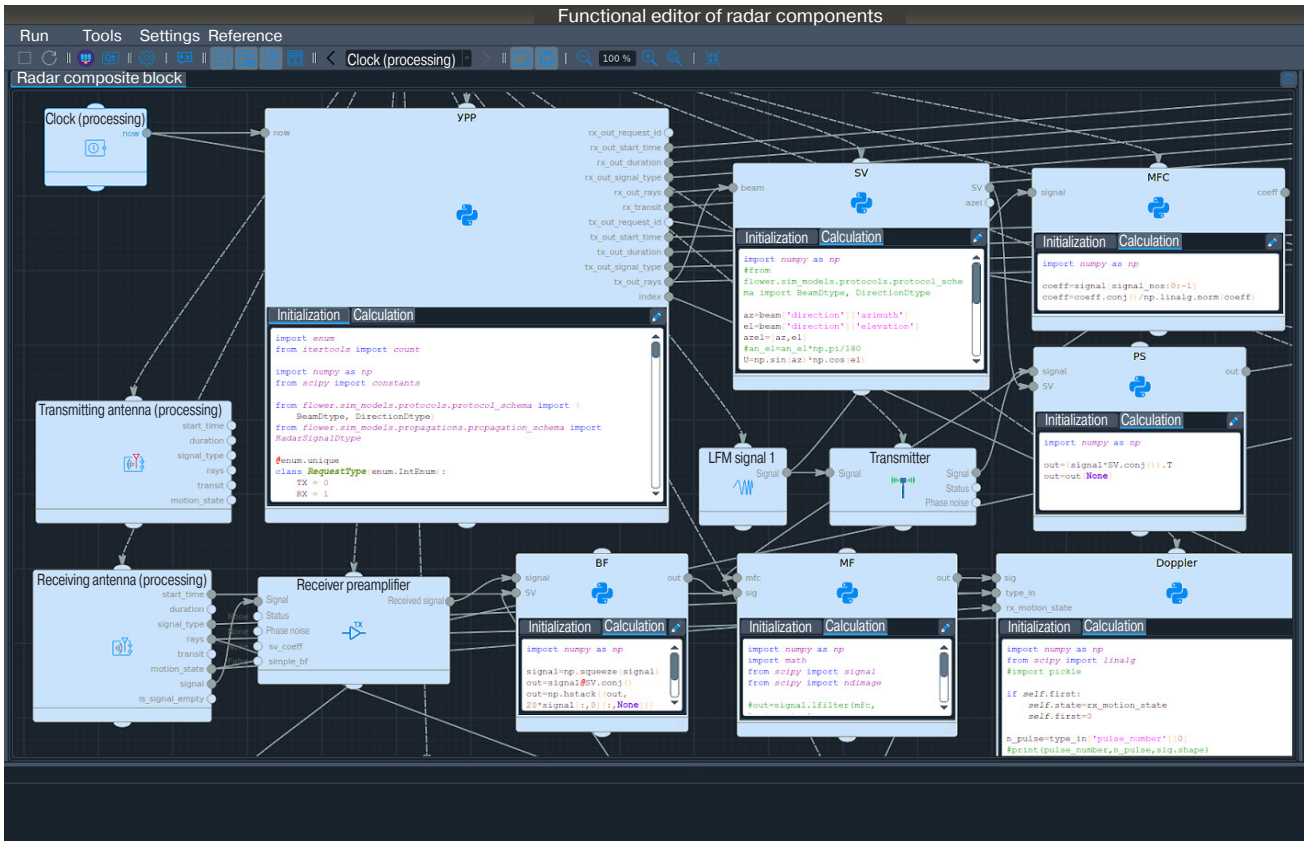

Fig. 1. Visual functional editor and radar model blocks

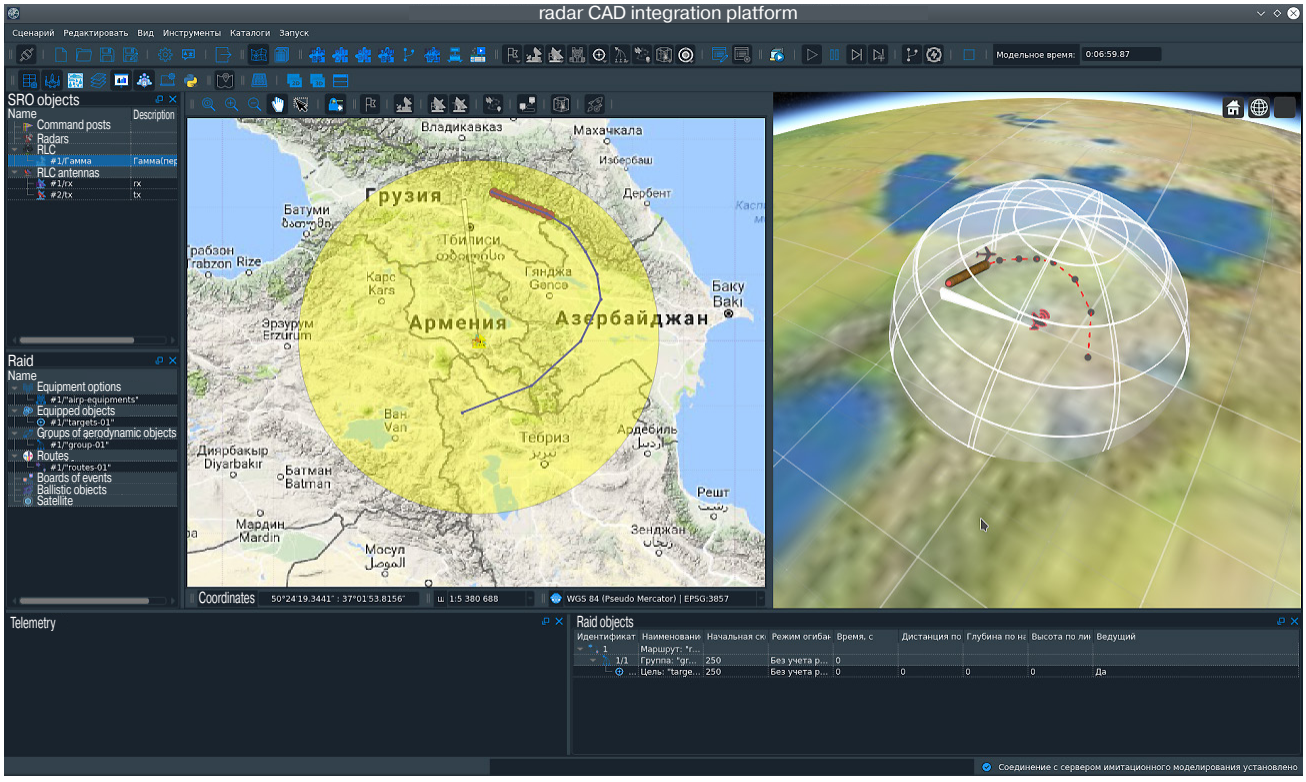

Fig. 2. Interface of the module of engineering calculation and simulation

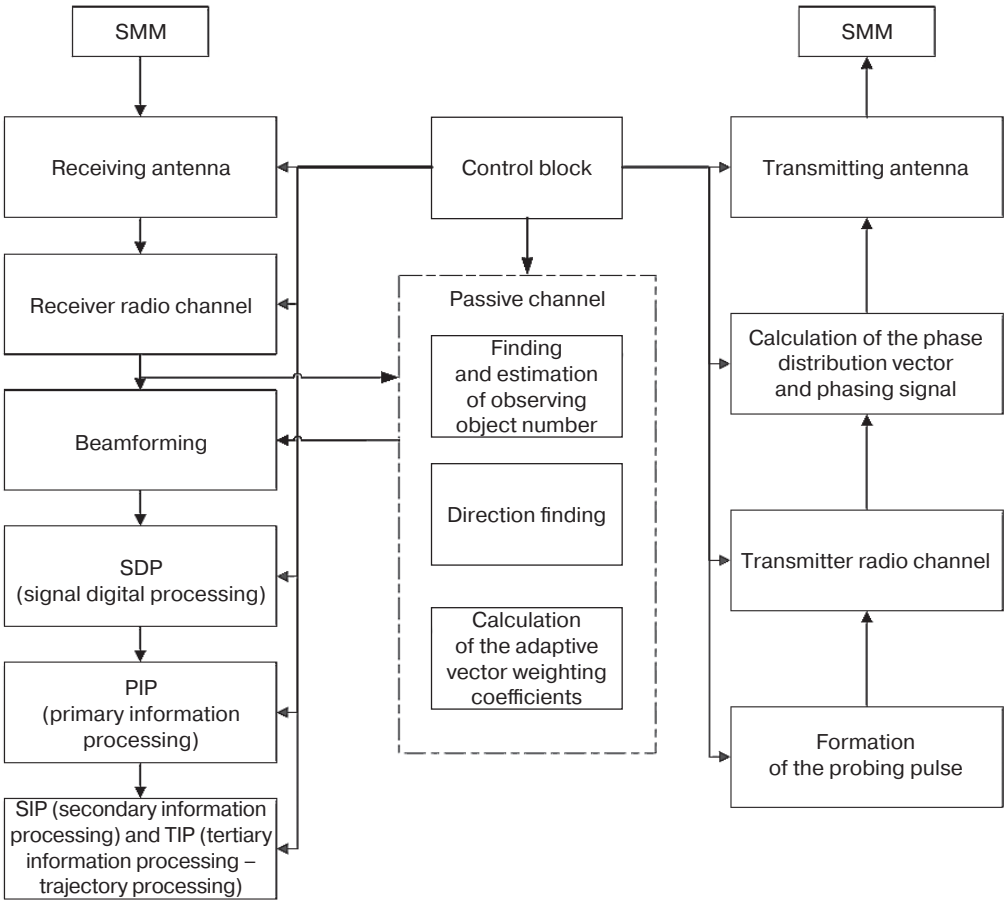

Fig. 3. Block-diagram of radar CAD

The radar model implements a passive channel for processing stochastic signals from external sources. In this case, training data comprising time samples with a DAA of length $K = 256$ are used.

2.2. Radar simulation algorithms

Algorithm for detecting stochastic signals

The model implements an asymptotically optimal algorithm for detecting stochastic signals using the decision statistics obtained from the generalized likelihood ratio test criterion [12]:

$$Q_{\mathrm{D}} = \frac{N\hat{\lambda}_1}{Tr\hat{\mathbf{R}}}, \quad (1)$$

where N is the number of DAA elements; $\hat{\mathbf{R}} = \frac{1}{K}\mathbf{X}\mathbf{X}^{\mathrm{H}}$ is the sample estimate of the correlation matrix; $\mathbf{X}$ is the training data package; Tr is the trace of the matrix; $\hat{\lambda}_1$ is the maximum eigenvalue of the matrix $\hat{\mathbf{R}}$.

Algorithm for estimating the number of stochastic signals

The model implements an asymptotically optimal algorithm for estimating the number of stochastic signals

$$\hat{M} = \arg\min_n \left(Q_n < d_n(\alpha)\right) - 1, \; n = 1, \ldots, N, \quad (2)$$

where $d_n(\alpha)$ is the threshold calculated from the given false alarm level α; Q_n is the decision statistic obtained from the generalized likelihood ratio test [13]:

$$Q_n = \frac{(N-n+1)\hat{\lambda}_n}{\sum_{i=n}^{N}\hat{\lambda}_i}, \quad (3)$$

where $\hat{\lambda}_i$ is the ith largest eigenvalue of the matrix $\hat{\mathbf{R}}$.

Algorithm for direction finding of sources of stochastic signals

For direction finding of sources of stochastic signals, the Capon algorithm is implemented, which uses the calculation of the spatial spectrum [14, 15]:

$$Q_{\mathrm{C}} = \frac{1}{\mathbf{V}^{\mathrm{H}}\hat{\mathbf{R}}^{-1}\mathbf{V}}, \quad (4)$$

where $\mathbf{V}$ is a hypothesis vector; $(\cdot)^{\mathrm{H}}$ is the Hermitian conjugacy symbol.

Adaptive spatial filtering (ASF) algorithm

The model implements the calculation of the adaptive weight vector according to the formula [14, 15]:

$$\mathbf{W} = \hat{\mathbf{R}}^{-1}\mathbf{S}, \quad (5)$$

where **S** is the steering vector.

All of the above algorithms are implemented in the blocks of the radar model in Python using the NumPy and SciPy modules.

3. SIMULATION MODELLING RESULTS

3.1. Simulation modeling scenario

To carry out the simulation, a model of a sector surveillance radar with electronic beam scanning was created. This model includes a passive channel that implements the processing of stochastic signals from external sources. The radar model was located in the area of St. Petersburg. Two azimuthally separated aerodynamic objects of observation were set (Fig. 4) with the option of installing stochastic signal sources on them. In terms of their presence, three scenarios were modeled:

1) no sources of stochastic signals;
2) one source of stochastic signals;
3) two sources of stochastic signals.

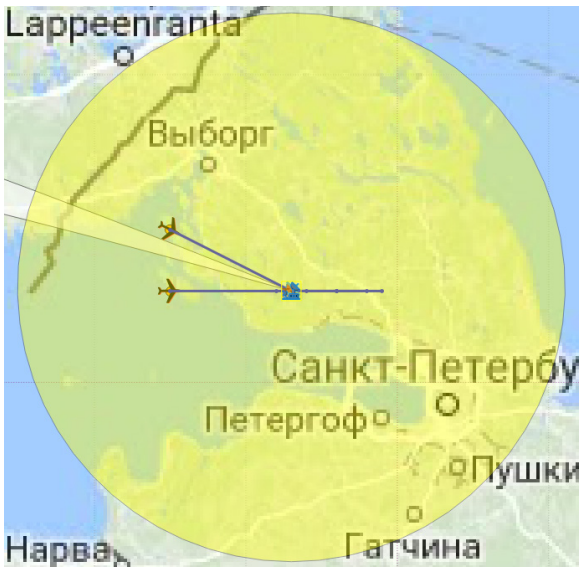

Fig. 4. Position of the radar and objects of observation

3.2. Results of the algorithms operation for detecting and estimating the number of sources

In the first scenario, the algorithms for detecting and estimating the number of sources showed the expected results—the sign of detection and estimate of the number are equal to zero. Figure 5 shows the result of the operation of these algorithms for several cycles of radar operation—the cycles of transmission and reception.

In the second scenario, the algorithms for detecting and estimating the number showed the expected results—the sign of detection and the estimate of the number of sources are equal to one (Fig. 6).

In the third scenario, the algorithms for detecting and estimating the number also showed the expected results—the detection sign is equal to one, while the estimated number is two (Fig. 7).

3.3. Results of the direction-finding algorithm

In the first scenario, there are no results, because the direction-finding algorithm is started only if the sign of detection is equal to one.

In the second scenario, one source of stochastic signals is located. Figure 8 shows the spatial spectrum in the generalized biconical coordinate system (GBCS) (the horizontal axis is the azimuth, the vertical axis is the elevation), built according to the results of the algorithm.

In the third scenario, two sources of stochastic signals are located. Figure 9 shows the spatial spectrum in the GBCS (the horizontal axis is the azimuth; the vertical axis is the elevation) constructed based on the results of the algorithm

The estimates of the angular coordinates of the sources of stochastic signals in the spherical coordinate system are as follows:

- 1st source: (1.3°; 0.3°), true position: (1.8°; −0.2°);
- 2nd source: (27.5°; 0.3°), true position: (27.2°; −0.2°).

As can be seen, the estimates coincide with the true position of the sources to within fractions of a degree. A further increase in the accuracy of the estimate is possible when using a grid of angles with a smaller discrete to construct the spatial spectrum.

3.4. Results of the ASF algorithm

In the absence of interfering signals, both objects of observation were detected, with marks being issued for them (yellow markers in Fig. 10). In this scenario, in the absence of interfering signals (the detection sign is equal to zero), the ASF algorithm was not activated, and a non-adaptive beam was formed for reception.

In the presence of one source of interfering signal placed on the right object of observation, the central object of observation was detected; marks were issues for it (yellow markers in Fig. 11, blue markers—the true position of the object of observation). No object of observation whose source comprised an

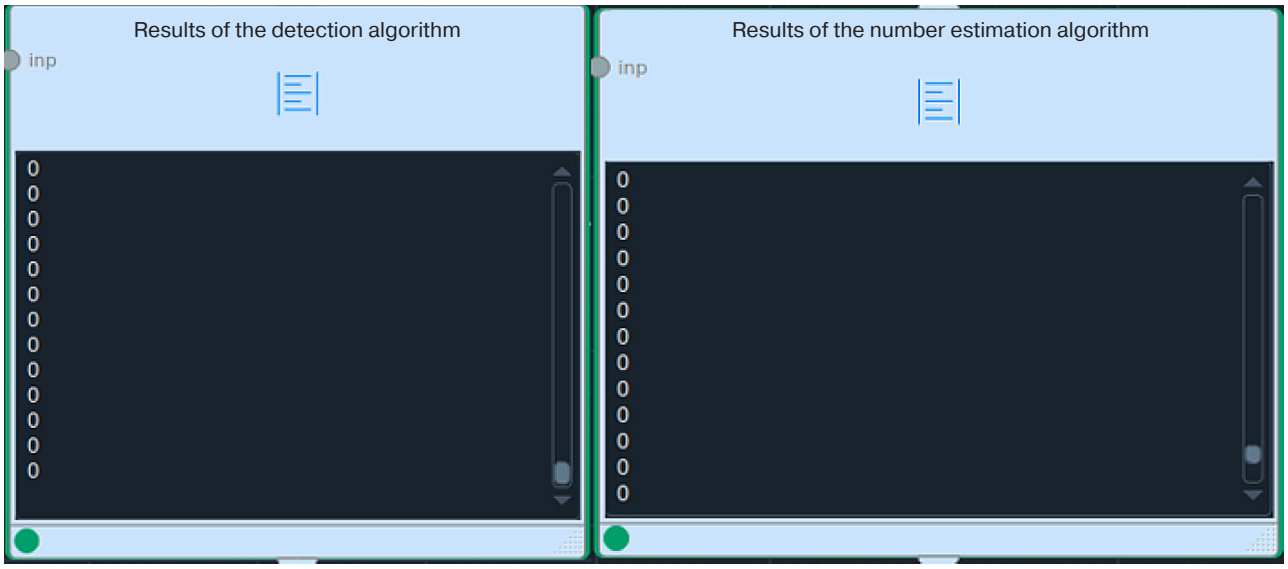

Fig. 5. Output of algorithms for detecting and estimating the number in a scenario 1

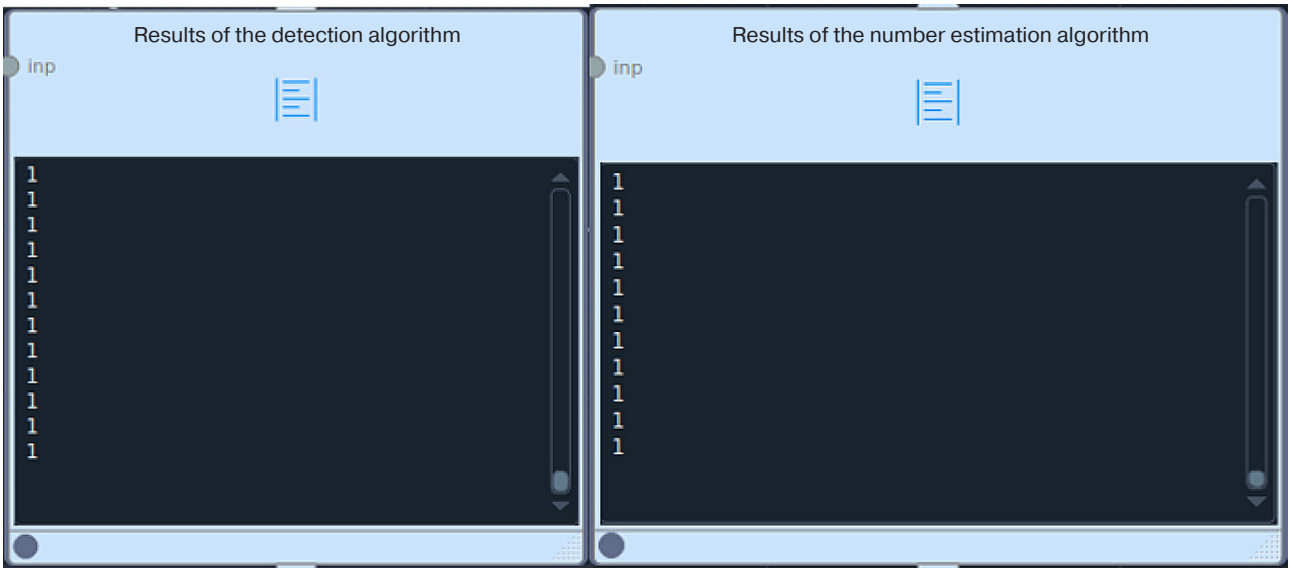

Fig. 6. Output of the algorithm for detecting and estimating the number in scenario 2

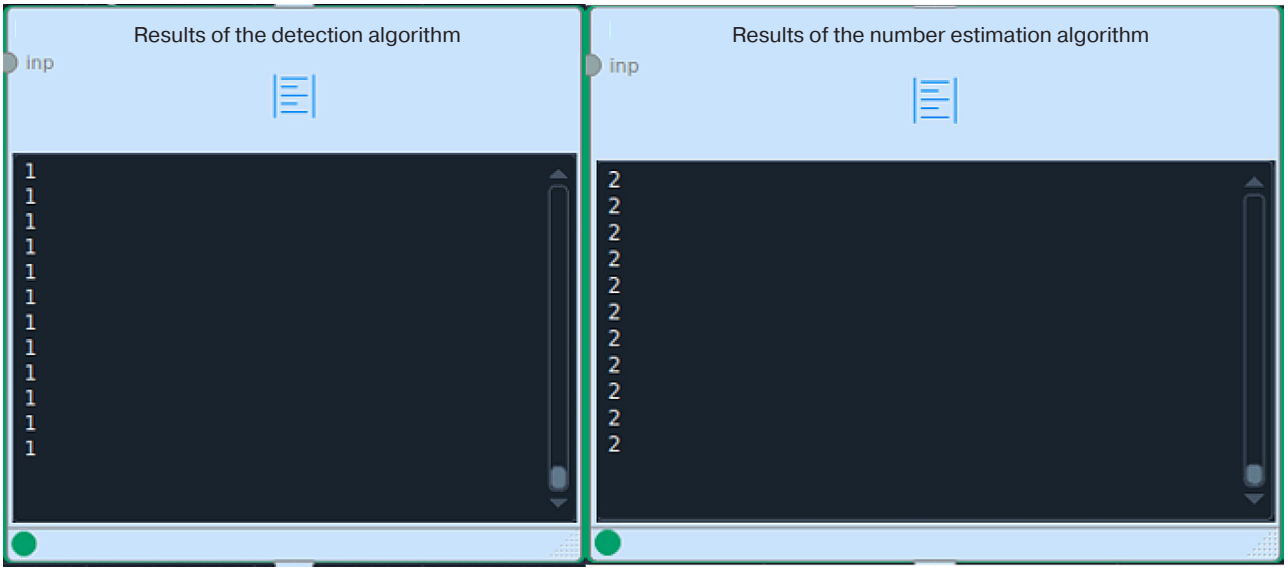

Fig. 7. Output of the algorithm for detecting and estimating the number in scenario 3

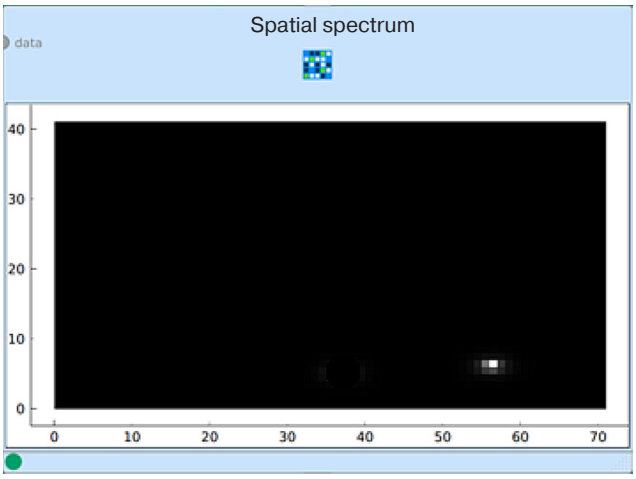

Fig. 8. Algorithm output for direction finding in Scenario 2

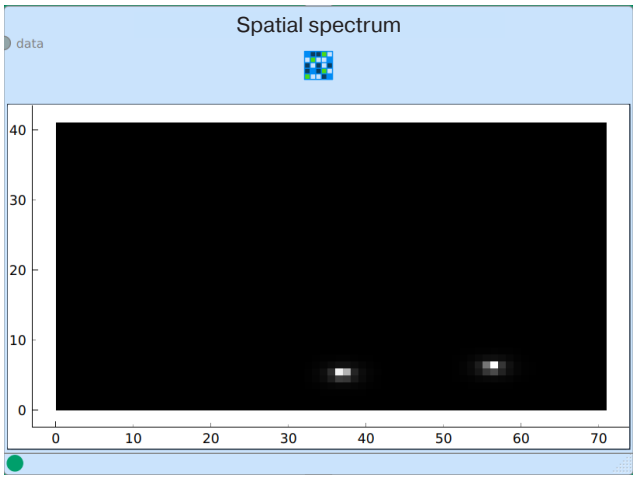

Fig. 9. Algorithm output for direction finding in Scenario 3

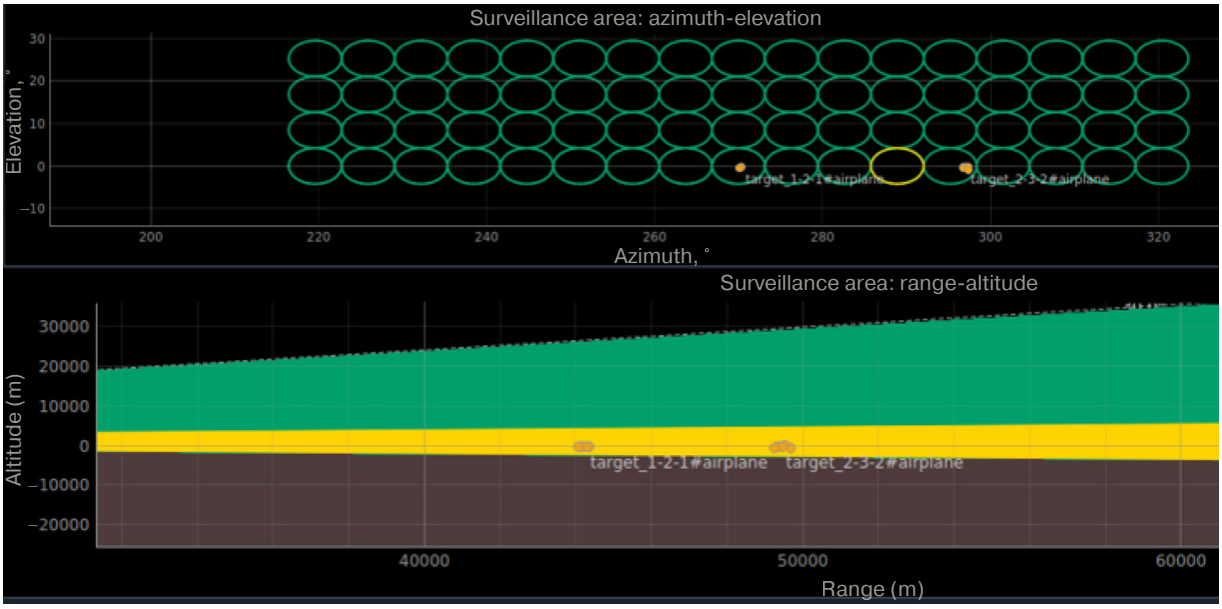

Fig. 10. Indicators "azimuth-elevation" and "range-altitude" in scenario 1

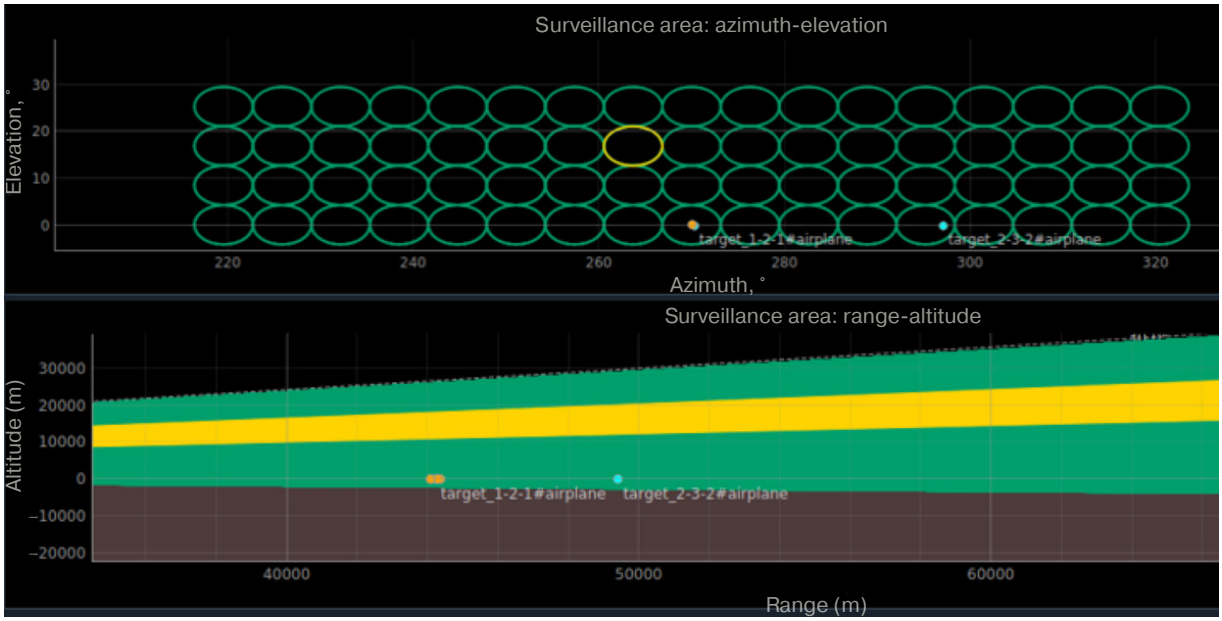

Fig. 11. Indicators "azimuth-elevation" and "range-altitude" in scenario 2

interfering signal was detected because the ASF algorithm cannot suppress an interfering signal if its angular direction coincides with the direction of the useful signal.

In the presence of two interfering signals, the objects of observation were not detected.

Let us estimate the efficiency of the ASF algorithm based on the results of the simulation. To do this, it is necessary to find the values of the following quantities before and after adaptation [16]:

- power of the useful signal at the output of the array;
- interference to noise ratio at the output in terms of power (INR);
- signal to interference + noise power ratio (SINR).

To calculate these values, the following parameters were calculated:

- useful signal output power

$$P_S = \sigma_S^2 \left| \mathbf{W}^H \mathbf{V}_S \right|^2, \quad (6)$$

where σ_S^2 is the signal power in the array element; $\mathbf{W}$ is the weight vector; $\mathbf{V}_S$ is the vector of the amplitude-phase distribution of the field of the useful signal in the array opening;

- output power of interferences and noises

$$P_{JN} = \mathbf{W}^H \hat{\mathbf{R}} \mathbf{W} = \frac{1}{K} \left\| \mathbf{W}^H \mathbf{X} \right\|^2, \quad (7)$$

where $\|\cdot\|$ is the Euclidean norm of the vector;

- intrinsic noise power at the array output

$$P_N = \sigma_N^2 \|\mathbf{W}\|^2, \quad (8)$$

where σ_N^2 is the intrinsic noise power in the array element.

To obtain a more accurate estimation, the data packet $\mathbf{X}$ used when calculating the output power of interference and noise was different from that used to calculate the adaptive weight vector. The estimates are given in Table. As follows from the presented results, the interference was suppressed almost completely to a level below the intrinsic noise of the antenna array.

Table. Results of evaluation of the effectiveness of ASF

Evaluated values	Before ASF	After ASF
P_S, dB	−94.4	−94.4
P_{JN}, dB	−85.0	−118.0
P_N, dB	−118.1	−118.1
INR, dB	33.1	−16.4
SINR, dB	−9.4	23.6

In order to illustrate the operation of the algorithm, Fig. 12 shows a section of the phased array antenna (PAA) pattern in scenario 2. The observed deep dip formed in the pattern in the direction of the interference confirms the correct operation of the algorithm.

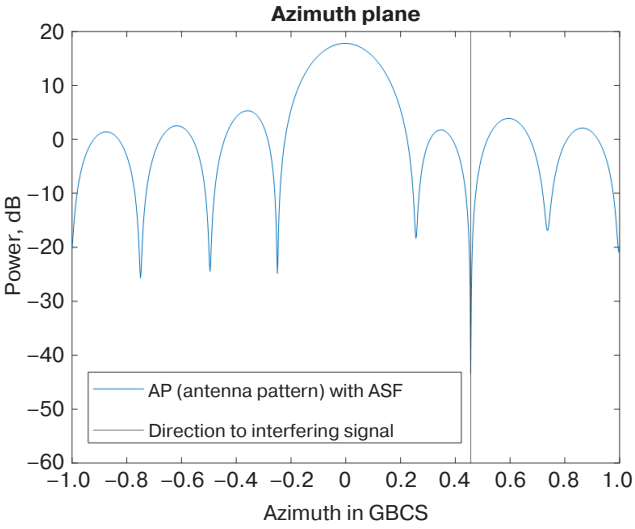

Fig. 12. Section of the PAA pattern

CONCLUSIONS

The Russian radar CAD system presents great opportunities for developing radar operation models, allowing the processing of various types of signals to be simulated in detail. For this purpose, a visual functional editor is used in which the radar model is built from a set of blocks. The module of engineering calculation and simulation allows the created radar model to be placed on the ground along with the preset raid scenario. To demonstrate these capabilities, a model of a sector surveillance radar with electronic beam scanning was created in which the implemented passive channel uses the processing of stochastic signals from external sources. Simulation modeling was carried out according to three scenarios of the aerospace environment. The results of the algorithms are fully consistent with the theoretical prediction.

Authors' contributions

M.Yu. Konopel'kin—conducting research, configuring radar model templates, setting a tactical task, setting up a noise/signal environment, and editing the text of the article.

S.V. Petrov—adaptation of the algorithms for using in a CAR radar and their implementation, script development, conducting simulation experiments, and writing the text of the article.

D.A. Smirnyagina—implementing the algorithms, conducting simulation experiments, analyzing the results obtained, and writing the text of the article.

REFERENCES

1. Sozinov P.A., Konoval'chik A.P., Saushkin V.P. Relevant questions of indigenous CAD development for radar engineering. *Vestnik vozdushno-kosmicheskoi oborony = Aerospace Defense Herald*. 2019;3(23):106–119 (in Russ.).
2. Sozinov P.A., Konoval'chik A.P. Basic approaches to the development of a domestic system of automated design of radar stations and current results. *Radiotekhnika = Radioengineering.* 2020;84(7–13):62–74 (in Russ.). https://doi.org/10.18127/j00338486-202007(13)-08
3. Konoval'chik A.P., Konopel'kin M.Yu., Shchiryi A.O., Arutyunyan A.A. Stages of designing advanced radar stations in specialized domestic CAD system. *Vestnik vozdushno-kosmicheskoi oborony = Aerospace Defense Herald.* 2020;4(28):111–119 (in Russ.).
4. Konoval'chik A.P. Computer-aided design of radar stations: principles for constructing the design process. *Vestnik vozdushno-kosmicheskoi oborony = Aerospace Defense Herald.* 2021;2(30):52–64 (in Russ.).
5. Konoval'chik A.P., Konopel'kin M.Yu., Plaksenko O.A., Shchiryi A.O. Statement of the task of development and preliminary architecture of the domestic CAD radar of a full end-to-end cycle. *Novye informatsionnye tekhnologii v avtomatizirovannykh sistemakh = New Information Technologies in Automated Systems.* 2017;20:127–130 (in Russ.).
6. Konoval'chik A.P., Plaksenko O.A., Shchiryy A.O. The concept of multi-level design of radars in the developed CAD radar of a full end-to-end cycle. *Fundamental'nyye problemy radioelektronnogo priborostroyeniya = Fundamental Problems of Radio-Electronic Instrumentation.* 2017;17(4):889–892 (in Russ.).
7. Konoval'chik A.P., Konopel'kin M.Y., Plaksenko O.A., Shchiryy A.O. Domestic system for computer-aided design of radar systems, complexes and stations, taking into account the means of aerospace attack. *Naukoyemkiye tekhnologii v kosmicheskikh issledovaniyakh Zemli = H&ES Research.* 2018;10(1):40–47 (in Russ.).
8. Konoval'chik A.P., Plaksenko O.A., Shchiryy A.O. Functions of simulating combat actions in the developed domestic CAD radar of a full end-to-end cycle. *Voprosy radioelektroniki= Issues of Radio Electronics*. 2018;3: 30–34 (in Russ.).
9. Konoval'chik A.P., Plaksenko O.A., Shchiryy A.O. Implementation of simulation modeling in the developed domestic CAD radar of a full end-to-end cycle. *Novyye informatsionnyye tekhnologii v avtomatizirovannykh sistemakh = New Information Technologies in Automated Systems*. 2018;21:290–293 (in Russ.).
10. Konoval'chik A.P., Plaksenko O.A., Shchiryy A.O. Substantiation of the appearance of promising radar stations using the developed domestic computer-aided design system. *Naukoyemkiye tekhnologii v kosmicheskikh issledovaniyakh Zemli = H&ES Research*. 2019;11(1): 4–11 (in Russ.).
11. Skolnik M.I. *Radar Handbook*. Third Edition. McGraw-Hill; 2008. 1328 p.

СПИСОК ЛИТЕРАТУРЫ

1. Созинов П.А., Коновальчик А.П., Саушкин В.П. Актуальные вопросы создания отечественной САПР для проектирования РЛС. *Вестник воздушно-космической обороны*. 2019;3(23):106–119.
2. Созинов П.А., Коновальчик А.П. Основные подходы к разработке отечественной системы автоматизированного проектирования радиолокационных станций и текущие результаты. *Радиотехника*. 2020;84(7–13): 62–74. https://doi.org/10.18127/j00338486-202007(13)-08
3. Коновальчик А.П., Конопелькин М.Ю., Щирый А.О., Арутюнян А.А. Этапы проектирования перспективных радиолокационных станций в специализированной САПР. *Вестник воздушно-космической обороны.* 2020;4(28):111–119.
4. Коновальчик А.П. Система автоматизированного проектирования радиолокационных станций: принципы построения процесса проектирования. *Вестник воздушно-космической обороны.* 2021;2(30): 52–64.
5. Коновальчик А.П., Конопелькин М.Ю., Плаксенко О.А., Щирый А.О. Постановка задачи разработки и предварительная архитектура отечественной САПР РЛС полного сквозного цикла. *Новые информационные технологии в автоматизированных системах.* 2017;20:127–130.
6. Коновальчик А.П., Плаксенко О.А., Щирый А.О. Концепция многоуровневого проектирования РЛС в разрабатываемой САПР РЛС полного сквозного цикла. *Фундаментальные проблемы радиоэлектронного приборостроения.* 2017;17(4):889–892.
7. Коновальчик А.П., Конопелькин М.Ю., Плаксенко О.А., Щирый А.О. Отечественная система автоматизированного проектирования радиолокационных систем, комплексов и станций с учетом средств воздушно-космического нападения. *Наукоемкие технологии в космических исследованиях Земли.* 2018;10(1):40–47.
8. Коновальчик А.П., Плаксенко О.А., Щирый А.О. Функции имитации боевых действий в разрабатываемой отечественной САПР РЛС полного сквозного цикла. *Вопросы радиоэлектроники.* 2018;3:30–34.
9. Коновальчик А.П., Плаксенко О.А., Щирый А.О. Реализация имитационного моделирования в разрабатываемой отечественной САПР РЛС полного сквозного цикла. *Новые информационные технологии в автоматизированных системах.* 2018;21:290–293.
10. Коновальчик А.П., Плаксенко О.А., Щирый А.О. Обоснование облика перспективных радиолокационных станций посредством разрабатываемой отечественной системы автоматизированного проектирования. *Наукоемкие технологии в космических исследованиях Земли.* 2019;11(1):4–11.
11. Skolnik M.I. *Radar Handbook*. Third Edition. McGraw-Hill; 2008. 1328 p.
12. Петров С.В. Синтез и анализ алгоритмов обнаружения стохастических сигналов в системах с многоэлементной антенной решеткой. *Антенны*. 2015;7: 29–36.

12. Petrov S.V. Synthesis and analysis of stochastic signal detection algorithms in the multi-element antenna array systems. *Antenny = Antennas*. 2015;7:29–36 (in Russ.).
13. Petrov S.V. Synthesis and analysis of the algorithm for estimating the number of stochastic signals in systems with a multi-element antenna array. *Antenny = Antennas.* 2015;9:15–22 (in Russ.).
14. Ratynskii M.V. *Adaptatsiya i sverkhrazreshenie v antennykh reshetkakh* (*Adaptation and Superresolution in Antenna Arrays*). Moscow: Radio i svyaz'; 2003. 200 p. (in Russ.).
15. Van Trees H.L. *Detection, estimation and modulation theory. Part IV. Optimum array processing.* Wiley; 2002. 1443 p.
16. Ratynskiy M.V. On the evaluation of adaptive spatial filtering efficiency. *Radiotekhnika = Radioengineering*. 2013;8:38–44 (in Russ.).
13. Петров С.В. Синтез и анализ алгоритма оценивания числа стохастических сигналов в системах с многоэлементной антенной решеткой. *Антенны.* 2015;9:15–22.
14. Ратынский М.В. *Адаптация и сверхразрешение в антенных решетках.* М.: Радио и связь; 2003. 200 с.
15. Van Trees H.L. *Detection, estimation and modulation theory. Part IV. Optimum array processing.* Wiley; 2002. 1443 p.
16. Ратынский М.В. Оценка эффективности адаптивной пространственной фильтрации. *Радиотехника.* 2013;8:38–44.

About the authors

Maxim Yu. Konopel'kin, Head of Department, "Almaz-Antey" Air and Space Defence Corporation (41, Vereiskaya ul., Moscow, 121471 Russia). E-mail: m.konopelkin@almaz-antey.ru. RSCI SPIN-code 6660-4641, https://orcid.org/0000-0002-0654-3845

Sergey V. Petrov, Cand. Sci. (Eng.), Lead Programmer, "Almaz-Antey" Air and Space Defence Corporation (41, Vereiskaya ul., Moscow, 121471 Russia). E-mail: sv.petrov@almaz-antey.ru. https://orcid.org/0000-0001-5370-9898

Daria A. Smirnyagina, Techician, "Almaz-Antey" Air and Space Defence Corporation (41, Vereiskaya ul., Moscow, 121471 Russia). E-mail: ponyoo@mail.ru. https://orcid.org/0000-0002-7237-2511

Об авторах

Конопелькин Максим Юрьевич, начальник отдела, Акционерное общество «Концерн воздушно-космической обороны «Алмаз-Антей» (121471, Россия, Москва, ул. Верейская, 41). E-mail: m.konopelkin@almaz-antey.ru. SPIN-код РИНЦ 6660-4641, https://orcid.org/0000-0002-0654-3845

Петров Сергей Викторович, к.т.н., ведущий программист, Акционерное общество «Концерн воздушно-космической обороны «Алмаз-Антей» (121471, Россия, Москва, ул. Верейская, 41). E-mail: sv.petrov@almaz-antey.ru. https://orcid.org/0000-0001-5370-9898

Смирнягина Дарья Алексеевна, техник, Акционерное общество «Концерн воздушно-космической обороны «Алмаз-Антей» (121471, Россия, Москва, ул. Верейская, 41). E-mail: ponyoo@mail.ru. https://orcid.org/0000-0002-7237-2511

Translated from Russian into English by Evgenii I. Shklovskii
Edited for English language and spelling by Thomas A. Beavitt

UDC 621.311.68
https://doi.org/10.32362/2500-316X-2022-10-5-60-72

RESEARCH ARTICLE

Development and research of uninterruptible power supply system for networks with supply voltage up to 24 V

Igor M. Sharov [@], Oleg A. Demin, Alexander A. Sudakov, Alexey D. Yarlykov

MIREA – Russian Technological University, Moscow, 119454 Russia
[@] Corresponding author, e-mail: ctosworld@gmail.com

Abstract

Objectives. Due to the continuous rapid development of renewable energy sources, requirements for secondary power supply systems keep increasing from year to year. Productive uptime for end users is dependent on the efficiency and stability of the power supply system. Such systems should be able to distribute and store energy from renewable sources having various parameters and configurations. Therefore, the present work is aimed at developing technical solutions for efficient uninterruptible secondary power supply systems in low voltage DC networks.

Methods. Advanced circuitry solutions are used for performing pulse conversions with high efficiency. The flexible hardware-software system is used for implementing the parameter control system.

Results. An uninterruptible power supply for low-voltage DC networks is developed. The description of subsystems and calculations for all main elements including the power ones are given. Using a contemporary component base, the system prototype is assembled, configured, and measured by parameters. The presented solutions allow achieving the universality of the system in terms of the input and output voltage range. Support for the fast-charging Power Delivery protocol is integrated. As well as regulating the battery charging current and voltage, the Li+ battery charging controller permits changes in the number of chargeable cells. The monitoring and control unit monitors network parameters and controls the system automation. Using a microcontroller as the control device, it is possible to easily change control parameters by changing software settings. Dual redundancy of the module monitoring the built-in battery parameters is used to ensure the reliability and safety of system functioning. Support for the standardized I^2C communication protocol with a separate power bus allows any necessary sensors to be connected for monitoring system parameters. External high-power devices controlled by a PWM signal may be added, if required. In the paper, the Li+ battery charging profile recommended by the manufacturer is provided.

Conclusions. The designed system provides stable power supply to end users at a power consumption up to 40 W for at least 45 min. The automation demonstrates reliable operation.

Keywords: uninterruptible power supply, control unit, charge controller, Power Delivery standard, charging curve, battery protection system, DC-DC converter, battery balancing

• **Submitted:** 09.11.2021 • **Revised:** 01.07.2022 • **Accepted:** 26.08.2022

For citation: Sharov I.M., Demin O.A., Sudakov A.A., Yarlykov A.D. Development and research of uninterruptible power supply system for networks with supply voltage up to 24 V. *Russ. Technol. J.* 2022;10(5):60–72. https://doi.org/10.32362/2500-316X-2022-10-5-60-72

Financial disclosure: The authors have no a financial or property interest in any material or method mentioned.

The authors declare no conflicts of interest.

НАУЧНАЯ СТАТЬЯ

Разработка и исследование системы бесперебойного питания в сетях с напряжением до 24 В

И.М. Шаров [@], О.А. Демин, А.А. Судаков, А.Д. Ярлыков

МИРЭА – Российский технологический университет, Москва, 119454 Россия
[@] Автор для переписки, e-mail: ctosworld@gmail.com

Резюме

Цели. От эффективности и стабильности систем электропитания зависит время бесперебойной работы конечных потребителей. Такие системы должны иметь возможность распределения и накопления энергии от возобновляемых источников с различными параметрами и конфигурациями. Развитие источников возобновляемой энергии постоянно увеличивает требования к системам вторичного электропитания. Целями работы являются разработка научно-обоснованных технических решений и создание эффективной системы бесперебойного вторичного питания в низковольтных сетях постоянного тока.

Методы. Использованы современные схемотехнические решения для выполнения импульсных преобразований с высокой эффективностью. Для реализации системы контроля параметров применен гибкий программно-аппаратный комплекс.

Результаты. Разработана система бесперебойного питания для низковольтных сетей постоянного тока. Приведено описание работы блоков системы и расчеты основных элементов, в т.ч. и силовых. С применением современной элементной базы собран прототип системы, проведена настройка и измерение ее параметров. За счет представленных решений достигается универсальность комплекса по диапазону входных и выходных напряжений. Интегрирована поддержка современного протокола быстрой зарядки Power Delivery. Примененный контроллер зарядки Li+ аккумуляторов позволяет изменять количество заряжаемых ячеек и регулировать токи и напряжения заряда аккумуляторной батареи (АКБ). Блок мониторинга и управления отслеживает текущие параметры сети и управляет автоматикой системы. Использование микроконтроллера в качестве управляющего устройства дает возможность изменения параметров управления без конструктивных изменений благодаря редактированию программного обеспечения. Для безопасности функционирования системы применено двукратное резервирование модуля контроля параметров встроенной аккумуляторной батареи. Поддержка стандартизированного протокола обмена данными по шине I^2C с отдельной шиной питания позволяет подключать любые необходимые датчики для отслеживания параметров системы. При необходимости могут быть добавлены сторонние устройства повышенной мощности, управляемые сигналом широтно-импульсной модуляции (ШИМ). Приведен рекомендуемый производителями профиль заряда Li+ АКБ.

Выводы. Спроектированная система позволяет обеспечивать стабильное электропитание потребителей с энергопотреблением до 40 Вт в течение времени не менее 45 мин. Автоматика демонстрирует безотказное функционирование.

Ключевые слова: система бесперебойного питания, блок управления, контроллер заряда, протокол Power Delivery, профиль заряда, блок защиты, DC-DC преобразователь, модуль балансировки

• **Поступила:** 09.11.2021 • **Доработана:** 01.07.2022 • **Принята к опубликованию:** 26.08.2022

Для цитирования: Шаров И.М., Демин О.А., Судаков А.А., Ярлыков А.Д. Разработка и исследование системы бесперебойного питания в сетях с напряжением до 24 В. *Russ. Technol. J.* 2022;10(5):60–72. https://doi.org/10.32362/2500-316X-2022-10-5-60-72

Прозрачность финансовой деятельности: Авторы не имеют финансовой заинтересованности в представленных материалах или методах.

Авторы заявляют об отсутствии конфликта интересов.

INTRODUCTION

Due to the development of renewable energy sources including their increased capacity, solutions are required for a number of problems associated with the conversion and storage of energy [1]. Automation systems used for these purposes should be developed using new circuit solutions aimed, among other things, at increasing operating efficiency, speed, and autonomy, at the same time as reducing heat generation, safely preventing abnormal operation, maintaining cost-effectiveness, etc. The standard output voltage of power systems in industrial automation and motor vehicles is 24 V. Such power systems can provide power to low-power devices in case of emergency.

Laying networks for emergency equipment is combined with additional time and material costs. This is especially true for emergency lighting systems in remote locations [2]. Such costs can be reduced by using a separate power supply units in the fixed version as a voltage source. Since the power consumption for sensor operation is low, the operating time of such units is satisfactory in the absence of recharging.

24 V power networks are also used in the security and fire safety systems [3]. In this setting, it is obvious that fail-safe power supply is required even under conditions of network failure. The Shtyl[1] and Bastion[2] companies produce uninterruptible power supplies (UPS) in the form of wall mount boxes. A 24 V power supply is also typically used by audio systems, for example, by a great number of device components manufactured by the MONACOR International company[3, 4]. Here, UPS systems can be integrated into devices in the form of modules or to ensure network continuity as a separate unit. It is also theoretically possible to use 24 V UPS systems to ensure the safety of trucks in the event of grid network failure[5]. UPS systems in the form of separate units are necessary attributes of equipment cabinets. Such systems must ensure safe and stable operation throughout their lifetime.

1. UPS SYSTEM

A conventional UPS system consists of two independent devices capable of operating both independently and together, thus expanding the possibilities of applying and reconfiguring the final product. The structural diagram of the UPS system is shown in Fig. 1.

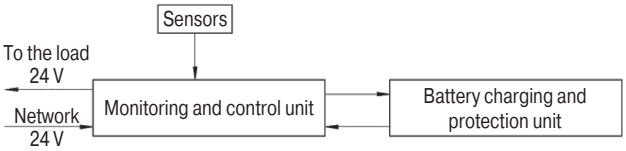

Fig. 1. Structural diagram of the UPS system

The UPS system consists of the monitoring and control unit, battery charging and protection unit, and external sensors. A similar system has been implemented in [4] but using a 220 V power supply.

The monitoring and control unit is designed for controlling the network and battery parameters, as well as the equipment temperature. At the moment of emergency shutdown, the unit commutates the system so that the necessary voltage is supplied from the battery charging and protection unit to the load. This provides the uninterrupted power supply of connected devices from the backup power supply. In addition, output currents and power are monitored while operating from the UPS system. Should the UPS permissible power consumption be exceeded, the load connected to the system is automatically switched off.

The battery charging and protection unit is designed for charging the built-in batteries and equalizing the potential between cells. When the built-in lithium-ion battery is discharged, backup power from any battery having voltage greater than 9 V—e.g., from widespread automotive lead-acid batteries—may be supplied. It is also possible to supply backup power from portable batteries supporting the Power Delivery fast-charging protocol. The unit duplicates critical system protection functions, preventing

[1] https://www.shtyl.ru/. Accessed August 29, 2022 (in Russ.).
[2] https://bast.ru/. Accessed August 29, 2022 (in Russ.).
[3] https://www.monacor.com/. Accessed August 29, 2022.
[4] MONACOR INTERNATIONAL GmbH & Co. KG; 2016. 164 p. https://www.blej24.com/catalogs/Monacor.pdf. Accessed August 29, 2022.
[5] *MAN TGA s 2000 g. Rukovodstvo po remontu i ekspluatatsii* (*MAN TGA from 2000 y. Repair and operation manual*). Monolit; 2015. 794 p. https://monolith.in.ua/catalog/rukovodstvo_po_remontu_man_tga_2000. Accessed August 29, 2022 (in Russ.).

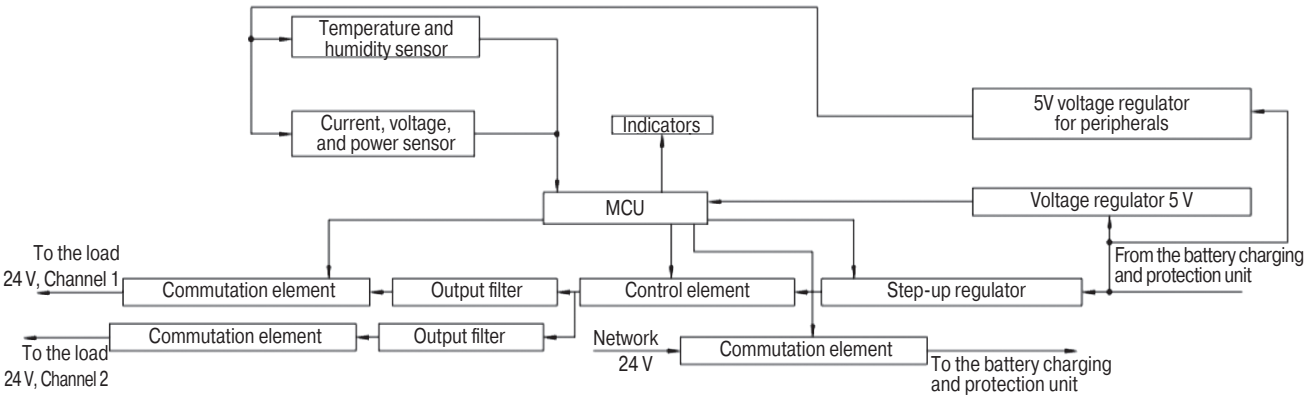

Fig. 2. Structural diagram of the monitoring and control unit

"overcharging" and deep discharging of the battery, as well as monitoring the temperature of the built-in battery using a thermistor.

2. MONITORING AND CONTROL UNIT

In the paper, the monitoring and control unit implemented on the ATmega 168 (Atmel Corporation (Microchip), USA) microcontroller (MCU) is considered [5]. Here, MCU with a clock frequency of 16 MHz, supply voltage, and logic levels of 5 V is used[6]. This version is selected due to its low cost and availability, an especially important factor under the present situation of crisis in the semiconductor industry. If necessary, it can be replaced without serious labor costs by a more productive and energy-efficient unit involving minor modifications of the circuit diagram. The structural diagram of the monitoring and control unit is shown in Fig. 2.

The circuit diagram of the monitoring and control unit shown in Figs. 3, 5, and 6 comprises two 5 V linear voltage regulators, MCU, state indicators, step-up (boost) regulator, three commutation elements, output filters, control element, and connector X1 for connecting sensors via I^2C bus with power supply.

The step-up regulator U1 (Fig. 3) is implemented on an XL6009 chip (XLSEMI, China). With an input voltage ranging from 5 V to U_{out}, its conversion efficiency may achieve 94% depending on the difference between input and output voltages. The conversion frequency is 400 kHz, while the maximum commutated current is 4 A. Soft start, thermal protection, and current limitation functions are built in[7]. The output voltage may be calculated by the following formula:

$$U_{out} = 1.25\left(1+\frac{R_{13}}{R_{14}}\right) = 1.25\left(1+\frac{18\ \text{k}\Omega}{1\ \text{k}\Omega}\right) = 23.75\ \text{V}. \quad (1)$$

Inductances L3 and L4 are switched in parallel for providing a given maximum conversion current. The converter chip has the control input for switching it on connected to the MCU pin via current limiting resistor R11. Resistor R12 connects the MCU pin of the microcircuit to "ground" for preventing spontaneous activation.

The field-effect transistor FET PSMN4R3-30BL (Nexperia, China) controlled by a PWM signal coming from MCU is used as the control element VT1 as described in [6]. This transistor is selected with allowance for power dissipation and the required output characteristics[8]; the control voltage produced by the divider R9, R10 is only 4.5 V.

The transistor output characteristic (Fig. 4) shows the transistor to be capable of commutating direct current up to 100 A at the control voltage of 4.5 V.

Although this value is much higher than necessary for steady-state operation, very high currents occur between C13, C15 and C21 when the output filters are powered due to the capacitors C13 and C15 having a rated capacity of 4700 μF. The equivalent series resistance of these capacitors is 55 mΩ; when unlocking the transistor gate[9], the peak current may be written as follows:

$$I_{peak} = \frac{U_{out}}{R_{ESR}} = \frac{23.75}{0.055} = 431.8\ \text{A}, \quad (2)$$

where U_{out} is the source voltage; R_{ESR} is the equivalent series resistance of the capacitor.

Here, the subsequent capacitive filter elements are not accounted for: the current is limited by the step-up

[6] High performance, low power AVR® 8-bit microcontroller, ATmega48/V/88/V/168/V, DS40002074A. Microchip Technology; 2018. 390 p. https://www.microchip.com/content/dam/mchp/documents/OTH/ProductDocuments/DataSheets/ATmega48_88_168_megaAVR-Data-Sheet-40002074.pdf. Accessed August 29, 2022.

[7] Switching current boost / buck-boost / inverting DC/DC converter, XL6009. Xinlong Semiconductor Technology; 2017. 8 p.

[8] N-channel MOSFET in D2PAK, PSMN4R3-30BL. Nexperia B.V.; 2017. 15 p.

[9] Matvienko V.A. *Fundamentals of electric circuit theory*: Textbook for universities; Yekaterinburg: UMTs UPI; 2016. 162 p. (in Russ.).

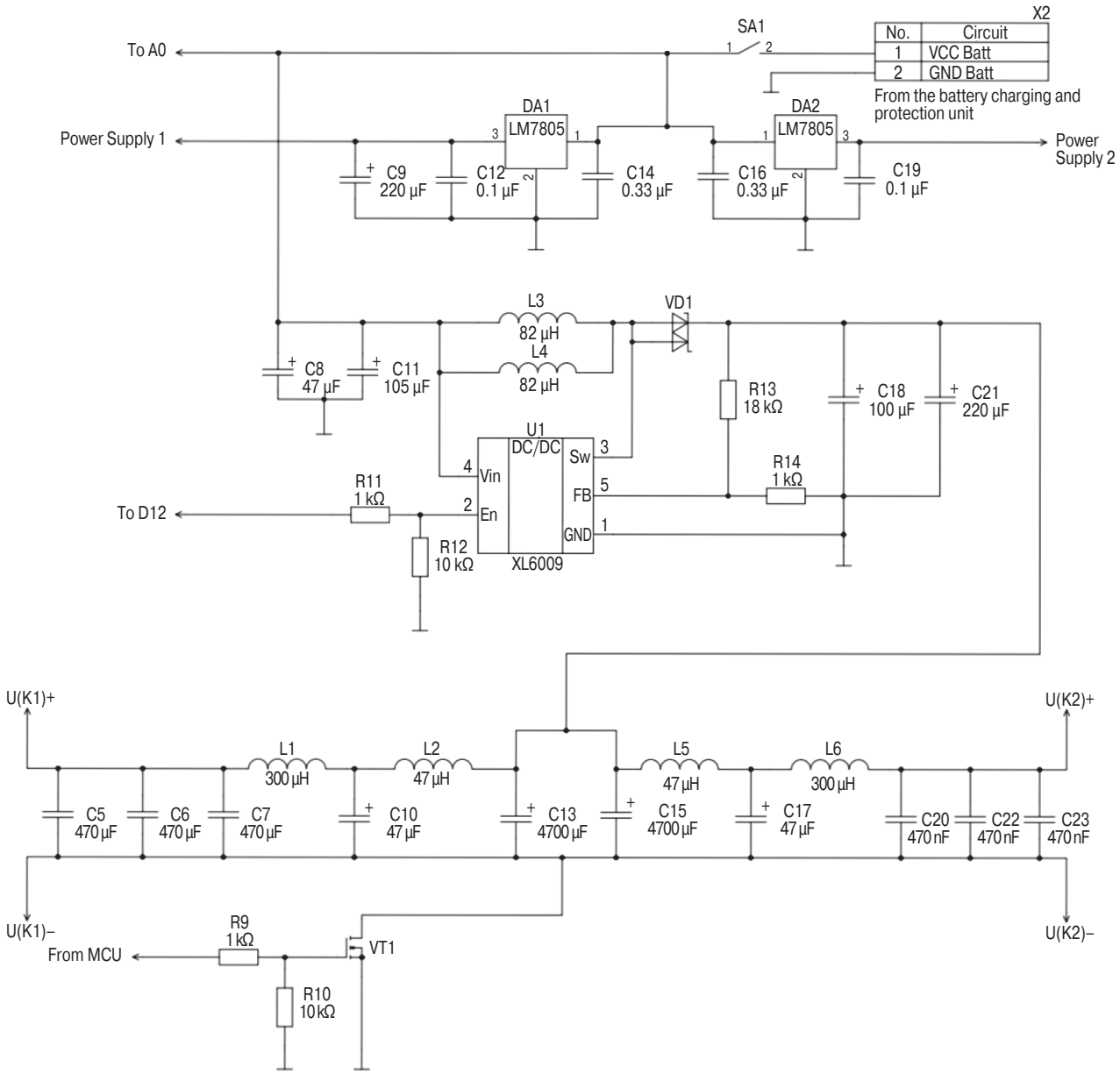

Fig. 3. Power supply circuit diagram of the monitoring and control unit. Here and in the following circuits, the designations of elements correspond to GOST 2.710-81[10]

voltage regulator U1, but not until its output capacities are discharged. Since the maximum peak current of the selected transistor is 465 A, the performance is not affected.

Each output filter is the LC ladder filter, as described in [7]. These are used for additional smoothing of pulsations after the boost converter.[11]

Both 5V linear voltage regulators are made on LM7805 chips (Inchange Semiconductor Company, China). The C14 and C16 capacitors filter input pulsations, while the C9, C12, and C19 capacitors filter the output ones.

The commutating elements K1–K3 (Fig. 5) are implemented on HK19F-DC5V-SHG relay (Ever-way Industry Co, China). The rated commutation current is 2 A at DC voltage 30 V[12]. The relay is controlled from MCU through optocouplers DA3–DA5. Resistors R15–R17 limit the current through the optocoupler and the LED used for indicating the state of elements K1–K3. This implementation allows for galvanic isolation of the MCU pin and the relay to protect MCU from line voltage as described in [8].

[10] GOST 2.710-81. Unified system for design documentation. Alpha-numerical designations in electrical diagrams. Moscow: Izdatel'stvo standartov; 1985 (in Russ.).

[11] Output noise filtering for DC/DC power modules. https://www.ti.com/lit/an/snva871/snva871.pdf. Accessed August 29, 2022.

[12] Subminiature DIP Relay, HK19F. Ever-Way Industry Company Limited; 2011. 3 p.

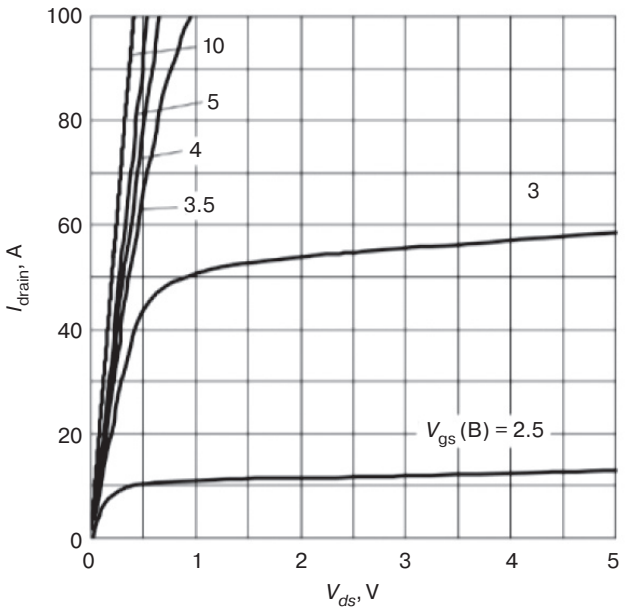

Fig. 4. Output characteristic of the PSMN4R3-30BL transistor. Dependence of the drain current I_{drain} on the drain–source voltage V_{ds} at fixed gate–source voltages V_{gs}

All the sensors used are connected via the I²C bus (Fig. 6). The INA219 chip (Texas Instruments, USA), which determines the current and voltage with an accuracy of ±0.2%[13], is used as the current, voltage, and power sensor. The SHT2 chip (Sensirion AG, Switzerland) is used as a temperature and humidity sensor; it has an accuracy of relative humidity ±2% and temperature ±0.3 °C.[14]

The LEDs HL1–HL4 displaying the remaining battery percentage along with the system operating mode are used as indicators; SB1 is the MCU reset button. The SB2 and SB3 clock buttons used for the forced shutdown of UPS output channels are connected to the MCU analog input DD1 through the resistive divider.

3. BATTERY CHARGING AND PROTECTION UNIT

The structural diagram of the battery charging and protection unit is shown in Fig. 7.

In the designed system, the load for this unit is produced by the control and monitoring unit. The circuit diagram of the battery-charging and protection unit is shown in Fig. 8, 10, and 11. The standalone pulse charge controller for the Li+ battery is implemented on a MAX1737 chip (Maxim integrated, USA) (Fig. 8). This controls the input current from the source, the output charging current, and the battery voltage. The allowable charging voltages range between 4.0 V per cell and 4.4 V per cell.

[13] Ugryumov E.P. *Digital circuitry*: Textbook for universities. 2nd ed.; BHV-Petersburg; 2007. 800 p. (in Russ.).

[14] Humidity and Temperature Sensor IC, SHT21. SENSIRION. CMOSens®; 2014. 15 p.

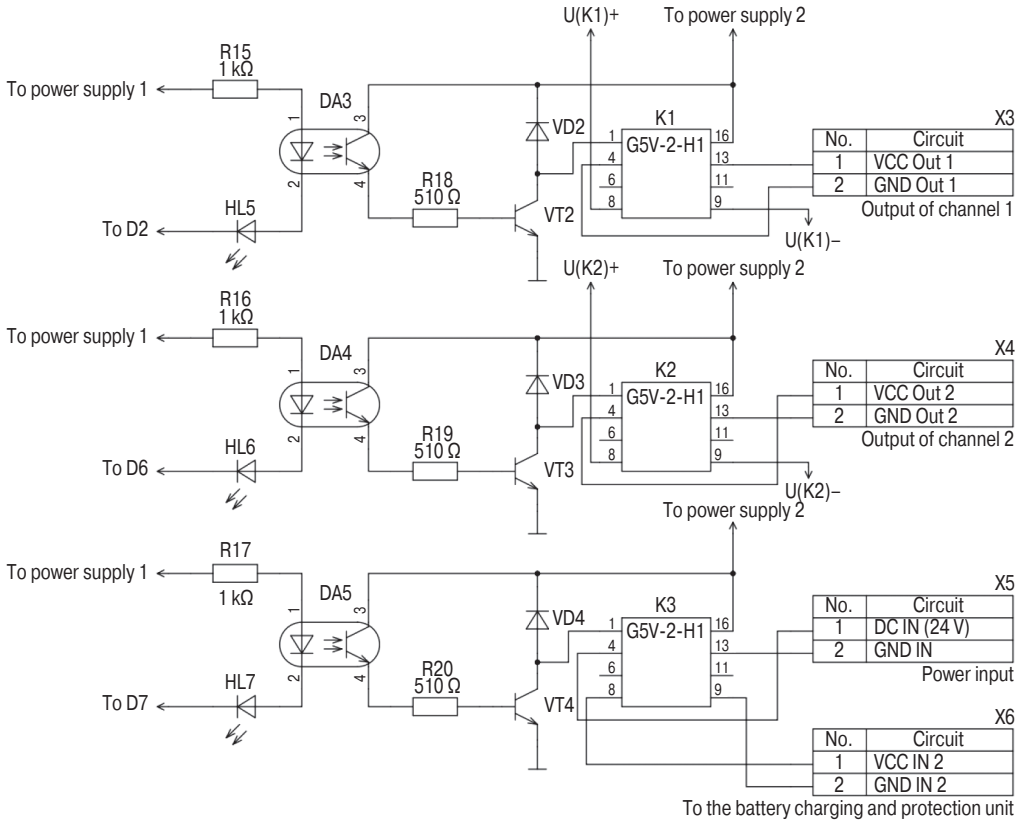

Fig. 5. Circuit diagram of commutating elements for the monitoring and control unit

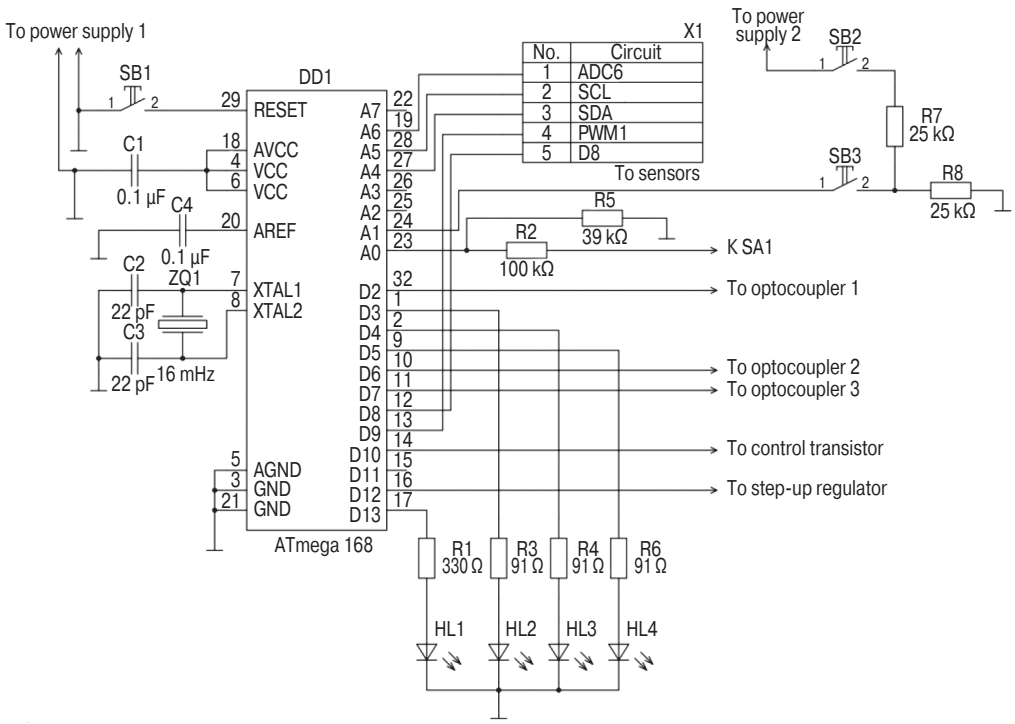

Fig. 6. Circuit diagram of the monitoring and control unit MCU

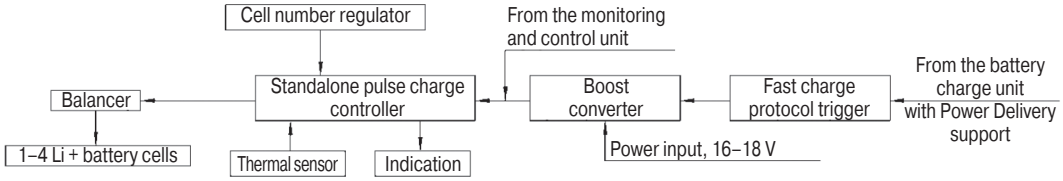

Fig. 7. Structural diagram of the battery charging and protection unit

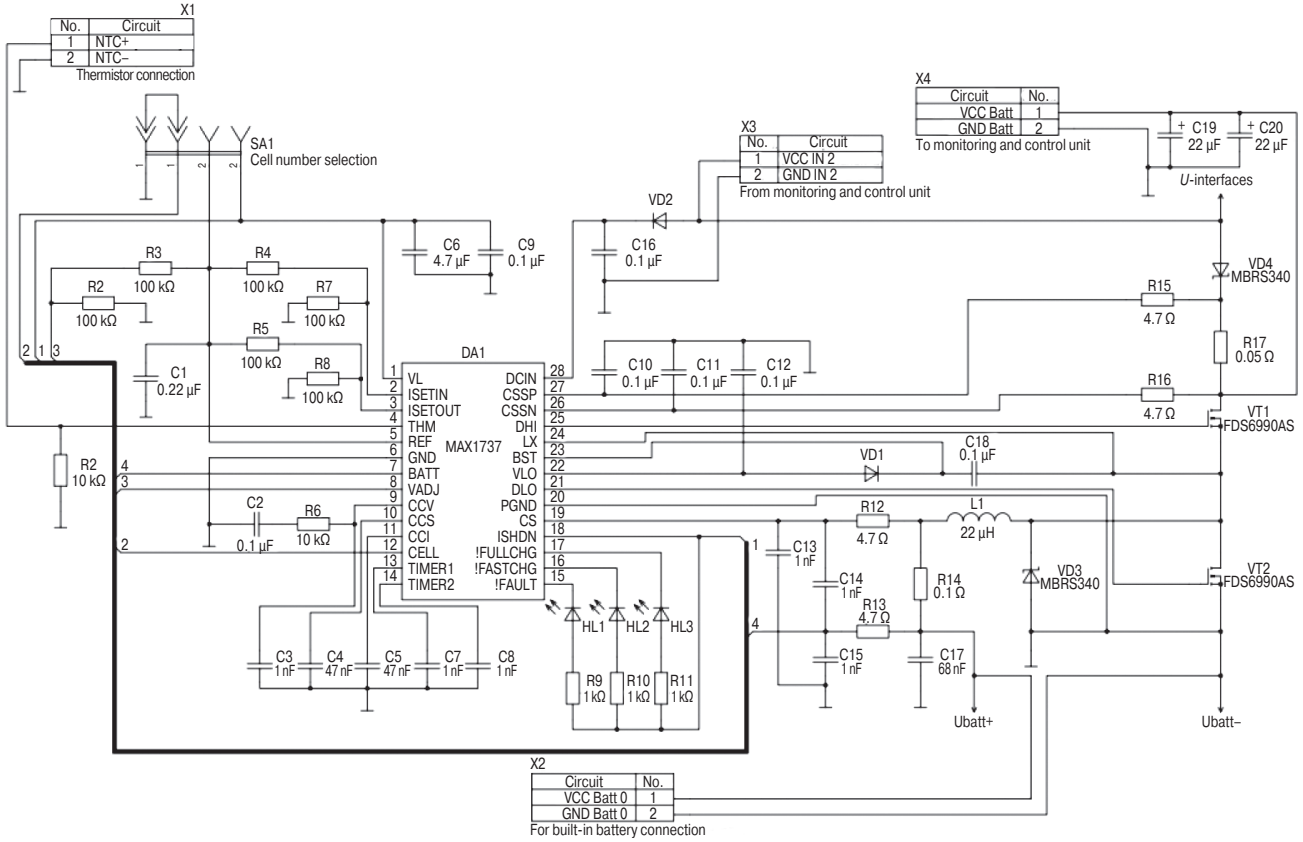

Fig. 8. Circuit diagram of the battery charging and protection unit controller

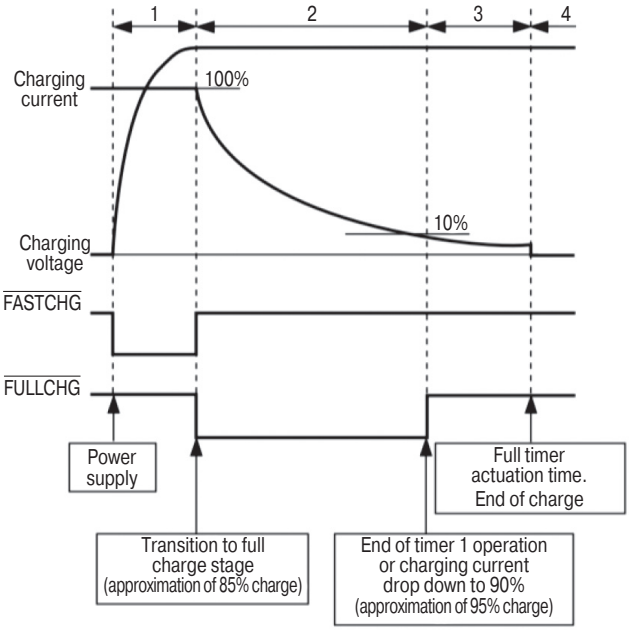

Fig. 9. Diagrams of voltage and current for charging profile

The external thermistor is connected via connector X1. The 10 kΩ resistor R1 is installed in the absence of a need for temperature monitoring. When the voltage of the built-in battery drops below the minimum threshold value U_{min} (3), the deep discharge protection system is activated; the load is switched off by transistors VT1 and VT2.

$$U_{min} = 2.5N \text{ V}, \quad (3)$$

where N is the number of connected cells.

The Li+ batteries are charged according to the specific charging profile, which is distinguished from those used with classic lead acid batteries. This is necessary for increasing the lifetime of the batteries as detailed in [9] and recommended for charging by many Li+ battery manufacturers. The diagram of the charging voltage and current as well as voltage diagrams of inverting pins for the fast charge (FASTCHG) and full charge (FULLCHG) stages are shown in Fig. 9.

The full charge cycle may be divided into 4 main stages:

1) fast charge stage—including non-linear changes in battery voltage while the current remains constant;
2) full charge stage—battery voltage reaches the predetermined value to remain constant, while the current decreases;
3) fill stage—initial current is decreased by 90% while the current change becomes almost linear;
4) completion stage—charging current becomes zero.

The maximum duration of each cycle is set by the charge controller's internal timers. The nominal value of capacitor C8 sets the running time of timer 2 responsible for the fast charge stage, amounting to 90 min at 1 nF. Should the controller fail in transiting to the next stage of the charge cycle within the time set by timer 2, the chip disables further battery charging and turns the error indicator on.

The nominal value of capacitor C7 sets the running time of timer 1 responsible for the full charge and fill stages, as well as for the pre-preparation time. At 1 nF, the full charge stage time is 90 min, while the fill stage time is 45 min. The pre-preparation includes checking the cell voltage for the minimum threshold value as well as checking the temperature. The checking time is 7.5 min. Should indicated values exceed the operating range, the controller turns an error message on and the charge cycle does not begin.

The LEDs HL1–HL3 are connected via current limiting resistors R9–R11 to inverting pins of the charge controller state indicator FAULT, FASTCHG, and FULLCHG.

The elements VT1, VT2, C17, L1, and VD3 form the DC voltage step-down converter. The transistor gates are controlled by chip DA1 (Maxim integrated, USA). This chip generates a PWM signal with variable fill factor depending on the input and the battery charging voltages and a frequency of 300 kHz. The claimed conversion efficiency ranges from 85% to 90%[15]. Although the output voltage ranges from 6 to 28 V, the input voltage should be higher than the minimum supply voltage of the charge controller:

$$U_{min\ chg} = U_{min} + 1.6 \text{ V}. \quad (4)$$

The voltage drop across resistor R17 sets the input current of the charge controller I_{in} as calculated by the following formula:

$$I_{in} = \frac{0.1}{R_{17}} \cdot \frac{U_{ISETIN}}{U_{REF}} = 1 \text{ A}, \quad (5)$$

where U_{ISETIN} is the voltage on pin 2 (SETIN) DA1 set by the voltage divider formed by resistors R4 and R7 with reference voltage at the input U_{REF} = 4.166–4.242 V.

The voltage drop across resistor R14, which regulates the battery charging current I_{chg}, is calculated by the following formula:

$$I_{chg} = \frac{0.2}{R_{14}} \cdot \frac{U_{ISETOUT}}{U_{REF}} = 1 \text{ A}, \quad (6)$$

where $U_{ISETOUT}$ is the voltage on pin I_{SETOUT} set by the voltage divider formed by resistors R5 and R8 with reference voltage at the input U_{REF}.

[15] Stand-alone switch-mode lithium-ion battery-charger controller, MAX1737, Data Sheet 19-1626. Maxim Integrated; 2017. 19 p.

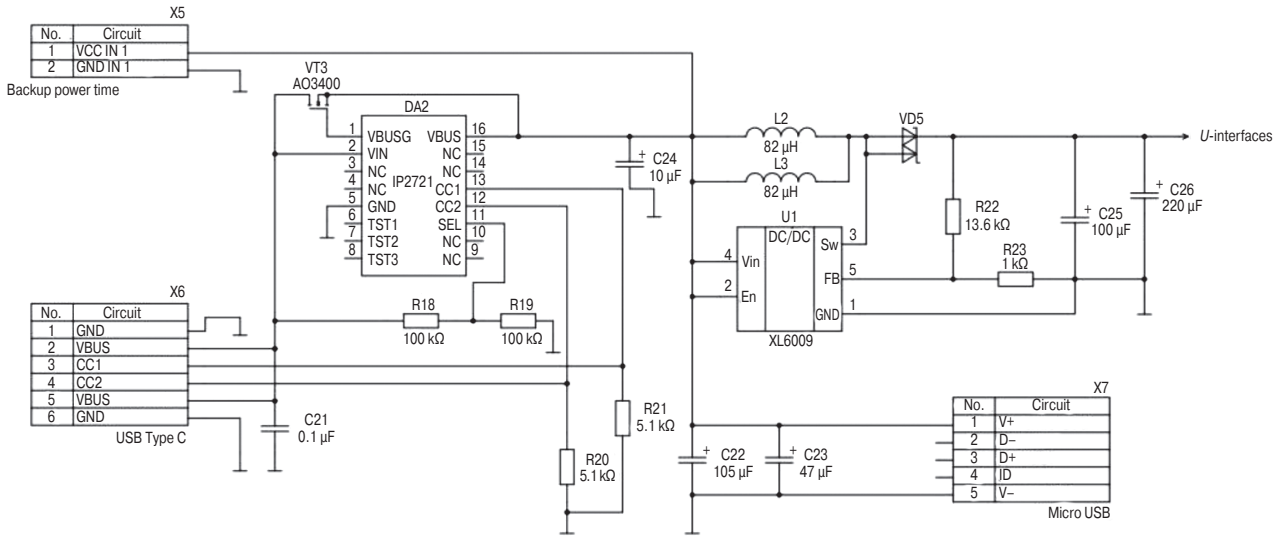

Fig. 10. Circuit diagram of the boost converter of the battery charging and protection unit

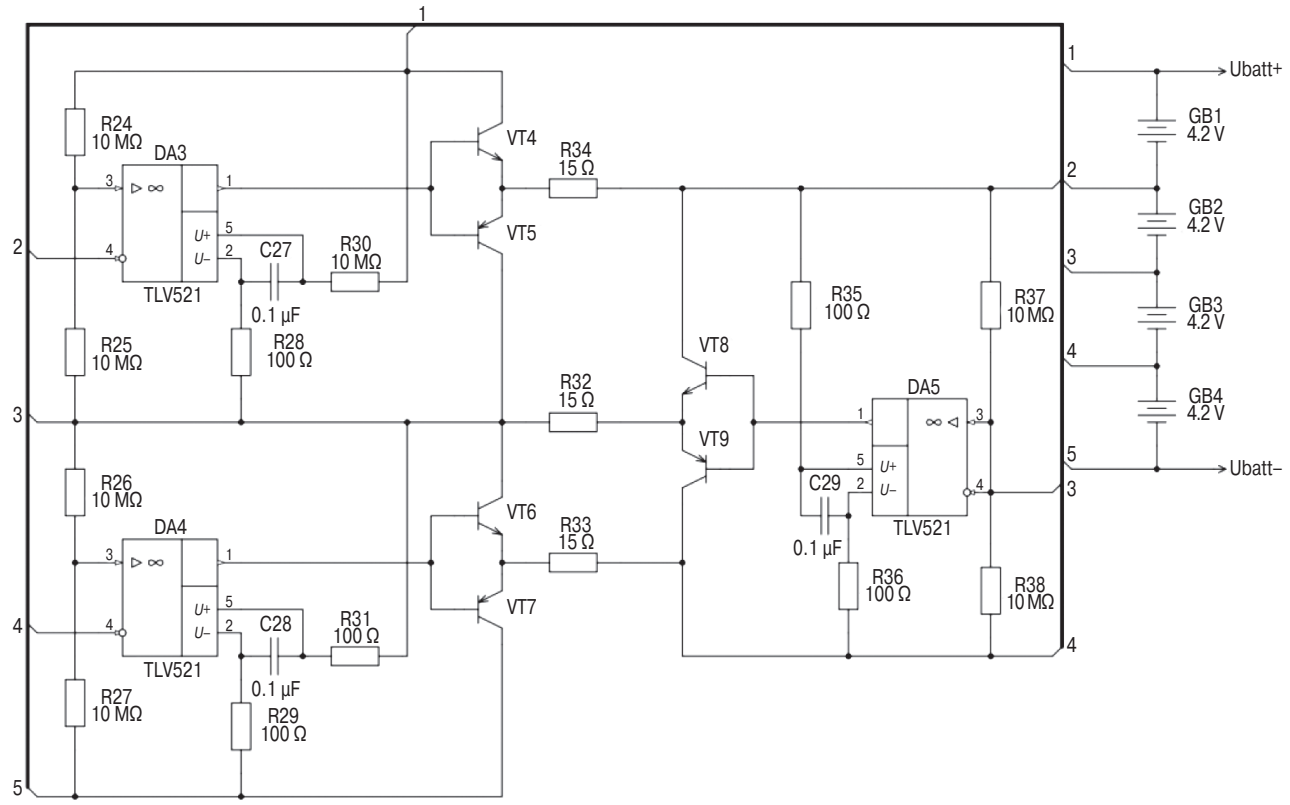

Fig. 11. Circuit diagram for the balancing module of the battery charging and protection unit

The boost converter in the battery charging and protection unit (Fig. 10) is used for generating the supply voltage of the charge controller. As a result, the input charging voltage range of the built-in battery is significantly extended, ranging from 5 to 28 V regardless of how many cells are connected due to the formation of a step-up/down converter.

The support of the Power Delivery fast charging protocol implemented in many modern consumer battery chargers is provided by the protocol trigger implemented on the IP2721 chip (Injoinic Technology Corp., China). Pin SEL sets one of the standard output voltages of the connected charger using data exchange protocol. When pin SEL is connected via resistor R18 to the power supply, the voltage at the battery charger unit is set to 12 V; when it is connected via resistor R19 to "ground", the voltage is set to 5 V.[16]

[16] TYPEC/PD2.0/PD3.0 Physical Layer IC for USB TYPEC input interfaces, IP2721. Injoinc Corp.; 2017. 7 p.

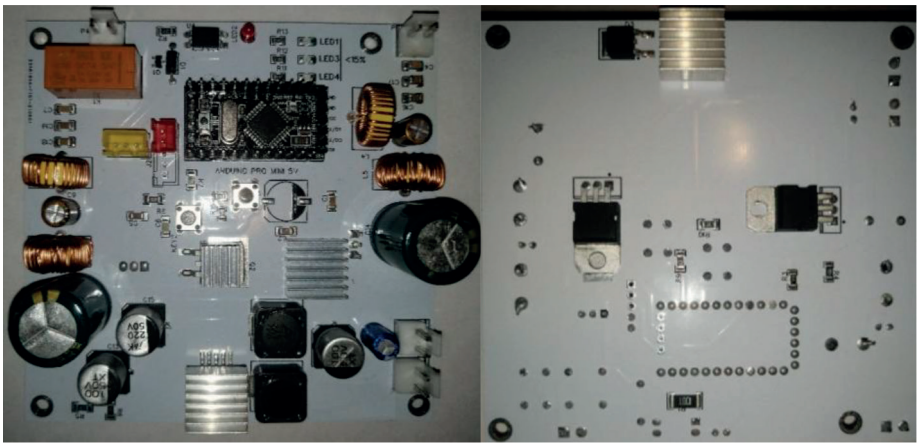

Fig. 12. Prototype for the monitoring and control unit: top and bottom views

Fig. 13. Prototype for the battery charging and protection unit: top and bottom views

The built-in cells are balanced by the balancing module using operational amplifiers DA3, DA4, and DA5 (Fig. 11). Each of these controls a pair of transistors by comparing the sum of voltages on two battery cells with voltage between two cells connected in series making allowance for the voltage[17] divider formed by a pair of resistors R24–R25 for DA3, R26–R27 for DA4 and R37–R38 for DA5. The built-in battery is formed by the cells of Li+ batteries GB1–GB4 connected in series. Operational amplifiers TLV521 (Texas Instruments, USA) are selected due to low power consumption[18], which increases energy efficiency.

The prototype design for the monitoring and control unit is shown in Fig. 12.

The prototype design for the battery charging and protection unit is shown in Fig. 13.

[17] Keep the balance – balancing of supercapacitors, ANP090. https://www.we-online.com/catalog/media/o671684v410%20ANP090a%20EN.pdf. Accessed August 29, 2022.

[18] NanoPower, 350nA, RRIO, CMOS Input, operational amplifier, TLV521, Data Sheet SNOSD26. Texas Instruments; 2016. 27 p.

4. RESEARCH FINDINGS ON CHARACTERISTICS OF THE DEVELOPED SYSTEM

For evaluating the output power of two channels, each channel is connected to a controlled electronic load. The constant power operating mode is set to 20 W per channel. The total power delivered by the system to the electronic load is about 40 W in this operating mode. Time diagrams for current, voltage, and power are drawn using the measuring tools built into the electronic load units.

Time diagrams for current, voltage, and power of the first channel are shown in Figs. 14 and 15.

Figure 14 shows that the change in the output voltage level during operation is 0.2 V. The actual output voltage level is 22.6 V differing from the calculated value U_{out}. This is due to the voltage drop across the output filters and the parameter spread of resistors R13, R14. The output current ripple is due to the operating principle of the controlled electronic load.

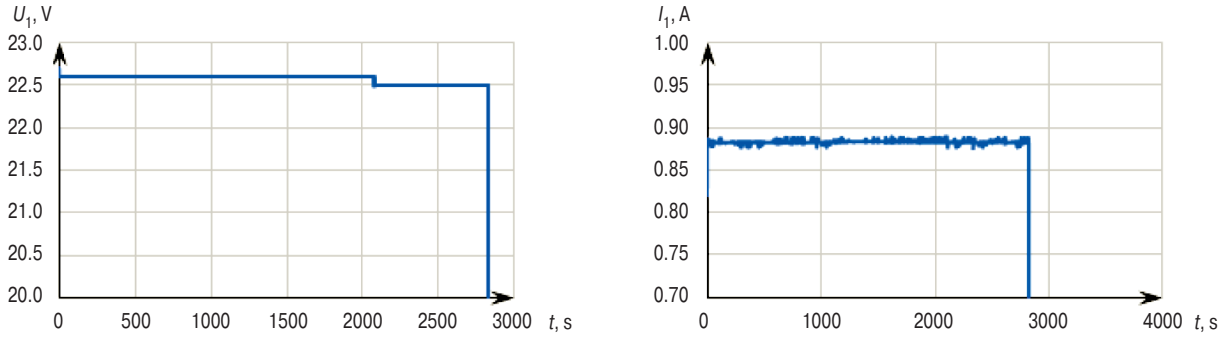

Fig. 14. Time diagrams for current and voltage of the first channel

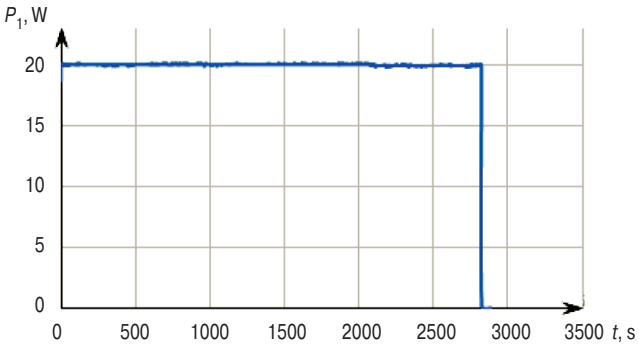

Fig. 15. Time diagram of the first channel power

Time diagrams of the second channel almost coincide with those of the first one making allowance for the insignificant parameter spread of the output filters. Time diagrams for the total current and power of two channels are shown in Fig. 16.

It may be seen from Figs. 14–16 that a sudden drop in the output voltage and power level occurs at t = 2800 s. This is due to automation; the voltage of built-in batteries drops below the critical value, they are completely discharged, and the charge controller disconnects them from the monitoring and control unit.

As can be seen from Fig. 16, the total output power is about 40 W, while the system operating time with such load is at least 45 min.

CONCLUSIONS

A prototype of an uninterruptible power system with the ability to change output voltage for required tasks has been created. Each unit has been tested separately along with their interaction.

The system generates stable output voltage of 22.6 V with a power of 20 W in each channel. The monitoring and control unit correctly displays the remaining percentage of the built-in battery charge in increments of 25% and enables shutdown of consumers when the built-in battery voltage falls below a specified threshold, thus duplicating the protection function of the battery charging and protection unit.

The battery charging and protection unit provides stable power supply to the monitoring and control unit for at least 45 min, successfully activating the fast-charging protocol when connected to the battery charger and protecting the built-in batteries from "overcharging."

It is intended to improve the developed system in future as follows:

- modification of output filters for reducing output voltage ripple;
- improvement of DC-DC converter input filters for reducing noise level;[19]

[19] Design and application considerations of input filter to reduce conducted emissions caused by DC/DC converter, No. 62AN101E Rev.003. ROHM Co., Ltd.; 2020. 7 p.

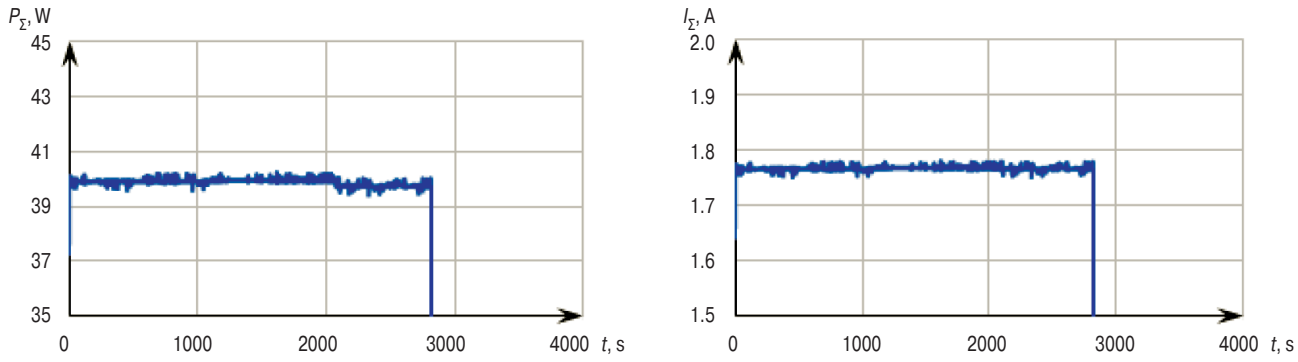

Fig. 16. Time diagrams for the total current and power of two channels

- replacement of transistor group in the balancing module for increasing maximum allowable balancing currents or using the balancing module for the same purpose;[20]
- increasing the output power and developing the inverter for providing the standard 220 V network voltage;
- implementing the control of the charge controller from MCU.

[20] Passive balancing allows all cells to appear to have the same capacity. https://softei.com/passive-balancing-allows-all-cells-to-appear-to-have-the-same-capacity. Accessed August 29, 2022.

Authors' contribution
All authors equally contributed to the research work.

REFERENCES

1. Lukutin B.V., Muravlev I.O., Plotnikov I.A. *Sistemy elektrosnabzheniya s vetrovymi i solnechnymi elektrostantsiyami*: uchebnoe posobie (*Power supply systems with wind and solar power plants*: textbook). Tomsk: Publishing House of Tomsk Polytechnic University; 2015. 128 p. (in Russ.).
2. Datsenko V.A., Sivkov A.A., Gerasimov D.Yu. *Montazh, remont i ekspluatatsiya elektricheskikh raspredelitel'nykh setei v sistemakh elektrosnabzheniya promyshlennykh predpriyatii*: uchebnoe posobie (*Installation, repair and operation of electrical distribution networks in power supply systems of industrial enterprises*: textbook). Tomsk: Publishing House of Tomsk Polytechnic University; 2007. 132 p. (in Russ.).
3. Traister J.E., Kennedy T. *Low voltage wiring: Security/Fire alarm systems*. NY: The McGraw-Hill Companies; 2002. 408 p.
4. Bityukov V.K., Lukht M.A., Mikhnevich N.G., Petrov V.A. Mother board of trainer with virtual front panel for study of linear voltage regulator characteristics. *Russ. Technol. J.* 2017;5(4):22–31 (in Russ.). https://doi.org/10.32362/2500-316X-2017-5-4-22-31
5. Revich Yu.V. *Programmirovanie mikrokontrollerov AVR: ot Arduino k assembleru* (*Programming of AVR microcontrollers: from Arduino to Assembler*). St. Petersburg: BHV-Petersburg; 2020. 448 p. (in Russ.). ISBN 978-5-9775-4076-6
6. Bityukov V.K., Simachkov D.S., Babenko V.P. *Istochniki vtorichnogo elektropitaniya* (*Secondary power sources*). Moscow; Vologda: Infra-Inzheneriya; 2020. 376 p. (in Russ.). ISBN 978-5-9729-0471-6
7. Milenina S.A., Milenin N.K. *Elektrotekhnika, elektronika i skhemotekhnika*: uchebnik i praktikum dlya vuzov (*Electrical engineering, electronics and circuit engineering*: textbook and workshop for universities). Moscow: Yurait; 2021. 406 p. (in Russ.). ISBN 978-5-534-04525-3
8. Gololobov V.N. *Skhemotekhnika s programmoi Multisim dlya lyuboznatel'nykh* (*CIRCUIT DESIGN with the Multisim program for the curious*). St. Petersburg: Nauka i tekhnika; 2019. 272 p. (in Russ.). ISBN 978-5-94387-880-0
9. Methekar P.N., et al. Optimum charging profile for lithium-ion batteries to maximize energy storage and utilization. *ECS Trans*. 2010;25(35):139–146. https://doi.org/10.1149/1.3414012

СПИСОК ЛИТЕРАТУРЫ

1. Лукутин Б.В., Муравлев И.О., Плотников И.А. *Системы электроснабжения с ветровыми и солнечными электростанциями:* учебное пособие. Томск: Изд-во Томского политехнического университета; 2015. 128 с.
2. Даценко В.А., Сивков А.А., Герасимов Д.Ю. *Монтаж, ремонт и эксплуатация электрических распределительных сетей в системах электроснабжения промышленных предприятий:* учебное пособие. Томск: Изд-во Томского политехнического университета; 2007. 132 с.
3. Traister J.E., Kennedy T. *Low voltage wiring: Security/Fire alarm systems*. NY: The McGraw-Hill Companies; 2002. 408 p.
4. Битюков В.К., Лухт М.А., Михневич Н.Г., Петров В.А. Системная плата учебного лабораторного стенда с виртуальной передней панелью для исследований характеристик линейных стабилизаторов. *Российский технологический журнал*. 2017;5(4):22–31. https://doi.org/10.32362/2500-316X-2017-5-4-22-31
5. Ревич Ю.В. *Программирование микроконтроллеров AVR: от Arduino к ассемблеру*. СПб.: БХВ-Петербург; 2020. 448 с. ISBN 978-5-9775-4076-6
6. Битюков В.К., Симачков Д.С., Бабенко В.П. *Источники вторичного электропитания*. Москва; Вологда: Инфра-Инженерия; 2020. 376 с. ISBN 978-5-9729-0471-6
7. Миленина С.А., Миленин Н.К. *Электротехника, электроника и схемотехника*: учебник и практикум для вузов. М.: Юрайт; 2021. 406 с. ISBN 978-5-534-04525-3
8. Гололобов В.Н. *Схемотехника с программой Multisim для любознательных*. СПб.: Наука и техника; 2019. 272 с. ISBN 978-5-94387-880-0
9. Methekar P.N., et al. Optimum charging profile for lithium-ion batteries to maximize energy storage and utilization. *ECS Trans*. 2010;25(35):139–146. https://doi.org/10.1149/1.3414012

About the authors

Igor M. Sharov, Student, Department of Radio Electronic Systems and Complexes, Institute of Radio Electronics and Informatics, MIREA – Russian Technological University (78, Vernadskogo pr., Moscow, 119454 Russia). E-mail: ctosworld@gmail.com. https://orcid.org/0000-0002-3391-3266

Oleg A. Demin, Student, Department of Radio Electronic Systems and Complexes, Institute of Radio Electronics and Informatics, MIREA – Russian Technological University (78, Vernadskogo pr., Moscow, 119454 Russia). E-mail: coin12@mail.ru. https://orcid.org/0000-0002-9864-5338

Alexander A. Sudakov, Assistant, Department of Radio Electronic Systems and Complexes, Institute of Radio Electronics and Informatics, MIREA – Russian Technological University (78, Vernadskogo pr., Moscow, 119454 Russia). E-mail: sudakov@mirea.ru. RSCI SPIN-code 4225-2792, https://orcid.org/0000-0001-6958-8111

Alexey D. Yarlykov, Assistant, Department of Radio Wave Processes and Technologies, Institute of Radio Electronics and Informatics, MIREA – Russian Technological University (78, Vernadskogo pr., Moscow, 119454 Russia). E-mail: yarlykov@mirea.ru. Scopus Author ID 57290652000, RSCI SPIN-code 3450-1587, https://orcid.org/0000-0002-7232-8588

Об авторах

Шаров Игорь Михайлович, студент, кафедра радиоэлектронных систем и комплексов Института радиоэлектроники и информатики ФГБОУ ВО «МИРЭА – Российский технологический университет» (119454, Россия, Москва, пр-т Вернадского, д. 78). E-mail: ctosworld@gmail.com. https://orcid.org/0000-0002-3391-3266

Демин Олег Александрович, студент, кафедра радиоэлектронных систем и комплексов Института радиоэлектроники и информатики ФГБОУ ВО «МИРЭА – Российский технологический университет» (119454, Россия, Москва, пр-т Вернадского, д. 78). E-mail: coin12@mail.ru. https://orcid.org/0000-0002-9864-5338

Судаков Александр Анатольевич, ассистент, кафедра радиоэлектронных систем и комплексов Института радиоэлектроники и информатики ФГБОУ ВО «МИРЭА – Российский технологический университет» (119454, Россия, Москва, пр-т Вернадского, д. 78). E-mail: sudakov@mirea.ru. SPIN-код РИНЦ 4225-2792, https://orcid.org/0000-0001-6958-8111

Ярлыков Алексей Дмитриевич, ассистент, кафедра радиоволновых процессов и технологий Института радиоэлектроники и информатики ФГБОУ ВО «МИРЭА – Российский технологический университет» (119454, Россия, Москва, пр-т Вернадского, д. 78). E-mail: yarlykov@mirea.ru. Scopus Author ID 57290652000, SPIN-код РИНЦ 3450-1587, https://orcid.org/0000-0002-7232-8588

Translated from Russian into English by Kirill V. Nazarov
Edited for English language and spelling by Thomas A. Beavitt

UDC 621.3.049.77
https://doi.org/10.32362/2500-316X-2022-10-5-73-91

REVIEW ARTICLE

Technology for the creation of ferroelectric regular domain structures using interfering elastic waves

Vladislav V. Krutov @, Alexander S. Sigov

MIREA – Russian Technological University, Moscow, 119454 Russia
@ Corresponding author, e-mail: v_krutov@mirea.ru

Abstract

Objectives. In many laboratories around the world, work is underway in the field of domain engineering of ferroelectrics. For a number of years, RTU MIREA has been conducting research on the creation of a high-performance technology for the formation of ferroelectric photonic and phononic crystals. The technology is characterized by a short duration of the technological cycle and provides the necessary depth of spatially periodic domain inversion. The key element of the technology is the combined effect of a uniform electric field and interfering high-frequency elastic waves that create a temperature grating. The technology is universal in relation to ferroelectrics of varying degrees of acoustic transparency, which is achieved by using highly dissipative liquid electrodes of a certain thickness. In this case, the energy of elastic waves practically does not penetrate into the ferroelectric, so the manifestation of undesirable effects is excluded. The purpose of this review article is to analyze the results of work carried out at RTU MIREA in the field of technology for the formation of ferroelectric regular domain structures (RDSs) during the period from 2008 to the present.

Methods. Provisions of the theory of propagation, refraction and interference of elastic waves in condensed media are used, in particular, the Newtonian model of a liquid as applied to shear waves, as well as computer simulation. When considering the main stages of the Double Pulse heterothermal technology for the formation of RDSs, methods of analysis and synthesis were applied.

Results. The possibility of forming not only micro-, but also submicron RDSs is shown. Recommendations are given on the choice of the type and specific properties of liquid electrodes, the angles between the direction of propagation of interfering waves, and their frequency. It is shown, in particular, that the use of highly dissipative ionic liquids as liquid electrodes creates favorable conditions for the formation of an RDS with a short period at room temperature. Thus, on shear waves with electrodes based on $LiPF_6$–PC at a frequency of 300 MHz, RDS with a period of about 2 μm can be created. The main technological parameters are determined both for the case of the action of longitudinal elastic waves and for the case of shear waves with horizontal polarization. The results are applicable to ferroelectrics such as lithium niobate, potassium titanyl phosphate, and lead zirconate titanate.

Conclusions. The proposed and studied methods are focused on the mass production of devices based on RDSs, in particular, on the manufacturing of optical parametric oscillators, acoustoelectronic devices, as well as terahertz wave generators and second harmonic oscillators. The technology has a short duration of the technological cycle, comparable to the polarization switching time in the used ferroelectric.

Keywords: domain engineering, ferroelectrics, temperature gratings, double pulse heterothermal technology, elastic waves, acoustic interference method

• **Submitted:** 11.05.2022 • **Revised:** 04.07.2022 • **Accepted:** 12.09.2022

For citation: Krutov V.V., Sigov A.S. Technology for the creation of ferroelectric regular domain structures using interfering elastic waves. *Russ. Technol. J.* 2022;10(5):73–91. https://doi.org/10.32362/2500-316X-2022-10-5-73-91

Financial disclosure: The authors have no a financial or property interest in any material or method mentioned.

The authors declare no conflicts of interest.

ОБЗОРНАЯ СТАТЬЯ

Технология формирования сегнетоэлектрических регулярных доменных структур с использованием интерферирующих упругих волн

В.В. Крутов [@], А.С. Сигов

МИРЭА – Российский технологический университет, Москва, 119454 Россия
[@] Автор для переписки, e-mail: v_krutov@mirea.ru

Резюме

Цели. Работы в области доменной инженерии в сегнетоэлектриках ведутся во многих лабораториях мира. На протяжении ряда лет в РТУ МИРЭА проводятся исследования по созданию высокопроизводительной технологии формирования сегнетоэлектрических фотонных и фононных кристаллов. Технология характеризуется малой продолжительностью технологического цикла и обеспечивает необходимую глубину пространственно-периодического инвертирования доменов. Ключевым звеном технологии является комбинированное воздействие однородного электрического поля и интерферирующих упругих волн высоких частот, создающих температурную решетку. Технология имеет универсальный характер в отношении сегнетоэлектриков различной степени акустической прозрачности, что достигается путем использования сильно диссипативных жидких электродов определенной толщины. При этом энергия упругих волн практически не проникает в сегнетоэлектрик, что исключает проявление нежелательных эффектов. Цель настоящей статьи – анализ результатов работ, выполненных в РТУ МИРЭА, в области технологии формирования сегнетоэлектрических регулярных доменных структур (РДС) в период с 2008 г. по настоящее время.

Методы. Использованы положения теории распространения, преломления и интерференции упругих волн в конденсированных средах, в частности ньютоновская модель жидкости применительно к сдвиговым волнам, а также компьютерное моделирование. При рассмотрении основных этапов биимпульсной гетеротермальной технологии формирования РДС применялись методы анализа и синтеза.

Результаты. Показана возможность формирования не только микро-, но также субмикронных РДС. Даны рекомендации по выбору типа и конкретных свойств жидких электродов, углов между направлением распространения интерферирующих волн, а также их частоты. Показано, что использование в качестве жидких электродов сильно диссипативных ионных жидкостей создает благоприятные условия для формирования РДС с малым периодом при комнатной температуре. Так, на сдвиговых волнах с электродами на основе $LiPF_6$–ПС на частоте 300 МГц могут быть созданы РДС с периодом около 2 мкм. Определены основные технологические параметры, как для случая воздействия продольных упругих волн, так и для случая сдвиговых волн с горизонтальной поляризацией. Результаты применимы к таким сегнетоэлектрикам как ниобат лития, титанил-фосфат калия, цирконат-титанат свинца.

Выводы. Предложенные и исследованные методы ориентированы на массовое производство устройств на основе РДС, в т.ч. на изготовление оптических параметрических генераторов, устройств акустоэлектроники, а также генераторов терагерцовых волн и генераторов второй оптической гармоники. Технология обладает малой продолжительностью технологического цикла, сопоставимой с временем переключения поляризации в используемом сегнетоэлектрике.

Ключевые слова: доменная инженерия, сегнетоэлектрики, температурные решетки, биимпульсная гетеротермальная технология, упругие волны, акустоинтерференционный метод

• **Поступила:** 11.05.2022 • **Доработана:** 04.07.2022 • **Принята к опубликованию:** 12.09.2022

Для цитирования: Крутов В.В., Сигов А.С. Технология формирования сегнетоэлектрических регулярных доменных структур с использованием интерферирующих упругих волн. *Russ. Technol. J.* 2022;10(5):73–91. https://doi.org/10.32362/2500-316X-2022-10-5-73-91

Прозрачность финансовой деятельности: Авторы не имеют финансовой заинтересованности в представленных материалах или методах.

Авторы заявляют об отсутствии конфликта интересов.

INTRODUCTION

Methods for creating photonic and phononic crystals based on ferroelectrics and multiferroics have recently been actively studied. Photonic and phononic crystals comprise regular domain structures (RDSs). Figure 1 schematically depicts a ferroelectric RDS of the side-by-side type.

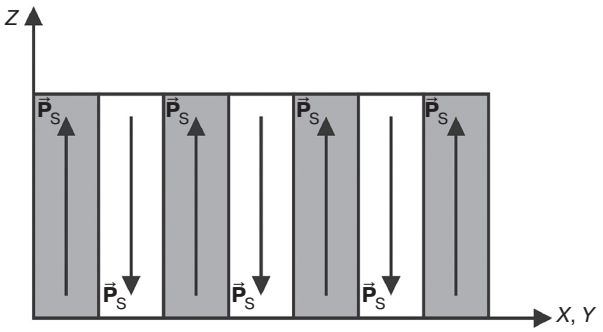

Fig. 1. Side-by-side RDS. Arrows depict the spontaneous polarization vector

Interest in RDSs is mainly due to their capability of performing various functions in acoustoelectronics [1], photonics [2, 3], as well as signal filtering and modulation devices [4, 5].

A number of methods for the creation of RDSs in ferroelectrics have been developed in laboratories around the world over the last 25 years (see, e.g., review [6]). A popular method [3] is based on the use of a nonuniform electric field generated by structured electrodes deposited by photolithography. Methods for "writing a domain pattern" using sequential scanning of the surface of a ferroelectric with a focused laser or electron beam [7] are of little use in the mass production of devices based on RDSs due to their long process cycle and shallow growth of domains. The method [8] based on moving the probe of an atomic force microscope over the ferroelectric surface also involves a long process cycle duration and provides only a shallow domain growth. The method of direct action of interfering laser beams on a single-domain ferroelectric [9] fails to produce a high-quality RDS. The generation of photoinduced charge carriers accompanying laser irradiation leads to undesirable effects such as the destruction of the temperature grating due to heat release by recombining carriers outside the antinodes of the interference pattern. Moreover, birefringence prevents the creation of contrasting temperature grating.

Methods for the creation of RDSs can be considered to be promising if they offer a minimum duration of the process cycle to provide a given depth of growth of domains and high quality RDS.

In recent years, there has been a search for "rapid" industry-oriented methods for the creation of RDSs that do not require the use of photolithography [10–13]. In particular, a method has been demonstrated [10] that allows the creation of surface quasi-periodic domain structures under the action of infrared laser pulses. The main advantage of this method consists in the possibility to produce rapidly domain structures without the use of photolithography. However, the method does not yet allow the creation of periodic domain structures with a given spatial period.

Methods for the creation of RDSs are also studied using a temperature grating induced by interfering elastic waves [13–16]. Such methods are based on the thermal interference principle, according to which local stimulation of domain switching is achieved by the pulsed uniform electric field action and temperature grating created by interfering waves. Figure 2 illustrates a pulsed interfering wave action with power density P and inverting uniform electric field of strength E. The corresponding technology of combined exposure is referred to as double pulse heterothermal (DPH) technology [14]. Selective switching of domains upon application of a uniform electric field is ensured owing to the decreased ferroelectric coercive field with increasing temperature [6]. In comparison with its analogs, this approach reduces the time of the formation of RDSs to values comparable to the polarization switching time of the ferroelectric.

Let us list the main stages of the DPH technology.

1. Creation of an interference pattern using a wave action pulse (creation of a temperature grating).
2. Polarization switching in heated areas of the temperature grating by a uniform electric field with strength $E \geq E_C$, where E_C is the coercive field.
3. Timely switching-off of the electric field upon reaching a given depth of domain growth, as well as in order to prevent lateral growth of domains.

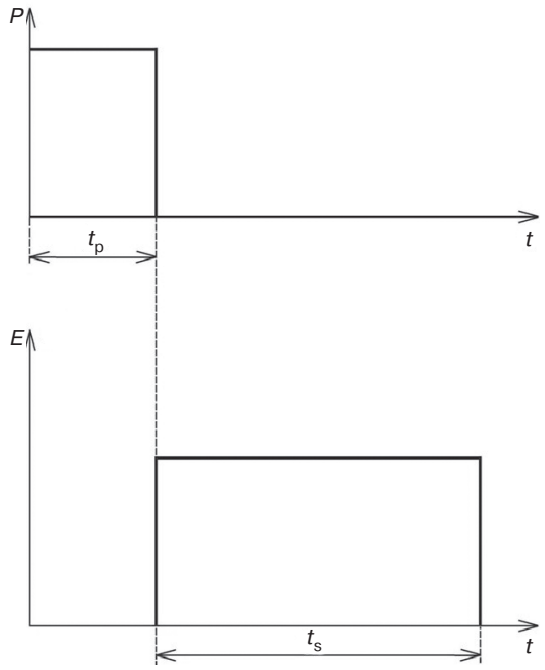

Fig. 2. A pulse of wave action with power density *P* and a pulse of an inverting uniform electric field of strength *E*. t_p is the thermal interference pulse duration, t_s is the duration of uniform electric field exposure

The pulse mode of heterothermal heating is crucial due to the need to prevent the destruction of the temperature grating by heat diffusion.

Since the domain inversion begins at the +*Z*-polar face of a ferroelectric [17, 18], it is expedient to create a temperature grating on the +*Z*-surface of a ferroelectric.

At the same time, in order to induce a contrast temperature grating using interfering waves, it is necessary to take into account the efficiency of the wave absorption in ferroelectrics. In particular, in lithium niobate and tantalate, the absorption is very low over a wide frequency range [19]. Consequently, upon entering a ferroelectric plate, the waves can be repeatedly reflected from its faces, which reduce the contrast of the temperature grating. Therefore, to prevent multiple reflections, it is necessary to create an absorbing layer near the +Z-polar face. In addition, at oblique incidences of ultrasound on the surface of both isotropic and anisotropic solids, birefringence occurs [19–22]. Of course, since the splitting of a refracted wave into longitudinal and transverse waves is highly undesirable when creating a contrasting temperature grating, it preferable that such an absorbing layer as an electrode for applying an inverting voltage be made of an electrically conductive liquid or a metal film. However, the deposition of a metal film is time consuming; moreover, the creation of long-lasting temperature gratings is prevented by the high thermal conductivity of metal materials.

In this article, we consider technology variants based on the use of a temperature grating induced by interfering elastic waves incident on a liquid electrode in contact with the +Z-surface of a ferroelectric (acoustic interference method). The results are applicable to such ferroelectrics as lithium niobate, potassium titanyl phosphate, and lead zirconate titanate.

1. CREATION OF RDSs USING LONGITUDINAL ELASTIC WAVES

1.1. Experimental setup. Calculation of the main parameters. Elastic waves frequency dilemma

Figure 3 shows the working section of the experimental setup intended to create RDSs both in bulk *Z*-cut ferroelectrics and ferroelectric *Z*-oriented films (the electrical circuit was described previously [6]). The operation of the experimental setup is based on the combined effect of two pulses: an interference pulse and an inverting pulse (see INTRODUCTION).

As shown in Fig. 3, an RDS is formed in the region adjacent to the interference pattern in ferroelectric *1* due to the local switching of domains by the uniform electric field using an electrically conductive absorbing liquid film *6* in contact with +*Z*-surface *9* of the ferroelectric. Film *6* functions as an electrode for applying voltage U_c, which performs the local switching of the spontaneous polarization $\vec{\mathbf{P}}_S$ on the temperature grating. The radio pulse U_{AI} is sent to the input of emitters *4* of longitudinal acoustic waves interfering in the area of overlapping beams. In this case, the temperature grating is created on the section of a film *6* that is covered by the interference pattern (the ultrasound absorption coefficient in the liquid film significantly exceeds the absorption in acoustic duct *3*). Due to being in direct contact with the +*Z*-surface, the temperature grating is translated into nucleating layer *8* of the ferroelectric by means of heat transfer. The voltage U_c is applied to both Z-surfaces *9* and *13* for selective reorientation of the domains under the heated areas in the antinodes of the interference pattern. In this case, to transfer the potential from electrode *12* to the −*Z*-surface through liquid *5*, the latter should also be electrically conductive (a "ferroelectric on a solid conductive substrate" variant is also possible).

Acoustic duct *3* of the electroacoustic (EA) module having two emitters *4* is made of a material having a low acoustic wave attenuation coefficient. The components of the circuit are pressed against the ferroelectric crystal through sealing rings *2* (rubber cuffs) using clamp *10*. In order to maintain a constant thickness of liquid film *6* under conditions of possible setup vibrations and ensure the stability of the interference pattern, restrictive protrusions are provided on acoustic block *3*.

Let us consider the algorithm for calculating the process parameters and numerical estimates. When

creating RDSs using the acoustic interference method, the following algorithm can be used for calculating the main process parameters [12]. Here, an RDS is to be created having spatial period d, width b, and length a on the Z-surface. In order to ensure translation of the temperature grating from film *6* to $+Z$-surface *9*, the film thickness must satisfy the condition $\delta << d$. Let, e.g., $\delta \approx d/8$.

Taking into account the damping of the wave according to the Bouguer–Lambert law and assuming that the angles of refraction are small, we choose a film with a thickness approximately equal to the skin depth $1/\alpha$, where α is the absorption coefficient of ultrasound in the film. Then, given that $\delta \approx d/8$, the absorption coefficient is written as

$$\alpha \approx 8/d. \tag{1.1}$$

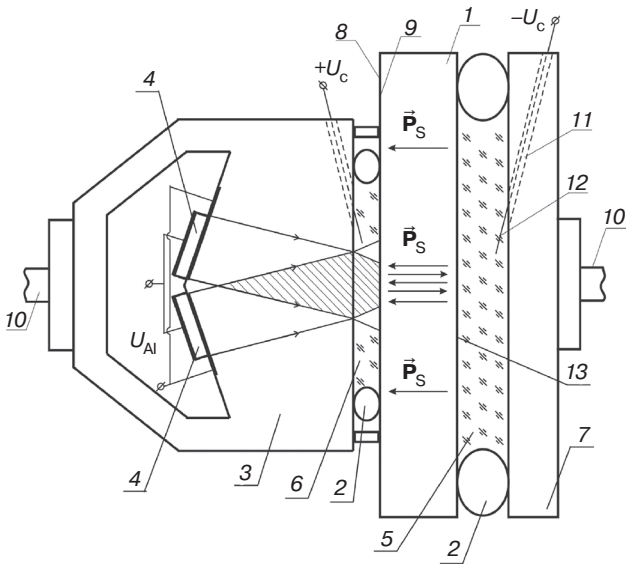

Fig. 3. Part of the setup for creating side-by-side RDSs

According to the Stokes–Kirchhoff formula, the frequency dependence of the absorption coefficient of acoustic waves in a liquid is quadratic: $\alpha = A \cdot f^2$, where A is a coefficient of proportionality. Then, using Eq. (1.1), the required ultrasound frequency is obtained as

$$f \approx \sqrt{8/dA}. \tag{1.2}$$

The period d of the interference pattern created by two beams propagating at an angle of 2β to each other is obtained

$$d = \lambda/(2\sin\beta) \tag{1.3}$$

Then the angle of incidence β of the beams on the absorbing film electrode is estimated at

$$\sin\beta \approx v_S A \cdot f/16, \tag{1.4}$$

where v_S is the speed of ultrasound in the acoustic duct of the EA module.

The aperture length p of each piezoelectric emitter is

$$p \approx a\sqrt{1 - Av_S^2/(32d)}, \tag{1.5}$$

where a is the RDS size (in the direction of the grating vector).

The length L of the acoustic duct of the EA module is found using the formula

$$L \approx \frac{p}{v_S}\sqrt{8d/A}. \tag{1.6}$$

The duration of the interference pulse t_p (for adiabatic heating in the antinodes) should be much less than the relaxation time of the temperature grating and can be estimated at [12]

$$t_p \approx 0.1 \cdot d^2/\chi, \tag{1.7}$$

where χ is the thermal diffusivity of the ferroelectric.

The acoustic pulse power incident on the absorbing film electrode (providing adiabatic heating in the antinodes) is calculated by the expression [23]

$$P_I \approx \frac{\rho_a C_a \chi \Delta T S}{1.6(1-R)d}\left(1 + \frac{8zC\rho}{dC_a\rho_a}\right), \tag{1.8}$$

where C_a, ρ_a, C, and ρ are the specific heat capacity and density of the absorbing film electrode and ferroelectric, respectively; z is the thickness of the nucleating ferroelectric layer; R is the coefficient of reflection from the absorbing film; ΔT is the temperature increment in the temperature grating; and S is the RDS area on the Z-surface.

This expression takes into account the energy consumption for local heating of the absorbing film-electrode and translation of the temperature grating into the nucleating layer of the ferroelectric (by heat transfer).

The pulsed power P_G of the microwave oscillator that is supplied to the input of the piezoelectric emitters is calculated by the formula

$$P_G \approx \frac{P_I \exp(2A_S f^2 L)}{\eta\left[1 - \left(\frac{K_{SW}-1}{K_{SW}+1}\right)^2\right]}, \tag{1.9}$$

where K_{SW} is the standing-wave coefficient in the radio path, η is the efficiency of the conversion of electrical energy into acoustic energy, and A_S is the coefficient of proportionality in the frequency dependence of the absorption coefficient of ultrasound for the material of the acoustic duct [11].

This expression takes into account the loss of acoustic energy in the acoustic duct as well as that due to the conversion of electrical energy into acoustic energy (both the dissipative loss and conversion loss are due to the reflection of the electromagnetic wave from the piezoelectric emitters).

The above expressions were used to calculate the main process parameters of the creation of RDSs in epitaxial *Z*-oriented lead zirconate titanate (PZT) films deposited on a conductive substrate. The RDSs formed in such films are used, e.g., in acoustoelectronics to create acoustic microwave filters [1]. Table 1 presents the results of calculations for an RDS with a width of $b = 25$ μm and a number of periods of $N = 20$ for two spatial period values $d = 0.8$ and 1.2 μm (these values correspond to the RDS created by scanning with an atomic force microscope probe in PZT films having a thickness of 0.2 μm [1]). The material of the liquid absorbing film electrode comprised an aqueous LiCl solution with a low thermal diffusivity ($0.14 \cdot 10^{-6}$ m^2/s), which significantly exceeds the value of this parameter for ferroelectrics. The material of the acoustic duct of the EA module was fused quartz. The following parameter values were used in the calculations [24, 25]: $A \approx 29.9 \cdot 10^{-15}$ s^2/m, $v_S \approx 5.96 \cdot 10^3$ m/s, $A_S \approx 0.015 \cdot 10^{-15}$ s^2/m, $\chi \approx 0.7 \cdot 10^{-6}$ m^2/s, $C = 300$ J $\cdot$ kg$^{-1}\cdot$K^{-1}, $\rho = 7.6 \cdot 10^3$ kg $\cdot$ m^{-3}, $C_a = 3800$ J $\cdot$ kg^{-1} $\cdot$ K^{-1}, $\rho_a = 1.05 \cdot 10^3$ kg $\cdot$ m^{-3}, $R = 0.5$, and $\Delta T = 5$ K.

Table 1 shows that the radio pulse power P_G at the input of the piezoelectric emitters does not exceed 0.1 W. Here it should be noted that the power P_G should not exceed the threshold value to avoid breakdown. This is especially important for gigahertz piezoelectric emitters in which thickness of the piezoelectric layer is quite small. The threshold value of the breakdown power depends on the material of the piezoelectric layer, its thickness, and other parameters, which is the subject of special studies.

From expressions (1.8) and (1.9), it follows that P_G can be reduced, in particular, by decreasing the temperature increment ΔT. Small ΔT values are acceptable in areas with a strong dependence of the coercive field on temperature. As the results of studying PZT showed [26], ΔT can be radically reduced near the Curie point, where the rate of decrease in the coercive field with increasing temperature is maximal.

As follows from expression (1.9), the power P_G can be reduced by decreasing the operating frequency f, the length L, and the absorption coefficient A_S in the acoustic duct of the EA module. In addition, P_G can be reduced by increasing the conversion efficiency η and decreasing the area S, as well as by reducing the reflection loss of the radio pulse from the piezoelectric emitter (by decreasing the standing-wave coefficient K_{SW} using impedance matching).

Expression (1.2) shows that frequency f can be decreased (at a given period d) by increasing the coefficient A of the absorbing film (by choosing appropriate electrolyte solution, solute concentration, and operating temperature).

The relaxation time of the temperature grating is $\tau_d \approx d^2/\chi$. In our calculations, for the period $d \approx 0.8$–1.2 μm, it is $\tau_d \approx 1$–2 μs, i.e., significantly exceeding the duration t_S of the inverting pulse, which for a PZT film is about 50 ns. Therefore, the temperature grating is preserved throughout the inverting pulse. At the same time, the duration of the process cycle (combined exposure to the interference and inverting pulses) is $t_C \approx t_p + t_S \leq 0.25$ μs (Table 1).

Let us estimate the elongation of the sample due to thermal expansion. For PZT, the thermal expansion coefficient is $k \approx 2 \cdot 10^{-6}$ K^{-1} [25]. Then, for a temperature grating having a temperature increment of $\Delta T = 5$ K, the relative elongation is $\Delta a/a \approx k \cdot \Delta T/2 \approx 0.47 \cdot 10^{-5}$. For an RDS with a length of $a \approx 20$ μm (which was used in the calculations), the elongation is $\Delta a \approx 10^{-10}$ m. The obtained value is four orders of magnitude smaller than the RDS periods given in Table 1.

Thus, using the developed model, the main process parameters of the creation of an RDS were estimated as applied to *Z*-oriented PZT films and liquid electrodes based on an aqueous LiCl solution. The calculations showed that, at room temperature (293 K), the creation of an RDS with a period on the order of one micrometer requires interfering elastic waves in the gigahertz range, the generation of which requires very expensive EA modules.

Note that the results of the estimation calculations were obtained for small angles of refraction and under the assumption that the thickness of the liquid electrode layer is approximately equal to the skin depth $\delta \approx d/8$.

As shown previously [27], in order to create an RDS with a small spatial period, including submicron structures, thin ferroelectric samples (i.e., films) should be used due to their specific heat transfer properties.

Table 1. Main process parameters of the creation of RDSs in PZT films

RDS period d, μm	Frequency f, GHz	Pulse duration t_p, μs	Acoustic duct length L, μm	Conversion efficiency η	Standing-wave coefficient K_{SW}	Power at input of liquid electrode P_I, W	Power at input of emitters P_G, W
$d = 1.2$	14.9	0.2	71	0.4	1.3	0.015	0.063
$d = 0.8$	18.3	0.09	38	0.3	1.4	0.019	0.094

The amplitude of the sound pressure of an elastic wave decreases by a factor of e at a distance of 1/α. Formula (1.2) for the carrier frequency of elastic waves was obtained under the assumption of small angles of refraction (for a liquid electrode with a thickness of 1/α). At the same time, after the wave is refracted at the acoustic duct–liquid interface at angle γ, the projection of the distance traveled by the wave onto the normal to the boundary is $\delta_0 = (1/\alpha)\cos\gamma$ ("reduced" skin depth). Earlier [15], for a liquid electrode with a thickness equal to the reduced skin depth, solutions were obtained for the carrier frequency (constructive frequency dilemma) as well as for the angles of refraction. The solutions for the angles of refraction have the form

$$\gamma_1 = \arccos\left(1.15\cos\left(\frac{\pi}{3}+\frac{1}{3}\arccos\frac{Av^2}{12.3d}\right)\right), \quad (1.10)$$

$$\gamma_2 = \arccos\left(1.15\cos\left(\frac{\pi}{3}-\frac{1}{3}\arccos\frac{Av^2}{12.3d}\right)\right), \quad (1.11)$$

where v is the speed of ultrasound in the liquid electrode.

The corresponding solutions for the frequency of interfering waves are given by the formulas

$$f_1 \approx \sqrt{\frac{8\cos\gamma_1}{dA}}, \quad (1.12)$$

$$f_2 \approx \sqrt{\frac{8\cos\gamma_2}{dA}}. \quad (1.13)$$

Based on the results of the modeling, we provided recommendations for choosing the frequency taking into account the state of the art of high-frequency ultrasonic piezoelectric emitters. As can be seen from formulas (1.12) and (1.13), it is advisable when operating at lower frequencies to use liquid electrodes having a high coefficient A value in the frequency dependence $\alpha = Af^2$ of the absorption coefficient of elastic waves.

Note that the values of the "lower" and "upper" frequencies of the elastic waves depend only on the properties of the liquid electrodes and the period of the domain structure.

Thus, the formation of an RDS (with given period d) is possible in two cases:

1) at the lower frequency f_1 with the angle of refraction γ_1 (formulas (1.10) and (1.12)), and
2) at the upper frequency f_2 with the angle of refraction γ_2 (formulas (1.11) and (1.13)).

The obtained results can be used to create similar experimental setups that require one to take into account the state of the art of high-frequency piezoelectric emitters.

1.2. Low-temperature operation

The cost of EA modules is known to sharply increase with increasing operating frequency of the piezoelectric emitter of elastic waves. Keeping in mind the high cost of manufacturing gigahertz piezoelectric emitters, let us consider an economical technological solution involving the use of ultrasonic waves at frequencies close to the lower limit of the microwave range ($f \approx 300$ MHz). As shown below, DPH technology can be used to create RDSs having parameters corresponding to those of the key elements of high-performance acoustoelectronic devices [28], as well as generators and detectors of terahertz radiation [2].

It can be shown that, for a liquid electrode of thickness δ equal to 1/2 of the reduced skin depth, i.e., $\delta = (1/2\alpha)\cos\gamma$, the formulas for the angle of refraction and the frequency f of elastic waves have the form

$$\gamma = \arccos\left(1.154\cos\left(\frac{\pi}{3}-\frac{1}{3}\arccos\frac{Av^2}{6.15d}\right)\right), \quad (1.14)$$

$$f \approx \sqrt{\frac{4\cos\gamma}{dA}}, \quad (1.15)$$

where d is the spatial limit of the RDS.

Solving the system of equations (1.14) and (1.15) gives formulas for the period of the RDS and the coefficient A:

$$d \approx \frac{0.81v}{f}\sqrt{\cos\gamma / \cos(\pi - 3\arccos(0.867\cos\gamma))}, \quad (1.16)$$

$$A \approx \frac{5}{vf}\sqrt{\cos\gamma \cdot \cos(3\arccos(0.867\cos\gamma) - \pi)}. \quad (1.17)$$

The angle of refraction is known to be related to the angle of incidence by Snell's law

$$\gamma = \arcsin\left(\frac{v}{v_S}\sin\beta\right). \quad (1.18)$$

For the phase and group velocities of the elastic wave to have the same direction, the material for the acoustic duct of the EA module should be isotropic. Among isotropic materials, the attenuation of elastic waves is lowest in fused quartz.

Let us consider the operation of an EA module made of fused quartz ($v_S \approx 5.96 \cdot 10^3$ m/s) in combination with a liquid electrode with a speed of ultrasound $v \approx 1.7 \cdot 10^3$ m/s. Previously [16], the frequency dependences of the period d and coefficient A of a liquid electrode were characterized according to expressions (1.16), (1.17), and (1.18).

Figure 4 illustrates the dependences of the period d on the frequency f for three EA modules with β = 10°, 12°, and 17°. For example, at a frequency of $f \approx 300$ MHz and an angle of incidence β ≈ 17°, an RDS with a period of $d \approx 38.0$ μm can be created. RDSs with such a period are used, in particular, in the manufacture of IR optical parametric oscillators [29, 30]. However, to create an RDS with such a period, an appropriate liquid electrode is required. Figure 5 presents the dependence of the coefficient A of the liquid electrode on the frequency f for the same EA modules. It can be seen that, to create an RDS with such a period, a liquid electrode with a very high value of the coefficient $A \approx 1060 \cdot 10^{-15}$ s^2/m is necessary. One of best-studied and most widely available conductive liquids is an aqueous solution of lithium chloride LiCl. However, at a frequency $f \approx 300$ MHz, the coefficient A of a LiCl solution is insufficiently high ($A \leq 550 \cdot 10^{-15}$ s^2/m) even when cooled to $T \approx 223$ K [31]. Therefore, an aqueous LiCl solution is inapplicable for creating an RDS with a period of $d \leq 40$ μm at a frequency close to $f \approx 300$ MHz.

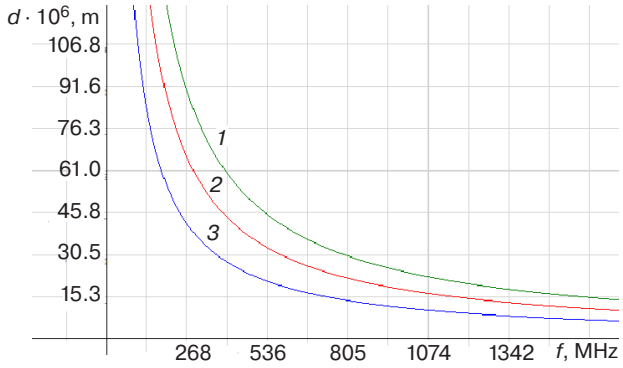

Fig. 4. Period d versus frequency f at three values of the angle of incidence β = (*1*) 10°, (*2*) 12°, and (*3*) 17°

As noted above, RDSs having a period $d \approx 40$–100 μm are the key elements of high-performance acoustic filters [28], as well as generators and detectors of terahertz radiation [2]. The possibility of creating an RDS with such values of the RDS period at a frequency $f \approx 300$ MHz has been demonstrated using a liquid electrode based on a LiCl solution at angles of incidence β < 17° [16]. For example, at β ≈ 10° at a given frequency (as follows from Figs. 4 and 5), the RDS period is $d \approx 80$ μm when using a liquid electrode with $A \approx 230 \cdot 10^{-15}$ s^2/m. This value of the coefficient A can be achieved by cooling the aqueous LiCl solution to a temperature of $T \approx 241$ K [31].

An EA module having a higher frequency $f \approx 670$ MHz has also been modeled [16]. At this frequency and lower temperature of $T \approx 233$ K, the possibility of creating an RDS with a period $d \approx 16$ μm has been demonstrated using a LiCl solution-based liquid electrode [31].

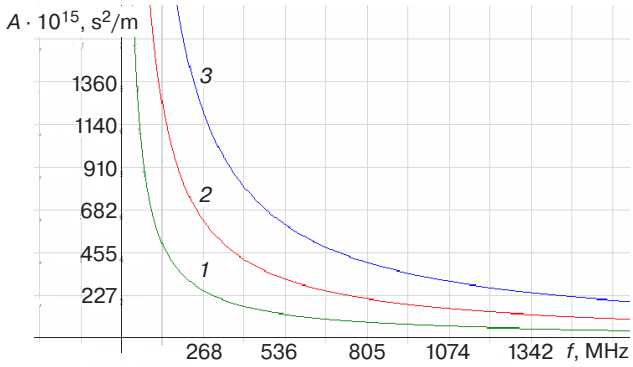

Fig. 5. Coefficient of liquid electrode versus frequency at three values of the angle of incidence β = (*1*) 10°, (*2*) 12°, and (*3*) 17°

In economical terms, EA modules operating at lower frequencies are generally more affordable. For example, domain structures with a period $d \approx 90$ μm can be created at a frequency of $f \approx 270$ MHz and β ≈ 10° using a liquid electrode with $A \approx 250 \cdot 10^{-15}$ s^2/m (e.g., a 7.7 M aqueous LiCl solution at $T \approx 238$ K [31]).

Significantly, RDSs with different periods d can be created using the same EA module (with a specified value of the angle of incidence β) by tuning the frequency within certain limits by means of various liquid electrodes and/or different temperatures.

2. CREATION OF RDSs USING LONGITUDINAL ELASTIC WAVES AND ELECTRODES BASED ON RTIL IONIC LIQUIDS

2.1. Main parameters of some highly dissipative RTIL at room temperature

The possibility of using the acoustic interference method to create RDSs using liquid electrodes based on an aqueous solution of lithium chloride was demonstrated in the previous section. However, the proposed technological solution requires cooling down to temperatures from 233 to 243 K.

In this section, we will discuss the possibility of creating RDSs at room temperature and frequencies near $f \approx 300$ MHz taking into account new data on the acoustic properties of liquid electrodes based on ionic liquids. Salts that melt at room temperature are referred to as room-temperature ionic liquids (RTIL). It will be shown that highly dissipative, electrically conductive RTILs such as 1-butyl-3-methylimidazolium bis(trifluoromethylsulfonyl)imide ([C_4mim][NTf_2]) and 1-hexyl-3-methylimidazolium bis(trifluoromethylsulfonyl)imide ([C_6mim][NTf_2]) create favorable conditions for the formation of RDSs using the acoustic interference method, implementing the technological solution [16] without cooling below

room temperature. The results are applicable to such ferroelectrics as $LiNbO_3$, $KTiOPO_4$, and PZT.

Let us consider the use of RTIL-based liquid electrodes in combination with a fused quartz acoustic duct. The experimental setup for the creation of RDSs using interfering elastic waves was described in section 1.1, as well as in the literature [12]. Figure 6 shows a fragment of this setup: (*1*) ferroelectric, (*2*) acoustic duct of the EA module, (*3*) piezoelectric emitter of longitudinal waves, (*4*) liquid electrode, and (*5*) +*Z*-surface of the ferroelectric. Here, P_S is the spontaneous polarization, β is the angle of incidence on the quartz–liquid interface, γ is the angle of refraction, and P_G is the power at the input of the piezoelectric emitters.

Previously [15], the thickness of the liquid electrode was assumed to be equal to the reduced skin depth $\delta_0 = (1/\alpha)\cos\gamma$. At the same time, in order to reduce the excessively high values of the coefficient *A*, the thickness of the liquid electrode should be selected to be somewhat lower than the reduced skin depth. Since a more significant decrease can lead to a decrease in the contrast of the temperature grating due to the reflection of a significant fraction of the ultrasound energy from the +*Z*-surface of the ferroelectric, this value should be approximately equal to 1/2–3/4 of the reduced skin depth. For example, if the thickness of the liquid electrode is taken to be 1/2 of the reduced skin depth, i.e., $\delta = (1/2\alpha)\cos\gamma$, then the angle of refraction γ, frequency *f*, period *d*, and coefficient *A* can be described by formulas (1.14), (1.15), (1.16), and (1.17), respectively.

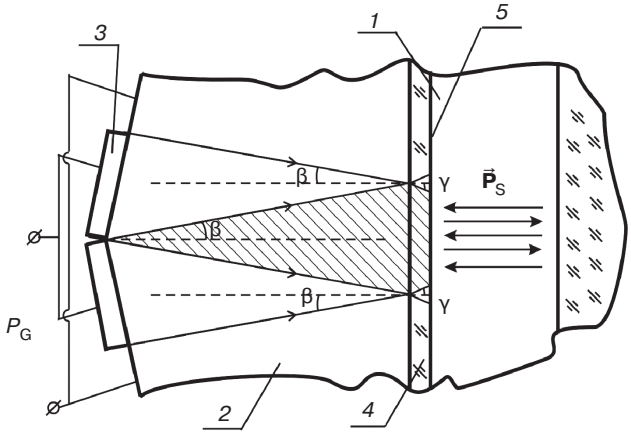

Fig. 6. Fragment of the experimental setup

Table 2 presents some parameters of four RTILs with high values of coefficient *A* at 293 K [32, 33]. It can be seen that these values are more than an order of magnitude higher than those of this coefficient for an aqueous lithium chloride solution at room temperature; as follows from expression (1.15), this allows RDSs to be created at much lower ultrasound frequencies.

Note also that the thermal diffusivity of the RTILs presented in Table 2 is very low (less than half that of water): $\chi \approx 0.6 \cdot 10^{-7}$ m^2/s. This makes it possible to create "long-lived" temperature gratings in RTIL-based liquid electrodes.

2.2. Results of computer modeling of the creation of RDSs at room temperature with ionic liquids

Figure 7 presents the dependence of the coefficient *A* of the liquid electrode on the frequency *f* according to expressions (1.17) and (1.18) for EA modules with angles of incidence β = 17°, 16°, 15°, and 14°. The required value of the coefficient *A* of the liquid electrode can be seen to decrease at a given frequency *f* with decreasing angle of incidence β on the quartz–RTIL interface.

An analysis of the radicands in expressions (1.16) and (1.17) shows that the minimum possible angle of incidence on the quartz–RTIL interface is β ≈ 13° (for liquids with a speed of sound of $v \approx 1260$ m/s). For angles β ≈ 13° and less, there is no real solution. In this case, this angle is independent of the chosen thickness of the liquid electrode, depending only on the v/v_S ratio. At the same time, as follows from Fig. 7, the selection of angles of incidence that significantly exceed β = 17° involves the need to use RTIL with a very high coefficient *A*, which is not always possible at room temperatures [32, 33].

Figure 8 illustrates the dependence of the period *d* on the frequency *f* according to expressions (1.16) and (1.15) for the same EA modules with specified incidence angles β = 17°, 16°, 15°, and 14°. Here, the period *d* of the formed RDS can be seen to increase for an EA module with a specified frequency *f* with decreasing angle of incidence β on the quartz–RTIL interface. Obviously, as follows from Fig. 7, the selection of an excessively low ultrasound frequency results in the need to find an RTIL

Table 2. Parameters of RTILs with high values of the coefficient *A* at an ultrasound frequency of $f \approx 300$ MHz and a temperature of 293 K

RTIL	Coefficient *A*, s^2/m	Speed of ultrasound *v*, m/s	Electrical conductivity σ, S/m	Reference
$[C_2mim][NTf_2]$	$450 \cdot 10^{-15}$	1260	0.9	[32]
$[C_4mim][NTf_2]$	$650 \cdot 10^{-15}$	1260	0.3	[32]
$[C_6mim][NTf_2]$	$800 \cdot 10^{-15}$	1260	0.2	[32]
$[C_4C_1pyr][NTf_2]$	$870 \cdot 10^{-15}$	1260	0.2	[33]

having a rather high value of the coefficient A, which, as noted above, is not always possible at room temperatures.

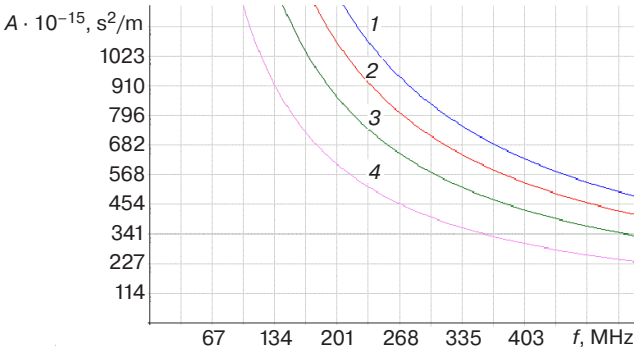

Fig. 7. Coefficient of liquid electrode versus ultrasound frequency at four values of the angle of incidence β = (*1*) 17°, (*2*) 16°, (*3*) 15°, and (*4*) 14°

For example, as follows from Fig. 8, using the EA module operating at a frequency of $f \approx 300$ MHz, at an angle of incidence $\beta \approx 15.5°$, an RDS with a period $d \approx 48$ μm can be created. At the same time, as follows from Fig. 7, to create such an RDS, an appropriate liquid electrode with $A \approx 650 \cdot 10^{-15}$ s²/m is required. As Table 2 shows, the ionic liquid [C_4mim][NTf_2] can be used as such a liquid electrode at a temperature of 293 K (with a conductivity $\sigma \approx 0.3$ S/m). As follows from Figs. 7 and 8, by using another RTIL such as the ionic liquid [C_6mim][NTf_2] (with $A \approx 800 \cdot 10^{-15}$ s²/m at the same temperature) at the same frequency, an RDS can be created having a period $d \approx 42$ μm (with an incidence angle $\beta \approx 16.7°$).

Table 3 presents other examples of creating RDS using RTIL at room temperature. At a frequency $f \approx 300$ MHz with the given RTIL, the spread in values of the angle of incidence β can be seen to comprise approximately 3 degrees.

In practical terms, the most interesting case arises when there is one type of RTIL and one EA module with a specified angle β. In this case, it is possible to create an RDS having a different period d by tuning the ultrasound frequency using the previously characterized [32, 33] temperature dependences of the coefficient A.

The rightmost column of Table 3 presents the estimated durations t_p of an interference pulse calculated for lithium niobate ($\chi \approx 1.54 \cdot 10^{-6}$ m²/s) using formula (1.7). For ferroelectrics having thermal diffusivities lower than that of lithium niobate, such as PZT [34], the corresponding values of the pulse duration t_p are several times longer.

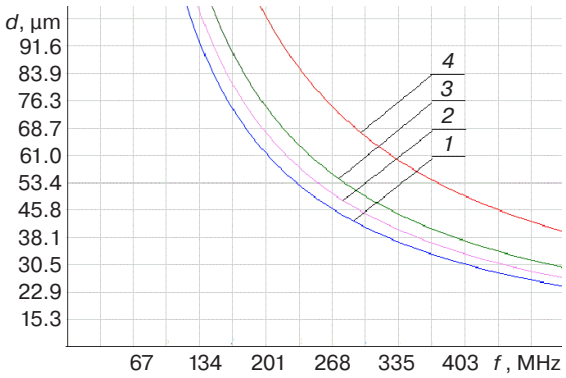

Fig. 8. Period d versus frequency at four values of the angle of incidence β = (*1*) 17°, (*2*) 16°, (*3*) 15°, and (*4*) 14°

The obtained results can be used, e.g., to develop and manufacture high-performance acoustic filters [28], generators of terahertz waves [2], and giant strain actuators [35, 36], especially in their mass production.

3. CREATION OF RDSs USING ELASTIC SHEAR WAVES

3.1. Calculation of the parameters of shear waves and some liquid electrodes in the Newtonian fluid model

In the previous section, we demonstrated the efficacy of using highly dissipative, electrically conductive RTILs as electrodes in the creation of RDSs at room temperature [37]. It is important to note that the use of these liquids opens up more opportunities in terms of choosing the type of elastic waves, since not only longitudinal, but also shear waves can propagate in them. A feature of shear waves is a very small depth of their penetration into the liquid [38]. This feature can significantly increase the efficiency of the technology.

The previously obtained [15] results showed that high values of the coefficient A for liquid electrodes allow the ultrasound frequency to be significantly reduced. Obviously, the use of shear waves can reduce the operating frequency. The use of shear waves can

Table 3. Estimated parameters for the creation of RDSs using ultrasound at a frequency $f \approx 300$ MHz and some RTILs at a temperature of 293 K

RTIL	Coefficient A, s²/m	Angle of incidence β, deg	RDS period d, μm	Pulse duration t_p, μs (for lithium niobate)
[C_2mim][NTf_2]	$450 \cdot 10^{-15}$	14.3	59	226
[C_4mim][NTf_2]	$650 \cdot 10^{-15}$	15.5	48	150
[C_6mim][NTf_2]	$800 \cdot 10^{-15}$	16.7	42	115
[C_4C_1pyr][NTf_2]	$870 \cdot 10^{-15}$	17.2	40	104

also be justified as follows. As is known, reflection and refraction of horizontally polarized shear waves do not result in the splitting of the wave into longitudinal and shear components at any angle of incidence. At the same time, when longitudinal waves are obliquely incident on the interface, the type of the wave is transformed, which may cause significant energy loss.

Whereas there are numerous publications on the use of longitudinal waves in liquids, corresponding studies into the use of shear waves, in particular, horizontally polarized ones, in liquids are not so abundant [39, 40].

As will be shown below, in some conductive liquids, giant values of the coefficient $A \approx (0.482–4.28) \cdot 10^{-10}$ s^2/m were obtained for shear waves at room temperatures. Note that the process of the creation of RDSs using longitudinal waves [37] used ionic liquids with $A \approx (0.2–0.8) \cdot 10^{-12}$ s^2/m (i.e., two orders of magnitude lower).

The experimental setup for the creation of RDS by the acoustic interference method using elastic waves was described in section 1 of this article, as well as in the literature [12, 15]. The setup described in this section differs by virtue of including piezoelectric emitters of shear waves, rather than longitudinal waves.

The wave amplitude decreases by a factor of e at the distance 1/α. For shear waves, 1/α is the depth of penetration of these waves into the liquid, which can be estimated at [38]

$$1/\alpha = \sqrt{\frac{2\eta_0}{\rho\omega}}, \quad (3.1)$$

where η_0 is the viscosity of the liquid at low frequencies, ρ is liquid density, and ω is the circular frequency of the shear waves.

For example, at a viscosity of 0.1 Pas, a density of 1400 kg/m^3, and a frequency f = 200 MHz, the penetration depth 1/α of a shear wave into the liquid is very small (324 nm). The quantity 1/α is also referred to as the skin depth. After the wave is refracted at the acoustic duct–liquid interface at angle γ, the wave amplitude decreases by a factor of e at a distance of 1/α, and the projection of the distance traveled by the wave onto the normal to this interface is $\delta_0 = (1/\alpha)\cos\gamma$ (reduced skin depth).

The velocity of shear waves propagating in a Newtonian fluid ($\omega\tau << 1$, where τ is the shear relaxation time) is described by the formula [40]

$$v \approx \sqrt{2\eta_0\omega/\rho}. \quad (3.2)$$

The coefficient of proportionality A for shear waves in the fluid can be readily found from expression (3.1)

$$A \approx \sqrt{\frac{\pi\rho}{\eta_0 f^3}}. \quad (3.3)$$

Using the condition $\omega\tau << 1$ of the Newtonian fluid model [40] and the values of the shear relaxation times τ of fluids that are given in Table 4, the maximum frequency f_N of shear waves in the model can be estimated at

$$f_N \approx 1/(4\pi\tau). \quad (3.4)$$

Table 4 presents the maximum frequencies f_N of shear waves (in the Newtonian fluid model) as calculated from formula (3.4) and some parameters of fluids used as electrodes: $LiPF_6$–PC electrolyte solution and the ionic liquid 1-butyl-3-methylimidazolium hexafluorophosphate ([C_4mim][PF_6], or [bmim][PF_6]).

For many materials at frequencies above approximately $f \approx 300$ MHz, the elastic waves are significantly attenuated in the acoustic duct of the EA module. To avoid this (other conditions being equal), a higher ultrasound power and more labor-intensive technology has to be used for manufacturing piezoelectric emitters. Based on this, and provided that the condition $f < f_N$ is met for each liquid, the frequencies $f \approx 70$ MHz and $f \approx 300$ MHz were chosen for preliminary estimation of the shear wave velocity v and the coefficient A. Table 5 presents the values of the shear wave velocity v and coefficient A calculated in the Newtonian model using formulas (3.2) and (3.3).

Table 5 shows that, for shear waves, these liquids have giant values of the coefficient $A \approx (0.482–4.28) \cdot 10^{-10}$ s^2/m

Table 4. Values of f_N and parameters of liquid electrodes at room temperature

No.	Liquid	Viscosity η_0, Pa·s	Density ρ, kg/m^3	Relaxation time τ, s	f_N, MHz	Electrical conductivity σ, S/m
1	$LiPF_6$–PC (2 mol/kg)	0.06 [41]	$1.2 \cdot 10^3$ [41]	$0.2 \cdot 10^{-9}$ [42]	400	0.2 [45]
2	[C_4mim][PF_6]	0.27 [43]	$1.38 \cdot 10^3$ [43]	$1.1 \cdot 10^{-9}$ [44]	72	0.1 [46]

Table 5. Values of the shear wave velocity v and coefficient A at frequencies not exceeding the maximum frequency f_N of the Newtonian model

No.	Liquid	$f < f_N$, MHz	v, m/s	A, s^2/m
1	$LiPF_6$–PC (2 mol/kg)	300	434.2	$0.482 \cdot 10^{-10}$
2	[C_4mim][PF_6]	70	414.9	$2.18 \cdot 10^{-10}$
3	$LiPF_6$–PC (2 mol/kg)	70	209.7	$4.28 \cdot 10^{-10}$

at room temperature. It is also noted that the velocity of the shear waves is several times lower than that of the longitudinal waves.

Taking into account the above limitations, computer modeling was performed to determine the angles of incidence of shear waves on the acoustic duct-liquid interface for given values of the RDS period and develop recommendations for choosing the frequency; the results are discussed in the next section.

3.2. Results of computer modeling for liquid electrodes based on [C_4mim][PF_6] and $LiPF_6$–PC at room temperature

A mathematical model of the effect of interfering elastic waves on a ferroelectric through a liquid layer whose thickness δ is smaller than the RDS half-period ($\delta \approx d/8$) and equal to the reduced skin depth $\delta_0 = (1/\alpha)\cos\gamma$ has been considered earlier[15].

It was determined [15] that, if the condition

$$d \geq 0.081 A v^2, \tag{3.5}$$

is met, then, for a given RDS period, the angle of refraction and the shear wave frequency are described by the expressions

$$\gamma = \arccos\left(1.15\cos\left(\frac{\pi}{3} - \frac{1}{3}\arccos\frac{Av^2}{12.3d}\right)\right), \tag{3.6}$$

$$f \approx \sqrt{\frac{8\cos\gamma}{dA}}. \tag{3.7}$$

We note that the elastic wave velocity v and the coefficient A in formulas (3.6) and (3.7) in the case of shear waves depend on the frequency according to (3.2) and (3.3), respectively.

From expressions (3.6) and (3.7), the following formula for the coefficient is obtained:

$$A \approx \frac{9.92}{vf}\sqrt{\cos\gamma\cos(3\arccos(0.867\cos\gamma) - \pi)}. \tag{3.8}$$

The radicand is nonnegative if $\gamma \geq 0.0475$.

Equating the right-hand sides of expressions (3.3) and (3.8) and taking into account expression (3.2), we obtain the equation for the angle of refraction of shear waves on the acoustic duct–liquid interface:

$$2.4927\cos\gamma\cos(3\arccos(0.867\cos\gamma) - \pi) = 1.$$

Solving this equation gives two values of the angle of refraction:

$$\gamma_1 = 0.455; \gamma_2 = 1.119. \tag{3.9}$$

The angle of refraction γ is known to be related to the angle of incidence β by Snell's law (1.18).

Using expressions (1.18) and (3.2), the frequency dependences of the angles of incidence β on the acoustic duct–liquid interface can be derived:

$$\begin{aligned}\beta_1 &= \arcsin\left(v_S \sin\gamma_1\sqrt{\frac{\rho}{4\pi\eta_0 f}}\right),\\ \beta_2 &= \arcsin\left(v_S \sin\gamma_2\sqrt{\frac{\rho}{4\pi\eta_0 f}}\right).\end{aligned} \tag{3.10}$$

Hence, the conditions follow:

$$v_S \sin\gamma_1\sqrt{\frac{\rho}{4\pi\eta_0 f}} \leq 1,\ v_S \sin\gamma_2\sqrt{\frac{\rho}{4\pi\eta_0 f}} \leq 1. \tag{3.11}$$

Obviously, the case of the smaller angle of incidence β_1 is of the greatest practical interest; since $\gamma_1 = 0.455 < \gamma_2 = 1.119$, this occurs at a lower frequency. In addition, to meet condition (3.11) at lower frequencies, it is advisable to use an EA module made of a material having a low shear wave velocity v_S. Paratellurite α-TeO_2 represents such a material in which the slowest shear sound wave velocity is $v_S = 0.61 \cdot 10^3$ m/s [47]. Then, condition (3.11) for the 2 mol/kg $LiPF_6$–PC liquid is satisfied at $f > f_{min1} \approx 113$ MHz; for the [C_4mim][PF_6] liquid, at $f > f_{min1} \approx 26$ MHz.

Figure 9 illustrates the frequency dependence of the angles of incidence β_1 and β_2 for the 2 mol/kg $LiPF_6$–PC liquid using the EA module based on paratellurite. It can be seen from Fig. 9 that the frequency f_{min2} (for the angles β_2) is approximately equal to 481 MHz for this liquid. In the Newtonian model used here, an RDS can be created at shear wave frequencies simultaneously higher than the frequency f_{min1} and lower than the maximum frequency f_N of the Newtonian model. Therefore, since the condition $f < f_N = 400$ MHz should be satisfied because for the 2 mol/kg $LiPF_6$–PC liquid, only the angles β_1 are of interest.

Similar frequency dependences of the angles of incidence β_1 and β_2 when using the EA module based on paratellurite were also characterized for the [C_4mim][PF_6] liquid. Table 6 presents the minimum frequencies f_{min1} and f_{min2} for these two liquids along with the angles β_1.

It is also necessary to determine the spatial period of the formed RDS. Taking into account expressions (3.3) and (3.7) and two values of the angle of refraction (3.9), we obtain the formulas for the frequency dependence of the RDS period:

$$d_1 = 8\cos\gamma_1 \Big/ \sqrt{\pi\rho f / \eta_0},\ d_2 = 8\cos\gamma_2 \Big/ \sqrt{\pi\rho f / \eta_0}. \tag{3.12}$$

Figure 10 presents the frequency dependences of the RDS period for the 2 mol/kg $LiPF_6$–PC liquid

Table 6. Minimum frequencies, operating frequency range Δf, angle of incidence β_1, and RDS period d_1, calculated for an acoustic duct made of α-TeO_2

No.	Liquid	f_{min1}, MHz	f_{min2}, MHz	Operating frequency range Δf, MHz	Angle of incidence β_1	RDS period d_1, μm	f_N, MHz
1	$[C_4mim][PF_6]$	26	123	30–70	1.410–0.703	10.4–6.8	72
2	$LiPF_6$–PC (2 mol/kg)	113	481	125–400	1.270–0.564	2.6–1.4	400

and the $[C_4mim][PF_6]$ liquid. These dependences can be used to determine the period of the created RDS at frequencies in the range from f_{min1} to f_N. In particular, for the 2 mol/kg $LiPF_6$–PC liquid, at frequencies in the range from f_{min1} = 113 MHz to f_N = 400 MHz; and for the $[C_4mim][PF_6]$ liquid, at frequencies in the range from f_{min1} = 26 MHz to f_N = 72 MHz.

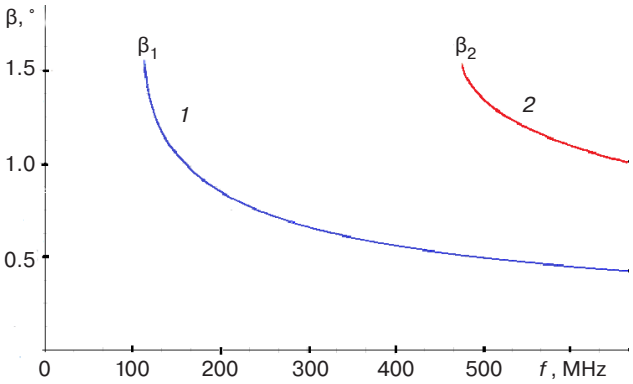

Fig. 9. Frequency dependence of the angles of incidence β_1 and β_2 on the paratellurite–liquid interface for the 2 mol/kg $LiPF_6$–PC liquid

Table 6 presents the results of calculating the minimum frequencies of shear waves, the range Δf of operating frequencies, the angles of incidence β_1, and the RDS period d_1 (for the EA module made of α-TeO_2) for two liquids. Obviously, in practice, the operating frequency range Δf is somewhat smaller than the difference $f_N - f_{min1}$ because the operating frequency is chosen not too close to the frequencies f_{min1} and f_N.

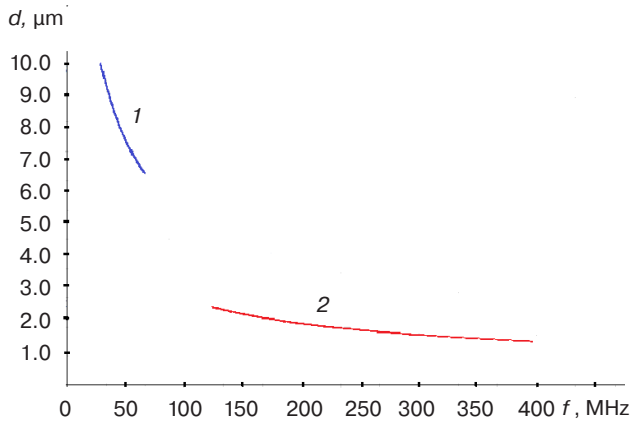

Fig. 10. Frequency dependence of the RDS period for the (*1*) $[C_4mim][PF_6]$ liquid and (*2*) 2 mol/kg $LiPF_6$–PC liquid

From Table 6, it can be seen that the use of a liquid electrode based on the 2 mol/kg $LiPF_6$–PC liquid enables the creation of an RDS with a period of 1.4–2.6 μm at frequencies of 400–125 MHz, respectively.

Thus, by using the acoustic interference method using shear waves, it is possible to create an RDS having a very small spatial period at room temperature with an EA module made of paratellurite, which is a significant advantage over the technology [37] using longitudinal waves.

CONCLUSIONS

The following are the main results obtained at RTU MIREA for the technology used for the creation of ferroelectric RDSs using interfering elastic waves.

1) The proposed technology for creating RDSs uses interfering elastic waves of high and ultrahigh frequencies. In this case, ultrasound is almost completely absorbed in liquid electrodes of a certain thickness and does not penetrate the ferroelectric, which prevents multiple reflections from opposite faces, increases the contrast of the acoustically induced temperature grating, and makes the technology universal (independent of the degree of acoustic transparency of the ferroelectric).
2) It is shown that, when using liquid electrodes based on lithium chloride, the creation of a RDS having a spatial period of several tens of micrometers at ultrasound frequencies of about 300 MHz requires cooling to temperatures of 233 to 243 K. It was also found that, at room temperature, the creation of an RDS requires liquid electrodes for which the coefficient of proportionality in the frequency dependence of the absorption coefficient of ultrasound is an order of magnitude greater than that of a lithium chloride solution.
3) It is shown that the use of such highly dissipative ionic liquids as $[C_4mim][NTf_2]$ and $[C_6mim][NTf_2]$ as liquid electrodes creates favorable conditions for the formation of a short-period RDS at room temperature. Recommendations are given on the choice of the type of ionic liquid, the values of the carrier frequency and pulse duration, as well as the angle of incidence of elastic waves on the fused quartz-liquid interface.

4) Using the Newtonian fluid model, a mathematical model is formulated for the creation of an RDS under the action of interfering shear waves on a ferroelectric through a liquid electrode layer was created. Recommendations are given for selecting the type of the liquid electrode, its thickness, the angle of incidence of shear waves at the paratellurite-liquid interface, as well as the carrier frequency and pulse duration at room temperature. To prevent the splitting of the shear wave at the acoustic duct-liquid interface into two components (longitudinal and shear), it is advisable to use horizontally polarized shear waves.
5) It is shown that shear waves at the same carrier frequency can be used to create an RDS having a spatial period an order of magnitude smaller than that created when using longitudinal waves. For example, whereas the use of longitudinal waves with electrodes based on the $[C_6mim][NTf_2]$ liquid at a frequency of 300 MHz allows an RDS to be created having a period of about 40 μm, shear waves with electrodes based on $LiPF_6$–PC at the same frequency can be used to produce an RDS having a period of about 2 μm.
6) The presented technology combines an extremely short process cycle duration with the necessary depth of domain inversion. In this case, the RDS formation time is comparable to the polarization switching time in the ferroelectric used. The technology can be used in the mass production of devices based on ferroelectric RDSs.

Authors' contribution. All authors equally contributed to the research work.

REFERENCES

1. Sarin Kumar A.K., Paruch P., Marré D., Pellegrino L., Tybell T., Ballandras S., Triscone J.M. A novel high frequency surface acoustic wave device based on piezoelectric interdigital transducers. *Integr. Ferroelectr.* 2004;63(1):55–62. https://doi.org/10.1080/10584580490458621
2. Kitaeva G.K., Kovalev S.P., Naumova I.I., Tuchak A.N., Yakunin P.V., Huang Y.C., Mishina E.D., Sigov A.S. Terahertz wave generation in periodically poled lithium niobate crystals fabricated using two alternative techniques. *Laser Phys. Lett*. 2013;10(5):055404–055409. https://doi.org/10.1088/1612-2011/10/5/055404
3. Yamada M., Nada N., Saitoh M., Watanabe K. First-order quasi-phase matched $LiNbO_3$ waveguide periodically poled by applying an external field for efficient blue second-harmonic generation. *Appl. Phys. Lett*. 1993;629(5):435–437. https://doi.org/10.1063/1.108925
4. Krutov V.V., Shchuka A.A., Mikhalevich V.G. Acoustic dispersive filters and acoustic microwave emitters based on ferroelectrics with spatial modulation of piezoelectric modulus. *Physics of Vibrations*. 2001;9(4):274–279.
5. Esin A.A., Akhmatkhanov A.R., Pavel'ev V.S., Shur V.Ya. Tunable $LiNbO_3$-based diffractive optical element for the control of transverse modes of a laser beam. *Komp'yuternaya optika = Computer Optics*. 2021;45(2):222–226 (in Russ.). https://doi.org/10.18287/2412-6179-CO-786
6. Krutov V.V., Sigov A.S., Shchuka A.A. Techniques for formation of ferroelectric photonic and phononic crystals. *Russ. Technol. J.* 2017;5(2):3–21 (in Russ.). https://doi.org/10.32362/2500-316X-2017-5-2-3-21

СПИСОК ЛИТЕРАТУРЫ

1. Sarin Kumar A.K., Paruch P., Marré D., Pellegrino L., Tybell T., Ballandras S., Triscone J.M. A novel high frequency surface acoustic wave device based on piezoelectric interdigital transducers. *Integr. Ferroelectr.* 2004;63(1):55–62. https://doi.org/10.1080/10584580490458621
2. Kitaeva G.K., Kovalev S.P., Naumova I.I., Tuchak A.N., Yakunin P.V., Huang Y.C., Mishina E.D., Sigov A.S. Terahertz wave generation in periodically poled lithium niobate crystals fabricated using two alternative techniques. *Laser Phys. Lett*. 2013;10(5):055404–055409. https://doi.org/10.1088/1612-2011/10/5/055404
3. Yamada M., Nada N., Saitoh M., Watanabe K. First-order quasi-phase matched $LiNbO_3$ waveguide periodically poled by applying an external field for efficient blue second-harmonic generation. *Appl. Phys. Lett*. 1993;629(5):435–437. https://doi.org/10.1063/1.108925
4. Krutov V.V., Shchuka A.A., Mikhalevich V.G. Acoustic dispersive filters and acoustic microwave emitters based on ferroelectrics with spatial modulation of piezoelectric modulus. *Physics of Vibrations*. 2001;9(4):274–279.
5. Есин А.А., Ахматханов А.Р., Павельев В.С., Шур В.Я. Скоростная модуляция поперечно-модового состава лазерных пучков с помощью дифракционных оптических элементов на основе $LiNbO_3$. *Компьютерная оптика*. 2021;45(2):222–226. https://doi.org/10.18287/2412-6179-CO-786
6. Крутов В.В., Сигов А.С., Щука А.А. Технология создания сегнетоэлектрических фотонных и фононных кристаллов. *Russ. Technol. J.* 2017;5(2):3–21. https://doi.org/10.32362/2500-316X-2017-5-2-3-21

7. Kokhanchik L.S., Irzhak D.V. Formation of regular domain structures and peculiarities of switching of the spontaneous polarization in lithium tantalate crystals during discrete electron irradiation. *Phys. Solid State*. 2010;52(2):306–310. https://doi.org/10.1134/S1063783410020137
[Original Russian Text: Kokhanchik L.S., Irzhak D.V. Formation of regular domain structures and peculiarities of switching of the spontaneous polarization in lithium tantalate crystals during discrete electron irradiation. *Fizika Tverdogo Tela*. 2010;52(2):285–289 (in Russ.).]
8. Volk T., Gainutdinov R., Zhang H. Domain patterning in ion-sliced $LiNbO_3$ films by atomic force microscopy. *Crystals*. 2017;7(5):137–145. https://doi.org/10.3390/cryst7050137
9. Sones C.L., Muir A.C., Ying Y.J., et al. Precision nanoscale domain engineering of lithium niobate via UV laser induced inhibition of poling. *Appl. Phys. Lett.* 2008;92(7):072905-3. https://doi.org/10.1063/1.2884185
10. Shur V.Ya., Mingaliev E.A., Kosobokov M.S., Makaev A.V. Domain structure evolution under multiple pulse heating of lithium niobate by infrared laser. *Ferroelectrics*. 2020;560(1):79–85. https://doi.org/10.1080/00150193.2020.1722886
11. Krutov V.V., Sigov A.S., Shchuka A.A., Kosinov A.A. Technological parameters of the formation of ferroelectric micro- and nanodomain structures by the acoustic interference method. In: *Fundamental Problems of Radioengineering and Device Construction INTERMATIC 2013: Proceedings of the International Scientific and Technical Conference.* 2013. Part 1. P. 139–142.
12. Krutov V.V., Sigov A.S., Shchuka A.A. Quick formation of micro- and nanodomain structures in ferroelectrics by microwave ultrasound interference. *Ferroelectrics*. 2015;476(1):69–74. https://doi.org/10.1080/00150193.2015.998522
13. Krutov V.V., Zasovin E.A., Sigov A.S., Shchuka A.A., Kabin D.V., Mikhalevich V.G. Technology for formation of photonic crystals using UHF elastic wave interference. In: *2008 CriMiCo – 18th International Crimean Conference Microwave and Telecommunication Technology, Conference Proceedings,* Sevastopol, Crimea: 2008; 793–794.
14. Krutov V.V., Zasovin E.A., Mikhalevich V.G., Sigov A.S., Shchuka A.A. Double pulse heterothermal technology for the formation of domain structures in ferroelectrics. *Phys. Solid State*. 2012;54(5):965–967. https://doi.org/10.1134/S1063783412050216
[Original Russian Text: Krutov V.V., Zasovin E.A., Mikhalevich V.G., Sigov A.S., Shchuka A.A. Double pulse heterothermal technology for the formation of domain structures in ferroelectrics. *Fizika Tverdogo Tela.* 2012;54(5):908–910 (in Russ.).]
15. Krutov V.V., Sigov A.S., Shchuka A.A. Phenomenon of formation of regular domain structures in ferroelectrics by uniform electric field and elastic waves: the dilemma of carrier frequencies. *Prikladnaya Fizika = Applied Physics.* 2018;3:53–58 (in Russ.). Available from URL: https://applphys.orion-ir.ru/appl-18/18-3/PF-18-3-53.pdf

7. Коханчик Л.С., Иржак Д.В. Формирование регулярных доменных структур и особенности переключения спонтанной поляризации в кристаллах танталата лития при дискретном облучении электронами. *Физика твердого тела*. 2010;52(2):285–289.
8. Volk T., Gainutdinov R., Zhang H. Domain patterning in ion-sliced $LiNbO_3$ films by atomic force microscopy. *Crystals*. 2017;7(5):137–145. https://doi.org/10.3390/cryst7050137
9. Sones C.L., Muir A.C., Ying Y.J., et al. Precision nanoscale domain engineering of lithium niobate via UV laser induced inhibition of poling. *Appl. Phys. Lett.* 2008;92(7):072905-3. https://doi.org/10.1063/1.2884185
10. Shur V.Ya., Mingaliev E.A., Kosobokov M.S., Makaev A.V. Domain structure evolution under multiple pulse heating of lithium niobate by infrared laser. *Ferroelectrics*. 2020;560(1):79–85. https://doi.org/10.1080/00150193.2020.1722886
11. Крутов В.В., Сигов А.С., Щука А.А., Косинов А.А. Технологические параметры формирования сегнетоэлектрических микро- и нанодоменных структур акустоинтерференционным методом. В сб.: *Фундаментальные проблемы радиоэлектронного приборостроения: материалы Международной научно-технической конференции «INTERMATIC–2013».* 2013. Ч. 1. С. 139–142.
12. Krutov V.V., Sigov A.S., Shchuka A.A. Quick formation of micro- and nanodomain structures in ferroelectrics by microwave ultrasound interference. *Ferroelectrics*. 2015;476(1):69–74. https://doi.org/10.1080/00150193.2015.998522
13. Крутов В.В., Засовин Э.А., Михалевич В.Г., Сигов А.С., Щука А.А., Кабин Д.В. Технология создания фотонных кристаллов с помощью интерференции упругих волн СВЧ диапазона. 18-я Междунар. Крымская конф. «*СВЧ техника и телекоммун. технологии*». Сб. науч. статей. Севастополь, Украина: 8–12 сент. 2008 г. С. 793–794.
14. Крутов В.В., Засовин Э.А., Михалевич В.Г., Сигов А.С., Щука А.А. Биимпульсная гетеротермальная технология формирования доменных структур в сегнетоэлектриках. *Физика твердого тела*. 2012;54(5):908–910.
15. Крутов В.В., Сигов А.С., Щука А.А. Образование регулярных доменных структур в сегнетоэлектриках при воздействии однородного электрического поля и упругих волн: дилемма несущих частот. *Прикладная физика.* 2018;3:53–57. URL: https://applphys.orion-ir.ru/appl-18/18-3/PF-18-3-53.pdf
16. Крутов В.В., Сигов А.С., Щука А.А. Создание сегнетоэлектрических доменных структур с использованием ультразвука вблизи нижней границы СВЧ-диапазона. *Прикладная физика.* 2018;6:60–63. URL: https://applphys.orion-ir.ru/appl-18/18-6/PF-18-6-60.pdf
17. Shur V.Y., Rumyantsev E.L., Batchko R.G., Miller G.D., Fejer M.M., Byer R.L. Domain kinetics in the formation of a periodic domain structure in lithium niobate. *Phys. Solid State*. 1999;41(10):1681–1687. https://doi.org/10.1134/1.1131068
18. Huang L., Jaeger N. Discussion of domain inversion in $LiNbO_3$. *Appl. Phys. Lett.* 1994;65(14):1763–1765. https://doi.org/10.1063/1.112911

16. Krutov V.V., Sigov A.S., Shchuka A.A. Creation of ferroelectric domain structures using ultrasound near the bottom of the UHF band. *Prikladnaya Fizika = Applied Physics*. 2018;6:60–63. Available from URL: https://applphys.orion-ir.ru/appl-18/18-6/PF-18-6-60.pdf
17. Shur V.Y., Rumyantsev E.L., Batchko R.G., Miller G.D., Fejer M.M., Byer R.L. Domain kinetics in the formation of a periodic domain structure in lithium niobate. *Phys. Solid State*. 1999;41(10):1681–1687. https://doi.org/10.1134/1.1131068
18. Huang L., Jaeger N. Discussion of domain inversion in $LiNbO_3$. *Appl. Phys. Lett.* 1994;65(14):1763–1765. https://doi.org/10.1063/1.112911
19. Kaino G. *Akusticheskie volny*. *Ustroistva, vizualizatsiya i analogovaya obrabotka signalov* (*Acoustic waves. Devices, visualization and analog signal processing*). Moscow: Mir; 1990. 652 p. (in Russ.). ISBN 5-03-001434-9
[Kino G.S. *Acoustic waves. Devices, Imaging and Analog Signal Processing.* Prentice-Hall; 1988. 601 p.]
20. Waterman P.C., Teutonico L.J. Ultrasonic double refraction in single crystals. *J. Appl. Phys.* 1957;28(2):266–270. https://doi.org/10.1063/1.1722721
21. Mott G. Reflection and refraction coefficients at a fluid-solid interface. *J. Acoust. Soc. Am*. 1971;50(3B):819–829. https://doi.org/10.1121/1.1912706
22. Ergin K. Energy ratio of the seismic waves reflected and refracted at a rock-water boundary. *Bull. Seismol. Soc. Am*. 1952;42(4):349–372. https://doi.org/10.1785/BSSA0420040349
23. Krutov V.V., Sigov A.S., Shchuka A.A. Acoustic interference method for the formation of micro- and nanodomain structures in ferroelectrics. In: *Metody sozdaniya, issledovaniya mikro-, nanosistem i ekonomicheskie aspekty mikro-, nanoelektroniki: IV Mezhdunarodnaya nauchno-tekhnicheskaya konferentsiya: sbornik statei* (*Methods of Creation, Research of Micro-, Nanosystems and Economic Aspects of Micro-, Nanoelectronics: IV International Scientific and Technical Conference: Collection of Papers*). Penza; 2013. P. 5–8 (in Russ.).
24. Kasper G., Tamm K. Sound propagation at GHz frequencies in aqueous LiCl solutions. *J. Chem. Phys.* 1980;72(9):5279–5289. https://doi.org/10.1063/1.439767
25. Kallaev S.N., Omarov Z.M., Bilalov A.R., Rabadanov M.Kh., Sadykov S.A., Bormanis K. Specific features of the thermal physical properties of relaxor ceramics based on lead zirconate titanate. *Phys. Solid State*. 2009;51(7):1524–1526. https://doi.org/10.1134/S106378340907052X
[Original Russian Text: Kallaev S.N., Omarov Z.M., Bilalov A.R., Rabadanov M.Kh., Sadykov S.A., Bormanis K. Specific features of the thermal physical properties of relaxor ceramics based on lead zirconate titanate. *Fizika Tverdogo Tela*. 2009;51(7):1436–1438 (in Russ.).]
26. Sidorkin A.S., Nesterenko L.P., Ryabtsev S.V., Sidorkin A.A. Frequency dependence of the coercive field and the internal bias field in ferroelectric thin films. *Phys. Solid State*. 2009;51(7):1348–1350. https://doi.org/10.1134/S1063783409070075
19. Кайно Г. *Акустические волны. Устройства, визуализация и аналоговая обработка сигналов.* М.: Мир; 1990. 652 с. ISBN 5-03-001434-9
20. Waterman P.C., Teutonico L.J. Ultrasonic double refraction in single crystals. *J. Appl. Phys.* 1957;28(2):266–270. https://doi.org/10.1063/1.1722721
21. Mott G. Reflection and refraction coefficients at a fluid-solid interface. *J. Acoust. Soc. Am*. 1971;50(3B):819–829. https://doi.org/10.1121/1.1912706
22. Ergin K. Energy ratio of the seismic waves reflected and refracted at a rock-water boundary. *Bull. Seismol. Soc. Am*. 1952;42(4):349–372. https://doi.org/10.1785/BSSA0420040349
23. Крутов В.В., Сигов А.С., Щука А.А. Акустоинтерференционный метод формирования микро- и нанодоменных структур в сегнетоэлектриках. В сб.: *Методы создания, исследования микро-, наносистем и экономические аспекты микро-, наноэлектроники:* IV Международная научно-техническая конференция: сборник статей. Пенза; 2013. С. 5–8.
24. Kasper G., Tamm K. Sound propagation at GHz frequencies in aqueous LiCl solutions. *J. Chem. Phys.* 1980;72(9):5279–5289. https://doi.org/10.1063/1.439767
25. Каллаев С.Н., Омаров З.М., Билалов А.Р., Рабаданов М.Х., Садыков С.А., Борманис К. Особенности теплофизических свойств релаксорной керамики на основе цирконата-титаната свинца. *Физика твердого тела*. 2009;51(7):1436–1438.
26. Сидоркин А.С., Нестеренко Л.П., Рябцев С.В., Сидоркин А.А. Частотная зависимость коэрцитивного поля и внутреннего поля смещения в тонких сегнетоэлектрических пленках. *Физика твердого тела*. 2009;51(7):1277–1279.
27. Крутов В.В., Сигов А.С., Щука А.А. Создание микро- и нанодоменных структур в сегнетоэлектрических пленках с использованием интерферирующего гиперзвука. *Доклады Российской Академии наук. Физика, технические науки*. 2016;469(2):173–176. https://doi.org/10.7868/S0869565216200093
28. Bassignot F., Haye G., Henrot F., Ballandras S., Courjon E., Lesage J.-M. New radio-frequency resonators based on periodically poled lithium niobate thin film and ridge structures. In: *2016. IEEE International Frequency Control Symposium* (*IFCS*). 2016:16302911. https://doi.org/10.1109/FCS.2016.7546793
29. Andreeva M.S., Andreeva N.P., Barashkov M.S., Mitin K.V., Shchebetova N.I., Krymskii M.I., Rogalin V.E., Akhmatkhanov A.R., Chuvakova M.A., Shur V.Ya. Optical parametric oscillator based on the periodically poled MgO:LN crystal with 4.1 μm wavelength and varied pulse duration. *Ferroelectrics*. 2016;496(1):128–134. https://doi.org/10.1080/00150193.2016.1155029
30. Myers L.E., Eckardt R.C., Fejer M.M., Byer R.L., Bosenberg W.R., Pierce J.W. Quasi-phase-matched optical parametric oscillators in bulk periodically poled $LiNbO_3$. *J. Opt. Soc. Am. B*. 1995;12(11):2102–2111. https://doi.org/10.1364/JOSAB.12.002102
31. Kasper G., Tamm K. Sound propagation at GHz frequencies in aqueous LiCl solutions. *J. Chem. Phys*. 1980;72(9):5279–5280. https://doi.org/10.1063/1.439767

[Original Russian Text: Sidorkin A.S., Nesterenko L.P., Ryabtsev S.V., Sidorkin A.A. Frequency dependence of the coercive field and the internal bias field in ferroelectric thin films. *Fizika Tverdogo Tela*. 2009;51(7):1277–11279 (in Russ.).]

27. Krutov V.V., Sigov A.S., Shchuka A.A. Formation of micro-and nanodomain structures in ferroelectric films by interfering hypersound. *Doklady Physics*. 2016;61(7): 332–334. https://doi.org/10.1134/S1028335816070077 [Original Russian Text: Krutov V.V., Sigov A.S., Shchuka A.A. Formation of micro-and nanodomain structures in ferroelectric films by interfering hypersound. *Doklady Akademii Nauk*. 2016;469(2):173–176 (in Russ.). https://doi.org/10.7868/S0869565216200093]
28. Bassignot F., Haye G., Henrot F., Ballandras S., Courjon E., Lesage J.-M. New radio-frequency resonators based on periodically poled lithium niobate thin film and ridge structures. In: *2016. IEEE International Frequency Control Symposium* (*IFCS*). 2016:16302911. https://doi.org/10.1109/FCS.2016.7546793
29. Andreeva M.S., Andreeva N.P., Barashkov M.S., Mitin K.V., Shchebetova N.I., Krymskii M.I., Rogalin V.E., Akhmatkhanov A.R., Chuvakova M.A., Shur V.Ya. Optical parametric oscillator based on the periodically poled MgO:LN crystal with 4.1 μm wavelength and varied pulse duration. *Ferroelectrics*. 2016;496(1):128–134. https://doi.org/10.1080/00150193.2016.1155029
30. Myers L.E., Eckardt R.C., Fejer M.M., Byer R.L., Bosenberg W.R., Pierce J.W. Quasi-phase-matched optical parametric oscillators in bulk periodically poled $LiNbO_3$. *J. Opt. Soc. Am. B*. 1995;12(11):2102–2111. https://doi.org/10.1364/JOSAB.12.002102
31. Kasper G., Tamm K. Sound propagation at GHz frequencies in aqueous LiCl solutions. *J. Chem. Phys*. 1980;72(9):5279–5280.https://doi.org/10.1063/1.439767
32. Zorębski M., Zorębski E., Dzida M., Skowronek J., Jężak S., Goodrich P., Jacquemin J. Ultrasonic relaxation study of 1-alkyl-3-methylimidazolium-based room-temperature ionic liquids: probing the role of alkyl chain length in the cation. *J. Phys. Chem. B*. 2016;120(14): 3569–3581. https://doi.org/10.1021/acs.jpcb.5b12635
33. Zorębski E., Zorębski M., Musiał M., Dzida M. Ultrasonic relaxation spectra for pyrrolidinium bis(trifluoromethylsulfonyl)imides: A comparison with imidazolium bis(trifluoromethylsulfonyl)imides. *J. Phys. Chem. B*. 2017;121(42):9886–9894. https://doi.org/10.1021/acs.jpcb.7b07433
34. Malyshkina O.V., Movchikova A.A., Kalugina O.N., Daineko A.V. Determination of thermal diffusivity coefficient of thin films by thermal square wave method. *Ferroelectrics*. 2011;424(1):28–35. https://doi.org/10.1080/00150193.2011.623637
35. Li F., Wang Q., Miao H. Giant actuation strain nearly 0.6% in a periodically orthogonal poled lead titanate zirconate ceramic *via* reversible domain switching. *J. Appl. Phys.* 2017;122(7):074103–074109. https://doi.org/10.1063/1.4997940
36. Wang Q., Li F. A low-working-field (2 kV/mm), large-strain (>0.5%) piezoelectric multilayer actuator based on periodically orthogonal poled PZT ceramics. *Sensors and Actuators A: Physical*. 2018;272:212–219. https://doi.org/10.1016/j.sna.2018.01.042

32. Zorębski M., Zorębski E., Dzida M., Skowronek J., Jężak S., Goodrich P., Jacquemin J. Ultrasonic relaxation study of 1-alkyl-3-methylimidazolium-based room-temperature ionic liquids: probing the role of alkyl chain length in the cation. *J. Phys. Chem. B*. 2016;120(14): 3569–3581. https://doi.org/10.1021/acs.jpcb.5b12635
33. Zorębski E., Zorębski M., Musiał M., Dzida M. Ultrasonic relaxation spectra for pyrrolidinium bis(trifluoromethylsulfonyl)imides: A comparison with imidazolium bis(trifluoromethylsulfonyl)imides. *J. Phys. Chem. B*. 2017;121(42):9886–9894. https://doi.org/10.1021/acs.jpcb.7b07433
34. Malyshkina O.V., Movchikova A.A., Kalugina O.N., Daineko A.V. Determination of thermal diffusivity coefficient of thin films by thermal square wave method. *Ferroelectrics*. 2011;424(1):28–35. https://doi.org/10.1080/00150193.2011.623637
35. Li F., Wang Q., Miao H. Giant actuation strain nearly 0.6% in a periodically orthogonal poled lead titanate zirconate ceramic *via* reversible domain switching. *J. Appl. Phys.* 2017;122(7):074103–074109. https://doi.org/10.1063/1.4997940
36. Wang Q., Li F. A low-working-field (2 kV/mm), large-strain (>0.5%) piezoelectric multilayer actuator based on periodically orthogonal poled PZT ceramics. *Sensors and Actuators A: Physical*. 2018;272:212–219. https://doi.org/10.1016/j.sna.2018.01.042

37. Krutov V.V., Sigov A.S., Shchuka A.A. A technique for the formation of ferroelectric regular domain structures using highly dissipative electrically conductive liquids at room temperature. *Ferroelectrics*. 2020;559(1):120–127. https://doi.org/10.1080/00150193.2020.1722013
38. Landau L.D., Lifshitz E.M. *Fluid Mechanics*. London: Pergamon Press; 1959. § 24.
39. Greenwood M.S., Bamberger J.A. Measurement of viscosity and shear wave velocity of a liquid or slurry for on-line process control. *Ultrasonics*. 2002;39(9):623–630. https://doi.org/10.1016/S0041-624X(02)00372-4
40. Kielczyński P., Pajewski W. Transmission of SH plane waves obliquely incident at a plane interface between an elastic solid and a viscoelastic liquid. *Acta Acust. United Acust*. 1990;71(1):21–27.
41. Yamaguchi T., Yonezawa T., Yoshida K., Yamaguchi T., Nagao M., Faraone A., Seki S. Relationship between structural relaxation, shear viscosity, and ionic conduction of $LiPF_6$/propylene carbonate solutions. *J. Phys. Chem. B*. 2015;119(51):15675–15682. https://doi.org/10.1021/acs.jpcb.5b08701
42. Yamaguchi T., Yoshida K., Yamaguchi T., Nagao M., Faraone A., Seki S. Decoupling between the temperature-dependent structural relaxation and shear viscosity of concentrated lithium electrolyte. *J. Phys. Chem. B*. 2017;121(37):8767–8773. https://doi.org/10.1021/acs.jpcb.7b04633
43. Yamaguchi T., Miyake S., Koda S. Shear relaxation of imidazolium-based room-temperature ionic liquids. *J. Phys. Chem. B*. 2010;114(24):8126–8133. https://doi.org/10.1021/jp1024137
44. Yamaguchi T., Nakahara E., Koda S. Quantitative analysis of conductivity and viscosity of ionic liquids in terms of their relaxation times. *J. Phys. Chem. B*. 2014;118(21):5752–5759. https://doi.org/10.1021/jp502631q

37. Krutov V.V., Sigov A.S., Shchuka A.A. A technique for the formation of ferroelectric regular domain structures using highly dissipative electrically conductive liquids at room temperature. *Ferroelectrics*. 2020;559:1:120–127. https://doi.org/10.1080/00150193.2020.1722013
38. Landau L.D., Lifshitz E.M. *Fluid Mechanics.* London: Pergamon Press; 1959. § 24.
39. Greenwood M.S., Bamberger J.A. Measurement of viscosity and shear wave velocity of a liquid or slurry for on-line process control. *Ultrasonics*. 2002;39(9):623–630. https://doi.org/10.1016/S0041-624X(02)00372-4
40. Kielczyński P., Pajewski W. Transmission of SH plane waves obliquely incident at a plane interface between an elastic solid and a viscoelastic liquid. *Acta Acust. United Acust*. 1990;71(1):21–27.
41. Yamaguchi T., Yonezawa T., Yoshida K., Yamaguchi T., Nagao M., Faraone A., Seki S. Relationship between structural relaxation, shear viscosity, and ionic conduction of $LiPF_6$/propylene carbonate solutions. *J. Phys. Chem. B*. 2015;119(51):15675–15682. https://doi.org/10.1021/acs.jpcb.5b08701
42. Yamaguchi T., Yoshida K., Yamaguchi T., Nagao M., Faraone A., Seki S. Decoupling between the temperature-dependent structural relaxation and shear viscosity of concentrated lithium electrolyte. *J. Phys. Chem. B*. 2017;121(37):8767–8773. https://doi.org/10.1021/acs.jpcb.7b04633
43. Yamaguchi T., Miyake S., Koda S. Shear relaxation of imidazolium-based room-temperature ionic liquids. *J. Phys. Chem. B*. 2010;114(24):8126–8133. https://doi.org/10.1021/jp1024137
44. Yamaguchi T., Nakahara E., Koda S. Quantitative analysis of conductivity and viscosity of ionic liquids in terms of their relaxation times. *J. Phys. Chem. B*. 2014;118(21):5752–5759. https://doi.org/10.1021/jp502631q
45. Kondo K., Sano M., Hiwara A., Omi T., Fujita M., Kuwae A., Yokoyama H. Conductivity and solvation of Li^+ ions of $LiPF_6$ in propylene carbonate solutions. *J. Phys. Chem. B*. 2000;104(20):5040–5044. https://doi.org/10.1021/jp000142f
46. Umecky T., Kanakubo M., Makino T., Aizawa T., Suzuki A. Effect of CO_2 dissolution on electrical conductivity and self-diffusion coefficients of 1-butyl-3-methylimidazolium hexafluorophosphate ionic liquid. *Fluid Phase Equilib*. 2013;357:76–79. https://doi.org/10.1016/j.fluid.2013.05.023
47. Ohmachi Y., Uchida N. Temperature dependence of elastic, dielectric, and piezoelectric constants in TeO_2 single crystals. *J. Appl. Phys*. 1970;41(6):2307–2311. https://doi.org/10.1063/1.1659223

45. Kondo K., Sano M., Hiwara A., Omi T., Fujita M., Kuwae A., Yokoyama H. Conductivity and solvation of Li^+ ions of $LiPF_6$ in propylene carbonate solutions. *J. Phys. Chem. B*. 2000;104(20):5040–5044. https://doi.org/10.1021/jp000142f
46. Umecky T., Kanakubo M., Makino T., Aizawa T., Suzuki A. Effect of CO_2 dissolution on electrical conductivity and self-diffusion coefficients of 1-butyl-3-methylimidazolium hexafluorophosphate ionic liquid. *Fluid Phase Equilib*. 2013;357:76–79. https://doi.org/10.1016/j.fluid.2013.05.023
47. Ohmachi Y., Uchida N. Temperature dependence of elastic, dielectric, and piezoelectric constants in TeO_2 single crystals. *J. Appl. Phys*. 1970;41(6):2307–2311. https://doi.org/10.1063/1.1659223

About the authors

Vladislav V. Krutov, Cand. Sci. (Eng.), Associate Professor, Department of Nanoelectronics, Institute for Advanced Technologies and Industrial Programming, MIREA – Russian Technological University (78, Vernadskogo pr., Moscow, 119454 Russia). E-mail: v_krutov@mirea.ru. https://orcid.org/0000-0003-1909-1435

Alexander S. Sigov, Academician at the Russian Academy of Sciences, Dr. Sci. (Phys.-Math.), Professor, President, MIREA – Russian Technological University (78, Vernadskogo pr., Moscow, 119454 Russia). E-mail: sigov@mirea.ru. ResearcherID L-4103-2017, Scopus Author ID 35557510600, RSCI SPIN-code 2869-5663, https://www.researchgate.net/profile/A_Sigov

Об авторах

Крутов Владислав Викторович, к.т.н., доцент, кафедра наноэлектроники Института перспективных технологий и индустриального программирования, ФГБОУ ВО «МИРЭА – Российский технологический университет» (119454, Россия, Москва, пр-т Вернадского, д. 78). E-mail: v_krutov@mirea.ru. https://orcid.org/0000-0003-1909-1435

Сигов Александр Сергеевич, академик РАН, д.ф.-м.н., профессор, президент ФГБОУ ВО «МИРЭА – Российский технологический университет» (119454, Россия, Москва, пр-т Вернадского, д. 78). E-mail: sigov@mirea.ru. ResearcherID L-4103-2017, Scopus Author ID 35557510600, SPIN-код РИНЦ 2869-5663, https://www.researchgate.net/profile/A_Sigov

Translated from Russian into English by Vladislav V. Glyanchenko
Edited for English language and spelling by Thomas A. Beavitt

Micro- and nanoelectronics. Condensed matter physics

Микро- и наноэлектроника. Физика конденсированного состояния

UDC 621.793.182
https://doi.org/10.32362/2500-316X-2022-10-5-92-99

RESEARCH ARTICLE

Comparison of magnetron sputtering systems for high-rate deposition of thick copper layers for microelectronic applications

Mariia V. Nazarenko [1, 2, @]

[1] *MIREA – Russian Technological University, Moscow, 119454 Russia*
[2] *RMT, Moscow, 115230 Russia*
[@] *Corresponding author, e-mail: m.v.makarova@list.ru*

Abstract

Objectives. When designing production equipment for the implementation of metal film deposition processes, the selection of technological sources for providing the required quality (structure, appearance), maximum process efficiency, and productivity, poses a challenging task. Since laboratory results often differ from issues faced in production processes, this choice becomes even more difficult under real production conditions due to a lack of sources for comparison. The purpose of the present work is therefore to compare magnetron deposition methods under real industrial conditions (planar extended magnetron, liquid-phase magnetron and cylindrical magnetron with a rotating cathode), identify their advantages and disadvantages along with features of thus-formed metal films, analyze the economic feasibility of each variant, and give practical recommendations for selecting a source when implementing the described process.

Methods. Films were deposited using magnetron sputtering system. Roughness was measured using a MarSurf PS1 profilometer. The structure of the films was studied using a Hitachi SU1510 scanning electron microscope. Film thicknesses were measured by X-ray fluorescence analysis using a Fisherscope X-RAY XDV-SDD measuring instrument.

Results. Sources of magnetron sputtering for the high-rate deposition of metallization layers under industrial conditions are considered. Obtained samples were compared according to the following criteria: deposition rate while maintaining the required quality, surface defects, film grain size, roughness, uniformity of the deposited layer, deposition efficiency (the ratio of the metal deposited directly onto the substrate to the amount of metal produced during the process). A comparison of the characteristics showed that the deposition rate for the liquid-phase magnetron is commensurate with the similar parameter for the cylindrical magnetron, exceeding the rate for the classical planar magnetron by about 4 times while maintaining the uniform appearance of the samples. The samples deposited with a liquid-phase magnetron had the highest roughness and the largest grain size. Although the cheapest method, liquid-phase magnetron sputtering achieved the lowest sputtering efficiency.

Conclusions. The choice of the deposition method depends on the problem to be solved. The rotatable magnetron system can be considered optimal in terms of cost, deposition rate, and quality of the deposited layers. Liquid-phase magnetron sputtering is recommended for low-cost high-speed deposition where there are no strict requirements for appearance, or in case of operation of small-sized equipment.

Keywords: magnetron, liquid phase magnetron, planar magnetron, rotatable magnetron, metal film deposition, deposition efficiency, productive methods, deposition rate, choice of deposition method

• **Submitted:** 07.02.2022 • **Revised:** 07.07.2022 • **Accepted:** 22.08.2022

For citation: Nazarenko M.V. Comparison of magnetron sputtering systems for high-rate deposition of thick copper layers for microelectronic applications. *Russ. Technol. J.* 2022;10(5):92–99. https://doi.org/10.32362/2500-316X-2022-10-5-92-99

Financial disclosure: The author has no a financial or property interest in any material or method mentioned.

The author declares no conflicts of interest.

НАУЧНАЯ СТАТЬЯ

Анализ источников магнетронного распыления для осаждения толстых слоев меди с высокой скоростью для изделий микроэлектроники

М.В. Назаренко [1, 2, @]

[1] *МИРЭА – Российский технологический университет, Москва, 119454 Россия*
[2] *ООО «РМТ», Москва, 115230 Россия*
[@] *Автор для переписки, e-mail: m.v.makarova@list.ru*

Резюме

Цели. При проектировании производственного оборудования для реализации процессов осаждения металлических пленок актуальной задачей является выбор технологических источников, которые должны обеспечивать требуемое качество (структуру, внешний вид), максимальные эффективность процесса и производительность. Однако в реальных производственных условиях сделать этот выбор сложно в связи с недостаточностью сравнительных материалов источников. Лабораторные результаты нередко отличаются от результатов на производстве. Цель работы – сравнить методы магнетронного осаждения в реальных промышленных условиях (планарном протяженном магнетроне, жидкофазном магнетроне и цилиндрическом магнетроне с вращающимся катодом), выявить их преимущества, недостатки и особенности формирования металлических пленок, проанализировать экономическую целесообразность выбора каждого из них и дать практические рекомендации выбора источника при реализации требуемого процесса.

Методы. Для осаждения пленок применены методы ионного распыления в магнетронных системах. Измерение шероховатости проводилось с помощью профилометра MarSurf PS1. Структура пленок изучалась с помощью растрового электронного микроскопа Hitachi SU1510. Толщины пленок измерялись методом рентгено-флуоресцентного анализа с помощью прибора Fisherscope X-RAY XDV-SDD.

Результаты. Рассмотрены источники магнетронного распыления для скоростного осаждения слоев металлизации в промышленных условиях. Проведено сравнение полученных образцов по критериям: скорость осаждения с сохранением требуемого качества, поверхностные дефекты, размер зерна пленки, шероховатость, равномерность осажденного слоя, эффективность осаждения (отношение металла, осажденного непосредственно на подложку, к количеству выработанного металла во время процесса). Сравнение характеристик показало, что скорость осаждения для жидкофазного магнетрона соизмерима с аналогичным параметром для цилиндрического магнетрона и превосходит примерно в 4 раза скорость для классического планарного магнетрона при сохранении единого внешнего вида образцов. Самой высокой шероховатостью и самым крупным размером зерна обладают образцы, осажденные жидкофазным магнетроном. Самой низкой эффективностью распыления обладает метод жидкофазного магнетронного распыления, который является самым дешевым.

Выводы. Выбор метода осаждения зависит от решаемой задачи. Оптимальным по стоимости, скорости осаждения и качеству осаждаемых слоев можно считать магнетрон с цилиндрическим вращающимся катодом. Жидкофазное магнетронное распыление рекомендовано использовать для дешевого скоростного осаждения, при котором нет жестких требований к внешнему виду, или в случае эксплуатации малогабаритного оборудования.

Ключевые слова: магнетрон, жидкофазный магнетрон, планарный магнетрон, цилиндрический магнетрон, осаждение металлических пленок, эффективность осаждения, производительные методы, скорость осаждения, выбор метода осаждения

• **Поступила:** 07.02.2022 • **Доработана:** 07.07.2022 • **Принята к опубликованию:** 22.08.2022

Для цитирования: Назаренко М.В. Анализ источников магнетронного распыления для осаждения толстых слоев меди с высокой скоростью для изделий микроэлектроники. *Russ. Technol. J.* 2022;10(5):92–99. https://doi.org/10.32362/2500-316X-2022-10-5-92-99

Прозрачность финансовой деятельности: Автор не имеет финансовой заинтересованности в представленных материалах или методах.

Автор заявляет об отсутствии конфликта интересов.

INTRODUCTION

In the rapidly developing field of microelectronics, there are constantly increasing requirements for devices whose integral part comprises boards on a ceramic base having a conductive copper layer. Copper conductive layers on ceramic substrates are used in devices such as switching boards, thermoelectric modules, power diodes, power transistors, and integrated circuits [1–6]. In terms of their dimensions, appearance, productivity, and cost, the increasing requirements for the quality and reliability of products in turn affects the materials and technological processes used in the manufacture of individual product elements. This leads among other things to the need to find more productive methods for the deposition of metallization coatings (copper, aluminum, titanium, etc.) as compared with traditional approaches.

However, the choice of the optimal method is difficult due to a lack of literature data providing such comparison criteria as surface roughness, grain size, surface structure, deposition rate, and cost of the deposited layer.

The purpose of the present work is therefore to analyze the methods of deposition of conductive layers according to the above indicated criteria on the example of copper layers.

DEPOSITION RATE

To date, the magnetron sputtering methods combining the highest deposition rates with a satisfactory quality of deposited coatings include:

- ion sputtering in magnetron systems with a liquid target (liquid-phase magnetron sputtering, LPMS) [6–9] (Fig. 1a);
- with an extended planar target [10] (Fig. 1b);
- with a cylindrical rotating target [11, 12] (Fig. 1c).

A high-quality coating is understood as one that minimizes the number of surface defects (droplet phase, various inclusions, craters) and internal defects (pores), but at the same time provides sufficient adhesion to ensure the performance of the product.

As a comparison, Table 1 shows the values of the deposition rate by the methods described. Presented data are obtained experimentally. The distance from the magnetron surface to the substrates is 100 mm. Aluminum nitride (AlN) with roughness Ra = 10 nm was used as substrates.

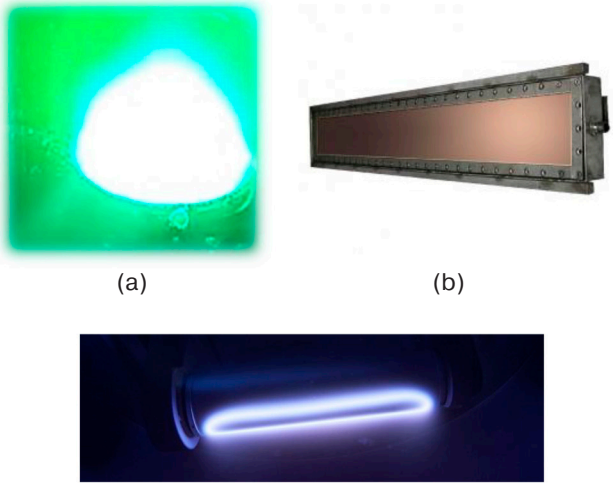

(a) (b) (c)

Fig. 1. View of magnetrons for technological applications: (a) liquid-phase magnetron, (b) planar magnetron, (c) cylindrical magnetron with a rotating cathode [7]

As compared with a cylindrical magnetron with a rotating target, it is impossible to achieve the same specific power at the cathode of an extended planar magnetron while maintaining the required quality of

Table 1. Comparison of the maximum deposition rates achieved on a fixed substrate

Magnetron sputtering system	With liquid target (crucible ∅86 mm)	With extended planar target (108 × 440 mm)	With cylindrical rotating target (450 × ∅152 mm)
Deposition rate	40 μm/min	10 μm/min	41 μm/min

Table 2. Comparison of surface roughness

Sample number	Magnetron sputtering system		
	With liquid target (crucible ∅86 mm)	With extended planar target (108 × 440 mm)	With cylindrical rotating target (450 × ∅152 mm)
1	68	31	51
2	70	28	44
3	98	26	51
4	89	29	42
Average value	81	28	42

Table 3. Grain size of copper surface

Grain size, μm	Magnetron sputtering system		
	With liquid target (crucible ∅86 mm)	With planar target (108 × 440 mm)	With cylindrical rotating target (450 × ∅152 mm)
Minimum	3	3	3
Maximum	20	6	11

the deposited films due to its overheating. This explains such a difference in the deposition rates.

As can be seen from Table 1, the deposition methods with a liquid and with a cylindrical rotating target have comparable results. However, a standard magnetron with an extended planar target does not provide such high deposition rates.

SURFACE ROUGHNESS

The values of the copper surface roughness (*Ra*, nm), which was measured using a MarSurf PS1 profilometer (Mahr GMBH, Germany), are presented in Table 2.

As can be seen, the classical magnetron with an extended planar target has the lowest roughness, which is explained by the low deposition rate. The method with a rotating cylindrical target has a roughness 1.5 times higher. The method with a liquid target has a roughness almost 4 times higher, which can become critical for some production tasks [13–15][1].

STRUCTURE OF THE FILMS

Figure 2 shows the surface structure and grain size. Studies were carried out on a Hitachi SU1510 scanning electron microscope (HITACHI, Japan). The grain size is indicated in Table 3.

Classical sputtering with a planar extended target provides the finest grain. For the magnetron with a cylindrical rotating target the grain size only 2 times larger. The method with a liquid target provides the largest grain, which is associated with a high thermal effect on the substrate caused by this type of a magnetron. By reducing the deposition rate on a fixed substrate to 20 μm/min, a grain size of up to 4 μm is achieved on a magnetron with a rotating cylindrical cathode, which is comparable to the grain size achieved on a planar magnetron with an extended target. However, the deposition rate is higher for a cylindrical magnetron.

THICKNESS UNIFORMITY OF DEPOSITED LAYER

The copper coating thickness was measured using a Fisherscope X-RAY XDV-SDD X-ray fluorescence thickness gauge (Fischer GMBH, Germany)[2]. Scanning was carried out in the center and along the perimeter of the substrate with an indent of 3 mm from the edge. An evaluation of the non-uniformity showed that sputtering methods having a liquid target and those

[1] *Pechatnye platy*: *Spravochnik*: v 2 kn. (*Printed circuit boards*: *Handbook*: in 2 books). Moscow: Tekhnosfera; 2018. Book 1. 1016 p. (in Russ).

[2] Dulov E.N., Ivoilov N.G. *X-ray spectral fluorescence analysis: teaching book for students of the Faculty of Physics.* Kazan: Kazan State University Press; 2008. 50 p. (in Russ.).

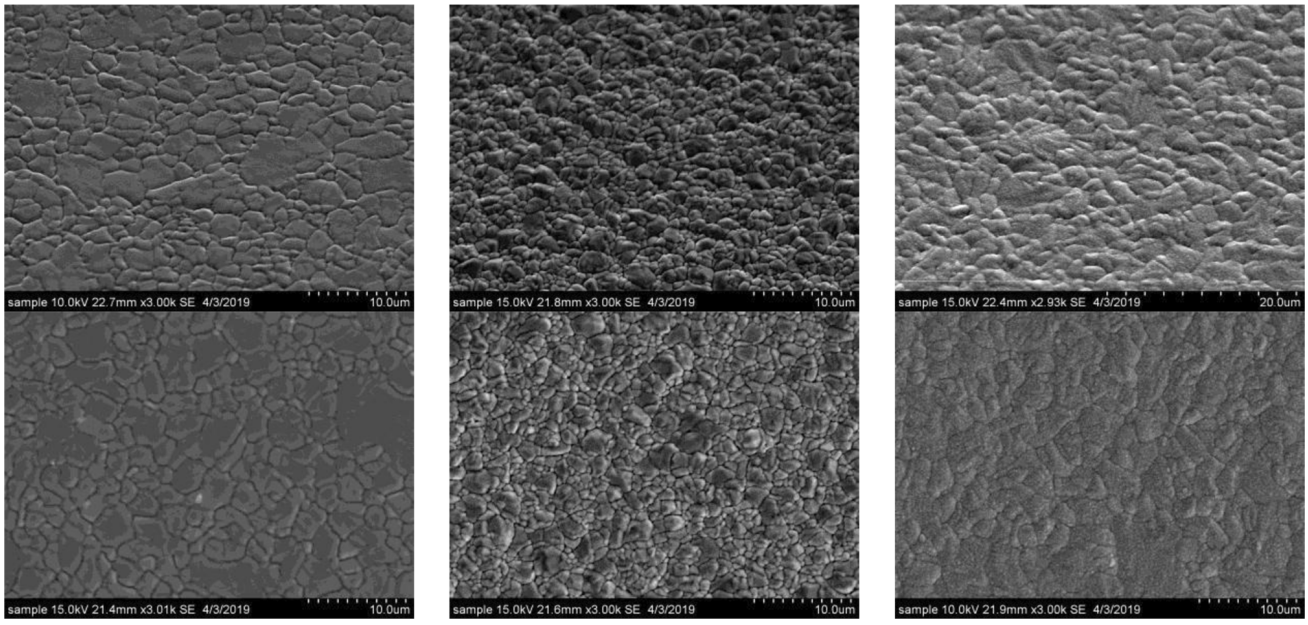

(a) (b) (c)

Fig. 2. View of the surface deposited using: (a) the LPMS method, (b) a planar magnetron with an extended target, (c) a magnetron with a cylindrical rotating target

Table 4. Evaluation of material efficiency

Parameter	Magnetron sputtering system		
	With liquid target (crucible ∅86 mm)	With planar target (108 × 440 mm)	With cylindrical rotating target (450 × ∅152 mm)
Fraction of material deposited on substrates, %	~20	~60	~90
Production of target material, %	~90–100	~45	~70
Efficiency, %	20	27	63

Table 5. Estimation of deposition cost of a 50 μm thick layer

Parameter	Magnetron sputtering system		
	With liquid target (crucible ∅86 mm)	With extended planar target (108 × 440 mm)	With cylindrical rotating target (450 × ∅152 mm)
Maximum loading of substrates in one process with dimensions of 60 × 48 mm	20	70	80
Number of processes on one target, pcs.	150 g (loading in the form of granules for 1 process)	5	40
Approximate cost per target, a.u.	1 kg – X	1 pc. – 4.5X	1 pc. – 29X
Cost of deposited layer per substrate, a.u.	~X/131	~X/80	~X/111

with a classical extended planar magnetron provide a layer non-uniformity of no more than ±5%, while for a magnetron with a cylindrical rotating target, the layer non-uniformity does not exceed ±3%.

SPUTTERING EFFICIENCY

The material utilization factor was estimated as follows: the fraction of the material removed from the target during its life cycle was multiplied by the fraction of the material that was deposited on the substrates. To convert to a percentage, the coefficient is multiplied by 100%. The calculation results are given in Table 4.

Calculations have shown that the most efficient sputtering is provided by a magnetron with a liquid target.

The cost of the deposited layer 50 μm thick was estimated taking into account the cost of the material and the efficiency of the deposited layer (Table 5).

The average price on the market of granulated vacuum-melted copper, *X* was taken as the base. The costs of a planar and a cylindrical rotating target are given in coefficients relative to the base cost of *X* arbitrary units (a.u.).

Despite the low efficiency of deposition, the magnetron with a liquid target is the most cost-effective due to the absence of the need to manufacture a target of complex shape. Regardless of the high cost of the target due to its increased efficiency, the magnetron with a rotating cylindrical target is close to the magnetron with a liquid target in terms of the cost of the "deposited layer."

CONCLUSIONS

The present work analyzed copper films obtained by magnetron sputtering using a cylindrical magnetron, a planar magnetron, and a liquid-phase magnetron. The comparison of deposition methods according to the criteria of "coating deposition rate," "coating structure and surface defects," "roughness," "uniformity of the deposited layer," "sputtering efficiency" and "economic feasibility" confirmed that there is no single universal method that offers optimal performance in terms of all these parameters. For example, the optimal cost of deposition is provided by the method of liquid-phase magnetron sputtering, where the relative cost of the deposited layer is *X*/131 a.u. This compares to *X*/111 a.u. in the case of cylindrical magnetron sputtering and *X*/80 a.u. in the case of a planar extended magnetron. At the same time, the LPMS method loses out to cylindrical magnetron sputtering in terms of surface structure criteria (roughness, grain size, and surface defects). The deposition rates of about 40 μm/min are comparable under the described conditions.

When choosing a coating deposition method, it is necessary to clearly understand the problem to be solved, namely, the requirements for productivity, coating quality (structure and defects), and cost. The magnetron with a cylindrical rotating cathode can be considered as optimal in terms of the cost of the deposited layer, the rate of deposition, and the quality of the deposited layers. However, due to the large dimensions of such sources, it cannot be used for small-sized vacuum chambers. It is recommended to use LPMS for inexpensive high-speed deposition, including operation in vacuum chambers with small dimensions. Although seemingly optimal, the deposition method using extended planar magnetron systems is outperformed by LPMS and cylindrical magnetrons.

REFERENCES

1. Yudintsev V. Global microelectronics development. New strategies. Part II. *Elektronika: Nauka. Tekhnologiya. Biznes = Electronics: Science. Technology. Business*. 2008;4:108–113 (in Russ.). Available from URL: https://www.electronics.ru/journal/article/413
2. Gromov G.G. Volumetric and thin-film thermoelectric modules. *Komponenty i tekhnologii = Components and Technologies*. 2014;9(158):87–92 (in Russ.). Available from URL: https://kit-e.ru/wp-content/uploads/15887.pdf
3. Parashchuk T., Sidorenko N., Ivantsov L., Sorokin A., Maksymuk M., Dzundza B., Dashevsky Z. Development of a solid-state multi-stage thermoelectric cooler. *J. Power Sources*. 2021;496:229821. https://doi.org/10.1016/j.jpowsour.2021.229821
4. Lavrentev M.G., Drabkin I.A., Ershova L.B., Volkov M.P. Improved extruded thermoelectric materials. *J. Electron. Mater.* 2020;49:2937–2942. https://doi.org/10.1007/s11664-020-07988-0
5. Dashevsky Z., Skipidarov S. Investigating the performance of bismuth-antimony telluride. In: Skipidarov S., Nikitin M. (Eds.). *Novel Thermoelectric Materials and Device Design Concepts*. 1st ed. Springer, Cham; 2019. P. 3–21. https://doi.org/10.1007/978-3-030-12057-3_1
6. Moiseev K.M., Nazarenko M.V. Use of magnetron sputtering with liquid target in manufacturing of electronic components for spacecraft. *AIP Conference Proceedings*. 2019;2171(1):170010. https://doi.org/10.1063/1.5133321

СПИСОК ЛИТЕРАТУРЫ

1. Юдинцев В. Развитие мировой микроэлектроники. Новое в стратегии. Часть II. *Электроника: Наука. Технология. Бизнес*. 2008;4:108–113. URL: https://www.electronics.ru/journal/article/413
2. Громов Г.Г. Объемные и тонкопленочные термоэлектрические модули. *Компоненты и технологии*. 2014;9(158):87–92. URL: https://kit-e.ru/wp-content/uploads/15887.pdf
3. Parashchuk T., Sidorenko N., Ivantsov L., Sorokin A., Maksymuk M., Dzundza B., Dashevsky Z. Development of a solid-state multi-stage thermoelectric cooler. *J. Power Sources*. 2021;496:229821. https://doi.org/10.1016/j.jpowsour.2021.229821
4. Lavrentev M.G., Drabkin I.A., Ershova L.B., Volkov M.P. Improved extruded thermoelectric materials. *J. Electron. Mater.* 2020;49:2937–2942. https://doi.org/10.1007/s11664-020-07988-0
5. Dashevsky Z., Skipidarov S. Investigating the performance of bismuth-antimony telluride. In: Skipidarov S., Nikitin M. (Eds.). *Novel Thermoelectric Materials and Device Design Concepts*. 1st ed. Springer, Cham; 2019. P. 3–21. https://doi.org/10.1007/978-3-030-12057-3_1
6. Moiseev K.M., Nazarenko M.V. Use of magnetron sputtering with liquid target in manufacturing of electronic components for spacecraft. *AIP Conference Proceedings*. 2019;2171(1):170010. https://doi.org/10.1063/1.5133321

7. Makarova M.V., Moiseev K.M. The problems of thick tin layers formation by ion sputtering in magnetron systems in target vapors. *Inzhenernyi zhurnal: nauka i innovatsii = Engineering Journal: Science and Innovation*. 2018;1(73) (in Russ). http:// doi.org/10.18698/2308-6033-2018-1-1717
8. Bleikher G.A., Krivobokov V.P., Yur'eva A.V. Analysis of the capabilities of magnetron sputtering systems for high-rate deposition of functional coatings. In: *Sovremennye tekhnologii, ekonomika i obrazovanie:* sbornik materialov II Vserossiiskoi nauchno-metodicheskoi konferentsii (*Modern Technologies. Economics and Education:* Collection of materials of the Second All-Russian Scientific and Methodological Conference). Tomsk: TPU; 2020. P. 51–52 (in Russ).
9. Kouptsov A.D., Vasiliev D.D., Sidorova S.V., Moiseev K.M. Design of a liquid-phase magnetron sputtering small-sized source for the vacuum coating system MVTU-11-1MS. *J. Phys.: Conf. Ser.* 2021;1799(1):012016. https://doi.org/10.1088/1742-6596/1799/1/012016
10. Shandrikov M.V., et al. Deposition of Cu-films by a planar magnetron sputtering system at ultra-low operating pressure. *Surface and Coatings Technology*. 2020;389:125600. https://doi.org/10.1016/j.surfcoat.2020.125600
11. Agrawal S. Development of rotatable magnetron. In: *33rd National Symposium on Plasma Science & Technology* (*PLASMA 2018*): Abstract Book. 2018. P. 172–173. Available from URL: http://www.pssi.in/documents/Abstract%20Book@Plasma%202018.pdf
12. Gudmundsson J.T., Lundin D. Introduction to magnetron sputtering. In: *High Power Impulse Magnetron Sputtering*. Elsevier; 2020. P. 1–48. https://doi.org/10.1016/B978-0-12-812454-3.00006-1
13. Belyakov S. Microchip assembly in Russia: reality and prospects. *Komponenty i tekhnologii = Components and Technologies*. 2014;(5):185–187 (in Russ). Available from URL: https://kit-e.ru/wp-content/uploads/154185.pdf
14. Sobotka S., Herrmann R. Intelligent transport of the 21st century. *Silovaya elektronika = Power Electronics*. 2010;1:12–15 (in Russ). Available from URL: https://power-e.ru/wp-content/uploads/2010_1_12.pdf
15. Makarova M.V., Moiseev K.M. Properties of copper films obtained by liquid-phase magnetron sputtering. In: *12-ya Mezhdunarodnaya nauchno-tekhnicheskaya konferentsiya "Vakuumnaya tekhnika, materialy i tekhnologii:"* Sbornik publikatsii (*12th International Scientific and Technical Conference "Vacuum technology, materials and technologies:"* Collection of publications). 2017. 5 p. (in Russ).

7. Макарова М.В., Моисеев К.М. Проблемы формирования толстых слоев олова методом ионного распыления в магнетронных системах в парах мишени. *Инженерный журнал: наука и инновации*. 2018;1(73). https://doi.org/10.18698/2308-6033-2018-1-1717
8. Блейхер Г.А., Кривобоков В.П., Юрьева А.В. Анализ возможностей магнетронных распылительных систем для высокоскоростного осаждения функциональных покрытий. *Современные технологии, экономика и образование*: сборник материалов II Всероссийской научно-методической конференции. Томск: Изд-во ТПУ; 2020. С. 51–52.
9. Kouptsov A.D., Vasiliev D.D., Sidorova S.V., Moiseev K.M. Design of a liquid-phase magnetron sputtering small-sized source for the vacuum coating system MVTU-11-1MS. *J. Phys.: Conf. Ser.* 2021;1799(1):012016. https://doi.org/10.1088/1742-6596/1799/1/012016
10. Shandrikov M.V., et al. Deposition of Cu-films by a planar magnetron sputtering system at ultra-low operating pressure. *Surface and Coatings Technology*. 2020;389:125600. https://doi.org/10.1016/j.surfcoat.2020.125600
11. Agrawal S. Development of rotatable magnetron. In: *33rd National Symposium on Plasma Science & Technology* (*PLASMA 2018*): Abstract Book. 2018. P. 172–173. URL: http://www.pssi.in/documents/Abstract%20Book@Plasma%202018.pdf
12. Gudmundsson J.T., Lundin D. Introduction to magnetron sputtering. In: *High Power Impulse Magnetron Sputtering*. Elsevier; 2020. P. 1–48. https://doi.org/10.1016/B978-0-12-812454-3.00006-1
13. Беляков С. Сборка микросхем в России: реальность и перспективы. *Компоненты и технологии*. 2014;5:185–187. URL: https://kit-e.ru/wp-content/uploads/154185.pdf
14. Соботка С., Херрманн Р. Интеллектуальный транспорт XXI века. *Силовая электроника*. 2010;1:12–15. URL: https://power-e.ru/wp-content/uploads/2010_1_12.pdf
15. Макарова М.В., Моисеев К.М. Свойства медных пленок, полученных методом жидкофазного магнетронного распыления. *12-я Международная научно-техническая конференция «Вакуумная техника, материалы и технологии»*: Сборник публикаций. 2017. 5 с.

About the author

Mariia V. Nazarenko, Postgraduate Student, Department of Nanoelectronics, Institute for Advanced Technologies and Industrial Programming, MIREA – Russian Technological University (78, Vernadskogo pr., Moscow, 119454 Russia); Leading Process Engineer, RMT (46, Varshavskoe sh., Moscow, 115230 Russia). E-mail: m.v.makarova@list.ru. RSCI SPIN-code 2797-9450, https://orcid.org/0000-0003-1707-8587

Об авторе

Назаренко Мария Владимировна, аспирант, кафедра наноэлектроники Института перспективных технологий и индустриального программирования, ФГБОУ ВО «МИРЭА – Российский технологический университет» (119454, Россия, Москва, пр-т Вернадского, д. 78); ведущий инженер-технолог, ООО «РМТ» (115230, Россия, Москва, Варшавское шоссе, д. 46). E-mail: m.v.makarova@list.ru. SPIN-код РИНЦ 2797-9450, https://orcid.org/0000-0003-1707-8587

Translated from Russian into English by Evgenii I. Shklovskii
Edited for English language and spelling by Thomas A. Beavitt

Analytical instrument engineering and technology

Аналитическое приборостроение и технологии

UDC 551.46.086
https://doi.org/10.32362/2500-316X-2022-10-5-100-110

RESEARCH ARTICLE

Measurement of capillary waves with a laser wave recorder

Viktor V. Sterlyadkin, Konstantin V. Kulikovsky @

MIREA – Russian Technological University, Moscow, 119454 Russia
@ *Corresponding author, e-mail: constantinkk@mail.ru*

Abstract

Objectives. Capillary waves on the sea surface play an important role in remote sensing, both in the optical and microwave wavelength ranges. However, processes of electromagnetic radiation scattering on a rough sea surface cannot be studied in the absence of reliable monitoring of the parameters of these capillary waves under natural conditions. Therefore, the aim of the present work was to develop methods for such monitoring purposes and test them under laboratory and field conditions.

Methods. Novel laser-based methods for recording capillary waves at frequencies up to 100 Hz were developed in the laboratory. The proposed remote methods, which do not interfere with the sea surface, are based on the recording of scattered laser radiation using a video camera.

Results. Under laboratory conditions, spatial profiles, time dependences of heights for all points of a laser sweep trajectory, and frequency power spectra were obtained. It is shown that slopes in capillary waves can reach 30° and that the amplitude of capillary waves at frequencies above 25 Hz does not exceed 0.5 mm. A new version of a scanning laser wave recorder was tested under natural conditions on an offshore platform. The measurements confirmed the possibility of measuring the parameters of sea waves on spatial scales covering 3 orders of magnitude: from units of millimeters to units of meters.

Conclusions. The developed wave recorder can be used to carry out direct measurements of “instantaneous” sea surface profiles with a time synchronization precision of 10^{-4} s and a spatial accuracy of better than 0.5 mm. The method makes it possible to obtain large series (21000) of «instantaneous» wave profiles with a refresh rate of 60 Hz, which opens up opportunities for studying the physics of wave evolution and the influence of wave parameters on the scattering of electromagnetic waves. The advantage of the method is the direct nature of the measurement of applicates and other wave characteristics not only in time but also in space. The entirely remote method does not distort the properties of the surface and is not affected by wind, waves, or sea currents. The possibility of using the proposed method under natural conditions at any time of the day and in a wide range of weather conditions has been experimentally ascertained.

Keywords: altimetry, spectrum of sea waves, capillary waves, atmosphere-ocean interaction, laser wave recorder, remote sensing

• **Submitted:** 03.02.2022 • **Revised:** 11.07.2022 • **Accepted:** 02.09.2022

For citation: Sterlyadkin V.V., Kulikovsky K.V. Measurement of capillary waves with a laser wave recorder. *Russ. Technol. J.* 2022;10(5):100–110. https://doi.org/10.32362/2500-316X-2022-10-5-100-110

Financial disclosure: The authors have no a financial or property interest in any material or method mentioned.

The authors declare no conflicts of interest.

НАУЧНАЯ СТАТЬЯ

Измерение капиллярных волн лазерным волнографом

В.В. Стерлядкин, К.В. Куликовский [@]

МИРЭА – Российский технологический университет, Москва, 119454 Россия
[@] *Автор для переписки, e-mail: constantinkk@mail.ru*

Резюме

Цели. Капиллярные волны на морской поверхности играют важную роль в задачах дистанционного зондирования как в оптическом, так и в микроволновом диапазонах длин волн. Однако исследовать процессы рассеяния электромагнитного излучения на взволнованной морской поверхности можно только при надежном контроле параметров этих капиллярных волн в натурных условиях. До настоящего времени не существовало методов измерения капиллярных волн в натурных условиях. Целью настоящей работы являлось создание таких методов и их проверка в лабораторных и натурных условиях.

Методы. В лаборатории были отработаны новые лазерные методы регистрации капиллярных волн на частотах до 100 Гц. Предложенные методы являются дистанционными, не искажающими поверхность. Они основаны на регистрации рассеянного лазерного излучения с помощью видеокамеры.

Результаты. В лабораторных условиях получены пространственные профили, временны́е зависимости высот для всех точек траектории лазерной развертки, частотные спектры мощности. Показано, что уклоны в капиллярных волнах могут достигать 30°, а амплитуда капиллярных волн на частотах выше 25 Гц не превышает 0.5 мм. В натурных условиях на морской платформе апробирована новая версия сканирующего лазерного волнографа. Измерения подтвердили возможность измерения параметров морского волнения на пространственных масштабах, охватывающих 3 порядка: от единиц миллиметров до единиц метров.

Выводы. Созданный волнограф позволяет проводить прямые измерения «мгновенных» профилей морской поверхности с временно́й синхронизацией в 10^{-4} с и пространственной точностью лучше 0.5 мм. Метод позволяет получать большие ряды (21 000) «мгновенных» профилей волнения с частотой обновления 60 Гц, что открывает возможности для исследования физики эволюции волнения, влияния параметров волнения на рассеяние электромагнитных волн. Достоинством метода является прямой характер измерения аппликат и всех характеристик волнения не только во времени, но и в пространстве. Метод полностью дистанционен, не искажает свойства поверхности, не подвержен влиянию ветра, волн и морского течения. Экспериментально в натурных условиях доказана возможность применения предложенного метода в любое время суток и в широком диапазоне погодных условий.

Ключевые слова: альтиметрия, спектр морского волнения, капиллярные волны, взаимодействие атмосферы и океана, лазерный волнограф, дистанционное зондирование

• **Поступила:** 03.02.2022 • **Доработана:** 11.07.2022 • **Принята к опубликованию:** 02.09.2022

Для цитирования: Стерлядкин В.В., Куликовский К.В. Измерение капиллярных волн лазерным волнографом. *Russ. Technol. J.* 2022;10(5):100–110. https://doi.org/10.32362/2500-316X-2022-10-5-100-110

Прозрачность финансовой деятельности: Авторы не имеют финансовой заинтересованности в представленных материалах или методах.

Авторы заявляют об отсутствии конфликта интересов.

INTRODUCTION

Capillary waves play a fundamentally important role in problems associated with the scattering of electromagnetic waves on a rough sea surface when solving inverse problems of remote sensing of the Earth from space. The influence of capillary waves can be clearly observed over a calm water area: due to gusts of wind, the surface becomes covered with small ripples, changing its color and darkening due to an increase in the absorption coefficient. Similar effects of a sharp increase in the absorption coefficient with the appearance of capillary waves are observed not only in the optical, but also in the microwave wavelength range. For this reason, capillary waves often turn out to be the determining factor when reconstructing the meteorological parameters of the atmosphere and the underlying surface from radiometric and optical measurements of the Earth from spacecraft.

In this regard, determining the detailed relationship between the parameters of capillary waves and the scattering characteristics of the sea surface becomes an important fundamental and applied problem. However, the difficulty of conducting such studies lies in the fact that, until recently, there have been no direct methods for remote determination of the parameters of capillary waves under natural conditions. While remote sensing methods are often used from under water to measure the parameters of gravity waves using acoustic reflections or laser beam refraction [1, 2], these measurements do not allow capillary waves to be recorded. When conducting measurements from offshore platforms or aircraft, laser altimetry methods can be used. However, spatial resolution in these cases is either absent [3] (single-point measurements) or limited to a few centimeters [4, 5]. For this reason, such methods cannot be used to record capillary waves, whose amplitude is measured in fractions of millimeters. It is also worth mentioning remote methods for measuring wave parameters based on stereo imaging [6]. However, such methods are not direct; moreover, their sensitivity is not sufficient for measuring the parameters of capillary waves.

There is a significant number of publications on methods for measuring artificial capillary waves in pools. A good analysis of these is given in [7, 8]. However, a common disadvantage of pool measurements is the presence of resonant edge effects that lead to distorted results. Although the theory of turbulence of gravity and capillary waves has been developed in many works[1] [9–13], we were not able to find any studies whose results included remote space-time measurements of the characteristics of capillary waves carried out under natural conditions.

The present work is aimed at creating a remote laser method for measuring waves from gravitational to capillary scales. The developed laser wave recorder model was tested both under laboratory and natural conditions. The paper provides a description of the method and measurement results.

In previous works [14, 15], we proposed novel laser methods for measuring the “instantaneous” shape of a rough sea surface. The basis of such methods involves laser scanning of the water surface with the beam trajectory recorded at the interface using a video camera. In this case, the beginning of the beam scan is synchronized with the start of recording the image on the sensor of the video camera. These methods can be used to remotely determine the detailed structure of all types of gravity and gravity-capillary waves across a wide range of weather conditions. The achieved accuracy of the method for measuring the interface height was 1 mm, while the accuracy of “tying” the entire trajectory to a single point in time was between 4 and 10 s. However, experimental verification of the proposed methods under natural conditions showed that their further development was required in order to be able to measure the purely capillary component of the waves. This was firstly due to the capillary component of the waves becoming significant for frequencies above 16 Hz, the traditional video sample rate of 25 Hz is not adequate for recording them: the recording frequency should be at least twice as high as the profile being recorded. Secondly, since the amplitude of capillary waves has a scale comparable to or less than 1 mm, the sensitivity of the method by which these waves will be recorded should be at the level of 0.5 mm or less. Thus, in the present work, the method of remote laser measurements of waves is improved to the level required for separately measuring the capillary component of the waves.

GENERATION OF CAPILLARY WAVES UNDER LABORATORY CONDITIONS AND THE TECHNIQUE OF LASER MEASUREMENTS

Laboratory measurements comprise an important step in creating a method for measuring capillary waves under marine conditions. As well as providing remote measurements of the parameters of the generated waves, Figure 1 shows a schematic of a laboratory setup that makes it possible to generate capillary waves of a given amplitude and frequency. Vibrations generated by a low frequency woofer and transmitted by a light rod to a round platform comprise a source of disturbances

[1] Filatov S.V. Nonlinear wave and vortex motions on the surface of a liquid. Cand. Sci. Thesis (Phys.-Math.). Chernogolovka; 2020. 82 p. (in Russ.). https://docplayer.com/170397192-Filatov-sergey-vasilevich-nelineynye-volnovye-i-vihrevye-dvizheniya-na-poverhnosti-zhidkosti.html

on the water surface. A ruler serves for recording the wavelength of the generated waves in the photographs. The stroboscope allows the image of capillary waves to be "stopped" if its frequency is consistent with that of the signal supplied to the woofer in order to obtain a clear image of the waves on the water surface in the reservoir and thus reliably measure the expanse of a set of several waves.

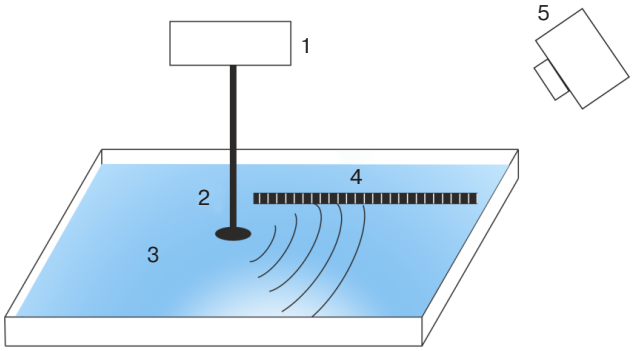

Fig. 1. Schematic of generating capillary waves in laboratory conditions:
1 – low-frequency woofer, 2 – vibrating platform, 3 – water surface, 4 – ruler, 5 – stroboscope

Photographs of the produced waves at different generator frequencies f are presented in Figs. 2a and 2b. In Fig. 2a, the frequency of produced waves f = 16 Hz corresponds to a gravity-capillary wave, while the frequency f = 60 Hz in Fig. 2b relates to purely capillary oscillations.

(a) (b)

Fig. 2. Images of surface waves at generation frequency f = 16 Hz (a) and at f = 60 Hz (b)

The created setup made it possible to find the dispersion relation between the angular frequency of the wave ω and the wavelength λ. The theoretical expressions for the dispersion and the phase velocity of waves have the form [16]:

$$\omega = \sqrt{kg + \frac{k^3\sigma}{\rho}}, \qquad (1)$$

$$U = \frac{\omega}{k} = \sqrt{\frac{g}{k} + \frac{k\sigma}{\rho}}, \qquad (2)$$

where $k = \frac{2\pi}{\lambda}$ is the wavenumber, g is the gravitational acceleration, and σ is the surface tension coefficient of the liquid.

In this equation, the first term under the root determines the gravitational part, while the second term is responsible for the capillary component. For pure water, σ = 72 mN/m, and the conditional boundary of the transition from predominantly gravitational to predominantly capillary waves corresponds to the equality of these terms. In this case, $k = \frac{\rho g}{\sigma} = 369\,\text{m}^{-1}$, and the wavelength corresponding to the boundary of the transition to capillary waves is λ_{bound} = 17 mm. The results of laboratory measurements are presented in Table.

Figure 3 shows the dispersion for surface waves. Here it should be noted that no special measures were taken to purify water from surfactants, resulting in a lowered value of σ. Optimization of the theoretical dependence for this parameter with respect to experimental measurements showed that the best approximation corresponds to σ = 45 mN/m. Note also that in laboratory measurements, the conditional wavelength λ_{bound} corresponding to the transition to the capillary component decreases in proportion to the surface tension coefficient.

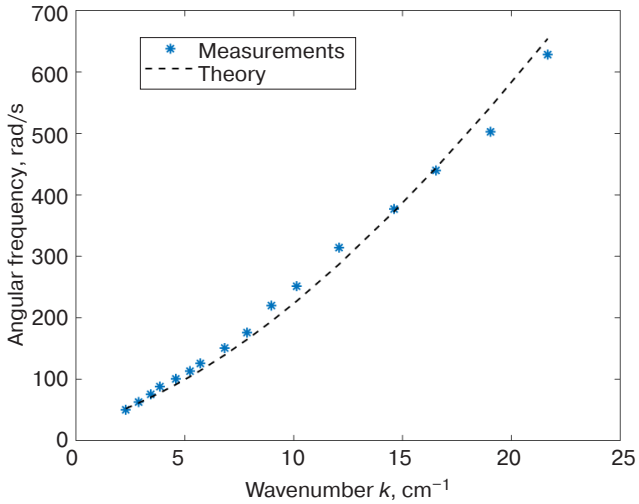

Fig. 3. Measured dispersion of gravity-capillary and capillary waves (σ = 45 mN/m)

It can be seen from the graph that the measured dispersion dependence is in good agreement with the theoretical dependence (1).

Table. Laboratory measurements

Frequency f, Hz	8	10	12	14	16	18	20	24	28	35	40	50	60	70	80	100
Wavelength λ, mm	27.5	22.0	18.3	16.3	13.7	12.0	11.0	9.2	8.0	7.0	6.2	5.2	4.3	3.75	3.6	2.9

The next step of the experiment was to register the amplitude of the emerging gravity-capillary waves. To do this, the surface was illuminated by laser radiation, which scanned along the surface with short stops at separate points. In a photograph, shown in Fig. 4, the boundary where the laser beams are scattered is clearly visible. Registration of surface movement during wave propagation is carried out using a video camera placed laterally with a recording frequency of 60 Hz. Laser beams scatter in water, when hit it, creating an almost vertical beam. The upper boundary of each beam corresponds to the water-air interface.

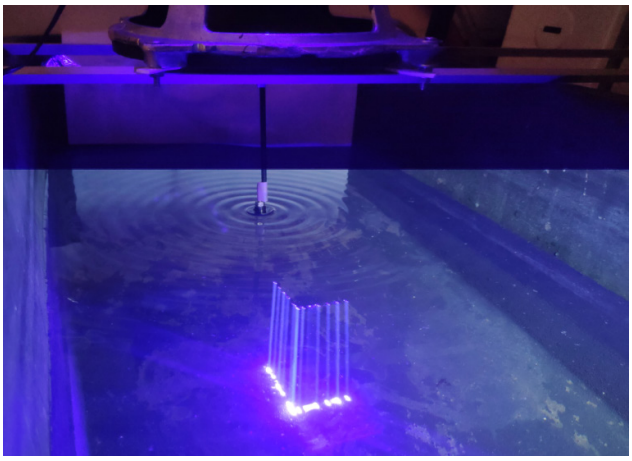

Fig. 4. Laser beams, when scattered in water, form a clear edge on the surface

However, such a measurement scheme did not allow recording the cross section of the surface and its profile. To solve this problem, the measurement scheme was changed. For this, a setup was assembled schematically shown in Fig. 5.

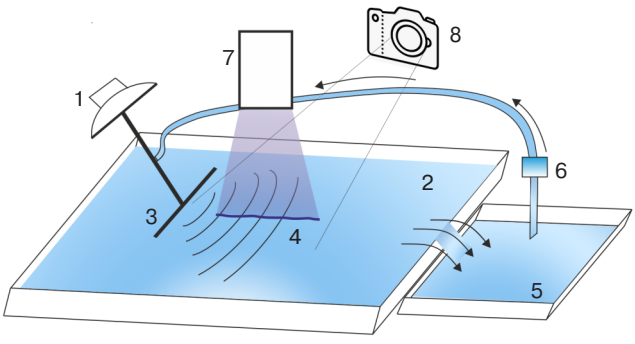

Fig. 5. Schematic of laboratory optical measurements of capillary waves: 1 – woofer, 2 – water surface, 3 – vibrating plate, 4 – interface illuminated by a scanning laser, 5 – lower reservoir, 6 – pump, 7 – electronically controlled scanner, 8 – video camera

In this experiment, the wave generator comprised a vibrating plate partially submerged in water. Vibrations from the woofer cone were transmitted to the water surface via a plate rigidly attached to the woofer. The woofer was powered via an amplifier using a sound generator, which allowed the amplitude and frequency of the plate vibrations to be changed over a wide range. Plane waves appearing on the water surface as a result of the displacement of the plate were illuminated by a scanning laser beam. To reduce the amount of dust particles settling on the surface, water was drained over the edge of the upper reservoir into the lower reservoir from which the water was returned to the upper bath by means of a pump. Laser radiation with a wavelength of 450 nm and power of about 1 W was swept on the surface along a straight line about 80 mm long using an electronically controlled scanner. The beam scattered at the interface was recorded from a laterally positioned video camera. In this case, the time of the beam sweep was close to the exposure time of video frames. An example of a video frame in which laser radiation is scattered onto a disturbed interface is shown in Fig. 6. The boundary of the water surface clearly visible in each frame can be converted into the height of the disturbance at each point of the ray trajectory taking the calibration of the video camera sensor into account. The presence of dust particles on the surface led to bright spots at their locations; however, draining the water significantly reduced their number to speed up the processing of frames.

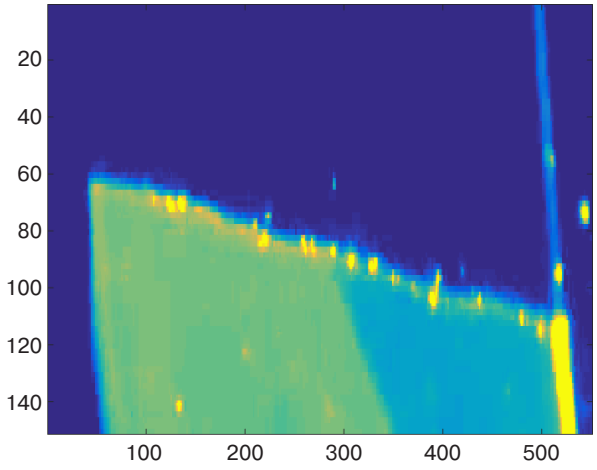

Fig. 6. Video frame of the wave surface, along which the capillary wave propagates

Video frames were processed for each column of the image. Figure 7 shows a graph of changes in the intensity of illumination along one of the columns of the frame. It can be seen that the boundary of the interface corresponding to the jump in intensity to a given level has a length of one pixel. Therefore, the height resolution of this method corresponds to the scale of one pixel, which in our experiment was 0.15 mm. The wave profile was recorded with sequential processing of all columns of the video frame.

Calibration of the video image and conversion of pixels to height in millimeters was carried out taking into account the position of the undisturbed surface and scaling according to the known image (*mire*). At the next stage, smoothing the profile with a sliding window turned out to be useful. Figure 8 shows examples of the wave profile for gravity-capillary and capillary waves of various frequencies, taking into account smoothing.

Although the vibration amplitude of the woofer cone and the rod disturbing the water surface in the reservoir did not change, the amplitude of the waves at frequencies above 16 Hz, which decreased with increasing frequency, did not exceed one millimeter. This indicates an increase

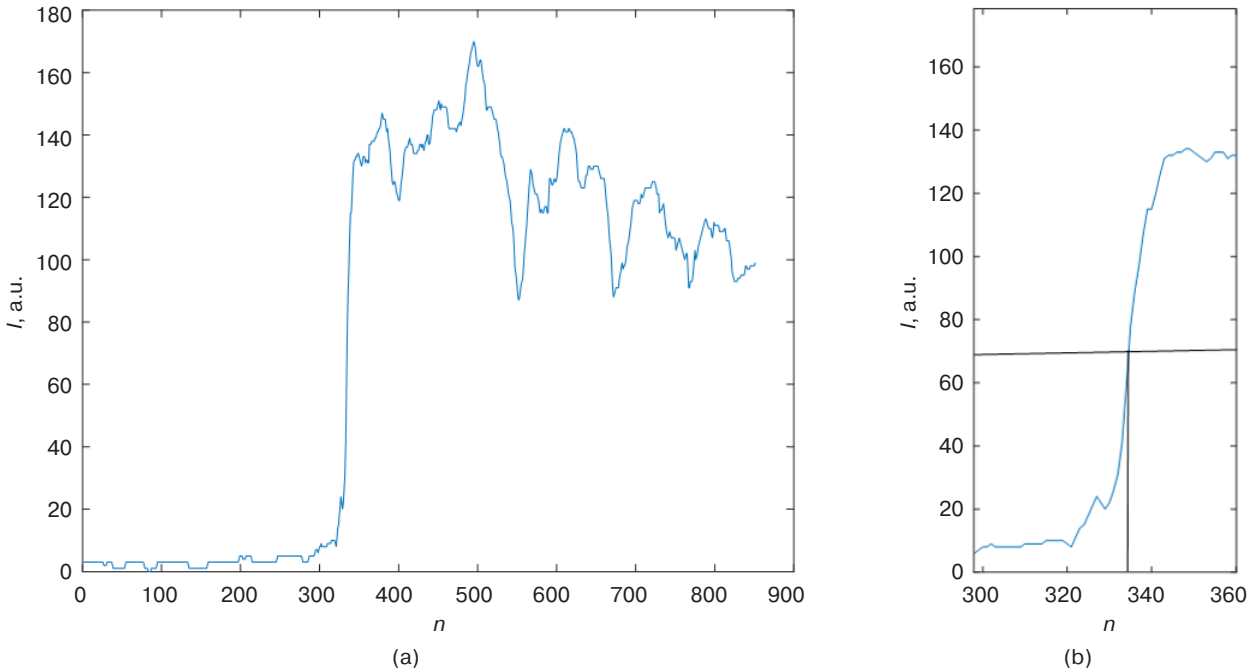

Fig. 7. Image intensity against the row number along one of the columns of the video frame in Fig. 5 (a) and the border of illumination clearly visible on an enlarged scale (b)

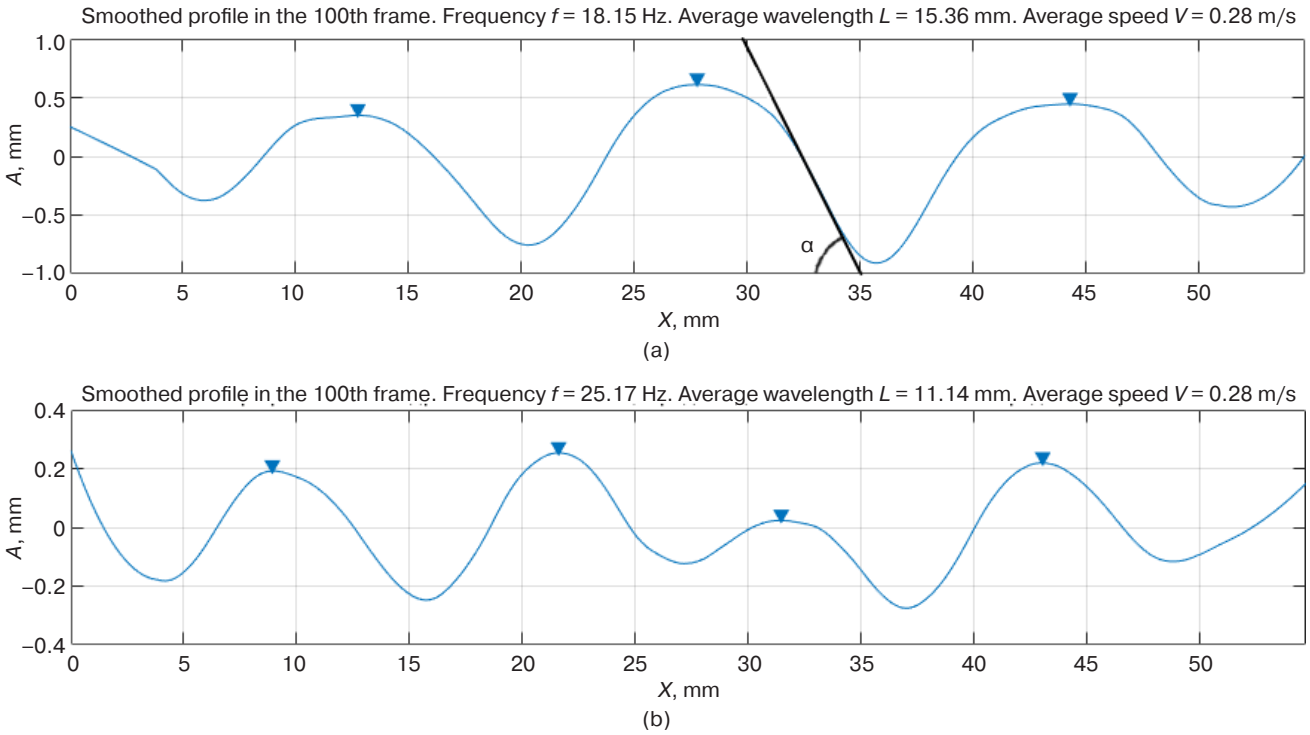

Fig. 8. Profile of capillary waves for a separate image frame: wave frequency 18 Hz (a), wave frequency 25 Hz (b)

in the attenuation coefficient with an increase in the frequency of capillary waves. In addition to the spatial image of capillary waves, the experiment made it possible to obtain the temporal variability of the applicate (height) at any point of the trajectory. Figure 9a shows the time dependence of the perturbation height. The power spectrum of the wave process is obtained via Fourier analysis of this dependence (Fig. 9b). The spectrum clearly registers the main frequency of the excited capillary waves, which corresponds to the vibration frequency of the woofer cone.

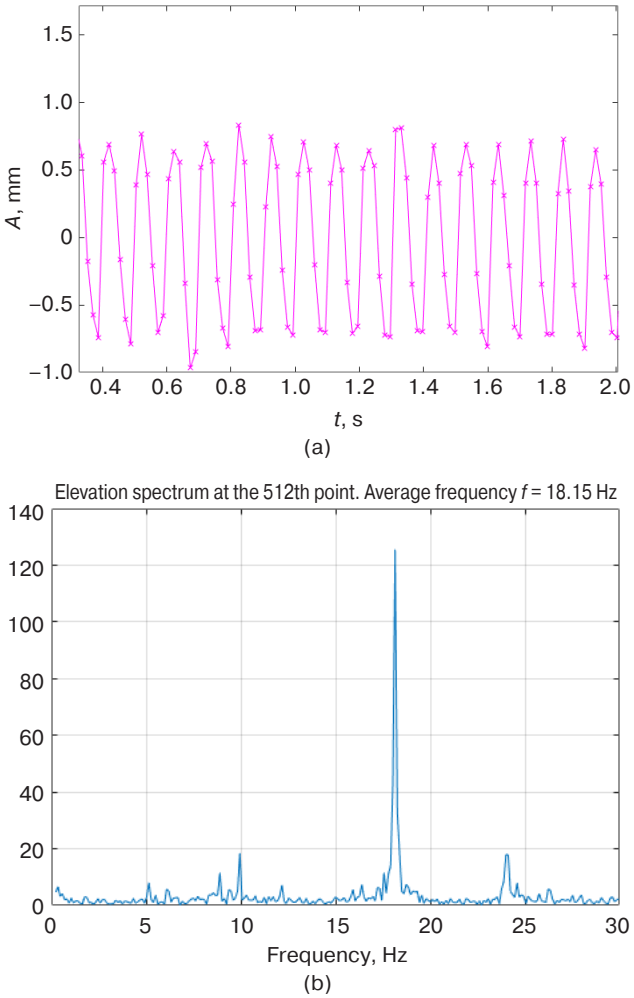

Fig. 9. Dependence of the height of the interface at one point of the trajectory on time (a) and the power spectrum in the 512th point (b)

The conducted laboratory studies of capillary waves made it possible to directly measure their main features and take these features into account when designing a marine wave recorder enabling to record the capillary component of sea waves. As a result of the analysis, a number of conclusions can be drawn. First, from the waveform in Fig. 8a it follows that the slopes in capillary waves can reach the level $\xi = tg(\alpha) = 2/5$, which is 23°. Under natural conditions, capillary waves are superimposed onto gravitational waves, increasing the overall slope of the surface area. Under marine conditions, the resulting slopes can be expected to reach 30° or more. In this case, a laser beam incident vertically down on the sea surface would deviate by more than 60°.

At frequencies of 25–30 Hz, it is not possible to create capillary waves with an amplitude greater than 0.5 mm. From this it follows that equipment used to measure the capillary component of sea waves under natural conditions at frequencies from 16 Hz to 30 Hz will require sensitivity at 0.5 mm or higher.

FIELD MEASUREMENTS OF CAPILLARY WAVES

In August 2021, the first field measurements were carried out using a scanning laser wave recorder, which made it possible to record capillary waves. The measurements were carried out from the sea pier of the Marine Hydrophysical Institute and from the stationary oceanographic platform of the Marine Hydrophysical Institute of the Russian Academy of Sciences, located in the town of Katsiveli in Crimea. Unlike the previous version of the wave recorder described in [14], the video recording frequency was increased from 25 Hz to 60 Hz. This made it possible to measure wave spectra up to 30 Hz, by which frequency the capillary component is already dominant. Recall that for pure water, starting from frequencies above 16 Hz, the capillary forces exceed the gravitational ones. A second improvement concerned the use of a zoom lens on a video camera, which increased the spatial resolution to 0.3–0.6 mm.

An example of a video frame received on August 26, 2021, at 20:47 Moscow time at the sea pier is shown in Fig. 10. The shape of the wave surface is clearly recorded in the image. For each 6-minute scanning session, it is possible to record 21 600 "instantaneous" spectra. These can be used as a basis for calculating both temporal and spatial wave spectra, one-dimensional and two-dimensional slopes on any scale, as well as the variability of wave parameters when the meteorological situation changes.

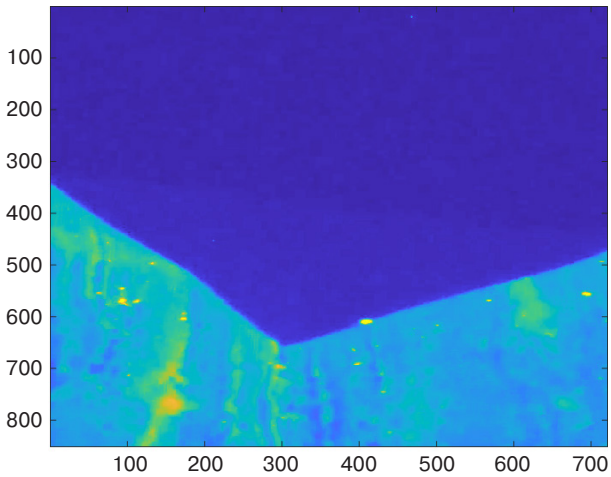

Fig. 10. Typical video frame of disturbance (values along axes are in pixels). Sampling frequency is 60 Hz

Figure 11 shows an example of a scanning realization dated August 26, 2021, for the dependence of the height on the frame number for one point of the trajectory (the total number of resolved points on the trajectory of the laser beam scan is 700). Figure 11a shows the entire scan, and Fig. 11b demonstrates a small segment of the scan on an enlarged scale.

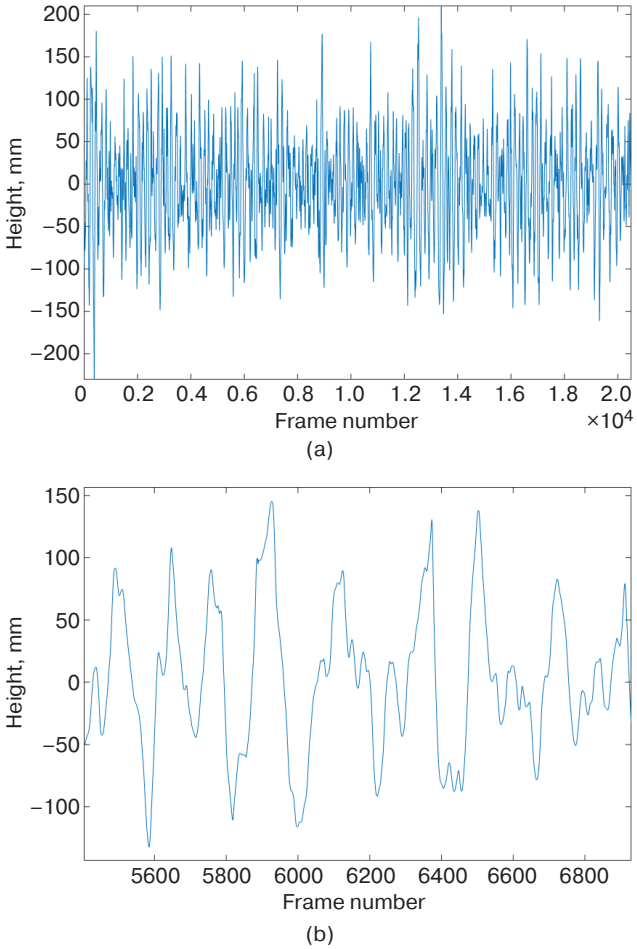

Fig. 11. An example of the dependence of the wave height on the frame number for one point on the scan trajectory (a), and a section of the recording on an enlarged scale (b)

The time spectrum of the resulting realization is of particular interest (Fig. 12). Traditionally, it is represented on a double logarithmic scale. There are three segments on the spectrum, whose slope characterizes various forms of waves. Here, the lowest frequency region of the spectrum (long wavelength) has a slope of −4.5 ± 0.3, while the middle region is responsible for gravitational waves and has a slope of −4.0 ± 0.2. The much less steep slope of the third region, which already takes capillary waves into account, is −2.6 ± 0.3. The obtained exponential dependence indices are in good agreement with the known theoretical and experimental data. Thus, the power dependence with a slope of −4.0 corresponds to the spectrum of V.E. Zakharova and

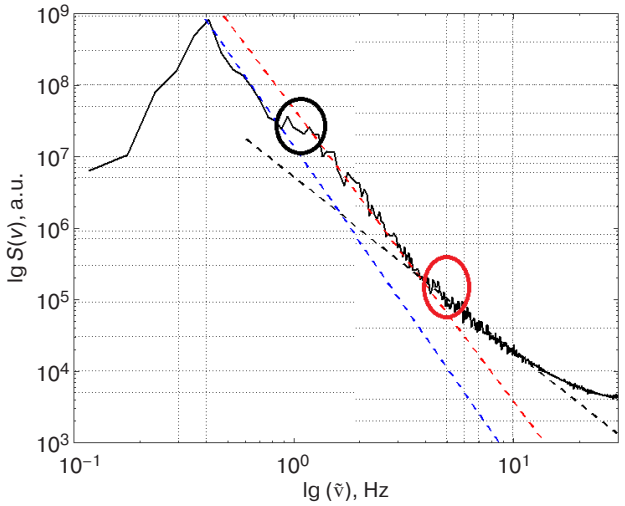

Fig. 12. Elevation spectrum at one point of the profile on a logarithmic scale for developing waves (August 26, 2021, Katsiveli, Crimea). The circles indicate the regions of transition from one spectrum slope to another

N.N. Filonenko [10], while the section with a slope of −4.5 forms a transitional regime to the Phillips spectrum $E \sim f^{-5}$ [12].

CONCLUSIONS

At this phase of research, the authors did not set the task of interpreting the spectral or other characteristics of waves. The purpose of this work was to create and test a new laser wave recorder under both laboratory and field conditions, in order to evaluate its capabilities for measuring the full spectrum of gravitational, gravity-capillary, and capillary waves under natural marine conditions. Under laboratory conditions, laser methods for recording capillary waves were tested, and the characteristics of waves at high frequencies were obtained: spatial profiles, time dependencies of heights for all points of the laser scan trajectory, as well as frequency power spectra. It is concluded that the slopes in capillary waves can reach 30°, while the amplitude at frequencies above 25 Hz does not exceed 0.5 mm. An important stage of the work was the testing of a new version of the scanning laser wave recorder under natural marine conditions. The measurements confirmed the feasibility of using the proposed laser method to measure the parameters of sea waves on spatial scales covering 3 orders: from millimeters to meters. We are not aware of world analogs having such characteristics. The method is patented [15]. The creation of a wave recorder that makes it possible to conduct direct measurements of "instantaneous" sea surface profiles synchronized within 10^{-4} s with a spatial accuracy of better than 0.5 mm opens up wide opportunities for studying the physics of wave evolution and the effect of waves on the scattering of electromagnetic waves. This is the first time such

opportunities have been opened up. The advantage of the method is that it provides direct measurements of applicates and all wave characteristics not only in time but also in the spatial domain. This makes it possible to obtain large series (21 000) of "instantaneous" wave profiles for each 6-minute scanning session. The described remote method, which does not distort the properties of the surface, is unaffected by wind, waves and sea currents. The possibility of using the proposed method to measure the proportion of foam on the sea surface at any time of the day and under a wide range of weather conditions has been experimentally demonstrated under field conditions.

Authors' contribution

The ideas of the proposed methods, hardware implementation, and assembly of the device, as well as the development of software for processing data were implemented by Professor V.V. Sterlyadkin and Senior Lecturer K.V. Kulikovsky, the staff of the Department of Physics at the MIREA – Russian Technological University.

REFERENCES

1. Holthuijsen L.H. *Waves in oceanic and coastal waters*. Cambridge University Press; 2010. 404 p. https://doi.org/10.1017/CBO9780511618536
2. Hashimoto N. Analysis of the directional wave spectrum from field data. In: *Advances in Coastal and Ocean Engineering.* Liu P.L.-F. (Ed.). Singapore: World Scientific. 1997;3:103–143. https://doi.org/10.1142/9789812797568_0004
3. Grare L., Lenain L., Melville W.K. Vertical profiles of the wave-induced airflow above ocean surface waves. *J. Phys. Oceanogr*. 2018;48(12):2901–2922. https://doi.org/10.1175/JPO-D-18-0121.1
4. Hwang P.A., Wang D.W., Walsh E.J., Krabill W.B., Swift R.N. Airborne measurements of the wave number spectra of ocean surface waves. Part I: Spectral slope and dimensionless spectral coefficient. *J. Phys. Oceanogr.* 2000;30(11):2753–2767. https://doi.org/10.1175/1520-0485(2001)031<2753:AMOTWS>2.0.CO;2
5. Allender J., Audunson T., Barstow S.F., Bjerken S., Krogstad H.E., Steinbakke P., Vartdal L., Borgman L.E., Graham C. The WADIC project; a comprehensive field evaluation of directional wave instrumentation. *Ocean Eng*. 1989;16(5–6):505–536. https://doi.org/10.1016/0029-8018(89)90050-4
6. Banner M.L., Jones I.S., Trinder J. Wavenumber spectra of short gravity waves. *J. Fluid Mech*. 1989;198:321–344. https://doi.org/10.1017/S0022112089000157
7. Falcon E., Mordant N. Experiments in surface gravity-capillary wave turbulence. *Annual Rev. Fluid Mech*. 2022;54:1–25. https://doi.org/10.1146/annurev-fluid-021021-102043
8. Brazhnikov M.Yu., Levchenko A.A., Mezhov-Deglin L.P. Excitation and detection of nonlinear waves on a charged surface of liquid hydrogen. *Instruments and Experimental Techniques*. 2002;45(6):758–763. https://doi.org/10.1023/A:1021418819539
9. Zakharov V.E. Weak turbulence in media with a decay spectrum. *J. Appl. Mech. Tech. Phys*. 1965;6(4):22–24. https://doi.org/10.1007/BF01565814
[Original Russian Text: Zakharov V.E. Weak turbulence in media with a decay spectrum. *Prikladnaya mekhanika i tekhnicheskaya fizika*. 1965;4:35–39 (in Russ.). Available from URL: https://www.sibran.ru/upload/iblock/2f5/2f55daccf31e1bdff4c6c44e436b4166.pdf]

СПИСОК ЛИТЕРАТУРЫ

1. Holthuijsen L.H. *Waves in oceanic and coastal waters*. Cambridge University Press; 2010. 404 p. https://doi.org/10.1017/CBO9780511618536
2. Hashimoto N. Analysis of the directional wave spectrum from field data. In: *Advances in Coastal and Ocean Engineering.* Liu P.L.-F. (Ed.). Singapore: World Scientific. 1997;3:103–143. https://doi.org/10.1142/9789812797568_0004
3. Grare L., Lenain L., Melville W.K. Vertical profiles of the wave-induced airflow above ocean surface waves. *J. Phys. Oceanogr*. 2018;48(12):2901–2922. https://doi.org/10.1175/JPO-D-18-0121.1
4. Hwang P.A., Wang D.W., Walsh E.J., Krabill W.B., Swift R.N. Airborne measurements of the wave number spectra of ocean surface waves. Part I: Spectral slope and dimensionless spectral coefficient. *J. Phys. Oceanogr.* 2000;30(11):2753–2767. https://doi.org/10.1175/1520-0485(2001)031<2753:AMOTWS>2.0.CO;2
5. Allender J., Audunson T., Barstow S.F., Bjerken S., Krogstad H.E., Steinbakke P., Vartdal L., Borgman L.E., Graham C. The WADIC project; a comprehensive field evaluation of directional wave instrumentation. *Ocean Eng*. 1989;16(5–6):505–536. https://doi.org/10.1016/0029-8018(89)90050-4
6. Banner M.L., Jones I.S., Trinder J. Wavenumber spectra of short gravity waves. *J. Fluid Mech*. 1989;198:321–344. https://doi.org/10.1017/S0022112089000157
7. Falcon E., Mordant N. Experiments in surface gravity-capillary wave turbulence. *Annual Rev. Fluid Mech*. 2022;54:1–25. https://doi.org/10.1146/annurev-fluid-021021-102043
8. Brazhnikov M.Yu., Levchenko A.A., Mezhov-Deglin L.P. Excitation and detection of nonlinear waves on a charged surface of liquid hydrogen. *Instruments and Experimental Techniques*. 2002;45(6):758–763. https://doi.org/10.1023/A:1021418819539
9. Захаров В.Е. Слабая турбулентность в средах с распадным спектром. *Прикладная механика и техническая физика*. 1965;4:35–39. URL: https://www.sibran.ru/upload/iblock/2f5/2f55daccf31e1bdff4c6c44e436b4166.pdf
10. Захаров В. Е., Филоненко Н. Н. Спектр энергии для стохастических колебаний поверхности жидкости. *Докл. АН СССР*. 1966;170(6):1292–1295. URL: http://www.mathnet.ru/links/ec2b951f99ebc10ab5bb4c2bf4fe5948/dan32646.pdf

10. Zakharov V.E., Filonenko N.N. Energy spectrum for stochastic oscillations of the surface of a liquid. *Dokl. Akad. Nauk SSSR*. 1966;170(6):1292–1295 (in Russ.). Available from URL: http://www.mathnet.ru/links/ec2b951f99ebc10ab5bb4c2bf4fe5948/dan32646.pdf
11. Zakharov V.E., Filonenko N.H. Weak turbulence of capillary waves. *J. Appl. Mech. Tech. Phys.* 1967;8:37–40. https://doi.org/10.1007/BF00915178
[Original Russian Text: Zakharov V.E., Filonenko N.H. Weak turbulence of capillary waves. *Prikladnaya mekhanika i tekhnicheskaya fizika*. 1967;5:62–67 (in Russ.). Available from URL: https://www.sibran.ru/upload/iblock/24e/24ea0a63fb235c70765e3dd7eceadeea.pdf]
12. Badulin S.I., Zakharov V.E. Phillips spectrum and a model of wind wave dissipation. *Theoret. and Math. Phys.* 2020;202(3):309–318. https://doi.org/10.1134/S0040577920030034
[Original Russian Text: Badulin S.I., Zakharov V.E. Phillips spectrum and a model of wind wave dissipation. *Teoreticheskaya i matematicheskaya fizika*. 2020;202(3):353–363 (in Russ.). https://doi.org/10.4213/tmf9801]
13. Lukaschuk S., Nazarenko S., McLelland S., Denissenko P. Gravity wave turbulence in wave tanks: Space and time statistics. *Phys. Rev. Lett*. 2009;103(4):044501. http://doi.org/10.1103/PhysRevLett.103.044501
14. Sterlyadkin V.V., Kulikovskii K.V., Kuzmin A.V., Sharkov E.A., Likhacheva M.V. Scanning laser wave recorder with registration of “instantaneous” sea surface profiles. *J. Atmos. Oceanic Technol*. 2021;38(8):1415–1424. https://doi.org/10.1175/JTECH-D-21-0036.1
15. Sterlyadkin V.V. *Scanning laser recorder recording “instant” shape of surface*: RU Pat. 2749727. Publ. 16.06.2021 (in Russ.).
16. Landau L.D., Lifshits E.M. *Teoreticheskaya fizika*: Uchebnoe posobie. V 10 t. T. VI. *Gidrodinamika* (*Theoretical Physics*: Textbook. In 10 v. V. VI. *Hydrodynamics*. Moscow: Nauka; 1986. 736 p. (in Russ.).
11. Захаров В.Е., Филоненко Н.Н. Слабая турбулентность капиллярных волн. *Прикладная механика и техническая физика*. 1967;5:62–67. URL: https://www.sibran.ru/upload/iblock/24e/24ea0a63fb235c70765e3dd7eceadeea.pdf
12. Бадулин С.И., Захаров В.Е. Спектр Филлипса и модель диссипации ветрового волнения. *Теоретическая и математическая физика*. 2020;202(3):353–363. https://doi.org/10.4213/tmf9801
13. Lukaschuk S., Nazarenko S., McLelland S., Denissenko P. Gravity wave turbulence in wave tanks: Space and time statistics. *Phys. Rev. Lett*. 2009;103(4):044501. http://doi.org/10.1103/PhysRevLett.103.044501
14. Sterlyadkin V.V., Kulikovskii K.V., Kuzmin A.V., Sharkov E.A., Likhacheva M.V. Scanning laser wave recorder with registration of «instantaneous» sea surface profiles. *J. Atmos. Oceanic Technol*. 2021;38(8):1415–1424. https://doi.org/10.1175/JTECH-D-21-0036.1
15. Стерлядкин В.В. *Сканирующий лазерный волнограф с регистрацией «мгновенной» формы поверхности*: Пат. RU № 2749727. Заявка № RU2020134068A; заявл. 16.102020; опубл.16.06.2021.
16. Ландау Л.Д., Лифшиц Е.М. *Теоретическая физика*: Учебное пособие. В 10 т. Т. VI. *Гидродинамика*. М.: Наука. Гл. ред. физ-мат. лит.; 1986. 736 с.

About the authors

Viktor V. Sterlyadkin, Dr. Sci. (Phys.-Math.), Professor, Department of Physics, Institute for Advanced Technologies and Industrial Programming, MIREA – Russian Technological University (78, Vernadskogo pr., Moscow, 119454 Russia). E-mail: sterlyadkin@mirea.ru. Scopus Author ID 6505940691, ResearcherID D-7125-2017, https://orcid.org/0000-0002-1832-8608

Konstantin V. Kulikovsky, Senior Lecturer, Department of Physics, Institute for Advanced Technologies and Industrial Programming, MIREA – Russian Technological University (78, Vernadskogo pr., Moscow, 119454 Russia). E-mail: constantinkk@mail.ru. Scopus Author ID 57223241696, https://orcid.org/0000-0001-9296-6424

Об авторах

Стерлядкин Виктор Вячеславович, д.ф.-м.н., профессор, кафедра физики Института перспективных технологий и индустриального программирования ФГБОУ ВО «МИРЭА – Российский технологический университет» (119454, Россия, Москва, пр-т Вернадского, д. 78). E-mail: sterlyadkin@mirea.ru. Scopus Author ID 6505940691, ResearcherID D-7125-2017, https://orcid.org/0000-0002-1832-8608

Куликовский Константин Владимирович, старший преподаватель, кафедра физики Института перспективных технологий и индустриального программирования ФГБОУ ВО «МИРЭА – Российский технологический университет» (119454, Россия, Москва, пр-т Вернадского, д. 78). E-mail: constantinkk@mail.ru. Scopus Author ID 57223241696, https://orcid.org/0000-0001-9296-6424

Translated from Russian into English by Evgenii I. Shklovskii
Edited for English language and spelling by Thomas A. Beavitt

UDC 811.134.2
https://doi.org/10.32362/2500-316X-2022-10-5-111-120

RESEARCH ARTICLE

Axiological aspects of teaching Spanish in the Soviet Union

Elena V. Novoselova,
Nadezhda I. Chernova @,
Nataliya V. Katakhova

MIREA – Russian Technological University, Moscow, 119454 Russia
@ Corresponding author, e-mail: chernova@mirea.ru

Abstract

Objectives. The paper analyzes core axiological aspects of Spanish teaching in higher educational institutions of the Soviet Union from the 1930s to the early 1980s based on various sources including textbooks, tutorials, etc.

Methods. The study is based on textual-analytic, historical-comparative, and structural methods.

Results. Scientific-pedagogical and sociological aspects of the subject are distinguished. The former are limited to the internal developmental logic of Spanish studies, while the latter refers to external circumstances, including ideological factors. The literature review shows that Spanish teaching in the USSR progressed topically from simple manuals aimed at consolidating linguistic basics to a more rigorous pedagogical development of Spanish language studies (grammar, phonetics, vocabulary, etc.) The authors identify two significant periods in the development of Soviet Spanish studies, with the first phase extending from the 1930s to the early 1960s, and the second—from the 1960s to the early 1980s.

Conclusions. The analysis showed that the formation and development of each period is associated with such events as the Spanish Civil War and the victory of the Cuban Revolution, which are not directly related to Spanish teaching. The first event coincided with the beginning of systematic Spanish teaching at the USSR universities, while the second redirected this process from Castilian to Latin American Spanish. However, the analysis of textbook and tutorial materials convincingly demonstrates that this process of redirection, which mainly concerns the selection of textual materials, remains incomplete. This supports a conclusion concerning the limited impact of ideology on the internal logic of the Spanish studies development in the USSR.

Keywords: Spanish, higher education, methodology, ideology, teaching of foreign languages

• **Submitted:** 14.06.2022 • **Revised:** 04.07.2022 • **Accepted:** 12.08.2022

For citation: Novoselova E.V., Chernova N.I., Katakhova N.V. Axiological aspects of teaching Spanish in the Soviet Union. *Russ. Technol. J.* 2022;10(5):111–120. https://doi.org/10.32362/2500-316X-2022-10-5-111-120

Financial disclosure: The authors have no a financial or property interest in any material or method mentioned.

The authors declare no conflicts of interest.

НАУЧНАЯ СТАТЬЯ

Аксиологические аспекты преподавания испанского языка в СССР

Е.В. Новосёлова,
Н.И. Чернова [@],
Н.В. Катахова

МИРЭА – Российский технологический университет, Москва, 119454 Россия
[@] Автор для переписки, e-mail: chernova@mirea.ru

Резюме

Цели. Целью статьи является анализ ведущих аксиологических аспектов преподавания испанского языка в высших учебных заведениях Советского Союза (с 1930-х до начала 1980-х гг.) на основе изучения содержания учебников, пособий и ряда других трудов.

Методы. В статье применяются текстологический, историко-сравнительный и структурный методы.

Результаты. На основе анализа указанных текстов авторы делают акцент на двух основных группах аспектов: научно-педагогических и вненаучных. Первые связаны с внутренней логикой развития испанистики как науки, вторые – со сторонними, внешними обстоятельствами, прежде всего, идеологическими. Анализ источников показывает, что тематически преподавание испанского в СССР проделало путь от простых пособий, нацеленных на закрепление основ языка, до углубленной разработки разнообразных конструктов испанского языка (грамматики, фонетики, лексики и т.д.). В хронологическом отношении дифференцированы два основных периода в развитии советской испанистики: с 1930-х до начала 1960-х гг. и с начала 1960-х до начала 1980-х гг.

Выводы. Анализ показал, что становление и развитие каждого из периодов связано с событиями, не имеющими к преподаванию испанского языка прямого отношения: гражданской войной в Испании и победой Кубинской революции. Следствием первого события стало начало систематического преподавания испанского в вузах СССР, а следствием второго – переориентация этого процесса с пиренейского варианта испанского на латиноамериканский. Однако содержание учебников и пособий убедительно демонстрирует, что эта переориентация не была полной и касалась преимущественно подбора текстовых материалов, что позволяет авторам прийти к выводу об ограниченности влияния идеологии на внутреннюю логику развития испанистики в СССР.

Ключевые слова: испанский язык, высшее образование, методология, идеология, преподавание иностранных языков

• **Поступила:** 14.06.2022 • **Доработана:** 04.07.2022 • **Принята к опубликованию:** 12.08.2022

Для цитирования: Новосёлова Е.В., Чернова Н.И., Катахова Н.В. Аксиологические аспекты преподавания испанского языка в СССР. *Russ. Technol. J.* 2022;10(5):111–120. https://doi.org/10.32362/2500-316X-2022-10-5-111-120

Прозрачность финансовой деятельности: Авторы не имеют финансовой заинтересованности в представленных материалах или методах.

Авторы заявляют об отсутствии конфликта интересов.

INTRODUCTION

The methods, approaches, and technologies of foreign language teaching have been always developed in tight integration with a number of other sciences, such as philosophy, pedagogics, psychology, psycholinguistics, and communication theory, whose data has been and is being productively implemented to assess the effectiveness and validity of the research. Today, the task of finding the most effective and rational ways of forming the foreign-language communicative competence of students remains still relevant [1].

Of the major European languages, Spanish came to Russia later than e.g., German, French, its systematic teaching and study beginning only during the twentieth century. In many respects, this can be attributed to the long period during which close relations between

Russia and Spain were absent[1]. This fact presents researchers with an interesting opportunity to analyze the formation and development of the teaching strategy for a particular subject over a limited period of time, as well as to evaluate the changes to which it has been subjected.

The present paper sets out to analyze axiological aspects of teaching Spanish in the USSR; in other words, its values (research, scientific, ideological, etc.). The composition of these values and degree of their influence on the pedagogical process are considered according to the logic of a comprehensive analysis of Spanish language textbooks for higher education institutions. Since school education does not rely directly on scientific achievements, it is considered to be beyond the scope of the study. Moreover, since we do not take a strictly historiographical approach, a comprehensive overview of works related to the topic also falls outside the scope of this this study. Readers interested in such a historiographical overview are recommended to consult the already published reviews [3, 4].

The chronological framework of the study covers the period from the 1930s to the early 1980s, the lower boundary being the beginning of teaching Spanish in higher educational institutions (HEIs) of the USSR and consequent appearance of the first university textbooks. The upper boundary is the beginning of *Perestroika,* whose impact on the educational process may require a separate study.

While separate works dealing with the analysis of related topics (history of relations between Russia and Spain, study of Spanish language and literature, etc.) are available, a comprehensive study of teaching Spanish in Soviet HEIs is yet to be published, hence the relevance of the present paper.

The evolution of Spanish studies can be summarized briefly as follows. At the early stage of Spanish studies formation, the grammar-translation method based mainly on the performance of lexical-grammatical exercises and reading, along with textual analysis, has prevailed in the teaching methodologies used [5]. Later, a tendency towards the prevalence of the conscious-practical method implying the priority given to the practical aspect of language proficiency, along with a systematic perception of grammar, can be identified[2]. This methodological transition can be seen as a consequence of the general development of Soviet pedagogics and the concomitant improvement of foreign language teaching methods.

[1] The main reason for this lies not so much in the geographical remoteness of the countries from each other as the fact that Spain and Russia became leading subjects of European politics at different times, in the 16th and 18th centuries, respectively. In other words, by the time Russia entered the Pan-European arena, Spain had already left it. In any case, regular diplomatic relations between the two countries were not established until the first half of the 18th century [2].

PRINCIPAL TRENDS OF TEACHING SPANISH IN THE USSR

In the Soviet Union higher education system, the Spanish language was first taught during the 1930s. This was not accidental since it was during this period that Spain and the USSR experienced a hitherto unprecedented convergence of destinies. During the Spanish Civil War (1936–1939), the Soviet Union actively supported the pro-Communist forces. That was a time of intense exchange between the two countries, not only in the military sphere, but also in cultural and social contexts. A number of Soviet writers, such as Ilya Ehrenburg and Mikhail Koltsov, visited Spain during those years [6]. In 1940, the well-known collection "Culture of Spain" was published in the USSR, being the first publication of its kind in Russian to include articles on various aspects of Spanish studies [7].

Due to the large number of Soviet professionals traveling to Spain during this period, the question of their appropriate linguistic training became paramount. In these circumstances, textbooks and manuals aiming at the most rapid mastery of the basics of the language started to appear. Textbooks for 1st–3rd year students of HEIs were among the first to be published in 1933 [8, 9]. Here we may mention the "Spanish Textbook: Elementary Course" published in 1937. According to its author, this publication was aimed at "the ability to read simple socio-political texts and to express one's thoughts simply but competently [10]." Such textbooks were notable not only for their concise grammatical material but also for the uniformity of the ideological agenda presented; they were largely based on texts and lexical items of the communist and anti-capitalist orientation including texts about Marx, Stalin, the conquest of Mexico by Cortés, etc. Since such an orientation was logical in the context of the civil war and associated ideological confrontation, its relevance to that time is not in question. However, the main methodological limitations of these manuals recognized to consist in a bias towards lexico-grammatical aspects of the language to the prejudice of phonetic features; in other words, the striking prevalence of the grammar–translation method over other important pedagogical principles.

In discussing early stages of Spanish teaching in this country, we should mention "Essays on the History of the Languages of Spain" by V.F. Shishmarev, being the first of its kind like the collection of essays on culture mentioned above. Even though this was not a Spanish textbook, it was actively used by Hispanists as a manual for studying the history of Iberian languages until other relevant works appeared. The author provides a panoramic view of the development of Spanish, Portuguese, Catalan, Galician, and Basque languages in

a broad historical context. Certainly, this work is not free from shortcomings; in particular, it contains inaccuracies and apparent errors related to the Spanish language of Latin America. For example, the author translates the word *huaca* as "tomb" and *alpaca* as "mountain goat" [11], which lexical items have been assimilated by Spanish from Quechua, the official language of the Inca Empire and the most widely spoken indigenous language in both Americas. However, such inadequacies do not significantly diminish the value of the work, especially when making allowance for the lack of materials on the languages of Latin America (which remains partly true today).

The defeat of pro-Communist forces in the Spanish Civil War had a certain impact on teaching Spanish in the USSR and on Spanish studies in general. Nevertheless, these areas continued to develop (as a major world power claiming primacy in science, the USSR could not remain ignorant of one of the world's most widely spoken languages). In addition to the work of Shishmarev, it is worth noting the "Spanish Language Courses for Higher Education Institutions" by O.K. Vasil'eva-Shvede [12], which continued the line of manuals mentioned above, as well as the first normative grammar of Spanish written by the author in co-authorship with Georgy Stepanov [13]. However, with the 1939 victory of Franco's Nationalists, a powerful ideological impetus, which might otherwise have contributed to the further activation of Soviet Spanish studies, was lost.

The Cuban Revolution (1953–1959) served as a new development vector, which, moreover, partly helped to redirect the focus of Spanish teaching from Castilian (Iberian) to the Latin American variants. However, the correlation of these language versions remains one of the most important and ambiguous issues in national teaching practice.

From that time up to the dissolution of the Soviet Union, linguistic connections were maintained primarily through the Soviet Union's diplomatic relationships with various Latin American countries (Soviet-Spanish diplomatic relations were interrupted for many years, only being resumed in 1977 [14]). This refers not only to Cuba but also to other countries having strong socialist and communist ideology (e.g., Ecuador, Peru, and Mexico). Since these processes undoubtedly had an influence on Spanish teaching in the USSR, it is necessary to assess and characterize this impact in more detail.

When analyzing the educational literature of this period, two major trends should be noted. The first is the absence of a rapid response to Cuban Revolution taking the form of new published materials, as did occur in the case of the Spanish Civil War. The second is the gradual increase in both the quantity and quality of works related to Spanish teaching published during the 1960s and 1970s.

The first can be explained in terms of the USSR not being as actively involved in the Cuban Revolution as it had been in the Spanish Civil War. Consequently, its position may be characterized as "wait-and-see," with the result that no hasty response to the events took the form of innovations in Spanish teaching. It was only when the victory of the Cuban Revolution became a *fait accompli* that Cuba and Latin America in general would become a subject of interest to textbook authors (this interest can be approximately dated to the early 1960s).

The second trend deserves special attention. Its most obvious reason is precisely the sharp increase in contacts with the Spanish-speaking world (the comparable factor occurred in the 1930s turned out to be short-lived, virtually disappearing with the end of the Spanish Civil War). In turn, the increase in contacts created a demand for Spanish-speaking professionals who would not just know the language, but also be able to master the entire complex of foreign language communicative competence. The consequence of this has been an increase in the number of HEIs offering the relevant training. This in turn resulted in an increase in the number of textbooks and manuals on the Spanish language, as well as in the formation of several significant academic centers offering both practical (teaching) and methodological (development of textbooks and manuals) training, as well as hosting theoretical research in the field of Spanish studies. Among these are the Moscow, Leningrad, and Kiev schools of Spanish studies.

A special place among the works of this period is occupied by Stepanov's monograph 'Spanish Language in Latin America' [15] based on the author's doctoral thesis (the same researcher also subsequently published a monograph 'On the Problem of Linguistic Variation. Spanish Language in Spain and America' [16], whose content largely overlaps with the work considered here). In the Russophone literature, this represents the first experience of creating such a compendium of the linguistic picture of Latin America. As Stepanov himself notes, his work was inspired by the need to study the American version of Spanish due to expanding contacts with this region [16]. While it would not have been possible to consider all versions of Spanish in Latin America equally in one monograph, this work established a clear direction for further research. The main result of the work is the author's compelling evidence for the need to study the American Spanish in detail, not as a deviation from the norm (i.e., the Castilian version), but as an independent linguistic unit. Unfortunately, a detailed study of Latin American Spanish in the USSR has not been widely

and systematically developed, despite the occasional publication of individual works [17–19]. In addition, this vector has only partially been implemented in the Spanish teaching practice, as will be described further in more detail.

This later period is characterized by an increase in the number of textbooks presenting general Spanish curricula of various orientations, including textbooks published for both linguistic and non-linguistic institutions. This indicates the growing popularity of Spanish as an object of study among students in various fields despite other major European languages like French and German continuing to be more prevalent.

In terms of their content and methodology, the considered works are characterized by a certain diversity. One of the first textbooks of this period for language universities is the 'Textbook of Spanish Language' by N.A. Velikopolskaya and V.I. Rodriguez–Danilevskaya published in 1963 [20]. In terms of methodology, this work is based on the principle of parallel mastering phonetic and lexico-grammatical skills. While the selection of lexical and textual material is quite standard, since it reflects everyday themes ("Home," "My Family," "At the Institute," etc.) and the contemporaneous realities of social life ("In the Lenin Museum," "November 7"), the authors also demonstrate a strong bias towards the literature of the Spanish Golden Age (fragments from the works by Lope de Vega and Francisco Gómez de Quevedo y Villegas) and realistic prose (Pedro Antonio de Alarcón and José Herrera Petere). The textbook also contains several texts on Argentinian and Uruguayan topics, which is rather unusual for Soviet textbooks due to the ideological difference between USSR and Argentina [21].

By way of comparison, we can analyze the textbooks for students attending non-linguistic universities. This includes, for example, the 'Spanish Textbook' for the first year of non-linguistic faculties of universities [22]. While it is methodologically similar to the previous one, the subject matter of many of the included texts ("Medical Equipment," "Vitamins," etc.) suggests that the course is addressed, among others, to physicians. This seems quite significant, since Spanish textbooks with such a narrow focus are rare in Russia.

The Spanish textbook written by Yu.A. Smychkovskaya is addressed to the HEI students of non-linguistic specialties. Featuring fairly standard content, it presents grammatical topics with increasing complexity and building in parallel lexical skills on the basis of texts of various topics: the first one covering domestic themes followed by some ideologically expressed texts about Latin America, Lenin, and the Cuban figure José Marti [23].

Discussing the increase in the number of textbooks and manuals, it is worth noting the presence of not only general Spanish language courses, but also a variety of specialized publications covering specific aspects of Spanish studies, such as lexicology, history of language, theoretical grammar, etc. Some of these special works are designed not only for future Hispanists but also to include a wider range of readers. An example is 'Spanish Language. Historical and Linguistic Essay', a brief training manual authored by S.P. Mamontov [24]. To some extent, the presence of such works is an indicator of widespread interest in Spanish language.

During this period, a fair amount of attention is paid to the development of grammatical understanding. Moreover, this applies not only to general courses of practical and theoretical grammar, but also such aspects as grammatical stylistics and situational speech grammar, thus indicating a certain level of research depth. Each of these aspects will be considered in more detail.

The acknowledged leading university textbook on theoretical Spanish grammar written by Vasil'eva-Shvede and Stepanov [25] focuses on morphology and syntax. The authors present the grammatical features of all parts of speech in the context of contemporaneous innovations, including the extensive use of foreign material, in the presentation of theoretical grammar. Although in this case, the analysis is based mainly on authentic Spanish material, this raises few questions concerning the difference between the Castilian and the Latin American version, since in grammatical terms, this is fairly insignificant (this, however, is not the case with lexis and phonetics). The most noticeable differences (e.g., in the use of personal pronouns) are marked by the authors' note.

An example of a more practical grammar course is the 'Spanish Language Handbook' written by S.I. Kanonich, in two volumes [26, 27]. It is obviously aimed at students already having a basic knowledge of Spanish grammar, since the first lessons include the analysis of past tenses. There is also a lexical component presented by texts on various topics. The first volume mainly consists of texts on everyday life topics, while the second contains a considerable amount of popular science and linguistic materials, such as "Louis Pasteur" or "Cuba."

The textbook 'Situational Speech Grammar of the Spanish Language', also written by Kanonich [28], representing the first work on this subject published in Russian, is aimed at advanced Spanish learners. Essentially, the work examines the stylistics of the language in terms of functional grammar. Moreover, situational speech grammar is considered by the author as a part of linguistic and cultural studies, being a necessary component of understanding social spheres of communication, without which it would be impossible to fully master the cultural component of foreign language communicative competence.

To a certain extent, Kanonich's works are complemented by the textbook on grammatical stylistics of Spanish language written by N.M. Firsova. The author focuses on the functional approach to language learning [29], i.e., its learning in the context of its subsequent practical application. Despite stylistic functions of grammar being less distinct than lexical functions, Firsova rightly draws attention to them, especially in the view of insufficient knowledge concerning these aspects of linguistic competence. Mastering stylistic functions of grammar features is of undeniable importance for future linguistic professionals since it allows them to achieve a high level of proficiency. Authentic Latin American materials, mostly of Cuban and Ecuadorian origin, are used to support the analysis.

Of great interest is the textbook on prepositions written by M.N. Deev, this being a traditionally difficult grammar topic [30]. Practically all Spanish prepositions are explained in sequence along with examples.

The important subject of the history of the Spanish language is covered in the textbook 'Historia de la Lengua Española' written by E.V. Litvinenko [31], which has successfully passed through several editions. This now classic work analyzes the formation and development of the Spanish language according to a historical perspective, from Vulgar Latin to the present state. However, its focus is firmly on the Castilian version, with practically no information on Latin American versions.

The specialized works addressed to students of Hispanic Studies can be analyzed on the basis of their subject matter and thematic orientation. In addition to the above-mentioned lexicology, language history, and grammar, reference should be also made to phonetics and the theory and practice of translation.

The increasing number of textbooks on Spanish phonetics [32–35] confirms the relevance of this topic for teaching practice. It is significant that these textbooks have been published consecutively at all three academic centers of Spanish studies mentioned above, thus demonstrating the demand for the subject and the intensity of its scientific development. In terms of methodology, these works are based on a theoretical approach, with much attention paid to analyzing and describing the organs of articulation, their position in pronouncing certain sounds, etc.

The material presented in the textbooks reflects the relevance of such problems as the orthoepic norm. In general, the authors solve it in favor of the Castilian version, citing the following considerations as arguments: the impossibility of defining a "Latin American" pronunciation norm [34]; the possibility of Latin American versions seeming ridiculous in Spain [35]. At the same time, some authors do include material on the phonetic features of Latin American Spanish [36]. This results in the paradoxical situation: despite Soviet Hispanists being mainly in contact with Latin American colleagues, they were taught the phonetic norms of the Castilian version in the first place.

It should be acknowledged that the Soviet school of Spanish studies has found itself in a difficult position in this respect; an entirely rational and satisfactory solution has yet to be found. There is no denying the above argument that no "Latin American" pronunciation norm exists as an objective reality. Although the corresponding term continues to be used in scientific literature and teaching practices, not only in Russia, it should be regarded as a conditional construct, being convenient in use, but only approximating reality. In turn, the linguistic reality Hispanists and all Spanish learners are confronted with is the variety of national versions of Latin American countries, which can differ from each other significantly.

Conversely, the phonetic norm of "classical" Castilian Spanish, it is treated as an objective reality in all the textbooks under consideration. However, it should be borne in mind here that Castilian Spanish also has a high degree of dialectical variability. This is typical not only for Latin America but also for Spain itself (there are Andalusian, Catalan, Galician, and a number of other dialects). Although the prescribed literary pronunciation norm does exist, is not absolute.

Among the works devoted to translation, the 'Textbook of Interpreting from Spanish for Institutes and Faculties of Foreign Languages' by various authors [37] along with 'Difficulties in translating from Spanish to Russian' by N.D. Arutyunova [38] should be highlighted. These textbooks are intended not just for future Spanish speakers but also for students having already mastered the language at a sufficiently high level. In the introduction, Arutyunova states that her work is aimed at 2–3 semester postgraduate students.

The first textbook is intended primarily for practicing interpreting skills, while the second one is focused to a greater extent on written translation in the context of fiction and sociopolitical literature. Despite the practical bent of the textbooks (aimed at developing a stable set of essential skills for high-quality translation), they also contain a considerable amount of theoretical material. This is especially true of the textbook by Arutyunova, which contains detailed reviews of the most grammatically complex aspects of the Spanish language (phrasal verbs, emphatic constructions, special cases of pronouns, etc.), which are traditionally given little attention in general grammar courses.

The textbook of interpreting, which also covers theoretical issues, is mainly focused on classifying and analyzing difficulties that arise during the process of interpretation. Special emphasis is placed on phonetic and lexical difficulties. This textbook is based mainly on the Latin American material, especially Cuban. The topics are also typical including the industrialization of Cuba, the struggle for independence in Colombia, etc. As Arutyunova notes, the materials appearing in the textbook are taken from Spanish and Latin American literature, as well as from the Communist press of Latin American countries. This is not surprising, due to the contacts actually being maintained between the Soviet Union and various Latin American countries, as noted above; for this reason, the focus on Latin American materials for teaching future Hispanists seems rational.

CONCLUSIONS

The review of the main textbooks, manuals, and other works having influenced the teaching process allows some conclusions to be drawn concerning axiological aspects of teaching Spanish in the USSR. These can be conveniently divided into two groups: (1) scientific and scientific-pedagogical; (2) sociological and other aspects (e.g., ideological). Although the boundary between these groups is not absolute, it can be drawn for the purposes of ensuring maximum clarity of the issue under study.

As the title of the paper implies, the scientific aspects are directly related to the development of Spanish studies as a theoretical discipline along with its teaching. This includes the methodology and thematic orientation of the studied material.

The highly diverse thematic component is characterized by a high level of scientific research. The significant contribution made by Soviet Hispanists to the study of various aspects of the Spanish language is duly reflected in its teaching.

Among nonscientific aspects, ideological aspects certainly stand out. Although Marxism-Leninism did not influence the philological methodology of the USSR as comprehensively as some other humanitarian disciplines (for example, history), the general ideological orientation of the state also strongly influenced the development of Spanish studies. As mentioned above, such events as the Spanish Civil War, the subsequent defeat of pro-Communist forces, as well as, conversely, the victory of the Cuban Revolution, had a direct impact on Spanish studies. In retrospect, these events have become clear markers reflecting the most important stages in the history of Soviet Spanish studies: the beginning of systematic study and teaching of Spanish language, as well as the redirection of this process from Castilian to reflect Latin American political and linguistic realities. However, this redirection process was not completed, with the Latin American component lacking proper acknowledgement in all the developed materials. Here we can clearly distinguish the internal logic of the theoretical development from the external ideological influences.

In conclusion, it has been demonstrated that Spanish teaching in the USSR can serve as an interesting example of combining internal and external influences of a different nature, which in varying degrees, directly or indirectly, affect the development of an academic subject.

Authors' contributions

E.V. Novoselova—literature review, writing the text of the article.

N.I. Chernova—research concept, generalization of the study results.

N.V. Katakhova—formulation of the conclusions, interpretation of the study results.

REFERENCES

1. Shokanova R.D., Tarasova E.N. Reproductive method in teaching Russian to foreign students and its innovative aspects. *Russ. Technol. J.* 2021;9(3):98–107 (in Russ.). https://doi.org/10.32362/2500-316X-2021-9-3-98-107
2. Alekseev M.P. Hispanistic in the context of Spanish-Russian cultural relationships. In: *Voprosy ispanskoi filologii* (*Questions of Spanish Philology*). Leningrad: Izd. Leningrad. Univ.; 1974. P. 10–25 (in Russ.).
3. Vasil'eva-Shvede O.K. Hispanistic in the USSR and actual problems of the Spanish philology. In: *Voprosy ispanskoi filologii* (*Questions of Spanish Philology*). Leningrad: Izd. Leningrad. Univ.; 1974. P. 25–49 (in Russ.).

СПИСОК ЛИТЕРАТУРЫ

1. Шоканова Р.Д., Тарасова Е.Н. Репродуктивный метод в обучении иностранных студентов русскому языку и его инновационные аспекты. *Russian Technological Journal.* 2021;9(3):98–107. https://doi.org/10.32362/2500-316X-2021-9-3-98-107
2. Алексеев М.П. Испанистика в свете испано-русских культурных связей. В сб.: *Вопросы испанской филологии.* Материалы I Всесоюзной конференции по испанской филологии. Л.: Изд-во Ленинградского университета; 1974. С. 10–25.

4. Suprun A.V. *Ispanskii yazyk: Bibliografiya inostrannoi literatury* (*Spanish language bibliography of the foreign literature*). Part 1: 1953–1963. Moscow: Institut Yazykoznaniya, Vsesoyuznaya biblioteka inostrannoi literatury; 1971. 61 p. (in Russ.).
5. Shchukin A.N. *Obuchenie inostrannym yazykam. Teoriya i praktika* (*Teaching foreign languages. Theory and practice*). Moscow: Filomatis; 2010. 476 p. (in Russ.). ISBN 978-5-98111-125-9
6. Bagno V.E. *Rossiya i Ispaniya: obshchaya granitsa* (*Russia and Spain: Common border*). St. Petersburg: Nauka; 2006. 477 p. (in Russ.).
7. *Kul'tura Ispanii* (*Spanish culture*). Moscow: Izd. Akad. Nauk SSSR; 1940. 497 p. (in Russ.).
8. Filippova O.N. *Uchebnik ispanskogo yazyka* (*Spanish textbook*). 2nd year. Moscow: MIV; 1933. 32 p. (in Russ.).
9. Kelyin V.F. *Uchebnik ispanskogo yazyka* (*Spanish textbook*). 3rd year. Moscow: MIV; 1933. 34 p. (in Russ.).
10. Vasil'eva O.K. *Uchebnik ispanskogo yazyka. Nachal'nyi kurs* (*Spanish textbook*: *Elementary course*). Moscow: Tovarishchestvo inostrannykh rabochikh v SSSR; 1937. 256 p. (in Russ.).
11. Shishmarev V.F. *Ocherki po istorii yazykov Ispanii* (*Essays on the history of languages of Spain*). Leningrad: Izd. Akad. Nauk SSSR; 1941. 338 p. (in Russ.).
12. Vasil'eva-Shvede O.K. *Kurs ispanskogo yazyka dlya vysshikh uchebnykh zavedenii* (*Spanish language courses for higher education institutions*). Moscow: Izdatelstvo literatury na inostrannykh yazykakh; 1948. 718 p. (in Russ.).
13. Vasil'eva-Shvede O.K., Stepanov G.V. *Grammatika ispanskogo yazyka* (*Spanish grammar*). Moscow: Izdatelstvo literatury na inostrannykh yazykakh; 1956. 384 p. (in Russ.).
14. Lipkin M.A., Volosyuk O.V., Yurchik E.E. (Eds.). *Istoriya Ispanii. Ot voiny za ispanskoe nasledstvo do nachala XXI veka* (*The history of Spain. From the war of the spanish succession to the beginning of the 21st century*). Moscow: Indrik; 2014. 872 p. (in Russ.). ISBN 978-5-91674-269-5
15. Stepanov G.V. *Ispanskii yazyk v stranakh Latinskoi Ameriki* (*Spanish language in Latin America*). Moscow: Izdatelstvo literatury na inostrannykh yazykakh; 1963. 202 p. (in Russ.).
16. Stepanov G.V. *K probleme yazykovogo var'irovaniya. Ispanskii yazyk Ispanii i Ameriki* (*On the problem of linguistic variation. Spanish language in Spain and America*). Moscow: Nauka; 1979. 327 p. (in Russ.).
17. Bylinkina M.I. *Smyslovye osobennosti ispanskogo yazyka argentintsev* (*Semantic features of the Spanish language of Argentines*). Moscow: Nauka; 1969. 202 p. (in Russ.).
18. Sinyavskii A.V. On the question of the unity of the Spanish language (on the probability of fragmentation of the Spanish language in Latin America). In: *Semantiki nekotorykh strukturnykh edinstv sovremennogo ispanskogo yazyka* (*Semantics of some structural units of the modern Spanish language*). Moscow: RUDN; 1978. P. 104–111 (in Russ.).
3. Васильева-Шведе О.К. Испанистика в СССР и актуальные проблемы испанской филологии. В сб.: *Вопросы испанской филологии.* Материалы I Всесоюзной конференции по испанской филологии. Л.: Изд-во Ленинградского университета; 1974. С. 25–49.
4. Супрун А.В. *Испанский язык: Библиография иностранной литературы*. Вып. 1: 1953–1963 гг. М.: Институт языкознания, Всесоюзная государственная библиотека иностранной литературы; 1970. 61 с.
5. Щукин А.Н. *Обучение иностранным языкам. Теория и практика*. М.: Филоматис; 2006. 476 с. ISBN 978-5-98111-125-9.
6. Багно В.Е. *Россия и Испания: общая граница.* СПб.: Наука; 2006. 477 с.
7. *Культура Испании*. М.: Издательство Академии Наук СССР; 1940. 497 с.
8. Филиппова О.Н. *Учебник испанского языка*. Курс II. М.: МИВ; 1933. 32 с.
9. Кельин В.Ф. *Учебник испанского языка.* Курс III. М.: МИВ; 1933. 34 с.
10. Васильева О.К. *Учебник испанского языка*. Начальный курс. М.: Товарищество иностранных рабочих в СССР; 1937. 256 с.
11. Шишмарев В.Ф. *Очерки по истории языков Испании.* Л.: Издательство Академии наук СССР; 1941. 338 с.
12. Васильева-Шведе О.К. *Курс испанского языка для высших учебных заведений*. М.: Издательство литературы на иностранных языках; 1948. 718 с.
13. Васильева-Шведе О.К., Степанов Г.В. *Грамматика испанского языка*. М.: Издательство литературы на иностранных языках; 1956. 384 с.
14. *История Испании. От войны за испанское наследство до начала XXI века;* под ред. Липкина М.А., Волосюк О.В., Юрчик Е.Э. М.: Индрик; 2014. 872 с. ISBN 978-5-91674-269-5
15. Степанов Г.В. *Испанский язык в странах Латинской Америки*. М.: Издательство литературы на иностранных языках; 1963. 202 с.
16. Степанов Г.В. *К проблеме языкового варьирования. Испанский язык Испании и Америки.* М.: Наука; 1979. 327 с.
17. Былинкина М.И. *Смысловые особенности испанского языка аргентинцев*. М.: Наука; 1969. 202 с.
18. Синявский А.В. К вопросу о единстве испанского языка (о вероятности фрагментации испанского языка в странах Латинской Америки). В сб.: *Семантики некоторых структурных единств современного испанского языка.* М.: Университет дружбы народов; 1978. С. 104–111.
19. Степанов Г.В. Этапы развития испано-американской диалектологии. В сб.: *Philologica. Исследования по языку и литературе. Памяти академика В.М. Жирмунского.* М.–Л.: Наука; 1973. С. 75–82.
20. Великопольская Н.А., Родригес-Данилевская В.И. *Учебник испанского языка*. М.: Издательство литературы на иностранных языках; 1963. 359 с.
21. Romero L.A. *Breve historia contemporánea de la Argentina*. Buenos Aires: Fondo de Cultura Económica de Argentina; 2007. 332 p. ISBN 978-950-557-393-6
22. Коршунова Я.Б. *Учебник испанского языка.* М.: Высшая школа; 1971. 282 с.

19. Stepanov G.V. Stages of development of Spanish-American dialectology. In: *Philologica. Issledovaniya po yazyku i literature. Pamyati akademika V.M. Zhirmunskogo* (*Philologica. Language and literature studies. To the memory of Academician V.M. Zhirmunskii*). Moscow–Leningrad: Nauka; 1973. P. 75–82 (in Russ.).
20. Velikopolskaya N.A., Rodriguez–Danilevskaya V.I. *Uchebnik ispanskogo yazyka* (*Textbook of Spanish language*). Moscow: Izdatelstvo literatury na inostrannykh yazykakh; 1963. 359 p. (in Russ.).
21. Romero L.A. *Breve historia contemporánea de la Argentina*. Buenos Aires: Fondo de Cultura Económica de Argentina; 2007. 332 p. (in Spanish). ISBN 978-950-557-393-6
22. Korshunova Ya.B. *Uchebnik ispanskogo yazyka* (*Spanish textbook*). Moscow: Vysshaya shkola; 1971. 282 p. (in Russ.).
23. Smychkovskaya Yu.A. *Ispanskii yazyk* (*Spanish language*). Kiev: Vischa shkola; 1975. 318 p. (in Russ.).
24. Mamontov S.P. *Ispanskii yazyk. Istoriko-lingvisticheskii ocherk* (*Spanish language. A historical and linguistic essay*). Moscow: RUDN; 1966. 46 p. (in Russ.).
25. Vasil'eva-Shvede O.K., Stepanov V.G. *Teoreticheskaya grammatika ispanskogo yazyka. Sintaksis chastei rechi* (*Theoretical grammar of the Spanish language. Morphology and syntax of parts of speech*). Moscow: Nauka; 1972. 349 p. (in Russ.).
26. Kanonich S.I. *Posobie po ispanskomu yazyku, 1 god* (*Spanish language handbook. 1st year*). Moscow: Prosveshchenie; 1971. 256 p. (in Russ.).
27. Kanonich S.I. *Posobie po ispanskomu yazyku. 2 god* (*Spanish language handbook. 2nd year*). Moscow: Prosveshchenie; 1971. 270 p. (in Russ.).
28. Kanonich S.I. *Situativno-rechevaya grammatika ispanskogo yazyka* (*Situational speech grammar of the Spanish language*). Moscow: Mezhdunarodnye otnosheniya; 1979. 208 p. (in Russ.).
29. Firsova N.M. *Vvedenie v grammaticheskuyu stilistiku sovremennogo ispanskogo yazyka* (*Introduction to grammatical stylistics of modern Spanish language*). Moscow: Vysshaya shkola; 1981. 160 p. (in Russ.).
30. Deev M.N. *Predlogi sovremennogo ispanskogo yazyka* (*Prepositions of the modern Spanish language*). Moscow: Visshaya shkola; 1973. 176 p. (in Russ.).
31. Litvinenko E.V. *Historia de la lengua española.* Kiev: Vishcha shkola; 1983. 215 p. (in Spanish).
32. Prigozhina R.N., Flores-Fernandez J.M. *Vvodnyi foneticheskii kurs ispanskogo yazyka* (*Phonetics of the Spanish language. Introductory course*). Moscow: Vysshaya shkola; 1975. 102 p. (in Russ.).
33. Vicente Rivas A.S. *Fonetika ispanskogo yazyka* (*Spanish phonetics*). Kiev: Vischa shkola; 1976. 71 p. (in Russ.).
34. Karpov N.V. *Fonetika ispanskogo yazyka. Teoreticheskii kurs* (*Spanish phonetics. Theoretical course*). Moscow: Vysshaya shkola; 1969. 233 p. (in Russ.).
35. Lebedeva N.A. *Fonetika ispanskogo yazyka. Vvodnyi kurs* (*Spanish phonetics. Introductory course*). Leningrad: Izd. Leningrad. Univ.; 1971. 54 p. (in Russ.).
36. Tamayo E. *Korrektivnyi kurs fonetiki ispanskogo yazyka* (*A remedial course of Spanish phonetics*). Moscow: Gosudarstv. tsentral. kursy zaochnogo obucheniya; 1965. 114 p. (in Russ.).
23. Смычковская Ю.А. *Испанский язык*. Киев: Вища школа; 1975. 318 с.
24. Мамонтов С.П. *Испанский язык. Историко-лингвистический очерк.* М.: Университет дружбы народов; 1966. 46 с.
25. Васильева-Шведе О.К., Степанов В.Г. *Теоретическая грамматика испанского языка. Синтаксис частей речи*. М.: Наука; 1972. 349 с.
26. Канонич С.И. *Пособие по испанскому языку*. Первый курс. М.: Просвещение; 1971. 256 с.
27. Канонич С.И. *Пособие по испанскому языку*. Второй курс. М.: Просвещение; 1971. 270 с.
28. Канонич С.И. *Ситуативно-речевая грамматика испанского языка*. М.: Международные отношения; 1979. 208 с.
29. Фирсова Н.М. *Введение в грамматическую стилистику современного испанского языка*. М.: Высшая школа; 1981. 160 с.
30. Деев М.Н. *Предлоги современного испанского языка*. М.: Высшая школа; 1973. 176 с.
31. Литвиненко Е.В. *История испанского языка* (*Historia de la lengua española*). Киев: Вища школа; 1983. 215 с.
32. Пригожина Р.Н., Флорес-Фернандес Х.М. *Вводный фонетический курс испанского языка*. М.: Высшая школа; 1975. 102 с.
33. Висенте-Ривас А.С. *Фонетика испанского языка*. Киев: Вища школа; 1976. 71 с.
34. Карпов Н.В. *Фонетика испанского языка*. Теоретический курс. М.: Высшая школа; 1969. 233 с.
35. Лебедева Н.А. *Фонетика испанского языка*. Вводный курс. Л.: Издательство Ленинградского университета; 1971. 54 с.
36. Тамайо Э. *Коррективный курс фонетики испанского языка*. М.: Государственные центральные курсы заочного обучения; 1965. 114 с.
37. Туровер Г.Я., Триста И.А., Долгопольский А.Б. *Пособие по устному переводу с испанского языка для институтов и факультетов иностранных языков.* М.: Высшая школа; 1967. 262 с.
38. Арутюнова Н.Д. *Трудности перевода с испанского языка на русский*. М.: Наука; 1965. 122 с.

37. Turover G.Ya., Trista I.A., Dolgopolsky A.B. *Posobie po ustnomu perevodu s ispanskogo yazyka dlya institutov i fakul'tetov inostrannykh yazykov* (*Textbook of interpreting from Spanish for institutes and faculties of foreign languages*). Moscow: Vysshaya shkola; 1967. 262 p. (in Russ.).
38. Arutyunova N.D. *Trudnosti perevoda s ispanskogo yazyka na russkii* (*Difficulties of translation from Spanish into Russian*). Moscow: Nauka; 1965. 122 p. (in Russ.).

About the authors

Elena V. Novoselova, Cand. Sci. (Hist.), Associate Professor, Foreign Languages Department, Institute of Radio Electronics and Informatics, MIREA – Russian Technological University (78, Vernadskogo pr., Moscow, 119454 Russia). E-mail: novosyolova@mirea.ru. Scopus Author ID 57223021781, RSCI SPIN-code 4025-5882, https://orcid.org/0000-0001-8593-8572

Nadezhda I. Chernova, Dr. Sci. (Pedagog.), Professor, Head of Foreign Languages Department, Institute of Radio Electronics and Informatics, MIREA – Russian Technological University (78, Vernadskogo pr., Moscow, 119454 Russia). E-mail: chernova@mirea.ru. Scopus Author ID 57194042371, RSCI SPIN-code 7391-4040, https://orcid.org/0000-0002-5685-9733

Nataliya V. Katakhova, Cand. Sci. (Pedagog.), Associate Professor, Foreign Languages Department, Institute of Radio Electronics and Informatics, MIREA – Russian Technological University (78, Vernadskogo pr., Moscow, 119454 Russia). E-mail: katakhova@mirea.ru. Scopus Author ID 57204175929, RSCI SPIN-code 2552-5380

Об авторах

Новосёлова Елена Владимировна, к.ист.н., доцент, кафедра иностранных языков Института радиоэлектроники и информатики ФГБОУ ВО «МИРЭА – Российский технологический университет» (119454, Россия, Москва, пр-т Вернадского, д. 78). E-mail: novosyolova@mirea.ru. Scopus Author ID 57223021781, SPIN-код РИНЦ 4025-5882, https://orcid.org/0000-0001-8593-8572

Чернова Надежда Ивановна, д.пед.н., профессор, заведующий кафедрой иностранных языков Института радиоэлектроники и информатики ФГБОУ ВО «МИРЭА – Российский технологический университет» (119454, Россия, Москва, пр-т Вернадского, д. 78). E-mail: chernova@mirea.ru. Scopus Author ID 57194042371, SPIN-код РИНЦ 7391-4040, https://orcid.org/0000-0002-5685-9733

Катахова Наталия Владимировна, к.пед.н., доцент, кафедра иностранных языков Института радиоэлектроники и информатики ФГБОУ ВО «МИРЭА – Российский технологический университет» (119454, Россия, Москва, пр-т Вернадского, д. 78). E-mail: katakhova@mirea.ru. Scopus Author ID 57204175929, SPIN-код РИНЦ 2552-5380

Translated from Russian into English by Kirill V. Nazarov
Edited for English language and spelling by Thomas A. Beavitt

MIREA – Russian Technological University.
78, Vernadskogo pr., Moscow, 119454 Russian Federation.
Publication date September 30, 2022.
Not for sale.

МИРЭА – Российский технологический университет.
119454, РФ, г. Москва, пр-т Вернадского, д. 78.
Дата опубликования 30.09.2022 г.
Не для продажи.


МИРЭА
Российский
технологический
университет